NASA CR-72756
MDC G0805

VEHICLE-SCALE INVESTIGATION OF A FLUORINE-HYDROGEN MAIN TANK INJECTION PRESSURIZATION SYSTEM

by
E. C. Cady and D. W. Kendle

MCDONNELL DOUGLAS ASTRONAUTICS COMPANY–WEST
Huntington Beach, California

Prepared for
NATIONAL AERONAUTICS AND SPACE ADMINISTRATION

NASA Lewis Research Center
Contract NAS 3-13306
Erwin A. Edelman, Project Manager

Requests for copies of this report should be referred to:

National Aeronautics and Space Administration
Scientific and Technical Information Facility
P. O. Box 33
College Park, Maryland, 20740

NAS CR-72756
MDC G0805

FINAL REPORT

VEHICLE-SCALE INVESTIGATION OF A FLUORINE-HYDROGEN MAIN TANK INJECTION PRESSURIZATION SYSTEM

by
E. C. Cady and D. W. Kendle

McDonnell Douglas Astronautics Company—West
Huntington Beach, California

prepared for

NATIONAL AERONAUTICS AND SPACE ADMINISTRATION

31 July 1970

CONTRACT NAS3-13306

NASA Lewis Research Center
Cleveland, Ohio
Erwin A. Edelman, Project Manager
Chemical and Nuclear Rocket Procurement Section

FOREWORD

This report was prepared by McDonnell-Douglas Astronautics Company-West, under Contract NAS 3-13306. The contract is administered by the National Aeronautics and Space Administration, Lewis Research Center, Chemical and Nuclear Rocket Procurement Section, Cleveland, Ohio. The NASA Project Manager for the contract is Mr. E. A. Edelman. This is the Final Report on the contract, and it summarizes the technical effort from 1 July 1969 to 31 July 1970.

ABSTRACT

A comprehensive analytical and experimental program is described that resulted in an advanced computerized analytical technique for predicting the performance of a fluorine-hydrogen Main Tank Injection (MTI) pressurization system for the full range of LH_2 - fueled space vehicles. The accuracy of the analysis was verified by a series of 17 tests of a full-scale MTI pressure control system in a 1000 ft^3 (28.3 M^3) flight-weight LH_2 tank. Prepressurization, constant-pressure hold, and LH_2 expulsion at controlled tank pressure were demonstrated over a wide range of ullage volumes, flowrates, tank pressures, and injector configurations, with reasonable ullage gas and tank wall temperatures and efficient fluorine usage.

CONTENTS

FIGURES

TABLES

SYMBOLS

a	Acceleration
A	Area
C_p	Specific heat at constant pressure
C_v	Specific heat at constant volume
d	Jet exit diameter, characteristic dimension
f	Fraction of interface heating to liquid
f_m	Ullage mixing fraction
Gr	Grashof number
h	Heat transfer coefficient
H	Specific enthalpy
K	Thermal conductivity
k	Constant
K'	Interface region limit coefficient
m	Mass
n	Evaporated liquid mass
N	Number of liquid nodes
Nu	Nusselt number
P	Pressure
Pr	Prandtl number
q	Heat
Re	Reynolds number
R	Universal gas constant
t	Time
T	Temperature
U	Velocity
V	Volume
w	Mass flow
W	Molecular weight
X	Distance on the vertical axis
Z	Gas compressibility factor

γ	C_p/C_v or polytropic exponent
Δ	Increment
ε	Error limit
ρ	Density
μ	Viscosity

Subscripts

b	Buoyancy
c	Combustion
C	Jet velocity core
fo	Forced
fr	Free
F	Flame
F_2	Fluorine
g	Gas
H_2	Hydrogen
HF	Hydrogen fluoride
i	Gas node index
inj	Injectant
j	Wall and hardware node index
J	Injectant jet flow
k	Liquid node index
L	Liquid
lim	Interface region limit
m	Maximum
M	Turbulent mixing
mix	Ullage mixing
R	Reaction
TT	Total tank
u	Ullage
vap	Vaporization
w	Wall
0	Initial

Superscripts

*	Intermediate conditions
'	Final conditions
.	Time derivative

SUMMARY

A comprehensive program was performed to analytically and experimentally determine the applicability of fluorine-hydrogen Main Tank Injection (MTI) to large-scale LH_2 - fueled space vehicles. A computerized analytical technique was developed to predict the performance of a large-scale, flight-type MTI pressure control system. The analytical model included provisions for heat transfer, injectant jet penetration, and ullage gas mixing. A large scale MTI control system was designed, fabricated, and tested in a 1000 ft^3 (28.3 M^3) flight-weight LH_2 tank. The 17 tests were performed at ullage volumes from 106 ft^3 (3 M^3) to 950 ft^3 (26.9 M^3), with both straight-pipe and diffuser-type injectors, and at varied LH_2 outflow and GF_2 injection flowrates. Pre-pressurization, constant-pressure hold, and LH_2 expulsion at controlled tank pressures of 43 psia (296 x 10^3 N/M^2) and 25 psia (172 x 10^3 N/M^2) were demonstrated. The analysis accurately predicted GF_2 usage, ullage gas and tank wall temperatures, and LH_2 quantities evaporated. The analysis was used to predict the performance of an MTI pressure control system for a Centaur vehicle configuration and mission specified by NASA. The study revealed that MTI could now be effectively applied to a space vehicle and that substantial pressurization system performance benefits would be realized.

INTRODUCTION

For cryogenic vehicles, particularly those that require multiburn operation, the tank pressurization system can contribute significantly to the weight, complexity, and cost of the propulsion feed system. A tank pressurization concept termed main tank injection (MTI) has been suggested as a means to reduce weight and increase system simplicity. MTI is a technique in which a hypergolic reactant is injected into a propellant tank, and the resultant heat release pressurizes the tank. When controllable, such a technique promises considerable performance and cost improvement, especially for an advanced hydrogen-fueled upper stage.

From July 1966 through April 1968, McDonnell Douglas Astronautics Company-West (MDAC-W) conducted an MTI pressurization research program under NASA Contract NAS 3-7963 to determine, analytically and experimentally, the feasibility, limitations, and operating characteristics of a propellant tank pressurization system that uses the heat generated by the injection of fluorine (F_2) into a liquid hydrogen (LH_2) tank to produce pressurizing gas by hydrogen propellant vaporization. This program was conducted in two phases: (1) small-scale phenomenological testing in glass apparatus and (2) medium-scale (105-gallon (.398 M^3)) feasibility testing with LH_2 expulsion.

The initial phase was an experimental investigation (encompassing a comprehensive series of 131 tests) of two general problem areas peculiar to the H_2-F_2 propellants for MTI: (1) the effect that a number of critical physical and chemical variables have on the hypergolicity of F_2 injected into an LH_2 tank and (2) the characteristics and behavior of the reaction products as they freeze in an LH_2 tank. The LH_2 pressurization tests were performed in small (5-in. (.127 M) - diameter by 10-in. (.254 M)) glass Dewars, with pressure and temperature measurements and Fastax motion pictures (at 4,000 pictures/sec) used to record each test.

The results of this initial effort led to the conclusion that H_2 and F_2 are generally hypergolic under the conditions that are normally present when MTI is used to pressurize a LH_2 tank; however, under certain conditions, it was found that the presence of about 1 percent (volume) oxygen in the injectant F_2 caused reaction inhibition, which was followed by F_2 freezing and, sometimes, destructive detonation. An increased injectant total enthalpy (warming) was required to overcome this inhibition and enable ignition before the injectant could freeze.

Despite the problems of injectant freezing and detonation, the feasibility and practicality of this pressurization technique were demonstrated in the small-scale glassware tests to the extent that medium-scale MTI pressurization tests could be confidently undertaken.

The second phase of the NAS 3-7963 program included full-scale injector design, fabrication, and testing in a 105-gallon (.398 M^3), high-pressure, heavy-weight LH_2 dewar tank. A series of 21 tests were performed with full-scale injectors in the 105-gallon (.398 M^3) LH_2 tank to demonstrate the feasibility of the pressurization technique, to define tank-pressure control limits, and to determine pressurization characteristics of three injector configurations: (1) ullage/simple (US), (2) submerged/aspirated (SA), and (3) submerged/simple (SS). The tests were performed with tank expulsion pressures from 10 (6.9×10^4) to 170 psig (117.2×10^4 N/M^2), F_2 flowrates from 0.001 (.00045) to 0.01 lb/sec (.0045 Kg/sec), and ullage fractions from 8 to 97 percent for multiple pre-pressurization and expulsion cycles.

The following results were noted:

1. The US injector exhibited reliable ignition and efficient pressurization through hydrogen vaporization and ullage heating. The submerged injectors (SS and SA) showed less efficient pressurization than the US mode, and these submerged injectors were susceptible to occasional injectant freezing and detonation.
2. The pressurization data were approximately correlated to simple pressurization models, and injector design requirements were established. The feasibility and overall controllability of the MTI pressurization technique was demonstrated.

The detailed results of the NAS 3-7963 program can be found in References 1, 2, and 3. The success of the medium-scale MTI tests indicated the need for an analytical method to predict MTI performance for any size of LH_2-fueled space vehicle, and to demonstrate a full-scale flight-type MTI pressurization system.

This report describes a program to analytically and experimentally determine the applicability of a MTI pressurization system to the full range of existing and potential hydrogen-fueled vehicles. The program consisted of five major tasks, as follows:

Task I — Pretest Analysis and Experiment Design

The objective of this task was to develop a computerized analytical technique for predicting the performance and behavior of a MTI pressurization system using ullage injection of ambient GF_2 into a LH_2 tank. The analytical procedure was to be of a level of sophistication similar to the analyses of Roudebush (Reference 4) or Epstein (Reference 5) and was to be used to establish the test plan and predict system performance for a test program using a large flight-weight LH_2 tank.

Task II — MTI System Design

The objective of this task was to design a large scale test system; including a 1000 ft^3 (28.3 M^3) Thor propellant tank and installation, the MTI control system and injectors, the instrumentation and data acquisition system, and the detailed test plan. The MTI control system/injector design task included design, fabrication, and hot firing operational checkout tests of the MTI control system/injectors.

Task III — MTI System Fabrication and Testing

The objective of this task was to fabricate and install the MTI injection system, test tank, instrumentation, and all auxiliary systems in the test facility at the MDAC Sacramento Test Center, and perform a series of pressurization and expulsion tests.

Task IV — Data Evaluation and MTI Analytical Modeling

The objective of this task was to evaluate and correlate the test results with the developed theoretical MTI model and revise the model as required. The modified MTI analysis was then used to predict the performance of an MTI pressurization system for a vehicle and mission specified by NASA.

Task V — Reporting

The objective of this task was to prepare and submit reports as required by NASA.

Although the work was performed in the five tasks described above, this report is organized to logically show the analytical study results, the experimental investigation design and results, and the results of the space vehicle performance predictions.

ANALYTICAL STUDY

The objective of the analytical study was to develop a general analytical model for predicting the performance and behavior of MTI pressurization of a LH_2 tank using ullage injection of GF_2. The resulting computerized analytical technique is designated as H819, MTI Pressurization Computer Program.

BASIC COMPUTER PROGRAM DESCRIPTION

Basic Assumptions and Capabilities

The most important characteristic of this pressurization analysis is its one-dimensional quality. Spatial variations in the system variables can occur only along the vertical tank axis; there are no radial or circumferential variations. There is no spatial variation in ullage pressure; fluid momentum and viscous processes are ignored. These aspects of the model are common to many pressurization analyses and have been compared extensively with experimental data and found to be valid (References 4 and 6). Buoyancy forces due to the local gravitational field tend to produce a stable thermal stratification in the gas and liquid, resulting in a temperature distribution which is essentially one-dimensional. Although nonuniform radial temperature distributions will obviously occur locally in the flame region for MTI, this flame region is believed to be small compared to the ullage volume, and does not invalidate the one-dimensional assumption for the heat transfer processes.

The thermal system for this pressurization analysts consists of four components: the tank wall, internal hardware (instrumentation, etc.), propellant liquid, and ullage gas. Any size and configuration may be specified for the tankage. The propellant is a pure single-component liquid and the ullage gas is pure propellant vapor. Real variable properties are used to describe the thermodynamic behavior of all materials. The temperature-specific enthalpy relationships are given for the wall, hardware, liquid, and gas. The gas conductivity and viscosity are also given for use in convective heat transfer coefficient formulas.

The tank is pressurized by means of heat input to the ullage from the injectant reaction; this heat input may vary arbitrarily with time. The propellant outflow may also vary arbitrarily with time. Heat is transferred from the ullage gas to the cooler surfaces of the tank wall, hardware, and liquid. The heat transferred to the liquid results in raising the liquid temperature and/or vaporizing liquid. All heat transfer rates may vary with time and the wall and hardware rates may also vary with location (axially). The heat input, propellant outflow, vaporization, and all heat transfer rates may be specified by internal calculations or by input tables (for parametric computations).

With the heat input and propellant outflow rates specified, the computer program calculates the temperature distributions in the wall, hardware, liquid and gas, as well as the liquid vaporization rate and tank pressure, all of which vary with time during the solution. These data may be output from the program as frequently as desired.

Finite Difference Approximations

There are two general approaches to the finite difference solution for a one-dimensional tank pressurization analysis: fixed point methods (as in References 4 and 7) and volume node methods (as in References 5 and 8). The node method has several important advantages for use with advanced pressurization analyses (Reference 8) and for the MTI application in particular. Generally, it provides the flexibility and versatility for describing the heat transfer and thermodynamic processes which are absolutely necessary for the development of an effective MTI analysis.

The computations are based on a finite difference representation of the physical system. The tank wall, internal hardware, propellant, and ullage are each divided by horizontal planes into a number of nodes, as shown schematically, in Figure 1, with the properties within each node being uniform. The gas and liquid are divided into nodes whose thickness and location can vary with time. The tank wall and hardware nodes are of equal axial thickness and are stationary. The size and number of these nodes is sufficient to give an adequate step function approximation to the continuous, axial variation of the system variables. Gas and liquid nodes may be subdivided or combined as required to meet solution accuracy criteria. The ullage partial mixing model

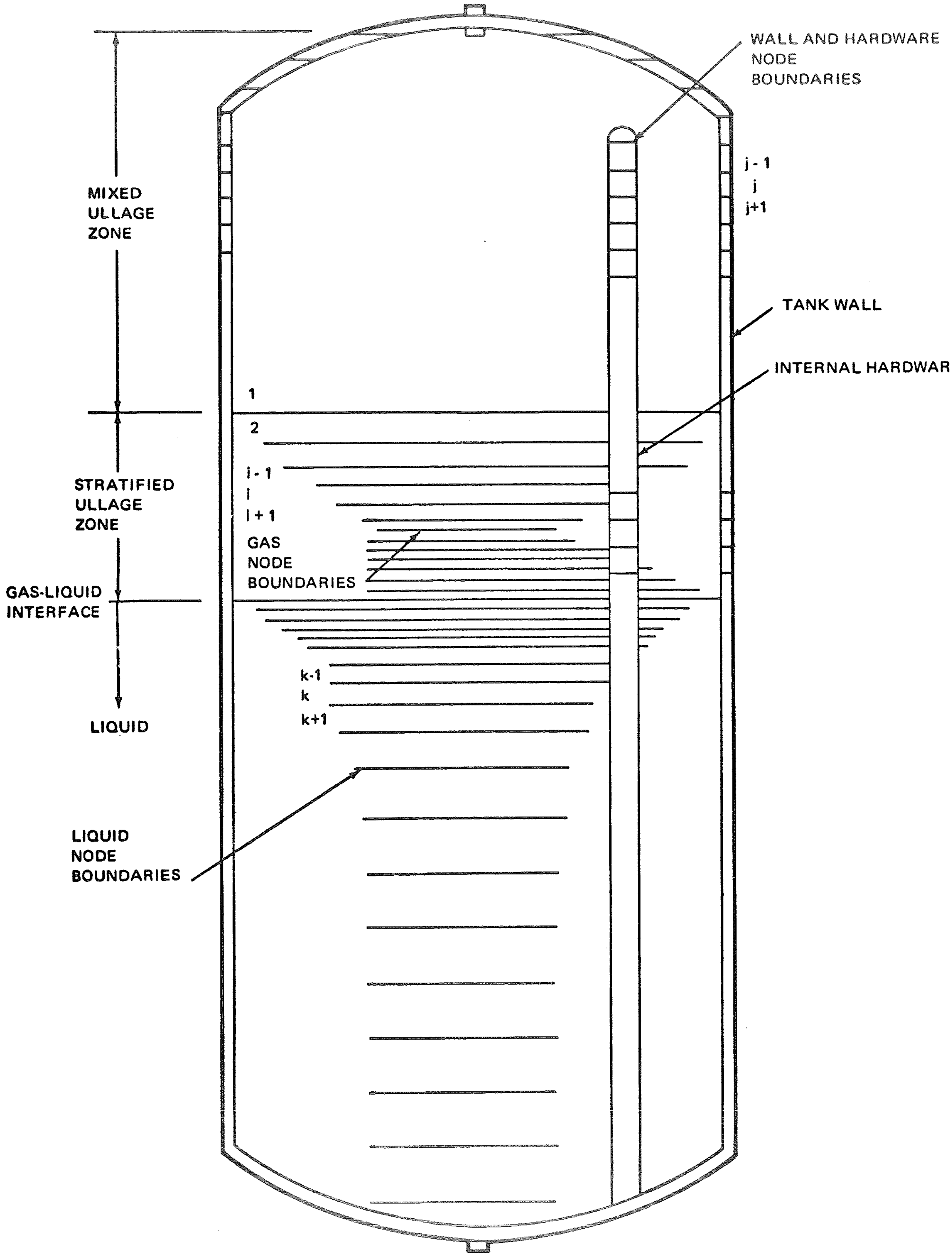

Figure I Finite Difference Node System

fits directly into this approximation of the physical system; the completely mixed zone is represented by the upper, single, large gas node.

The volume of each liquid and gas node is bounded by the top and bottom node boundary planes and by the solid surface of the tank wall and the internal hardware. Heat transfer takes place between each gas node and the solid surfaces with which it is in contact. The physically simultaneous processes of heat transfer and pressure change are assumed to take place sequentially as isobaric heat transfer and isentropic pressure change. The numerical solution is obtained by calculating the change in the state of each node in the system during each successive time step throughout the total solution time span. The state of each node is determined from equilibrium, conservation relationships.

Ullage Mixing

A key feature of the MTI analysis is the ullage mixing model; it relates directly to the heat input process from the GF_2/GH_2 reaction, and also to the heat and mass transfer occurring at the gas-liquid interface. The basis for this model is that the injectant gas inflow interacts with the ullage gas in the region near the injector, causing agitation and mixing. This gas mixing results in a region of nearly uniform temperature in the top part of the tank ullage. Nonuniformities do exist directly in the injectant flow path, particularly with the MTI flame; however, in the vicinity of the wall and hardware heat transfer surfaces away from the flame, a mixed ullage region of nearly uniform temperature is obtained. The validity of this model was established initially by experimental data from GH_2/LH_2 pressurization tests (Reference 9) and was verified subsequently by the MTI tests conducted during this investigation.

The extent of the mixed ullage region is determined by the injectant flowrate, the injector configuration and the ullage conditions. The GF_2 enters the ullage with a downward velocity and momentum. Since the flame reaction causes this flow to have a high temperature and low density relative to the surrounding ullage, the downward flow is retarded and decelerated by buoyancy forces. The jet velocity also decays due to turbulent mixing with the surrounding gas. These processes cause the injectant flow to be decelerated to a zero velocity and turned into a reverse flow pattern at some point in the ullage. This zero velocity point is the limit of the region of direct interaction of the injectant flow with the ullage and is related to the depth of the resulting mixed ullage region. A model for predicting this jet penetration depth from the analysis of buoyancy and turbulent mixing processes has been established.

The limit of the downward flow path of the injectant is necessarily also the limit of the heat source region from the MTI flame. Therefore, all heat released from the GF_2/GH_2 reaction goes into the mixed ullage region, the large upper node shown in Figure 1, except for that which is transferred to the liquid at the gas-liquid interface.

The dominant mode of heat transfer at the gas-liquid interface results from direct impingement of the injectant flow upon the liquid surface. This flow impingement causes penetration and disruption of the liquid surface, increased surface area exposure and fluid agitation. The net result is a high rate of convective heat transfer. This impingement condition can only occur when the injectant flow completely penetrates the ullage, otherwise this interface mechanism is inoperative.

When the ullage is only partially mixed, the remaining gas below the mixed zone undergoes thermal stratification in the usual manner as shown in Figure 1.

Overall Computer Program Computations

An overall flow chart for program H819 is shown in Figure 2. The sequence of computations occurring during a single time step is described in Figure 3. The description of the program computations and the list of equations given below follow the general order of the flow chart in Figure 3.

Program Operating Modes

A number of options are provided throughout the program to tailor the computation to a variety of requirements. Two principal operating modes are available: the fluorine injection mass flowrate history is specified by input and the resulting tank pressure history solution is calculated (injectant supply mode); or, the tank pressure history is specified by input and the required fluorine injection mass flowrate history is calculated (injectant demand mode). A pressure switch option is also available in which the upper and lower limits

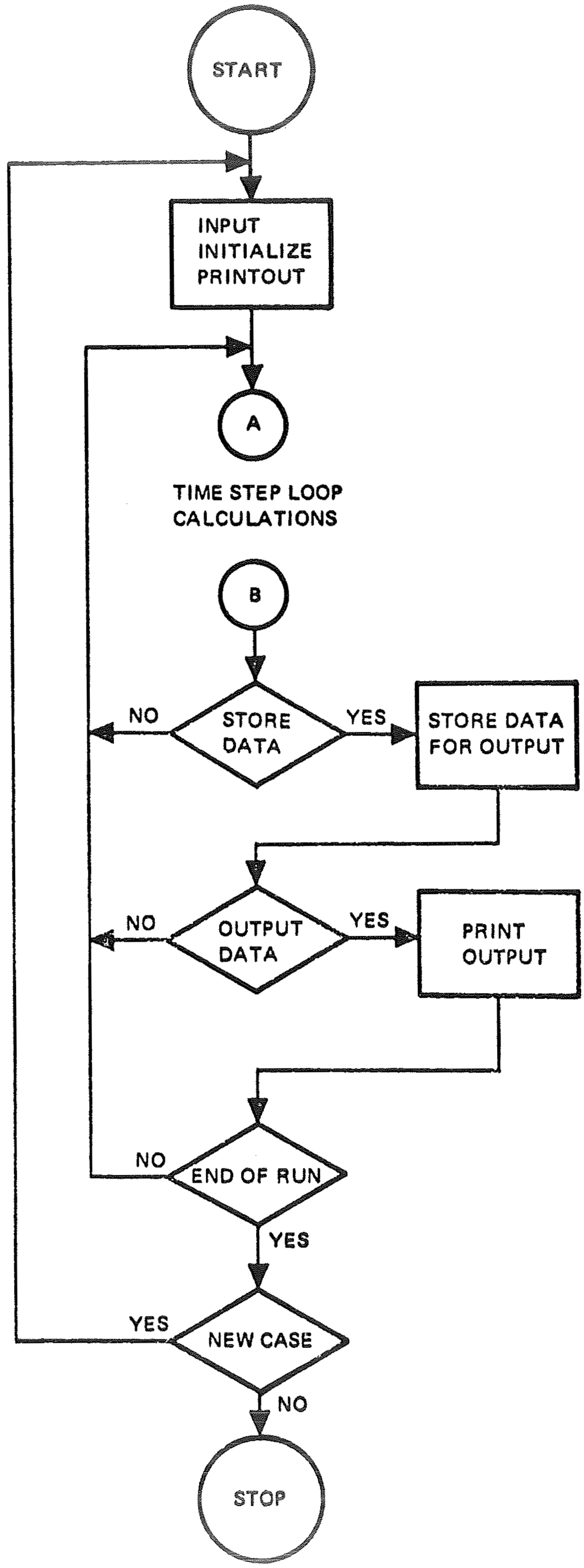

Figure 2. Program H819 Flow Chart

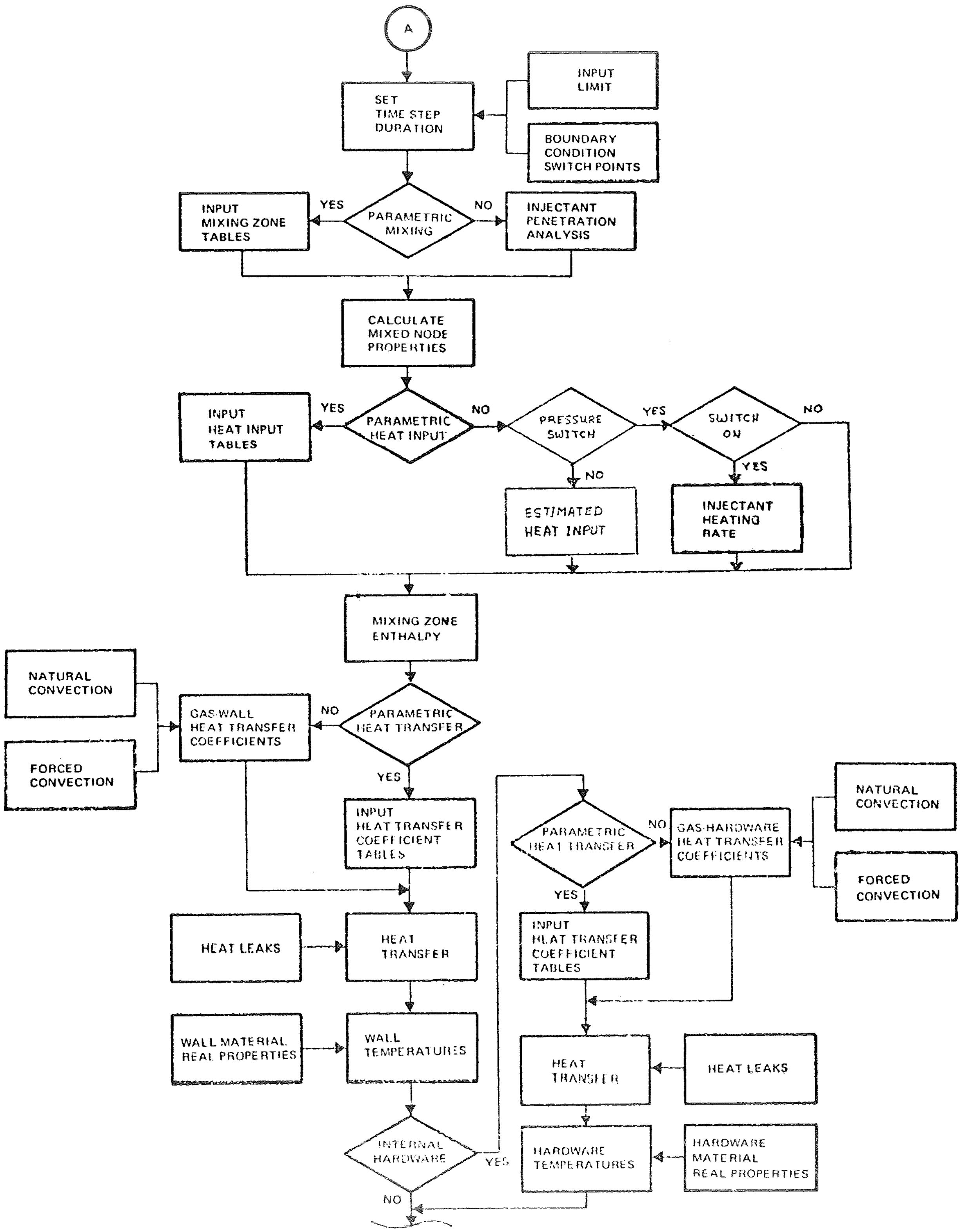

Figure 3. Time Step Loop Flow Chart

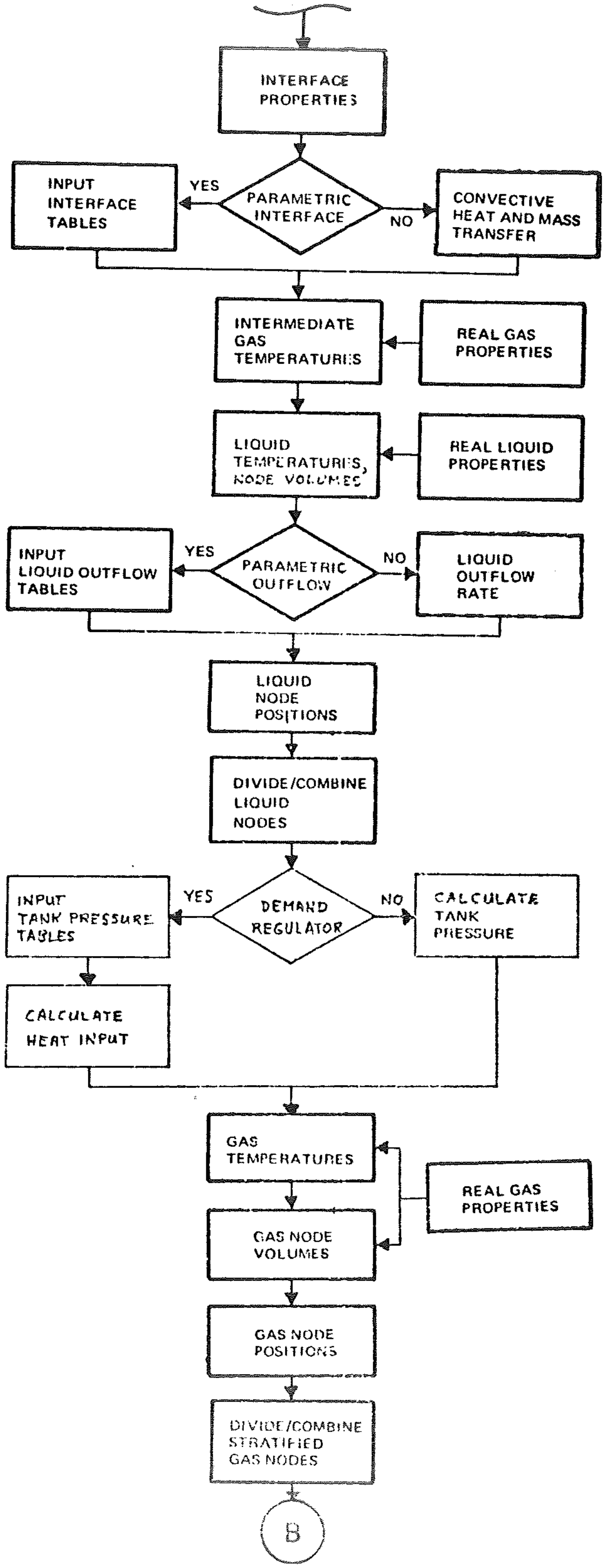

Figure 3 (Cont'd). Time Step Loop Flow Chart

of the desired operating pressure band are specified and the fluorine flow is switched on/off to maintain the pressure within that band. This option resembles the specified pressure history input, but the program actually operates in the injectant supply mode with the fluorine flow being controlled internally rather than by input. The fluorine flowrate during the switch-on periods may be specified either by the input history tables or by pressure bottle blowdown equations.

Tank Configuration

The tank configuration is specified by input tables which give the net cross section area (tank cross section minus hardware cross section), wall circumference, wall thickness, hardware circumference and hardware thickness at each input axial location. From this input table, a working table is generated by interpolation for use in the program computations. This table has its values at evenly spaced vertical node locations indexed from tank top to bottom and includes the accumulated tank volume, the wall and hardware effective heat transfer circumferences and their respective node masses. The effective heat transfer circumference accounts for the slant height of the solid surface at each node location; it is the actual tank wall or hardware area exposed to the ullage between the boundaries of the node, divided by the vertical distance between these boundaries. The exposed wall and hardware areas are multiplied by their respective thicknesses to give the node masses. In the program calculations, the wall area is obtained by multiplying the heat transfer circumference by the vertical height of the node.

Initial Conditions

At the start of the computation it is necessary to define the initial state of the system. The tank pressure and liquid level are input and the temperature distributions in the ullage gas, liquid, tank wall and internal hardware are specified by input tables. The node initial properties are determined from these by linear interpolation.

Notation for Equations

In the following equations, the index numbers of the gas, wall and liquid nodes are noted by subscripts i, j, and k, respectively. A variable value at the start of a time step, before it is modified by any computations, is without a superscript. An intermediate value of a variable which occurs at some point in the computation is noted by an asterisk (*) superscript. A final value of a variable at the end of a sequence of calculations is noted by a prime (') superscript. Determination of a dependent variable value Y for an independent variable value X from a table by linear interpolation is indicated by the notation Y<X>. A summary of this notation and the definition of symbols used in the following equations are given in the Symbols section.

Jet Penetration Depth and Ullage Mixing

The jet penetration depth into the ullage is determined from the condition of the ullage gas and the injectant entering the tank. Isentropic expansion of the GF_2 across the injector valve is assumed; the temperature T_{Jo} of the GF_2 at the injector exit is

$$T_{Jo} = T_{F_2} \left(\frac{P}{P_{F_2}} \right)^{\frac{\gamma - 1}{\gamma}} \tag{1}$$

where P is the known tank pressure, and T_{F_2} and P_{F_2} are the temperature and pressure of the GF_2 upstream of the injector valve. There are three options for determining T_{F_2} and P_{F_2}:

1. T_{F_2} and P_{F_2} are constant
2. T_{F_2} is constant and P_{F_2} is calculated from a polytropic pressure bottle blowdown equation
3. Both T_{F_2} and P_{F_2} are calculated from a polytropic pressure bottle blowdown equation.

The GF_2 mass flow rate $\dot{w}_J$ is either input (option 1 only) or determined from a choked orifice equation. The fluorine density at the injector exit is

$$\rho_{Jo} = \frac{W_{F_2} P}{R\ T_{Jo}} \tag{2}$$

and the injector inlet velocity for a cross section area A_J is

$$U_{Jo} = \frac{1.25\ \dot{w}_J}{\rho_{Jo}\ A_J} \tag{3}$$

where the factor 1.25 gives the centerline velocity for a fully developed turbulent pipe flow. Figure 4 shows details of the injectant flow and flame structure.

The jet penetration depth is determined by both buoyancy and turbulent jet mixing effects. The basic equation for the deceleration of the jet centerline velocity due to buoyancy is

$$\frac{1}{2}\ \rho_j\ d(U_j^2) = a\ (\rho_j - \rho_u)\ dX \tag{4}$$

or

$$d(U_j^2) = 2a\ (1 - \frac{\rho_u}{\rho_j})\ dX \tag{5}$$

Since the ullage may be at near LH_2 temperatures initially, a compressibility factor is included in the equation for ρ_u but the warmer jet is assumed to be a perfect gas; Equation (5) becomes

$$d(U_j^2) = 2a \left(1 - \frac{T_j}{M_j}\ \frac{M_u}{Z_u T_u}\right) dX \tag{6}$$

where T_j is the temperature and M_j is the molecular weight on the centerline of the jet, which vary with distance X in the flame structure. The variation in velocity due to turbulent jet mixing must also be specified. A literature search was conducted to find applicable analyses and data on the structure of turbulent jets and flames. Two analyses were found which were considered appropriate for nonreacting jets.

Kleinstein (Reference 10) has developed an analysis of axially symmetric compressible turbulent free jets which results in a simple equation for the axial decay rates and compares very well with experimental data. The

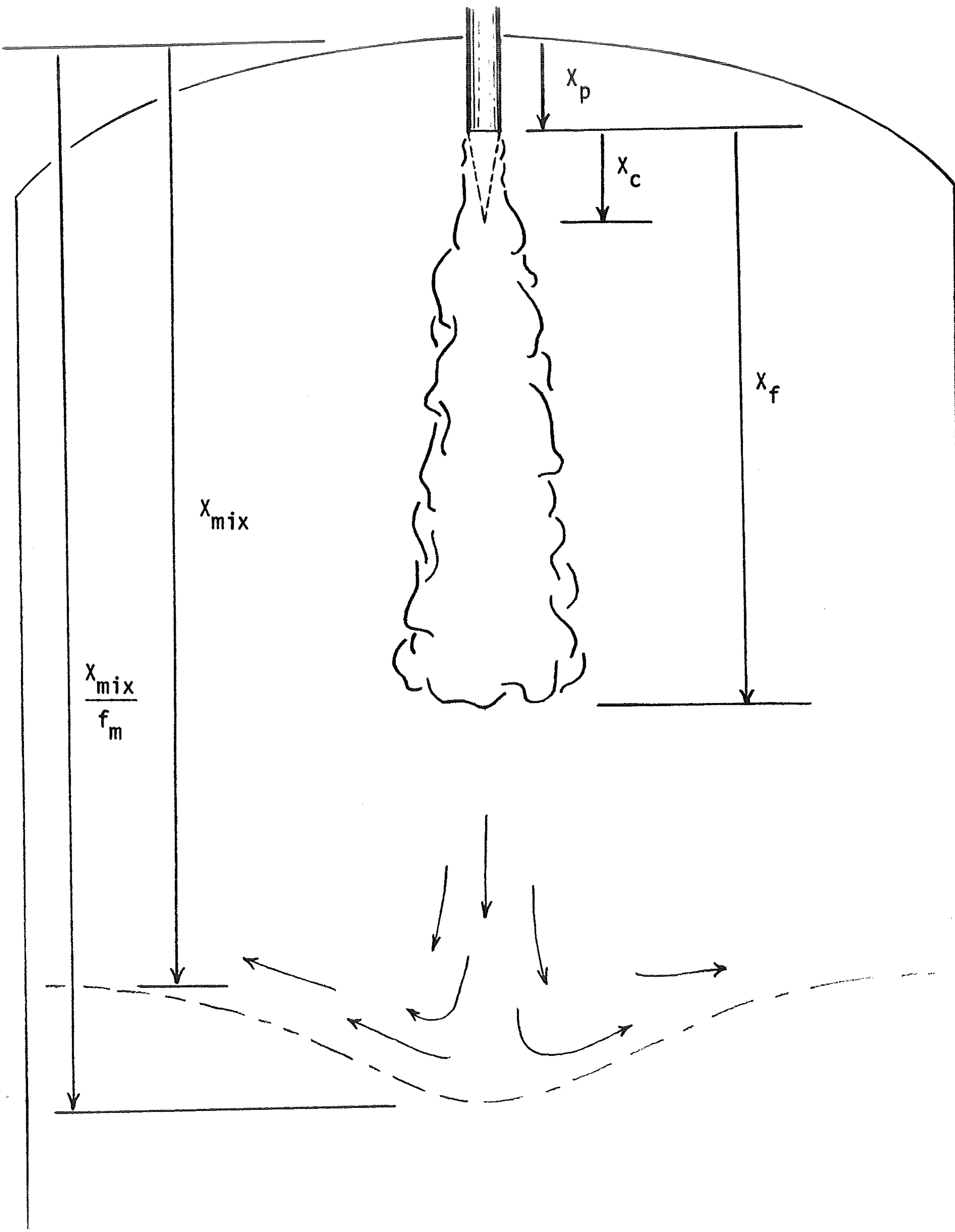

Figure 4. Injectant Flow and Flame Structure

centerline velocity, temperature and mass concentration of the jet fluid (Y_j/Y_{jo}) respectively are given by the single equation

$$\frac{U_j}{U_{Jo}}, \frac{T_J - T_u}{T_{Jo} - T_u}, \frac{Y_J}{Y_{Jo}} = 1 - \exp\left\{-1/\left[K\frac{X}{r}\left(\frac{\rho_u}{\rho_{Jo}}\right)^{1/2} - 0.70\right]\right\} \tag{7}$$

where k = 0.074, 0.102, and 0.104, respectively, and $\frac{X}{r}\left(\frac{\rho_u}{\rho_{jo}}\right)^{1/2} \geq 9.46$, 6.86, and 6.73, respectively. The limits on the latter term indicate the extent of the initial core lengths.

Experiments have shown that the radial distributions of velocity and temperature in a variable density jet are similar except near the jet exit. Laufer (Reference 11) has derived equations which are valid for this self-preserving region. The jet centerline velocity is given by

$$\frac{U_J}{U_{Jo}} = 19.2\left(\frac{X - X_o}{\theta}\right)^{-1} \tag{8}$$

and the temperature by

$$\frac{T_J - T_u}{T_{Jo} - T_u} = 15.9\left(\frac{X - X_o}{\theta}\right)^{-1} \tag{9}$$

where

$$\theta = \sqrt{\frac{\rho_{Jo}}{\rho_u}\frac{d^2}{8}} \tag{10}$$

is the "momentum diameter" and X_o is the "virtual origin" of the similar jet. Figure 5 from Reference 11 shows the comparison of this analysis with experimental data.

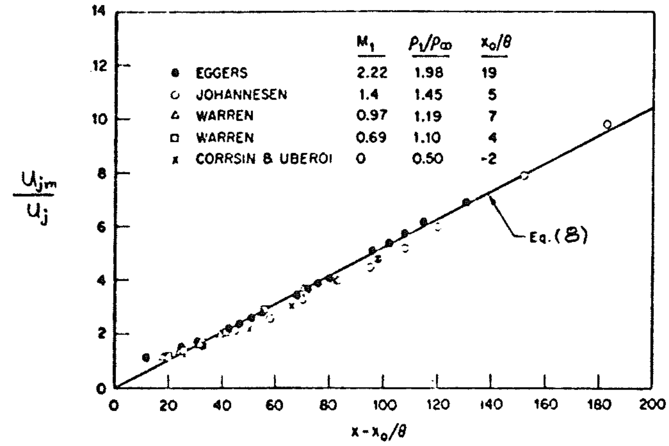

Center velocity in the circular jet.

Notes: Source - Reference 11

M_1 = Mach No.

$\rho_1/\rho_\infty = \rho_{jo}/\rho_u$

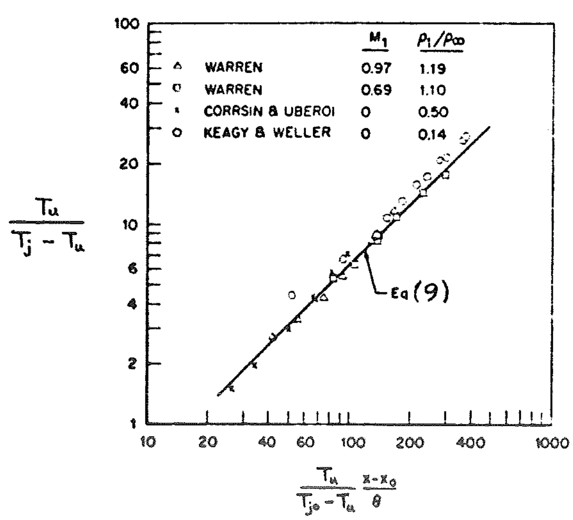

Center temperature in the circular jet.

Figure 5. Comparison of Laufer's Analysis with Experimental Data

Kleinstein's equations were considered preferable since they are valid for the entire jet length starting from the core limit. Laufer's equations were derived for the self-preserving region of the jet and were not intended for use in the region close to the jet exit.

In deriving the final form of the jet penetration equations and programming the associated computer subroutines, it was desirable to obtain a closed form solution for the penetration depth. A numerical integration was used in the preliminary stage of this investigation because the added flexibility was necessary. In the final version of the computer program, an explicit equation for the centerline velocity decay would be both convenient and less costly in machine time. Judged on this criterion, Kleinstein's equations were found to be less suitable than Laufer's since integration of the former produced a cumbersome result. After further study of these two analyses and comparisons with experimental data, it was concluded that the accuracy of Laufer's equations is equal to that of Kleinstein's except for a very small region near the jet exit. Since the jet penetration regularly extends to lengths on the order of a hundred jet-exit diameters, the relatively small inaccuracies in a region extending only a few jet diameters from the exit will have an insignificant effect on the calculated result. Therefore, it is satisfactory to use the simpler equations of Laufer.

Laufer's equations for the jet centerline functions are of the form $K\theta(X - X_0)^{-1}$, where K is a constant, θ is the momentum diameter, X is the distance from the jet exit and X_0 is the distance to the virtual origin. For the low subsonic jet-exit velocities encountered in this application, the value of X_0 was found to vary in a range from -0.5d to 0.5d where d is the jet exit diameter. Since X is often on the order of 100d, this variation in X_0 is insignificant, therefore, X_0 is set equal to its average value of zero. This approximation further simplifies the use of Laufer's equations.

The physical environment encountered by the jet in tank pressurization cannot be defined as easily as it is in the analysis and experimental work described by Laufer. The jet is flowing in a finite ullage volume with possible reverse flow; the jet flow is against an adverse pressure gradient which decelerates the jet; and the ullage which is assumed to be quiescent is subjected to the general turbulent motion of ullage mixing. These factors are not amenable to precise mathematical description. It was anticipated that Laufer's results would require empirical adjustment to obtain agreement with observed tank pressurization performance. Reference 9 reports exnerimental data for GH_2 pressurization of an LH_2 tank with a straight-pipe injector which are suitable for correlation with this analysis. For this purpose equations were derived for a nonreacting jet.

The jet penetration solution is evaluated mostly within the large mixed-region node and normally extends a relatively shorter distance into lower nodes. Since the centerline temperature at a large distance from the jet exit would not immediately be affected by a change in the surrounding ullage, it is acceptable to ignore this factor and simplify the analysis. Therefore, the ullage temperature T_u in Equation (9) is replaced by T_o which designates the mixed ullage region temperature, giving

$$T_j = T_o + (T_{jo} - T_o)\ 15.9\,\theta X^{-1} \tag{11}$$

The ullage density in Equation (10) is also taken as that of the mixed ullage node. Substituting Equation (9) into Equation (6) and integrating from X_1 to X_2 gives

$$\Delta(u_j^2)_b \Big|_{X_1}^{X_2} = 2a\left[\left(1 - \frac{T_o}{Z_u T_u}\right)\left(X_2 - X_1\right) - \frac{\left(T_{jo} - T_o\right)}{Z_u T_u}\ 15.9\ \theta \ln\left(\frac{X_2}{X_1}\right)\right] \tag{12}$$

where the subscript b indicates that this is the velocity squared decrement due to buoyancy only. The decrement due to jet mixing is given directly by Equation (8).

$$\Delta(u_j^2)_m \Big|_{X_1}^{X_2} = (u_{jo}\ 19.2\theta)^2\ \left(X_2^{-2} - X_1^{-2}\right) \tag{13}$$

The total change in jet centerline velocity squared is the sum

$$\Delta(u_j^2) \Big|_{X_1}^{X_2} = \Delta(u_j^2)_b \Big|_{X_1}^{X_2} + \Delta(u_j^2)_m \Big|_{X_1}^{X_2} \tag{14}$$

In the core region at the jet exit the second term is zero.

Solving Equation (14) for the point at which $U_j = 0$ gives the jet penetration limit. This analysis was added to the Tank Pressurization Computer Program and cases were run for the experimental conditions reported in Reference 9. It was found that multiplying the constants in Equations (8) and (9) by 1.2 to give values of 23.0 and 19.1, respectively, resulted in excellent agreement with the experimental data for the jet penetration depth shown in Figure 6.

With this modification in the equations, the pressurant mass was calculated as a function of expulsion time for the 1, 3/4 and 1/2-inch (.0254, .019 and .0127 M) diameter straight-pipe injectors and is compared in Figure 7 with the experimental data from Reference 9. These results are an excellent verification of the partially mixed ullage model. The deviations between calculated and experimental data are probably influenced by interface heat and mass transfer.

For the reacting MTI jet, Equation (9) must be replaced by the centerline variation of temperature within and downstream from the flame. The jet centerline velocity equation for the reacting MTI jet is assumed to be the same as for the nonreacting jet:

$$\frac{u_j}{u_{jo}} = \frac{X_c}{X} \quad X > X_c \tag{15}$$

where X_c is the velocity core length. The temperature equation is modified by using the flame length X_F as the effective temperature core length:

$$\frac{T_j - T_u}{T_{jm} - T_u} = \frac{X_F}{X} \quad X > X_F \tag{16}$$

In the flame region, a linear increase in centerline temperature is assumed

$$\frac{T_j - T_{jo}}{T_{jm} - T_{jo}} = \frac{X - X_c}{X_F - X_c} \quad X_c < X \leq X_F \tag{17}$$

and T_j remains equal to T_{jo} in the velocity core region ($X \leq X_c$).

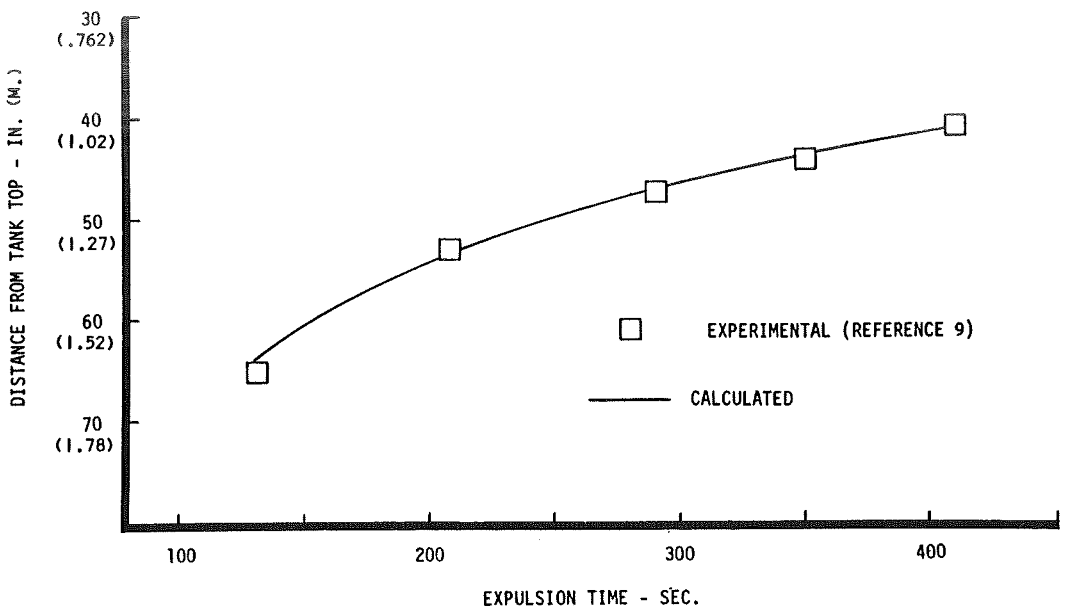

Figure 6. Depth of Mixed Ullage Zone at End of Expulsion

R316

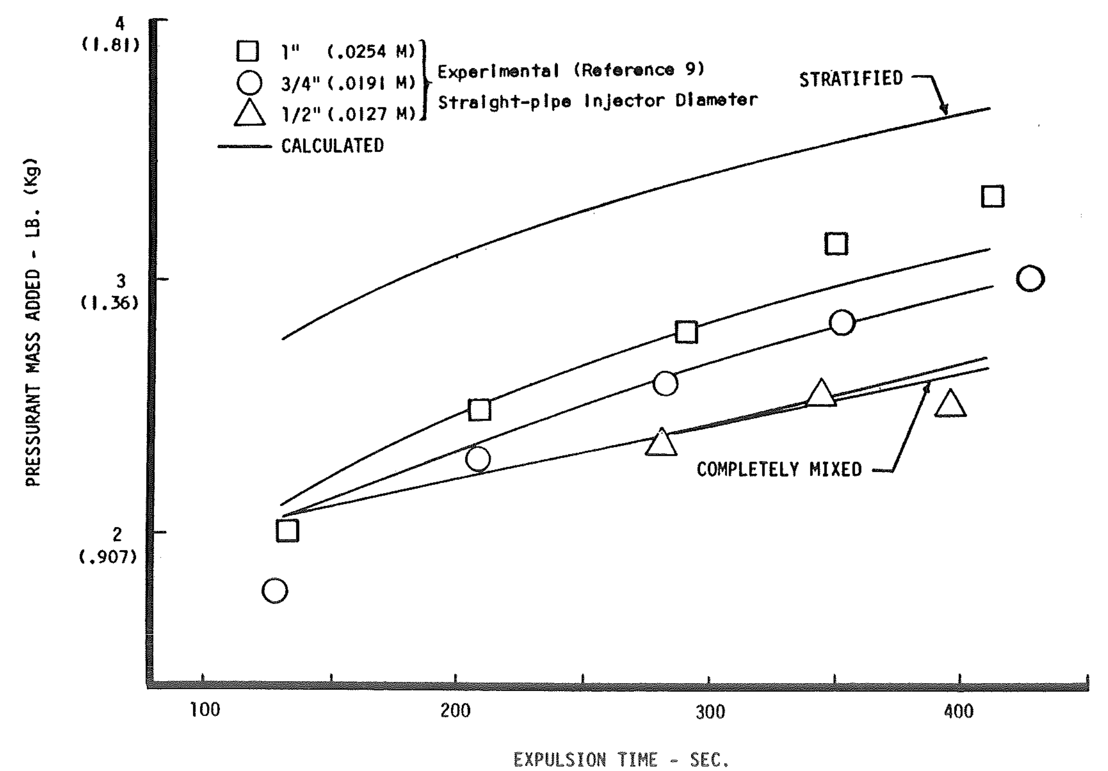

Figure 7. Pressurant Gas Added to Tank During Expulsion of Propellant

Laufer (Reference 11) derives an equation for the centerline mass concentration of the jet fluid which is of the same form as the temperature equation. Assuming this is true also for the MTI jet gives

$$Y_j = \frac{X_F}{X} \quad X > X_F \tag{18}$$

$$Y_j = \frac{X - X_c}{X_F - X_c} \quad X_c < X \leq X_F \tag{19}$$

where Y_j is the mass fraction of HF, equal to one at the maximum temperature point and zero in the surrounding medium and at the jet exit. The jet centerline molecular weight is then given by

$$M_j = \frac{M_{H_2} \, M_{HF}}{Y_j \, (M_{H_2} - M_{HF}) + M_{HF}} \quad X > X_F \tag{20}$$

$$M_j = \frac{M_{F_2} \, M_{HF}}{Y_j \, (M_{F_2} - M_{HF}) + M_{HF}} \quad X_c < X \leq X_F \tag{21}$$

where M is molecular weight.

In all regions of the jet flow, the centerline velocity-squared decrement from location X_1 to X_2 due to turbulent mixing with the surrounding ullage is given by

$$\Delta(u_J{}^2)_m \Big|_{X_1}^{X_2} = u_{Jo}^2 \, X_c{}^2 \left(\frac{1}{X_2^2} - \frac{1}{X_1^2} \right) \tag{22}$$

The centerline velocity-squared decrement due to buoyancy forces on the hot, downward flowing jet is found by combining and integrating the above equations giving three different equations for the three regions of the jet structure: the velocity core, the flame zone, and beyond the flame zone.

Velocity core zone ($X \le X_c$):

$$\Delta(u_J^2)_b \Bigg|_{X_1}^{X_2} = 2a \left(1 - \frac{T_{Jo}\, W_{H_2}}{W_{F_2}\, Z_u T_u}\right) (X_2 - X_1) \tag{23}$$

Flame zone ($X_c < X \le X_F$):

$$\Delta(u_J^2)_b \Bigg|_{X_1}^{X_2} = 2a \left\{ A(X_2 - X_1) + \frac{B}{2}\left[(X_2 - X_c)^2 - (X_1 - X_c)^2 \right] + \frac{C}{3} \left[(X_2 - X_c)^3 - (X_1 - X_c)^3 \right] \right\}$$

$$A = 1 - \frac{T_{Jo}\, W_{H_2}}{W_{F_2} Z_u T_u}$$

$$B = -\frac{W_{H_2} \left[T_{Jo}\left(W_{F_2} - W_{HF}\right) + W_{HF}\left(T_{Jm} - T_{Jo}\right)\right]}{W_{F_2}\, W_{HF}\, Z_u T_u\, (X_F - X_c)} \tag{24}$$

$$C = -\frac{W_{H_2}\left(W_{F_2} - W_{HF}\right)\left(T_{Jm} - T_{Jo}\right)}{W_{F_2}\, W_{HF}\, Z_u T_u \left(X_F - X_c\right)^2}$$

Beyond the flame zone ($X > X_F$):

$$\Delta(u_J^2)_b \Bigg|_{X_1}^{X_2} = 2a \left[D\,(X_2 - X_1) + E \ln\left(\frac{X_2}{X_1}\right) - F\left(\frac{1}{X_2} - \frac{1}{X_1}\right) \right]$$

$$D = 1 - \frac{T_o}{Z_u T_u}$$

$$E = -\frac{X_F\left[T_o\left(W_{H_2} - W_{HF}\right) + W_{HF}\left(T_{JM} - T_o\right)\right]}{W_{HF}\, Z_u T_u} \tag{25}$$

$$F = -\frac{X_F^2\left(W_{H_2} - W_{HF}\right)\left(T_{JM} - T_o\right)}{W_{HF}\, Z_u T_u}$$

The total centerline velocity-squared decrement is the sum of the mixing and buoyancy contributions

$$\Delta(u_J^2) \Big|_{X_1}^{X_2} = \Delta(u_J^2)_m \Big|_{X_1}^{X_2} + \Delta(u_J^2)_b \Big|_{X_1}^{X_2} \qquad (26)$$

To complete this derivation, the flame length X_F must be defined.

The photographic data from the NAS 3-7963 tests were reviewed in conjunction with the test oscillograph data. Most of the high speed motion pictures of the ullage tests showed no details of the H_2-F_2 flame. The camera was aimed, due to geometrical considerations, at a point below where the flame could penetrate, except for high pressure injection tests. Even in most of these tests, the gross over exposure of the film caused by the intense brightness of the flame obliterated all detail. However, in the case of test number 11, good motion pictures were obtained, and the extreme tip of the flame could be seen during the latter part of the prepressurization and initial part of the expulsion.

In appearance, the flame was quite bright and flickered at the edge of visibility. This allowed the length of the flame to be determined fairly accurately. By reconstructing the geometry of the camera angle, test tank and injector dimensions, etc., it was found that the flame first became visible at 15.6 inches (.396 M) (or 87 nozzle diameters) and the maximum extent of the flame was at 19.25 inches (.49 M) (or 107 nozzle diameters). The flickering appearance of the flame clearly indicated that it was not a laminar diffusion flame of stable contour, but rather, a turbulent flame. The transition from diffusion flames to turbulent flames occurs at Reynolds numbers from 2000 to 10,000, depending on the combustants. Our injection Reynolds number of 36,600 indicates that transition to a turbulent flame should have occurred.

Analysis of the flow conditions for the MTI jet indicated that the velocity core, calculated from the modified equation (5), was about 30 diameters long; the flame thus extended an average of 67 diameters beyond the velocity core. The growth of the total length of the flame from 87 to 107 diameters was attributed to the growth of the velocity core as the ullage heated up. It is known (Reference 12) that the length of turbulent flames does not vary appreciably with injectant velocity; therefore, a constant length of 67 diameters beyond the velocity core was chosen for the flame, giving the definitions

$$X_c = 23.0\,\theta \tag{27}$$

$$X_F = X_c + 67d \tag{28}$$

both measured from the jet exit. These variables are substituted into the foregoing jet penetration equations.

Equation (26) is evaluated to find the location X_2 at which $u_J^2 = 0$, which is the limit of jet penetration. The values of the ullage compressibility factor and temperature (Z_u and T_u) will be different for each gas node of the computer program model so that the limits X_1 and X_2 cannot extend beyond the limits of a single gas node in the evaluation of this equation. At the jet exit, located a distance X_p from the tank top in the i_p node (usually $i_p = 1$),

$$u_J^2 = u_{Jo}^2 \tag{29}$$

The first velocity decay calculation is

$$u_{J,i_p+1}^2 = u_J^2 + \Delta(u_J^2) \Bigg|_{X_p}^{X_{i_p+1}} \tag{30}$$

and subsequently

$$u_{J,i+1}^2 = u_{J,i}^2 + \Delta(u_J^2) \Bigg|_{X_i}^{X_{i+1}} \tag{31}$$

for each increment in i. In each evaluation, Z_uT_u is set equal to Z_iT_i for that node. The gas node containing the location of the penetration limit X_{mix} is identified by the conditions

$$u_{J,i}^2 > 0 \;; \quad u_{J,i+1}^2 \leq 0 \tag{32}$$

A bisection iteration technique is then used within this node ($i = i_{mix}$) to determine two X-locations which satisfy

$$2\,\frac{X_2 - X_1}{X_2 + X_1} \le \epsilon \qquad (33)$$

where $U_J^2 \ge 0$ at X_1, $U_J^2 \le 0$ at X_2 and ϵ is a specified error limit. The penetration depth is the average of X_1 and X_2.

The penetration depth is the maximum possible extent of the mixed ullage region. If the ullage mixing process is completely effective, the mixing depth X_{mix} will equal the penetration depth. This requires that the gas velocity in the jet flow field be dissipated in random turbulent mixing in the affected ullage region. However, if a recirculating flow field is induced in the ullage by the injectant flow, permitting some heated gas from the reaction zone to reach upper levels of the ullage without complete mixing, then some degree of temperature stratification will result. This effect is represented by a mixing fraction factor f_m which is a measure of the effectiveness of the ullage mixing. The ullage mixing depth is given by

$$X_{mix} = f_m\,\frac{X_1 + X_2}{2} \qquad (34)$$

where X_1 and X_2 are defined by Equation (33).

The gas node containing X_{mix} is divided at that point into two separate nodes. All nodes located above X_{mix} are combined into a single upper mixed ullage node and its mass and specific enthalpy are determined:

$$m_{mix} = \sum_{i=1}^{i_{mix}} m_i \qquad (35)$$

$$H_{mix} = \frac{\sum_{i=1}^{i_{mix}} m_i H_i}{m_{mix}} \qquad (36)$$

The gas node indices are then adjusted with $i = i_{max}$ becoming $i = 1$ and so forth.

Injectant Reaction Heating

The heat addition rate may be determined in three ways depending on the operating mode. The fluorine inflow rate $\dot{w}F_2$ may be read from input tables or calculated from a pressure bottle blowdown equation (initial conditions input) and multiplied by the GF_2/GH_2 heat of reaction H_R to give

$$\dot{q}'_{inj} = \dot{w}'_{F_2} \Delta H_R \tag{37}$$

or, if the pressure history is input and the fluorine flow is calculated, the heating rate from the previous time step is used as an estimate

$$\dot{q}'_{inj} = \dot{q}_{inj} \tag{38}$$

The first intermediate specific enthalpy of the mixed ullage node after heat addition is

$$H_1^* = H_1 + \frac{\dot{q}'_{inj} \Delta t}{m_1} \tag{39}$$

and the intermediate temperature is determined by interpolation from the gas specific enthalpy tables

$$T_1^* = T \langle H_1^* \rangle \tag{40}$$

Gas-Wall Heat Transfer

The gas and liquid are divided into nodes whose thickness and location can vary with time. The tank wall and internal hardware nodes are of equal axial thickness and are stationary. The gas and liquid node boundaries do not generally coincide with the wall and hardware node boundaries. (This discussion will refer to gas-wall heat transfer, but the treatment with hardware nodes is the same.) One gas node can exchange heat with more than one wall node, or with only a part of one wall node, and vice versa. The heat transfer equation is

$$\dot{q}_{ij} = h_{ij} A_{w,ij} (T_i - T_{wj}) \tag{41}$$

where the subscript i identifies the gas node and j the wall node. $A_{w,ij}$ is the wall area at which the i and j nodes are in contact; $A_{w,ij} = 0$ when the nodes are not in contact.

The heat transfer coefficient, h_{ij}, is based on the experimental results described in that section. In the tank ullage, free convection is always present, and the turbulent heat transfer coefficient for free convection to a vertical flat plate is found from

$$\frac{h_{fr} d}{K} = 0.13 \; (GR \cdot PR)^{1/3} \tag{42}$$

(taken from Reference 13.) In the mixed zone of the ullage, while injection occurs, forced convection heat transfer is also present, and is evaluated from

$$\frac{h_{fo} d}{K} = 0.037 \; (Re)^{4/5} \; (PR)^{1/3} \tag{43}$$

(taken from Reference 14.) The heat transfer coefficients are assumed to be additive:

$$h_{ij} = h_{fr} + h_{fo} \tag{44}$$

In the free convection equation the characteristic dimension d, appearing in the Grashof number, cancels out, but the forced convection coefficient is a function of $d^{-1/5}$. This is a very weak function, with 1000 percent change in d resulting in only a 58 percent change in h_{fo}, thus the characteristic dimension is arbitrarily set at one foot. This dimension is not particularly related to tank size, but rather to the probable size of characteristic turbulent eddies in the ullage.

The velocity appearing in the Reynolds number is evaluated as

$$U = .12 \; u_{Jo} \tag{45}$$

as is described below in the section on Experimental results.

The total heat transfer to a single wall node is

$$\Delta q_j = \Delta t \sum_i \dot{q}_{ij} \tag{46}$$

and from a single gas node,

$$\Delta q_i = \Delta t \sum_j \dot{q}_{ij} \tag{47}$$

The specific enthalpies of the gas and wall nodes are known prior to the heat transfer, and are calculated after heat transfer as

$$H_i^* = H_i - \Delta q_i/m_i \tag{48}$$

$$H_{wj}' = H_{wj} + \Delta q_i/m_{wj} \tag{49}$$

The intermediate gas node temperatures (before pressure change) and the new wall node temperatures are found from the specific enthalpy tables.

Gas-Liquid Interface Heat and Mass Transfer

The dominant mode of interface heat transfer is due to direct impingement of the injectant flow on the liquid surface. While other secondary mechanisms of interface transfer may be in effect under other conditions, only this dominant mode is presently treated in the analysis.

When the injectant jet flow reaches the liquid surface and has not decayed to a zero centerline velocity, the jet will then continue its downward flow, penetrating into the liquid, until the zero velocity condition is reached. The penetration depth into the liquid is calculated in the same manner as the ullage penetration depth, after making the substitution of $W_{H_2} P/R \rho_{L,k}$ for $Z_u T_u$ in Equations (19) through (21). This change replaces the ullage gas node density with the liquid node density. The resulting liquid penetration depth X_L is measured from the liquid surface.

The degree of agitation experienced by the liquid and the gas at the interface as well as the variation in the exposed liquid surface area are all related to the velocity of the jet at the liquid surface and hence to the depth of penetration of the gas jet into the liquid. Therefore, the overall gas-liquid heat transfer rate is expressed as a function of X_L. Correlations with experimental data for liquid hydrogen pressurization have indicated the form

$$\dot{q}_g = K\ X_L^2 \tag{50}$$

where $\dot{q}_g$ is the heat transfer rate from the ullage gas to the interface and K is empirically determined. (See the section on Computer Analysis of Experimental Results.) The heat transfer rate from the interface to the liquid is a fraction of $\dot{q}_g$

$$\dot{q}_L = f\ \dot{q}_g \tag{51}$$

The difference between what is transferred to and from the interface results in vaporization of liquid at the interface

$$\dot{q}_{vap} = \dot{q}_g - \dot{q}_L \tag{52}$$

The interface temperature is determined from a saturation temperature table as a function of the tank pressure; the liquid heat of vaporization H_{vap} and the liquid and gas saturation specific enthalpies are determined from tables as a function of the interface temperature. The rate of liquid vaporization is given by

$$\dot{n} = \frac{\dot{q}_{vap}}{\Delta H_{vap}} \tag{53}$$

The heat transferred from the interface to the liquid is distributed in a restricted region below the interface of depth X_{lim} equal to X_L.

A uniform distribution of the interface transfer heating within this region is assumed, with the heat transferred to each node given by

$$\Delta H_{L,k} = \frac{\left(X_{k+1} - X_k\right)}{X_{lim}} \frac{\dot{q}_L \Delta t}{m_{L,k}} \tag{54}$$

for $X_{k+1} \leq X_{lim}$ and

$$\Delta H_{L,k} = \frac{\left(X_{lim} - X_k\right)}{X_{lim}} \frac{\dot{q}_L \Delta t}{m_{L,k}} \tag{55}$$

for $X_{k+1} > X_{lim}$. The liquid node specific enthalpy is

$$H'_{L,k} = H_{L,k} + \Delta H_{L,k} \tag{56}$$

and the second intermediate specific enthalpy of the single mixed ullage node is

$$H_1^{**} = H_1^{*} - \frac{\dot{q}_g \Delta t}{m_1} \tag{57}$$

The gas node and the affected liquid nodes are checked against the respective saturation specific enthalpies to correct any supersaturation conditions which may have occurred. If a node is super-saturated, sufficient mass is condensed or evaporated from the node such that the latent heat involved will bring the remaining node mass to a saturated condition. This mass transfer is added to that from Equation (53). The transferred mass is distributed in the same proportional manner as described above for the transferred heat. The final liquid node temperatures are determined by interpolation from the liquid specific enthalpy tables

$$T'_{L,k} = T_L \left\langle H'_{L,k} \right\rangle \tag{58}$$

and the second intermediate gas temperature is similarly

$$T_1^{**} = T \left\langle H_1^{**} \right\rangle \tag{59}$$

A second intermediate gas temperature is calculated only when interface heat transfer is occurring. In the remaining discussion, no distinction will be made between the first and second intermediate values.

Liquid Outflow and Node Positions

The mass outflow rate $\dot{w}_L$ is usually specified by input although an option is available to determine it as a function of the tank pressure. The liquid nodes remaining after outflow are determined by finding the maximum value of N' which satisfies

$$\sum_{k=N'}^{N} m_{L,k} \geq \dot{w}_L \Delta t \tag{60}$$

where N and N' are the indices of the bottom liquid nodes before and after outflow. The mass of the new bottom node after outflow is

$$m'_{L,N'} = m_{L,N'} + \sum_{k=N'+1}^{N} m_{L,k} - \dot{w}_L \Delta t \tag{61}$$

where the summation term is zero if N' = N. The density of each liquid node is determined for its temperature from tables

$$\rho'_{L,k} = \rho_L \langle T'_{L,k} \rangle \tag{62}$$

and each node volume is

$$V'_{L,k} = \frac{m'_{L,k}}{\rho'_{L,k}} \tag{63}$$

These nodes are then relocated in the tank.

The tank configuration is specified in part by a table giving the accumulated tank volume as a function of the distance from the tank top for each wall node location, $V_{T,j} \langle X_j \rangle$. With V_{TT} equal to the total tank volume, the successive locations of the upper node boundaries are found by interpolation in the tank volume table

$$X_{L,n} = X_L \langle V_{TT} - \sum_{k=n}^{N'} V'_{L,k} \rangle \tag{64}$$

where n is a specific liquid node index. The upper boundary of the top liquid node, $X_{L,1}$, is the gas-liquid interface location.

After the liquid nodes have been relocated, their thicknesses $(X_{L,k+1} - X_{L,k})$ are checked against the maximum and minimum limits and node splitting and combining are carried out as needed.

Tank Pressure

Depending on the operating mode, the tank pressure may be specified by input tables or calculated as a function of the heat input and other operating parameters. In the latter case, intermediate gas node densities are calculated

$$\rho_i^* = \frac{W_{H_2}\, P}{Z_i R\, T_i^*} \tag{65}$$

where Z_i is the node compressibility factor determined at the old pressure and the intermediate node temperature. With γ_i determined in the same way, the new tank pressure P' is given by the polynomial

$$0 = \left[\sum_i \frac{m_i'}{\rho_i^*} - V_u\right] + \left[\sum_i \frac{m_i'}{\rho_i^* \gamma_i}\right] \ln\left(\frac{P}{P'}\right) + \left[\frac{1}{2!} \sum_i \frac{m_i'}{\rho_i^* \gamma_i{}^2}\right] \ln^2\left(\frac{P}{P'}\right) + \dots$$

$$\dots + \left[\frac{1}{n!} \sum_i \frac{m_i'}{\rho_i^* \gamma_i{}^n}\right] \ln^n\left(\frac{P}{P'}\right) \tag{66}$$

which results from a series expansion of the pressure term in the ullage volume conservation equation. The root of this equation (for n = 9) which lies closest to ln (P/P') = 0 is found using the Newton-Raphson iteration technique.

Gas Node Final Conditions

Heat transfer is assumed to be isobaric and pressure change isentropic. The enthalpy change due to heat transfer gave the intermediate gas node temperature from the specific enthalpy tables. The final temperature of each gas node after the pressure change is calculated from the isentropic relationship

$$T_{ii}' = T_i^* \left(\frac{P'}{P}\right)^{\frac{\gamma_i - 1}{\gamma_i}} \tag{67}$$

and the node specific enthalpies are found from the table. The final gas density is calculated from

$$\rho_i' = \frac{W_{H_2} P'}{Z_i' R T_i'} \tag{68}$$

and the gas node volume is

$$V'_i = \frac{m_i'}{\rho_i'} \tag{69}$$

The location of the gas node boundaries above the liquid surface is then determined according to the successive node volumes in the same manner described for the liquid nodes in the previous section.

Injectant Reaction Heating Correction

The necessary final condition for a time step loop calculation is that the sum of the gas node volumes exactly equal the available ullage volume from the tank top to the liquid surface. If the gas node final conditions calculated in the previous section do not satisfy this requirement, heat is added or removed from the mixed ullage node to obtain exact agreement. The final temperature must be

$$T_1' = \frac{W_{H_2} P' V_1'}{Z_1' R m_1'} \tag{70}$$

where V_1' is the volume to be filled by the first gas node. The final specific enthalpy from the tables is

$$H_1' = H\langle T_1' \rangle \tag{71}$$

and the corrected fluorine inflow rate is

$$\dot{w}_{F_2}' = \frac{\dot{q}'_{inj} - \frac{H_1' - H_1^*}{\Delta t}}{\Delta H_R} \tag{72}$$

where H_i^* is used to refer to the node specific enthalpy before correction. In the operating mode for which Equation (37) is used to determine $\dot{q}'_{inj}$, the required correction will be negligible. However, when Equation (38) is used for an estimated $\dot{q}'_{inj}$, the correction can be significant.

With the thermodynamic state of the gas nodes completely determined and the node boundaries located, the node thicknesses $(X_{i+1} - X_i)$ are then checked against the maximum and minimum limits and node splitting and combining are carried out as needed. The mixed ullage node is excepted from this node thickness regulation.

Physical Properties Data

Variable physical properties of the gaseous and liquid hydrogen and the wall and hardware materials are utilized throughout the program computations. These properties are generally specified as temperature dependent tables which are read by linear interpolation. The compressibility factor Z and ratio of specific heats γ for hydrogen are also a function of pressure (density) and are evaluated by equations which were derived from the Benedict, Webb, Rubin equation of state as modified by Strobridge (Reference 15).

Specific enthalpy tables are included for the gas, liquid, wall and hardware. Wall and hardware densities complete the specification of the structural materials. Stainless steel, aluminum and titanium properties are currently in use. The liquid density, vapor pressure and heat of vaporization tables are included for use in the interface calculations. Gas thermal conductivity, viscosity and specific heat tables are given for use in the heat transfer coefficient calculations. The specific heat table is generated internally from the gas specific enthalpy table.

A table of gas compressibility factors is also included as a function of both temperature and pressure. Linear interpolation in this table is not sufficiently accurate for use in the near-saturated region. The table value is used as an estimate to evaluate the gas density. The gas density and temperature are then used in the equation

$$
\begin{aligned}
Z(\rho, T) = \Bigg\{ & A_1 T\rho + A_1 A_2 T\rho^2 + A_3 \rho^2 + \rho^2 \left(\frac{A_4}{T} + \frac{A_5}{T^2} + \frac{A_6}{T^4} \right) \\
& + A_7 A_1 T \rho^3 + A_8 \rho^3 + A_9 T \rho^4 + e^{-A_{17}\rho^2} \left[\rho^3 \left(\frac{A_{10}}{T^2} + \frac{A_{11}}{T^3} + \frac{A_{12}}{T^4} \right) \right. \\
& \left. + \rho^5 \left(\frac{A_{13}}{T^2} + \frac{A_{14}}{T^3} + \frac{A_{15}}{T^4} \right) \right] + A_{16} \rho^6 \Bigg\} \frac{1}{\rho R T}
\end{aligned}
\tag{73}
$$

to give the final value of the compressibility factor. The ratio of specific heats

$$
\gamma(\rho, T) = \frac{C_p(\rho, T)}{C_v(\rho, T)} \tag{74}
$$

is evaluated using

$$
\begin{aligned}
C_v(\rho, T) = {} & B_1 + B_2 T + B_3 T^2 + B_4 T^3 + B_5 T^4 + B_6 T^5 \\
& - R - \left[\rho \left(\frac{2A_4}{T^2} + \frac{6A_5}{T^3} + \frac{20\ A_6}{T^5} \right) \right. \\
& + \frac{1}{2A_{17}} \left(\frac{6A_{10}}{T^3} + \frac{12A_{11}}{T^4} + \frac{20A_{12}}{T^5} \right) \left(1 - e^{-A_{17}\rho^2} \right) \\
& \left. + \frac{1}{2A_{17}^2} \left(\frac{6A_{13}}{T^3} + \frac{12A_{14}}{T^4} + \frac{20A_{15}}{T^5} \right) \left(1 - e^{-A_{17}} \left[1 + A_{17} \rho^2 \right] \right) \right]
\end{aligned}
\tag{75}
$$

and

$$C_p(\rho,T) = C_v(\rho,T) + \frac{T\left[\left(\frac{\partial P}{\partial T}\right)_\rho\right]^2}{\rho^2\left(\frac{\partial P}{\partial \rho}\right)_T} \tag{76}$$

where

$$\begin{aligned}\left(\frac{\partial P}{\partial T}\right)_\rho = {} & A_1\rho + A_1A_2\rho^2 - \rho^2\left(\frac{A_4}{T^2} + \frac{2A_5}{T^3} + \frac{4A_6}{T^5}\right) \\ & + A_7A_1\rho^3 + A_9\rho^4 - e^{-A_{17}\rho^2}\left[\rho^3\left(\frac{2A_{10}}{T^3} + \frac{3A_{11}}{T^4} + \frac{4A_{12}}{T^5}\right)\right. \\ & \left. + \rho^5\left(\frac{2A_{13}}{T^3} + \frac{3A_{14}}{T^4} + \frac{4A_{15}}{T^5}\right)\right]\end{aligned} \tag{77}$$

and

$$\begin{aligned}\left(\frac{\partial P}{\partial \rho}\right)_T = {} & A_1T + 2A_1A_2T\rho + 2A_3\rho + 2\rho\left(\frac{A_4}{T} + \frac{A_5}{T^2} + \frac{A_6}{T^4}\right) + 3A_7A_1T\rho^2 \\ & + 3A_8\rho^2 + 4A_9T\rho^3 - 2A_{17}\rho e^{-A_{17}\rho^2}\left[\rho^3\left(\frac{A_{10}}{T^2} + \frac{A_{11}}{T^3} + \frac{A_{12}}{T^4}\right)\right. \\ & \left. + \rho^5\left(\frac{A_{13}}{T^2} + \frac{A_{14}}{T^3} + \frac{A_{15}}{T^4}\right)\right] \\ & + e^{-A_{17}\rho^2}\left[3\rho^2\left(\frac{A_{10}}{T^2} + \frac{A_{11}}{T^3} + \frac{A_{12}}{T^4}\right) + 5\rho^4\left(\frac{A_{13}}{T^2} + \frac{A_{14}}{T^3} + \frac{A_{15}}{T^4}\right)\right] + 6A_{16}\rho^5\end{aligned} \tag{78}$$

The constants in these equations are given in Table I.

TABLE I

CONSTANTS FOR EQUATIONS (73) AND (75)

A_1	=	$0.8208199823 \times 10^{+2}$	A_{10}	=	$-0.1070380625 \times 10^{+11}$
A_2	=	$0.2062278898 \times 10^{+2}$	A_{11}	=	$0.1016369054 \times 10^{+13}$
A_3	=	$-0.1292792029 \times 10^{+6}$	A_{12}	=	$-0.1938431002 \times 10^{+14}$
A_4	=	$-0.7237230137 \times 10^{+7}$	A_{13}	=	$0.3857308627 \times 10^{+13}$
A_5	=	$0.1159242745 \times 10^{+9}$	A_{14}	=	$-0.6757463236 \times 10^{+15}$
A_6	=	$-0.1010879875 \times 10^{+11}$	A_{15}	=	$0.1462114653 \times 10^{+17}$
A_7	=	$0.3176293970 \times 10^{+3}$	A_{16}	=	$0.5254992259 \times 10^{+11}$
A_8	=	$0.2581305967 \times 10^{+7}$	A_{17}	=	$0.1800100800 \times 10^{+4}$
A_9	=	$0.2410669065 \times 10^{+6}$			

B_1	=	$0.4977816011 \times 10^{+1}$
B_2	=	$-0.3384077523 \times 10^{-2}$
B_3	=	$0.3521443738 \times 10^{-3}$
B_4	=	$-0.1435633178 \times 10^{-4}$
B_5	=	$0.2303247505 \times 10^{-6}$
B_6	=	$-0.1038316229 \times 10^{-8}$

Program Output

Two types of output data format are generated by the program. A summary table is printed which gives the values of selected parameters at each time step in the solution; these include the mixed ullage zone temperature, fluorine flowrate, tank pressure and several others. An example of this output is given in Figure 8. The second output format is a complete description of the thermodynamic state of the system, giving the temperature profiles of the ullage gas, liquid, tank wall and internal hardware. The volume, density and mass of the nodes are also printed for the gas and liquid. This output format is also shown in Figure 8. These printouts always occur for the initial and final conditions and may be printed out at any time during the solution as specified by input.

TEST NO. 2, 50 C/C ULLAGE

TIME (SEC)	PRESSURE (PSIA)	TEMP. (GR)	WT. F2 (LB)	EVAP. (LB)	F2 FLOW (LB/SEC)	XMIX (FT)	XMIX/XIF	UL. VOL. (FT3)	XLPLN (FT)	PF2 (PSIA)	UJO (FT/SEC)
0.00	15.00	235.50	0.00000	0.00000	0.00000	0.000	0.000	533.233	0.000	305.0	0.0
.10	15.57	62.77	.00644	0.00000	.06435	4.212	.371	533.233	0.000	304.8	63.9
.20	16.14	63.30	.01287	0.00000	.06432	4.682	.412	533.233	0.000	304.7	63.0
.30	16.42	65.29	.01930	0.00000	.06429	4.707	.415	533.233	0.000	304.5	62.2
.40	16.69	67.28	.02572	0.00000	.06426	4.737	.417	533.233	0.000	304.4	61.5
.50	16.96	69.29	.03215	0.00000	.06423	4.763	.420	533.233	0.000	304.2	60.7
.60	17.23	71.34	.03856	0.00000	.06419	4.791	.422	533.233	0.000	304.1	60.0
.70	17.51	73.41	.04498	0.00000	.06416	4.818	.424	533.233	0.000	303.9	59.2
.80	17.78	75.49	.05139	0.00000	.06413	4.844	.427	533.233	0.000	303.8	58.5
.90	18.05	77.58	.05780	0.00000	.06410	4.870	.429	533.233	0.000	303.6	57.8
1.00	18.32	79.67	.06421	0.00000	.06406	4.899	.432	533.233	0.000	303.5	57.2
1.10	18.58	81.76	.07061	0.00000	.06403	4.923	.434	533.233	0.000	303.3	56.6
1.20	18.85	83.87	.07701	0.00000	.06400	4.951	.436	533.233	0.000	303.2	55.9
1.30	19.11	85.97	.08341	0.00000	.06397	4.973	.438	533.233	0.000	303.0	55.3
1.40	19.37	88.06	.08980	0.00000	.06394	5.000	.440	533.233	0.000	302.9	54.8
1.50	19.63	90.19	.09619	0.00000	.06390	5.025	.443	533.233	0.000	302.7	54.2
1.60	19.89	92.31	.10258	0.00000	.06387	5.050	.445	533.233	0.000	302.6	53.6
1.70	20.15	94.44	.10896	0.00000	.06384	5.069	.447	533.233	0.000	302.4	53.1
1.80	20.40	96.56	.11535	0.00000	.06381	5.093	.449	533.233	0.000	302.3	52.6
1.90	20.66	98.69	.12172	0.00000	.06378	5.120	.451	533.233	0.000	302.1	52.1
2.00	20.91	100.81	.12810	0.00000	.06374	5.142	.453	533.233	0.000	301.9	51.6
3.00	23.34	122.03	.19181	0.00000	.06371	5.164	.455	533.233	0.000	300.4	51.1
4.00	25.55	142.36	.25520	0.00000	.06339	5.370	.473	533.233	0.000	298.9	47.0
5.00	27.50	160.50	.31827	0.00000	.06307	5.546	.489	533.233	0.000	297.4	43.7
6.00	29.17	176.77	.38103	0.00000	.06276	5.686	.501	533.233	0.000	295.9	41.3
7.00	30.86	191.67	.44347	0.00000	.06244	5.801	.511	533.233	0.000	294.5	39.4
8.00	32.31	205.50	.50560	0.00000	.06213	5.896	.519	533.233	0.000	293.0	37.9
9.00	33.26	218.47	.56742	0.00000	.06182	5.981	.527	533.233	0.000	291.5	36.6
10.00	34.39	230.46	.62893	0.00000	.06151	6.056	.533	533.233	0.000	290.1	35.4
11.00	35.47	242.01	.69013	0.00000	.06120	6.118	.539	533.233	0.000	288.6	34.4
12.00	36.46	252.80	.75102	0.00000	.06090	6.177	.544	533.233	0.000	287.2	33.5
13.00	37.42	263.32	.81162	0.00000	.06059	6.231	.549	533.233	0.000	285.7	32.7
14.00	38.33	273.43	.87191	0.00000	.06029	6.277	.553	533.233	0.000	284.3	32.0
15.00	39.20	283.17	.93189	0.00000	.05999	6.325	.557	533.233	0.000	282.9	31.3
16.00	40.04	292.67	.99158	0.00000	.05969	6.365	.561	533.233	0.000	281.5	30.7
17.00	40.85	301.89	1.05098	0.00000	.05939	6.403	.564	533.233	0.000	280.1	30.1
18.00	41.53	310.90	1.11007	0.00000	.05910	6.445	.568	533.233	0.000	278.7	29.6
19.00	42.40	320.22	1.16888	0.00000	.05880	6.269	.552	533.233	0.000	277.3	29.1
20.00	43.14	329.74	1.22739	0.00000	.05851	6.103	.538	533.233	0.000	275.9	28.6
20.21	43.30	331.73	1.23986	0.00000	.05822	6.137	.541	533.233	0.000	275.6	28.1
20.31	43.27	331.41	1.23986	0.00000	-.00000	6.142	.541	533.233	0.000	275.6	28.0
21.31	42.97	328.14	1.23986	0.00000	-.00000	6.141	.541	533.233	0.000	275.6	28.0
22.31	42.66	325.06	1.23986	0.00000	-.00000	6.127	.540	533.233	0.000	275.6	28.2
23.31	42.40	322.14	1.23986	0.00000	-.00000	6.113	.539	533.233	0.000	275.6	28.3
24.31	42.14	319.36	1.23986	0.00000	-.00000	6.106	.538	533.233	0.000	275.6	28.4
25.31	41.90	316.74	1.23986	0.00000	-.00000	6.093	.537	533.233	0.000	275.6	28.6
26.31	41.67	314.23	1.23986	0.00000	-.00000	6.086	.536	533.233	0.000	275.6	28.7
27.31	41.45	311.84	1.23986	0.00000	-.00000	6.073	.535	533.233	0.000	275.6	28.8
27.99	41.31	310.30	1.23986	0.00000	-.00000	6.067	.534	533.233	0.000	275.6	28.9
28.99	42.19	321.39	1.29802	0.00000	.05816	6.057	.534	533.233	0.000	274.3	29.0

Figure 8. H819 Program Output - Time Step Data

TEST NO. 2, 50 0/0 ULLAGE

ELAPSED TIME	=	197.2142	ULLAGE FRACTION	=	.819	PRESSURANT MASS	=	0.00000	CONDENSED MASS	=	0.0000
TIME STEP DURATION	=	2.0000	LIQUID REMOVED	=	296.810	VENTED MASS	=	0.00000	EVAPORATED MASS	=	0.0000
TIME STEP COUNT	=	176	LIQUID REMAINING	=	183.708	TOTAL ULLAGE MASS	=	34.58315	CONDENSATION RATE	=	0.000000
GAS NODES	=	30	OUTFLOW RATE	=	2.860	INFLOW RATE	=	0.00000	HEAT TO INTERFACE	=	0.000
LIQUID NODES	=	1	PRESSURE (PSIA)	=	34.694	ULLAGE VOLUME	=	830.04294	HEAT TO LIQUID	=	0.000

X	T	HW	RHO	VOL	MASS
0.000000	721.2890	8.6842	.0090379	412.96990	3.73237
8.931827	563.8292	6.1262	.0115619	26.31291	.30423
9.461463	466.3039	6.2776	.0133306	12.27127	.16358
9.708370	442.6969	6.6531	.0147031	12.37565	.18196
9.957377	390.3031	6.4203	.0164237	10.36507	.17023
10.165930	364.9576	6.7928	.0178342	10.35782	.18472
10.374337	336.0052	6.5916	.0192566	10.93414	.21055
10.594340	306.7936	6.9556	.0210795	9.95800	.20991
10.794702	280.7757	6.6930	.0226998	10.81311	.24546
11.012269	252.4367	6.9222	.0257949	20.20669	.52123
11.418843	214.2398	6.8767	.0304119	18.47526	.56187
11.790578	182.3055	7.0493	.0357779	16.79074	.60074
12.128420	142.5271	5.8223	.0459088	20.56129	.94394
12.542128	101.6617	4.8651	.0650203	18.04029	1.17298
12.905112	79.1808	4.1094	.0848409	18.72376	1.58854
13.281647	67.7817	2.7969	.1008012	13.04637	1.31509
13.544350	65.6984	3.1666	.1044563	12.86257	1.34358
13.803154	64.6814	2.3665	.1063464	12.88321	1.37008
14.062373	63.6508	3.0534	.1082795	12.90876	1.39775
14.322107	62.6149	2.0036	.1104242	12.91996	1.42668
14.582066	61.6468	2.8743	.1124536	12.95601	1.45695
14.842756	60.4565	3.2866	.1150761	12.93653	1.48869
15.103043	59.5467	2.4868	.1171475	12.99228	1.52201
15.364457	58.6715	3.1785	.1192325	13.03389	1.55406
15.626708	57.6950	2.4123	.1211515	13.07939	1.58459
15.889875	57.0100	3.1599	.1234230	13.09750	1.61653
16.153406	56.1059	3.5920	.1258425	13.11161	1.65002
16.417225	55.1560	2.8227	.1284999	13.11443	1.68520
16.681097	54.1068	3.9197	.1315837	13.08855	1.72224
16.944448	51.2157	2.6681	.1410758	18.83637	2.65736
17.323449	36.0000		4.4400000	183.70790	815.66307

	X	TW	TH
1	.216600	474.7846	532.8842
2	.649800	473.0182	532.4681
3	1.083000	472.6616	532.3089
4	1.516200	479.7965	532.3668
5	1.949400	479.7870	532.3650
6	2.382600	479.7833	532.3645
7	2.815800	479.7811	532.3636
8	3.249000	479.7802	532.3635
9	3.682200	479.7803	532.3635
10	4.115400	479.7803	532.3635
11	4.548600	479.7804	532.3635
12	4.981800	479.7775	532.3628
13	5.415000	479.7552	532.3549
14	5.848200	479.6585	532.3113
15	6.281400	476.4790	531.6455
16	6.714600	467.8150	524.5084
17	7.147800	457.9040	516.9537
18	7.581000	442.6952	503.6291
19	8.014200	416.6609	477.6425
20	8.447400	372.2730	429.0355
21	8.880600	303.3436	345.8680
22	9.313800	263.4753	297.8161
23	9.747000	226.7126	253.8372
24	10.180200	198.5693	220.5792
25	10.613400	175.2692	191.9782
26	11.046600	153.2363	167.5102
27	11.479800	132.2694	143.7357
28	11.913000	111.7651	119.7355
29	12.346200	92.7176	97.6970
30	12.779400	76.1830	78.6753
31	13.212600	67.9289	69.1435
32	13.645800	64.4054	64.8884
33	14.079000	62.6420	63.1258
34	14.512200	60.9199	61.3992
35	14.945400	59.2611	59.7288
36	15.378600	57.7185	58.2226
37	15.811800	56.1740	56.6797
38	16.245000	54.7144	55.0842
39	16.678200	52.9534	53.6021
40	17.111400	47.1367	49.3948

Figure 8. (Cont'd) H819 Program Output - Node Thermodynamic Data

COMPUTER ANALYSIS OF EXPERIMENTAL RESULTS

GF_2 Usage and Ullage Gas Temperature

Two of the most important parameters in the prediction of MTI performance are GF_2 usage and the temperature of the ullage gas (which directly affects tank wall heating). These parameters are directly related to the degree of ullage mixing. With good ullage mixing, the ullage gas temperature is lower, heat transfer to the wall is lower, and thus, GF_2 requirements are minimized. The reverse is also true: less mixing, higher temperatures, and greater GF_2 usage. In the initial prediction of large tank performance during the tests the ullage was assumed to be completely (100 percent) mixed to the depth of the predicted injectant penetration. By 100 percent mixed, or with the ullage mixing fraction $f_m = 1.0$, it is meant that the ullage is at a uniform temperature (for heat transfer purposes) to the depth of penetration of the injectant jet. With $f_m < 1.0$, the injectant jet penetration itself is not directly affected, but the mixed depth is less, and thus the temperature in the mixed region is higher.

Evaluation of the temperature profile data from the experimental program indicated that for many tests the temperatures were not uniform over a substantial depth, but tended to stratify with time, with the upper dome region getting much warmer than the lower part of the ullage. On the other hand, data from some tests (7, 12 and 13) showed very deep uniform temperature profiles.

For the initial data correlation attempts, the factors in the jet penetration equations were manipulated in an attempt to reduce the penetration depth (and thus mixing depth) to the degree necessary for temperature profile correlation. This could not be accomplished by any rational means. Therefore, it was assumed, for heat transfer computation purposes, that the ullage mixing depth was some fraction of the jet penetration depth. The effect of ullage mixing fraction on ullage temperature is shown in figure 9 for test 2. The predicted uniform

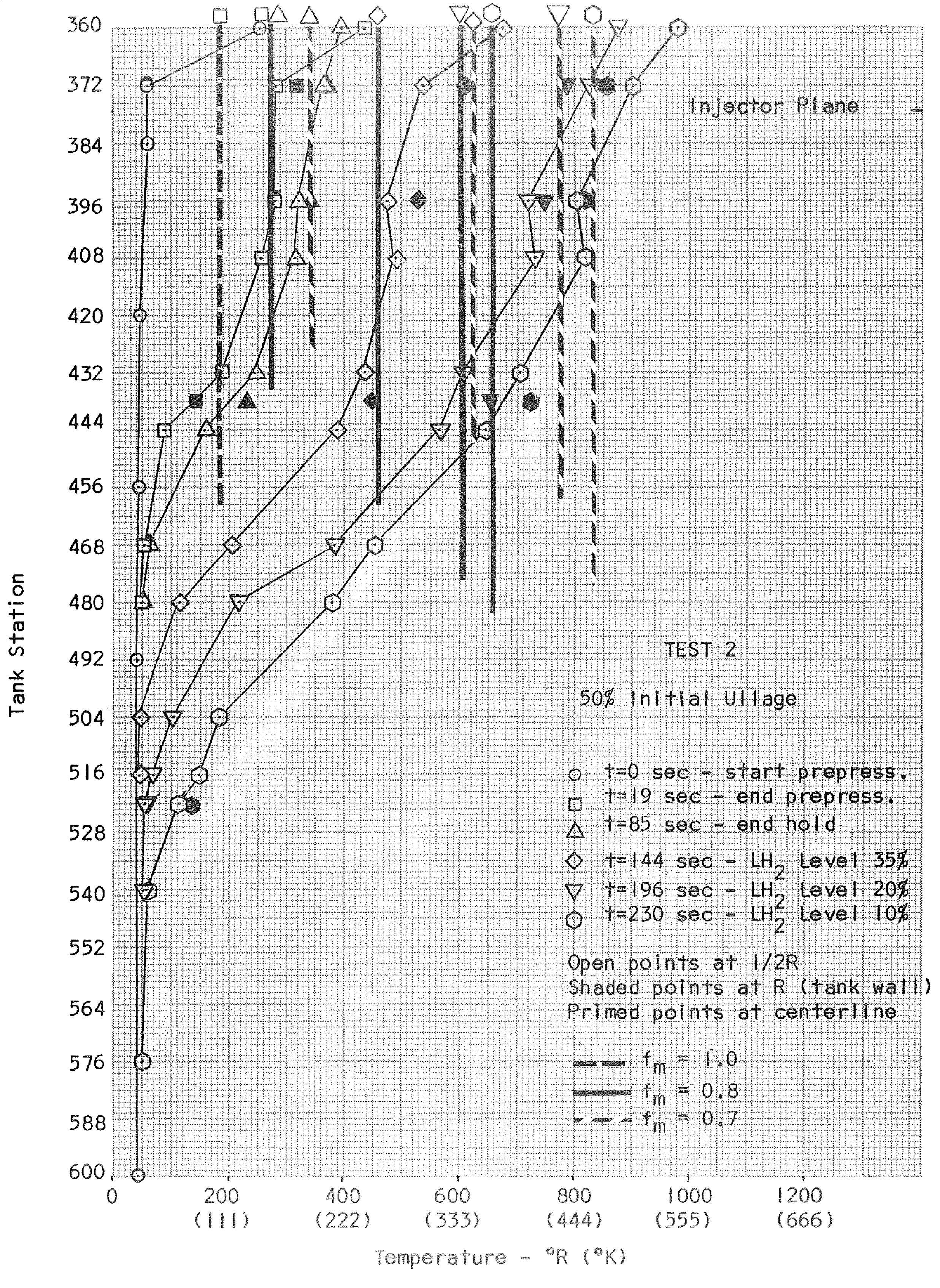

Figure 9. Temperature Correlation for Test 2

temperature and depth for different values of f_m are superimposed on the experimental temperature profile. Only the mixed zone profile is shown; the lower ullage drops to LH_2 temperature at the interface. With $f_m = 1.0$, the ullage temperatures, are too cold, the jet penetration (mixing) depth too deep, and the GF_2 usage too low (.88 lbs (.40 K_g) compared to actual 1.29 lbs (.585 K_g) GF_2). On the other hand $f_m = 0.8$ at the start of the test and dropping to $f_m = 0.7$ at the end of the test gives rather good temperature correlation. To evaluate this effect further, only the large ullage cases were examined, assuming no LH_2 interface heat or mass transfer. In general, it was found that using a constant $f_m = 0.8$ gave acceptable correlation, as shown in figures 10 to 14. In test 3 (figure 10) and other tests, the actual temperature rises somewhat following prepressurization, but the predicted temperatures do not change. This is thought to be due partly to sensor lag during prepressurization, and partly to the fact that the program immediately ceases all mixing and heat transfer when the injector closes following prepressurization, when in fact these processes would continue for a finite time, therefore the actual control system would be required to add more energy than predicted. The predicted GF_2 usage for the appropriate f_m assumption is shown in Table 2 and agrees with the actual GF_2 usage within 15 percent for the large ullage tests except for test 13. The temperature profiles for test 13 are poorly correlated by $f_m = 0.8$, but are well correlated by $f_m = 1.0$ as shown in figure 15. Also, the predicted GF_2 usage for test 13, assuming $f_m = 1.0$ is much closer to the experimental value Apparently, the critical parameters in this test behaved in a manner such that the 100 percent ullage mixing assumption is correct. Examination of the test conditions revealed that this was a low pressure test (~24 psia (166 x 10^3 N/M^2)) with a very short prepressurization time (~3 sec) and that very little energy was required to maintain pressure. The injector valve was open only 10 percent to 17 percent of the time. For the other large ullage tests, except test 14, the prepressurization took much longer, and the injector valve was open a significantly larger percent of the time.

This behavior suggested that the injectant flow for fairly long prepressurization times sets up a circulating flow field in the tank, with reverse (upward) flow near the wall which decreased random turbulent mixing and led to ullage temperature stratification. This made the ullage gas behave as if it was correctly described by an ullage mixing fraction of less than 1.0. This does not

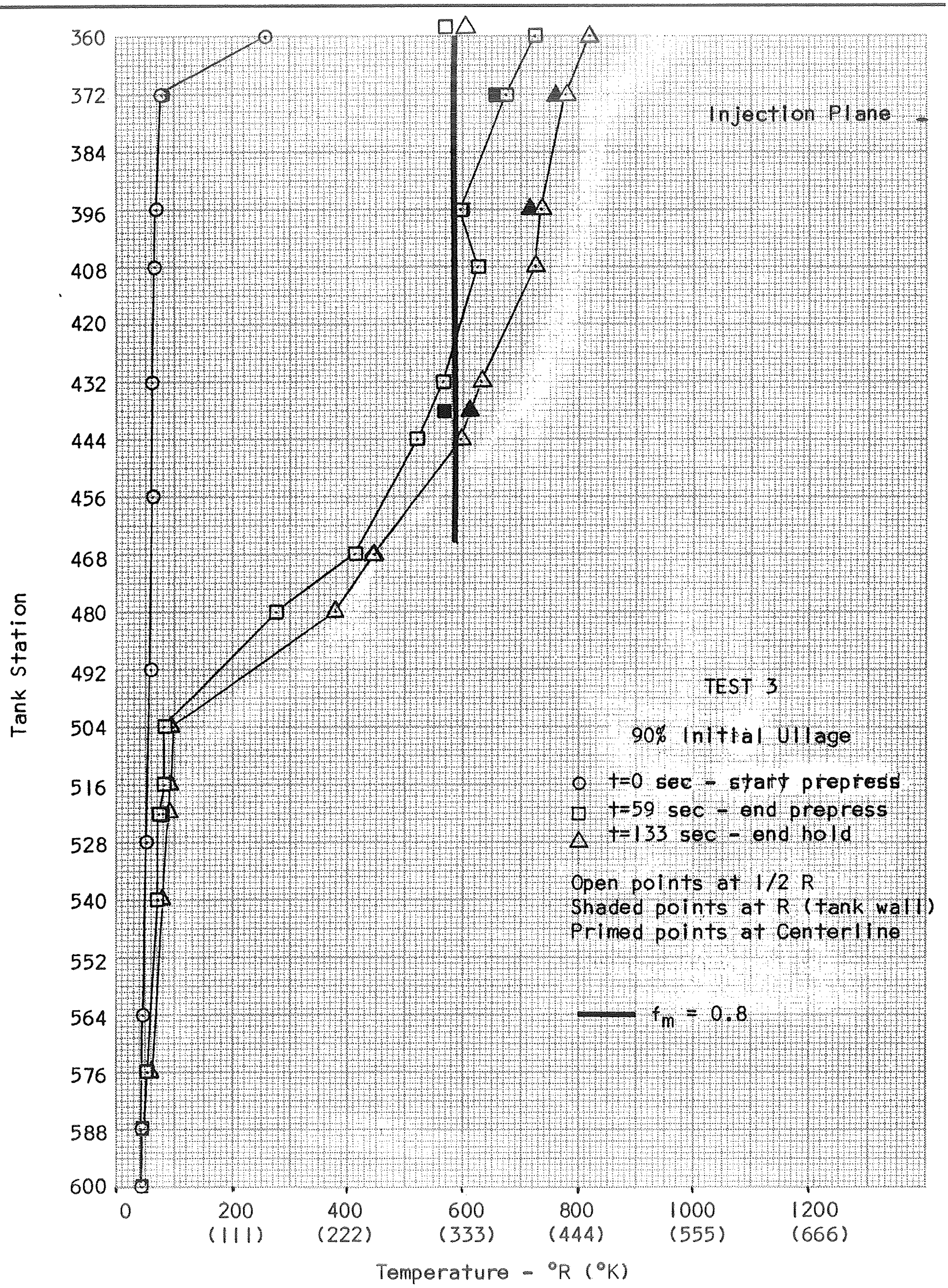

Figure 10. Temperature Correlation for Test 3

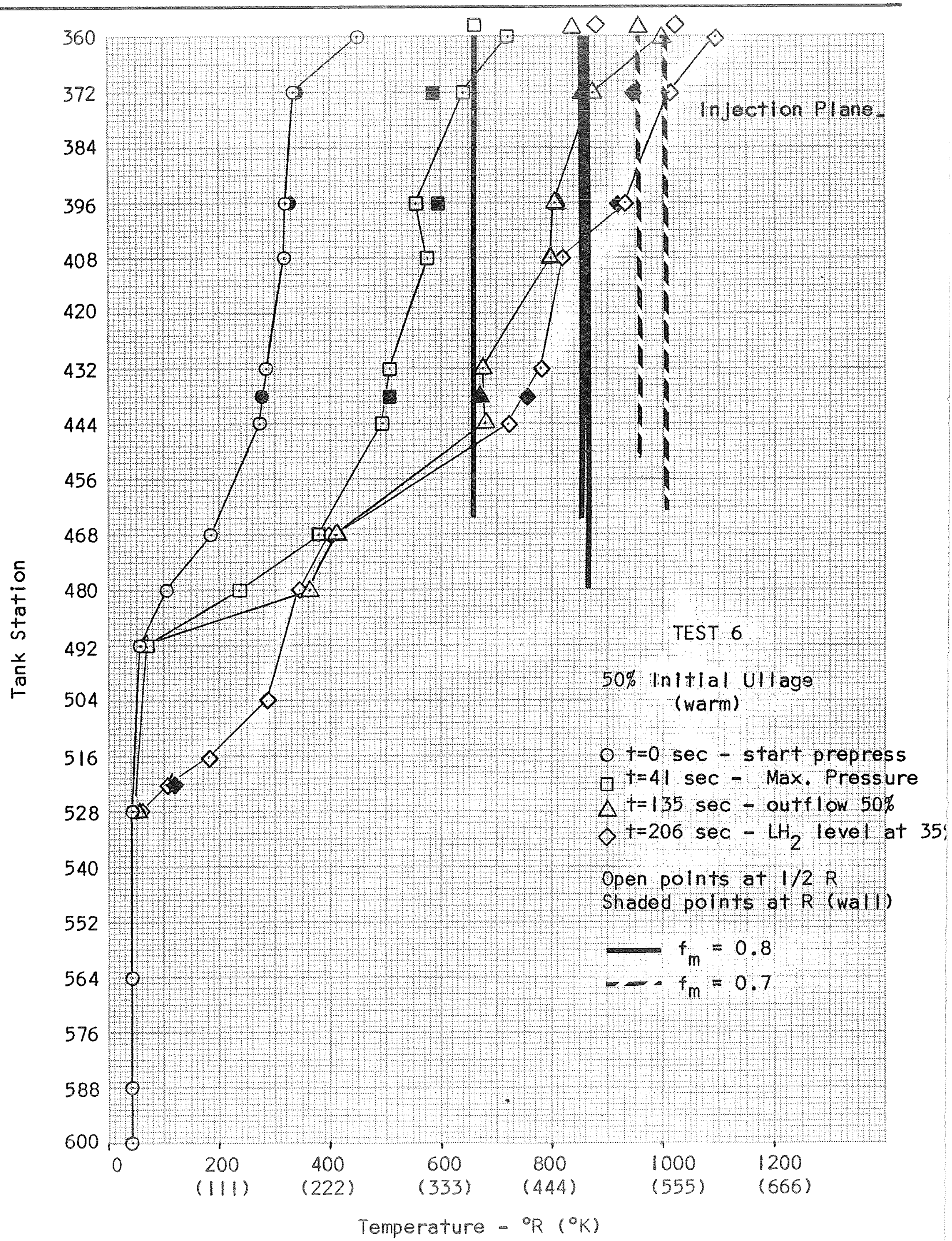

Figure 11. Temperature Correlation for Test 6

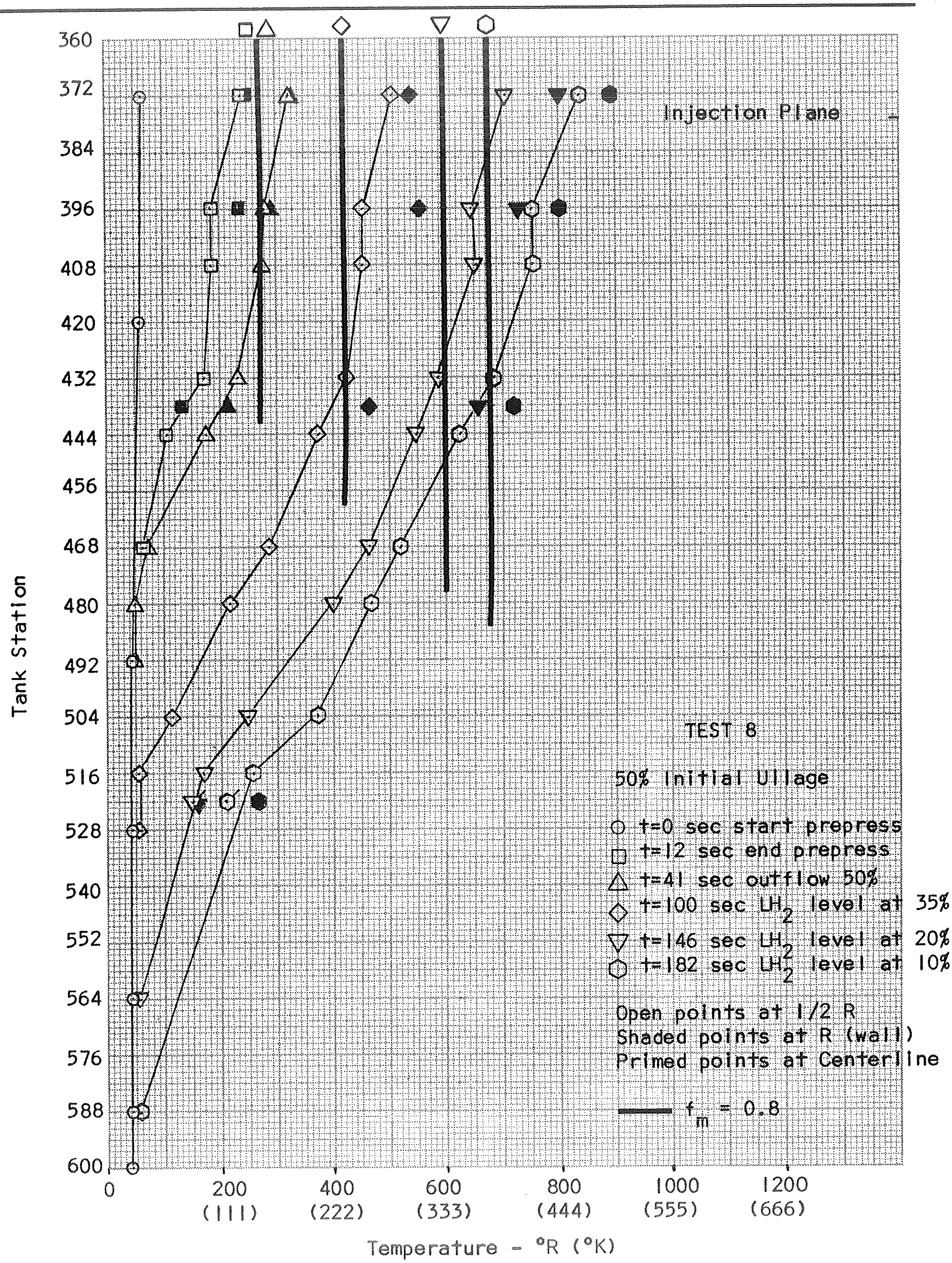

Figure 12. Temperature Correlation for Test 8

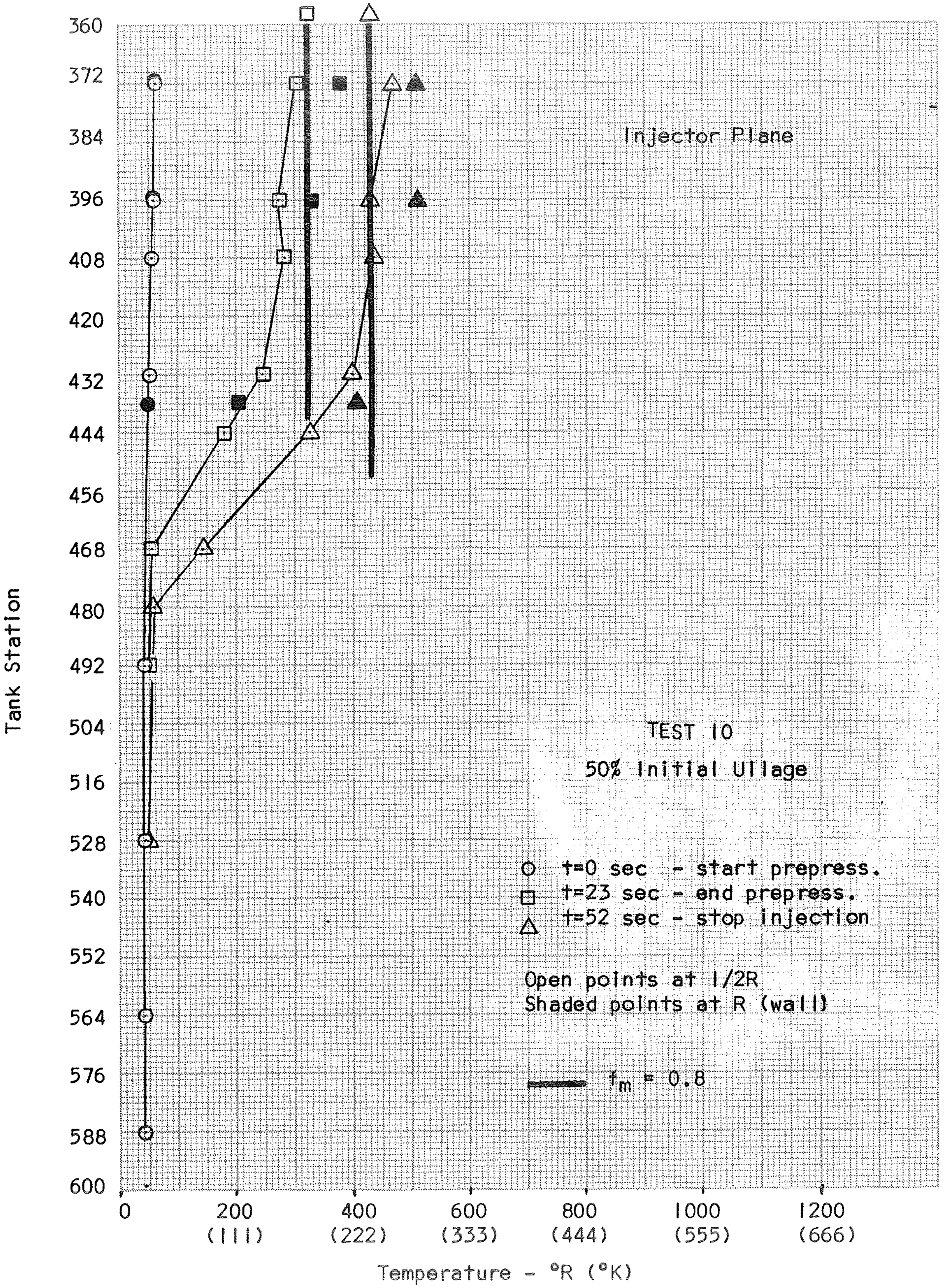

Figure 13. Temperature Correlation for Test 10

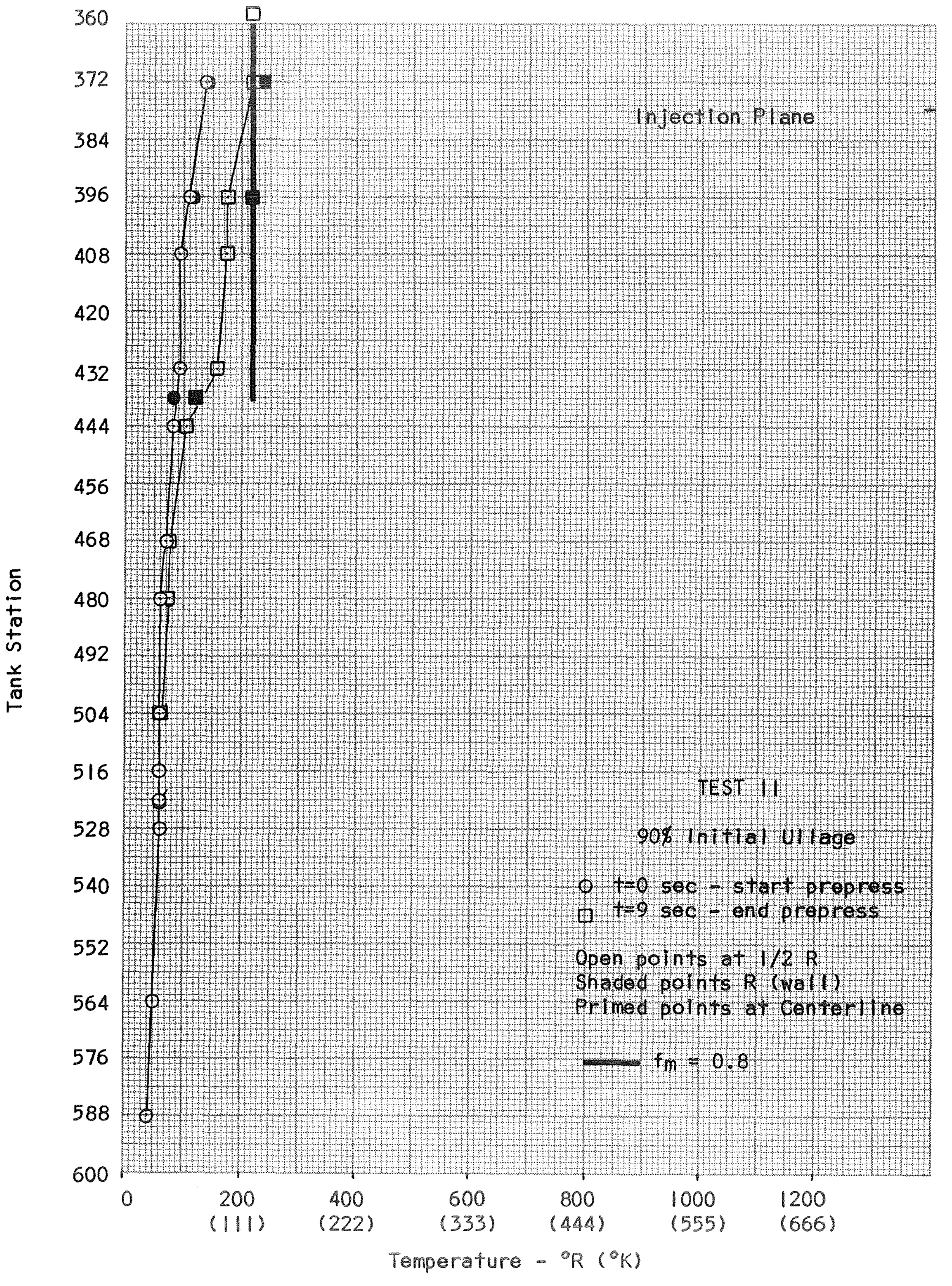

Figure 14. Temperature Correlation for Test 11

TABLE 2

COMPARISON OF PREDICTED AND ACTUAL GF_2 USAGE

Test	Time (sec)	Actual GF_2 Weight (lb)	(Kg)	Predicted GF_2 Weight (lb)	(Kg)	Error (%)
1	12.7	.912	.414	.955	.433	+ 5.1
2	19.2	1.290	.585	1.102	.500	-14.6
	85	1.730	.785	1.480	.672	-14.5
	144	3.630	1.648	3.127	1.420	-13.9
	196	5.630	2.556	5.380	2.444	- 4.5
	230	6.680	3.033	6.800	3.087	+ 1.8
3	59	3.52	1.597	3.78	1.717	+ 7.4
	133	5.42	2.460	5.44	2.468	+ 0.4
4	4	.190	.086	.196	.089	+ 3.2
	23	.416	.189	.196	.089	--
	65	1.200	.545	.976	.443	-18.6
	109	2.610	1.184	2.480	1.127	- 5.0
5	3.2	.236	.107	.273	.124	+15.7
	75	.417	.189	.273	.124	--
	130	.974	.442	.919	.417	- 5.6
	164	1.842	.836	2.138	.970	+15.9
	215	4.165	1.890	4.484	2.037	+ 7.6
6	41	2.125	.965	2.05	.931	- 3.5
	135	5.105	2.317	5.469	2.484	+ 7.1
	206	6.73	3.054	7.218	3.278	+ 7.2
		γ = 1.15				
7	1	.078	.035			
	8	.078	.035			
	134	.300	.136			
	235	.601	.273			
	418	1.580	.717			
	582	2.940	1.334			
	780	6.340	2.885			
	902	8.960	4.070			
		γ = 1.0				
7	1	.078	.035	.045	.020	-42.0
	8	.078	.035	.045	.020	-42.0
	134	.300	.136	.437	.198	+45.6
	235	.687	.312	.879	.399	+28.0
	418	.805	.820	1.686	.765	- 6.6
	582	3.350	1.521	3.19	1.448	- 4.8
	780	7.050	3.200	6.29	2.854	-10.8
	902	9.800	4.450	9.954	4.513	+ 1.5

TABLE 2 (Continued)

Test	Time (sec)	Actual GF_2 Weight (lb)	(Kg)	Predicted GF_2 Weight (lb)	(Kg)	Error (%)
8	12.5	.902	.409	1.02	.463	+13.1
	41	1.138	.516	1.243	.565	+ 9.2
	100	3.030	1.375	2.85	1.293	- 5.9
	146	5.050	2.292	5.21	2.366	+ 3.2
	182	6.32	2.867	6.76	3.068	+ 7.0
9	4	.260	.118	--	--	--
10	23	1.27	.576	1.32	.600	+ 3.9
	52	2.42	1.098	2.48	1.127	+ 2.5
11	9	.317	.144	.319	.145	+ 0.6
		$\gamma = 1.15$				
12	.8	.062	.028			
	4	.062	.028			
	112	.284	.129			
	200	.544	.247			
	287	1.030	.468			
		$\gamma = 1.0$				
12	.8	.062	.028	.036	.016	-42.0
	4	.062	.028	.036	.016	-42.0
	112	.284	.129	.378	.172	+34.0
	200	.570	.259	.868	.394	+52.0
	287	1.185	.538	1.493	.679	+26.0
				$f_m = 0.8$		
13	3	.287	.130	.296	.134	+ 3.1
	120	1.149	.521	1.847	.839	+60.7
				$f_m = 1.0$		
13	3	.287	.130	.249	.113	-13.2
	120	1.149	.521	1.320	.600	+14.9
14	3	.188	.085	.160	.073	-14.9
	146	.549	.249	.530	.241	- 3.5
	266	1.595	.724	1.531	.695	- 4.0
	334	3.100	1.407	2.785	1.265	-10.5
15	25	1.215	.551	1.26	.572	+ 3.7
	30	1.37	.622	1.41	.640	+ 2.9
	98	3.65	1.657	4.00	1.816	+9.6
16	4	.252	.114	.134	.061	-47.0
	56	.985	.447	1.121	.509	+13.8
	115	3.150	1.430	3.395	1.540	+ 7.8
	169	4.730	2.147	5.383	2.445	+11.7
17	70	1.735	.788	1.967	.893	+13.4

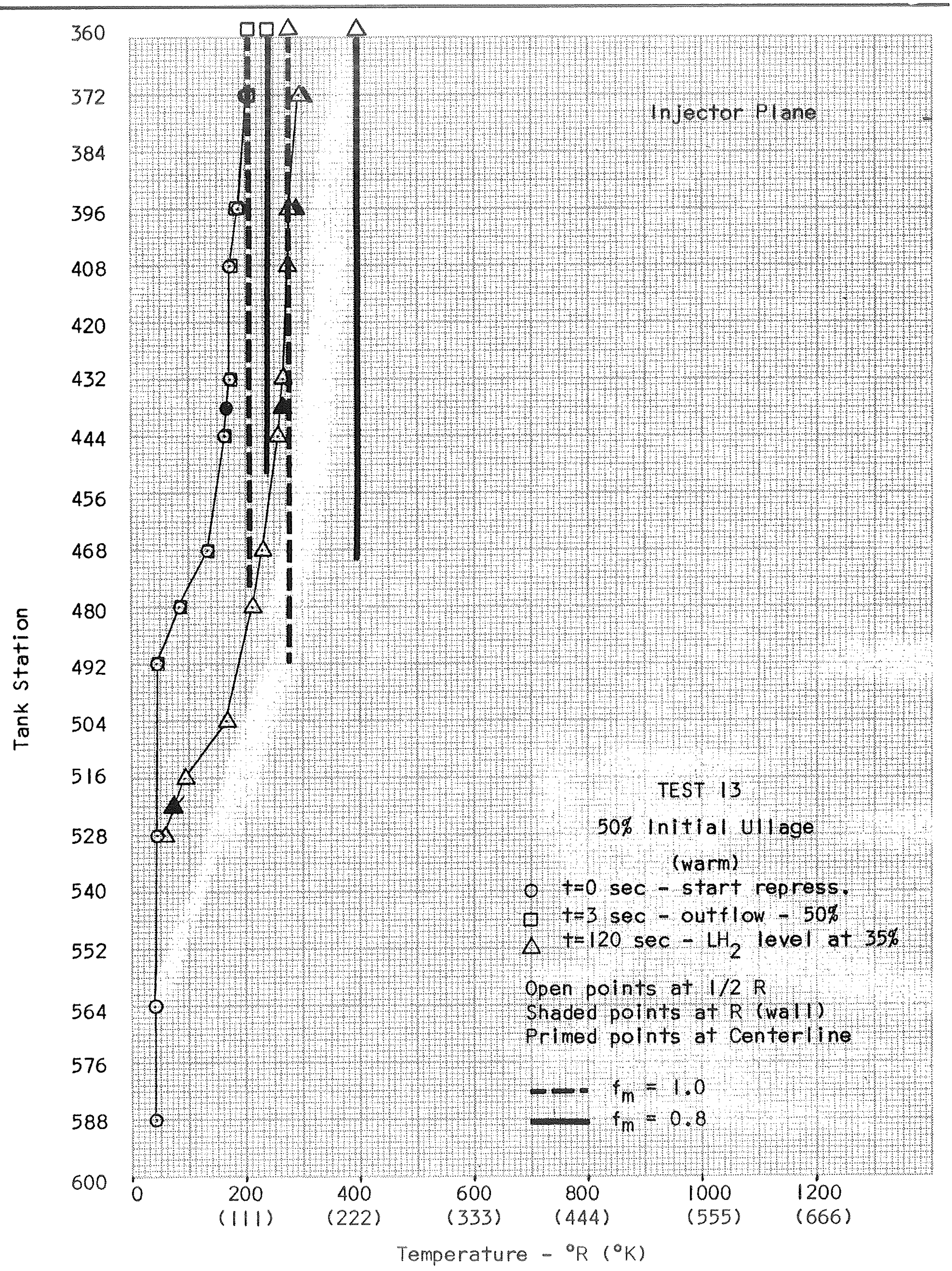

Figure 15. Temperature Correlation for Test 13

mean that this circulation reduced the injectant jet penetration by the fraction f_m, but only that it resulted in stratification of the ullage, so that for heat transfer purposes the ullage behaved as if it were less mixed (warmer). Apparently, for test 13, the circulating flow field never got started or maintained because of the short prepressurization time and small injector on-time fraction. It was initially hoped that a criterion could be established to predict the onset of this circulation so that for a particular case, one could predict whether the ullage would behave as if 80 percent mixed or 100 percent mixed. Examination of the data from test 14 showed that this was not possible. Test 14 also had a prepressurization time of 3 seconds and an injector on-time fraction even smaller initially than test 13, and yet test 14 behaved as if it were 80 percent mixed (or even 75 percent mixed, as shown in figure 16). Clearly, the circulating flow field (if real) was established in test 14. The only other difference between tests 13 and 14, was that the initial ullage condition for test 13 was warmer than for test 14. Perhaps an initially warm ullage tends to resist establishment of the circulating flow field.

It appears that the proposed flow field is generally present, and that under some combination of ullage parameters it may be possible to avoid or suppress it; however, a rational flow field onset criterion cannot be formulated from a single data point. It is equally apparent that when the injector valve is open for substantial time periods, the ullage behaves as if it were 80 percent to 70 percent mixed (e.g., see figure 11 for test 6 where the injector valve was open continuously). Most of the GF_2 usage occurs when the injector valve is open for substantial periods, and therefore, accurate GF_2 usage prediction is most important for this regime. Because of this, using $f_m = 0.8$ as standard for all computations gives accurate GF_2 usage predictions for most cases (see Table 2) and is conservative for cases where 100 percent ullage mixing might occur.

For the small ullage cases, prepressurization is also rapid, and the injector-on time fraction could be small initially; but, in these cases, LH_2 interface heat and mass transfer are occurring which may obscure the effects of ullage mixing. Actually, for the high pressure tests (~43 psia (296 x 10^3 N/M^2)), the injector-on time fraction quickly gets quite large (especially

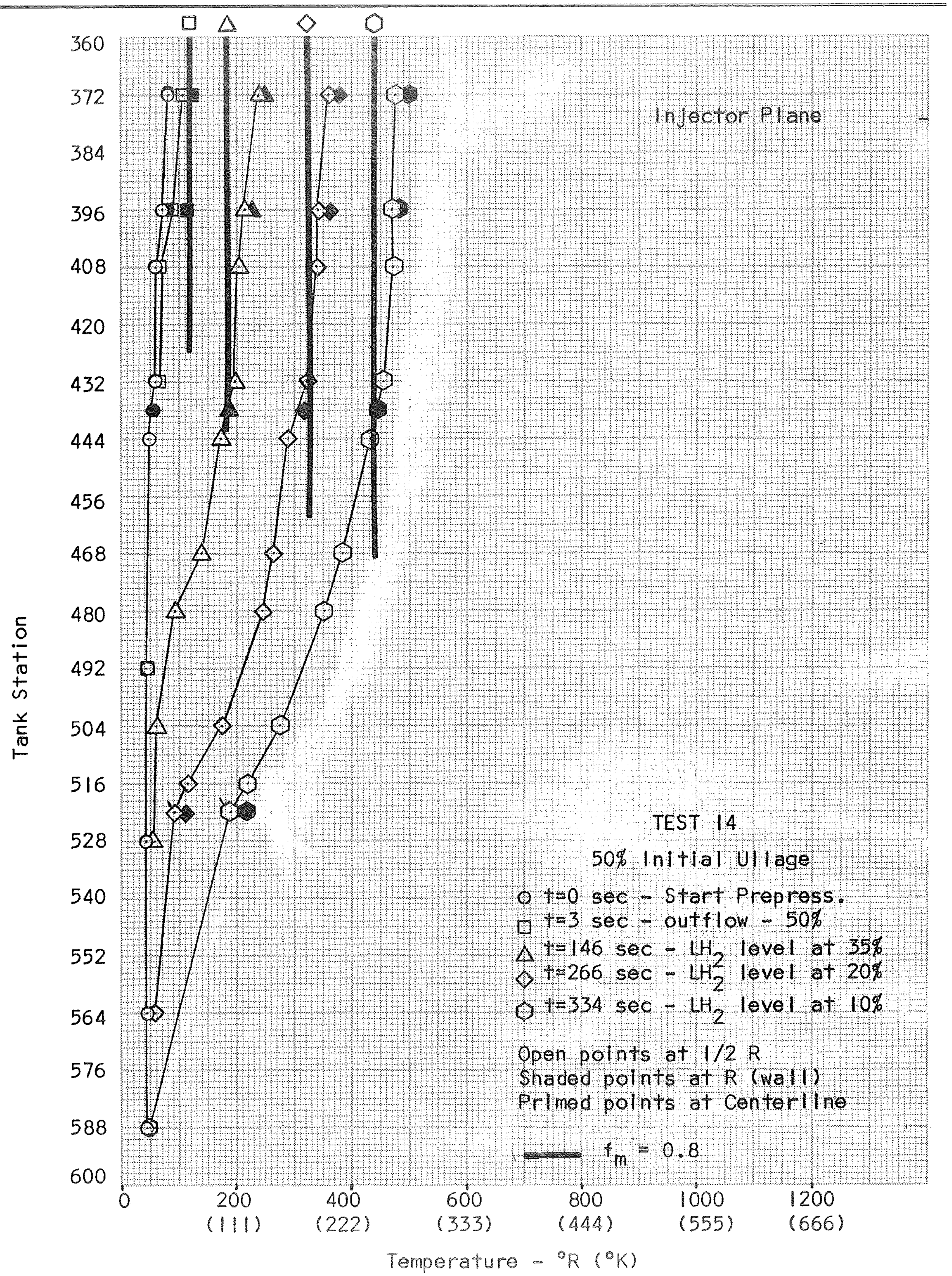

Figure 16. Temperature Correlation for Test 14

with high LH_2 outflow rates). Therefore, $f_m = 0.8$ was assumed in the ullage, and the LH_2 interface heat and mass transfer was analyzed. The form of the interface heat transfer equation based on analysis of LH_2 tank pressurization data from Reference 9 was

$$\dot{q}_g = K\, X_L^{\,2} \tag{79}$$

where X_L was the depth of LH_2 penetration by the pressurant jet. The data from Reference 9 were correlated by assuming K was constant; however, this assumption gave poor results with the MTI data and led to difficulties with situations where the heat transferred to the interface was greater than the total equivalent heat injected into the tank. It was found that using $K = .6\, \dot{q}_c$ (where $\dot{q}_c$ was the equivalent heat input rate from injection), heat losses to the bulk liquid equal to 20 percent of the $\dot{q}_g$, and $f_m = 0.8$ gave excellent temperature correlation for tests 4 and 5 as shown in figures 17 and 18, and accurately predicted the GF_2 usage (see Table 2). The LH_2 evaporation predicted with these assumptions agreed well with data from the ullage mass calculations described below in the section on mass and enthalpy balances.

For tests 7 and 12, the prepressurization time is very short, the injector on-time fraction is very small, and the temperature profiles indicate deep jet penetration and uniform temperatures. Therefore, as one might expect, the assumption of $f_m = 0.8$ gives poor temperature correlation and high GF_2 usage predictions. However, the assumption of $f_m = 1.0$ also gives only fair temperature correlation; the predicted temperatures are somewhat high and the evaporation is quite low. The mass balances (described below) indicated that test 7 should evaporate about 6 lbs (2.7 Kg) of LH_2 and test 12, about 5 lbs (2.3 Kg). With the assumptions of $K = .6\, \dot{q}_c$ and $f_m = 1.0$, only half this quantity of LH_2 was evaporated.

Tests 7 and 12 are at low pressure, are quite long in duration, and have a surface layer of saturated LH_2 caused by external heat leak. With this saturated layer, the heat transfer to the interface would cause only evaporation, with no losses to bulk liquid heating. The interface heat transfer would not necessarily depend on liquid penetration depth, because of the very short injector on-times which would mean very transient LH_2 penetration. It

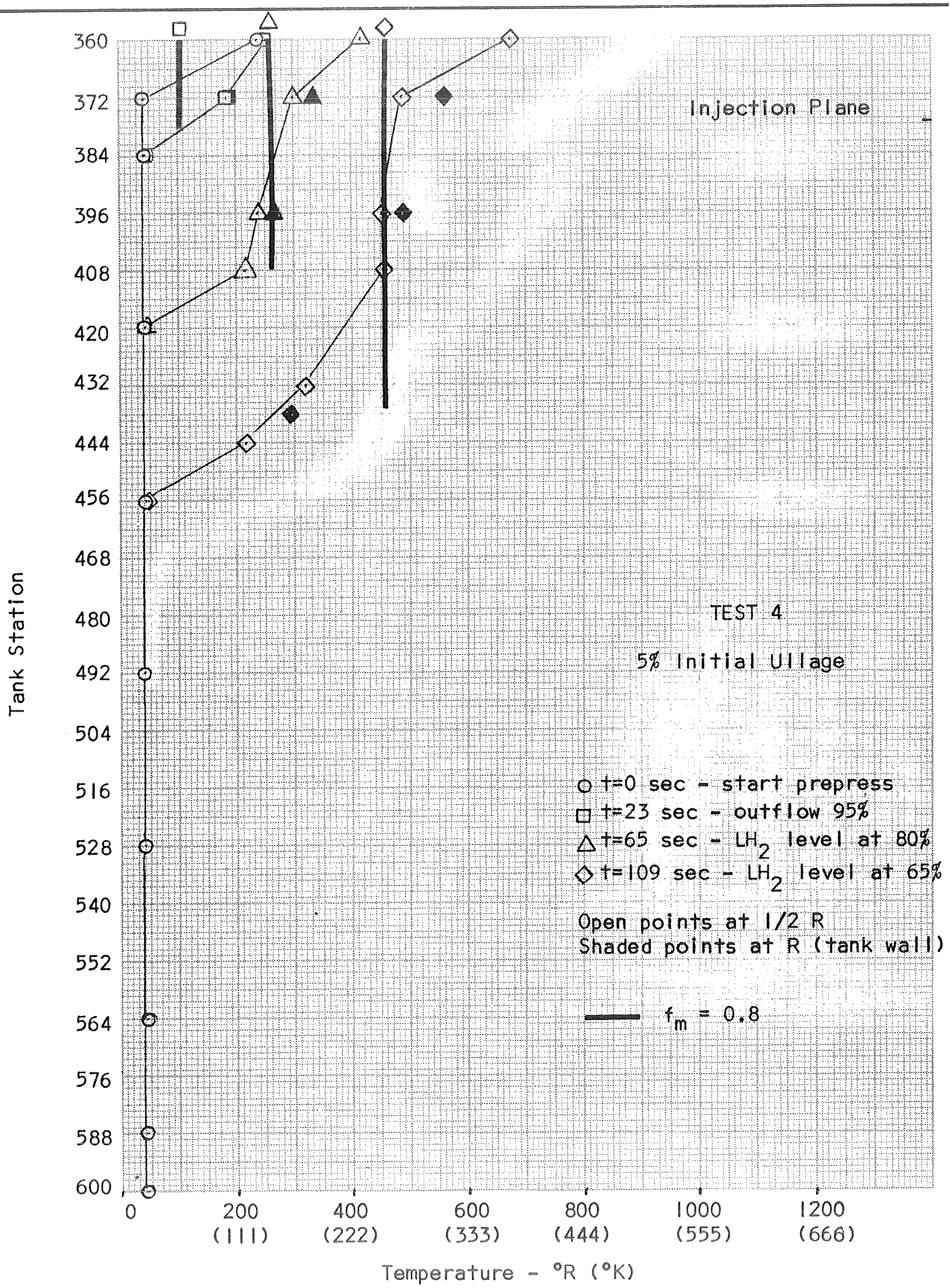

Figure 17. Temperature Correlation for Test 4

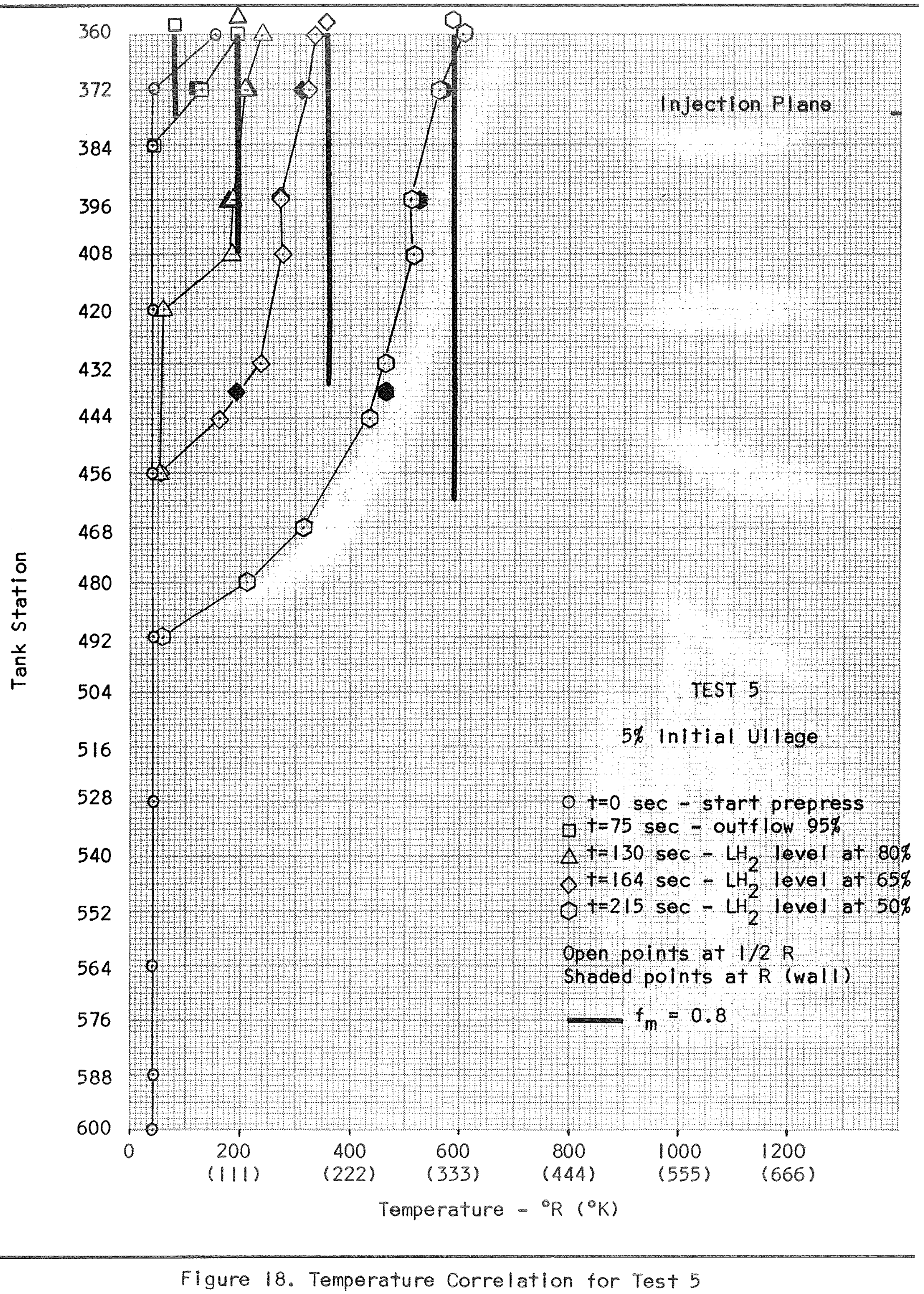

Figure 18. Temperature Correlation for Test 5

was more likely that evaporation would depend simply on the available energy in the ullage; thus, simply as a fraction of $\dot{q}_c$. It was found that assuming

$$f_m = 0.9 \tag{80}$$

and

$$\dot{q}_g = .25\ \dot{q}_c \tag{81}$$

with no LH_2 bulk losses gave a much better temperature correlation and GF_2 usage and evaporation prediction, as shown in figures 19 and 20, and Table 2. In tests 7 and 12, it was thought that because of low GF_2 usage and long test times, the GF_2 expansion in the storage cylinder may have been near-isothermal rather than polytropic (see discussion in section on Experiment Results). Table 2 supports this contention for tests 7 and 12. Even with this assumption, the agreement for test 12 is poor. The transient nature of the GF_2 flow in test 12 may account for this deviation.

The diffuser injector tests (15 to 17) were evaluated with the same factors as the straight-pipe injector tests. It was found that $f_m = 0.8$, which was generally appropriate for the straight pipe tests, gave very high temperatures for the diffuser tests. On the other hand, $f_m = 1.0$ gave excellent correlations as shown in figures 21 to 23. This change in f_m is attributed to the spreading of the diffuser flow field, which would interact more extensively with the ullage gas and promote more effective mixing. The GF_2 usage was predicted reasonably well with this assumption as shown in Table 2.

The correlation for the 5 percent ullage case (test 16) is shown in figure 22. The predicted temperatures are somewhat high, but the agreement is still quite good. It is probable that the interface equation predicts too little evaporation for the diffuser, which would account for the higher temperatures. The predicted GF_2 usage in Table 2 is also somewhat high, except for prepressurization, where the calculated lower evaporation and liquid losses result in more rapid and more efficient prepressurization.

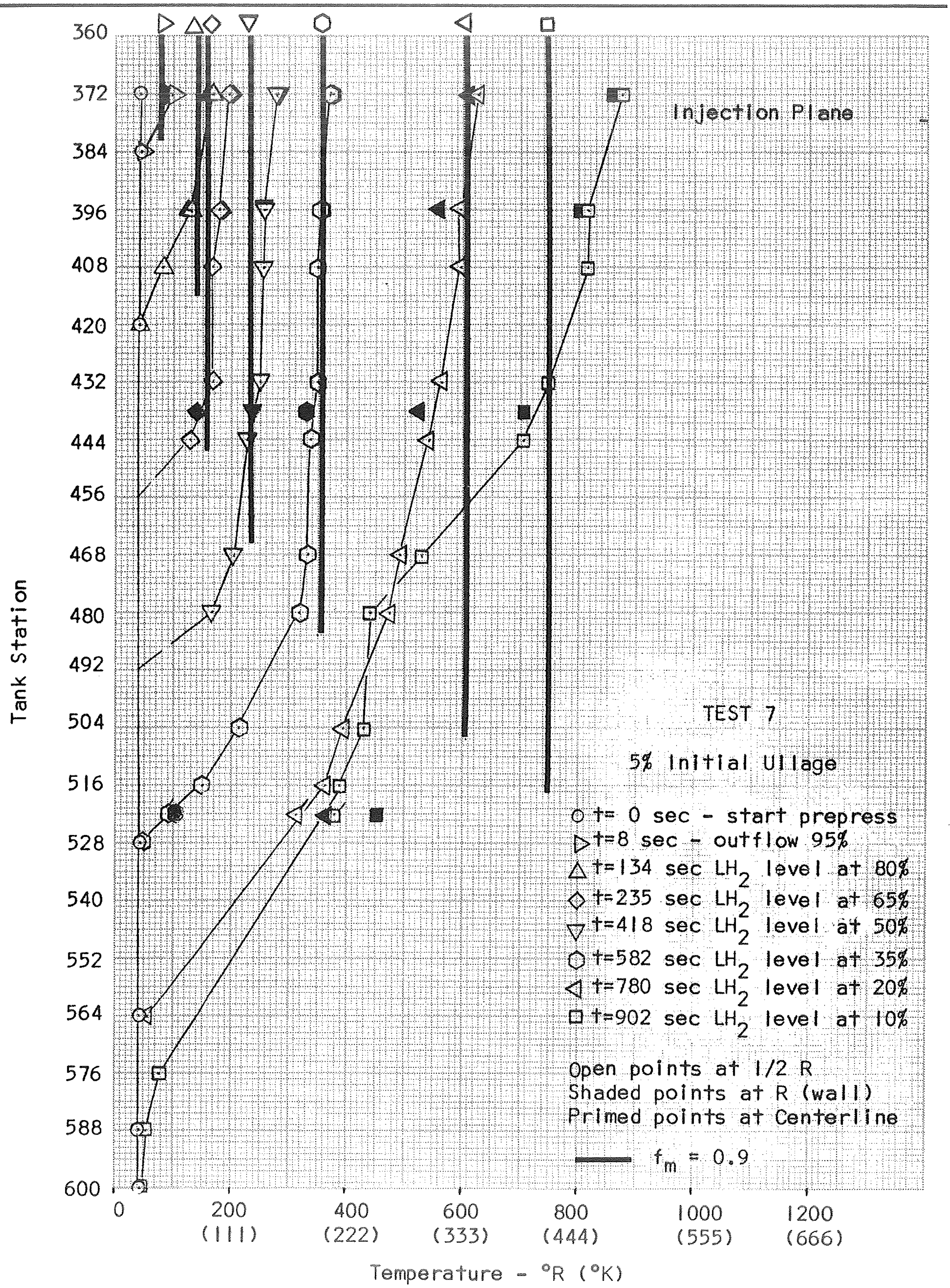

Figure 19. Temperature Correlation for Test 7

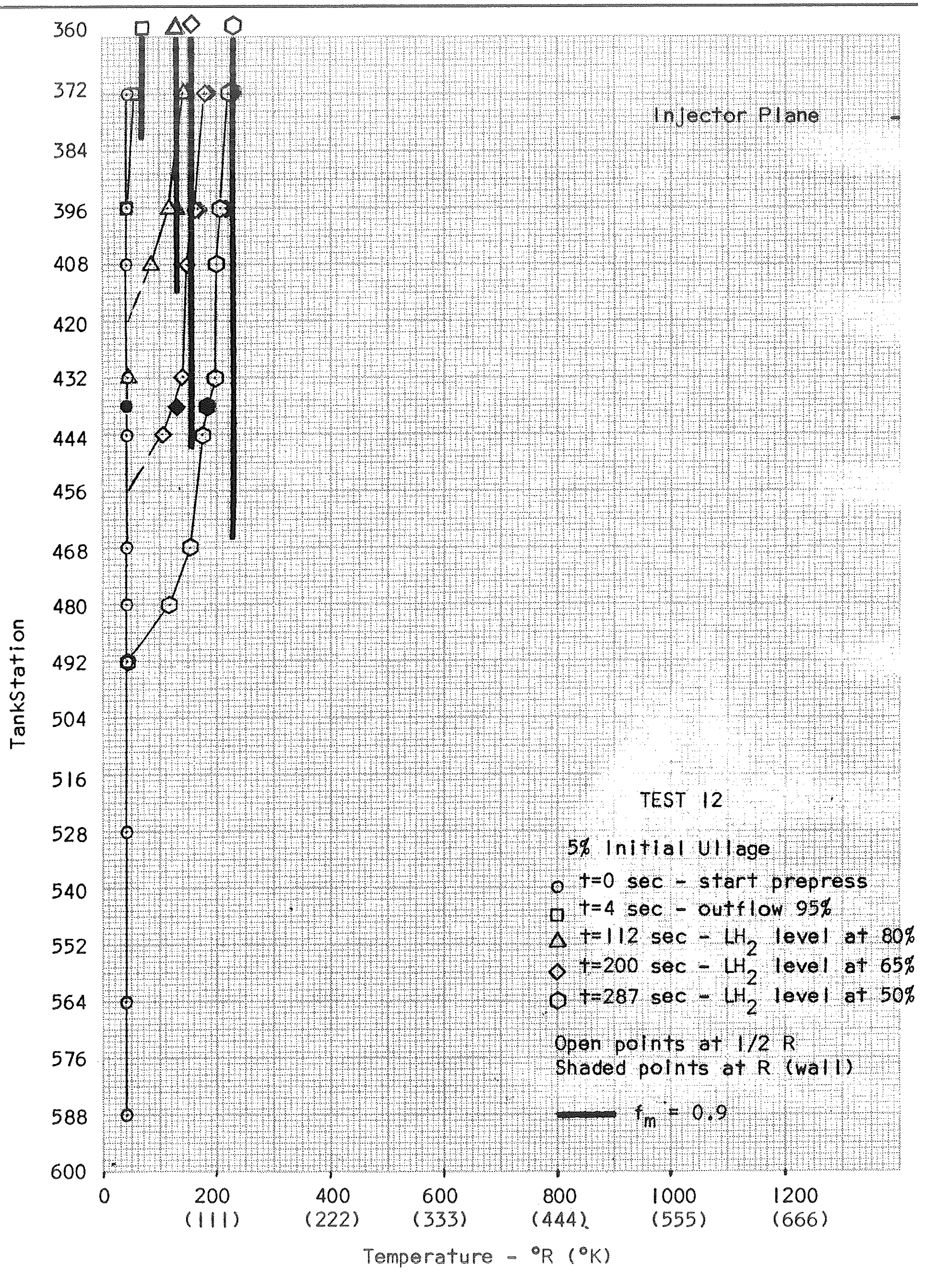

Figure 20. Temperature Correlation for Test 12

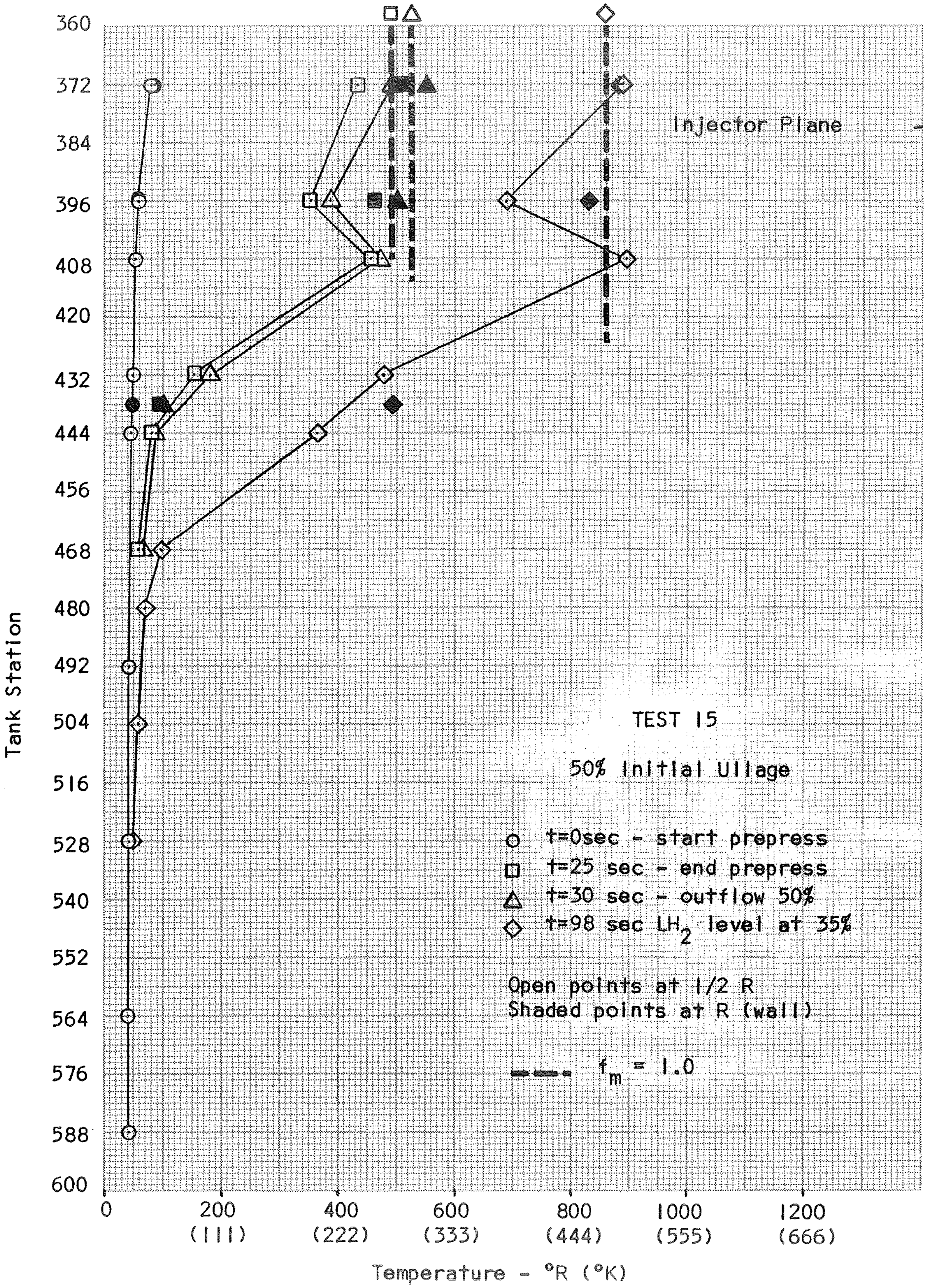

Figure 21. Temperature Correlation for Test 15

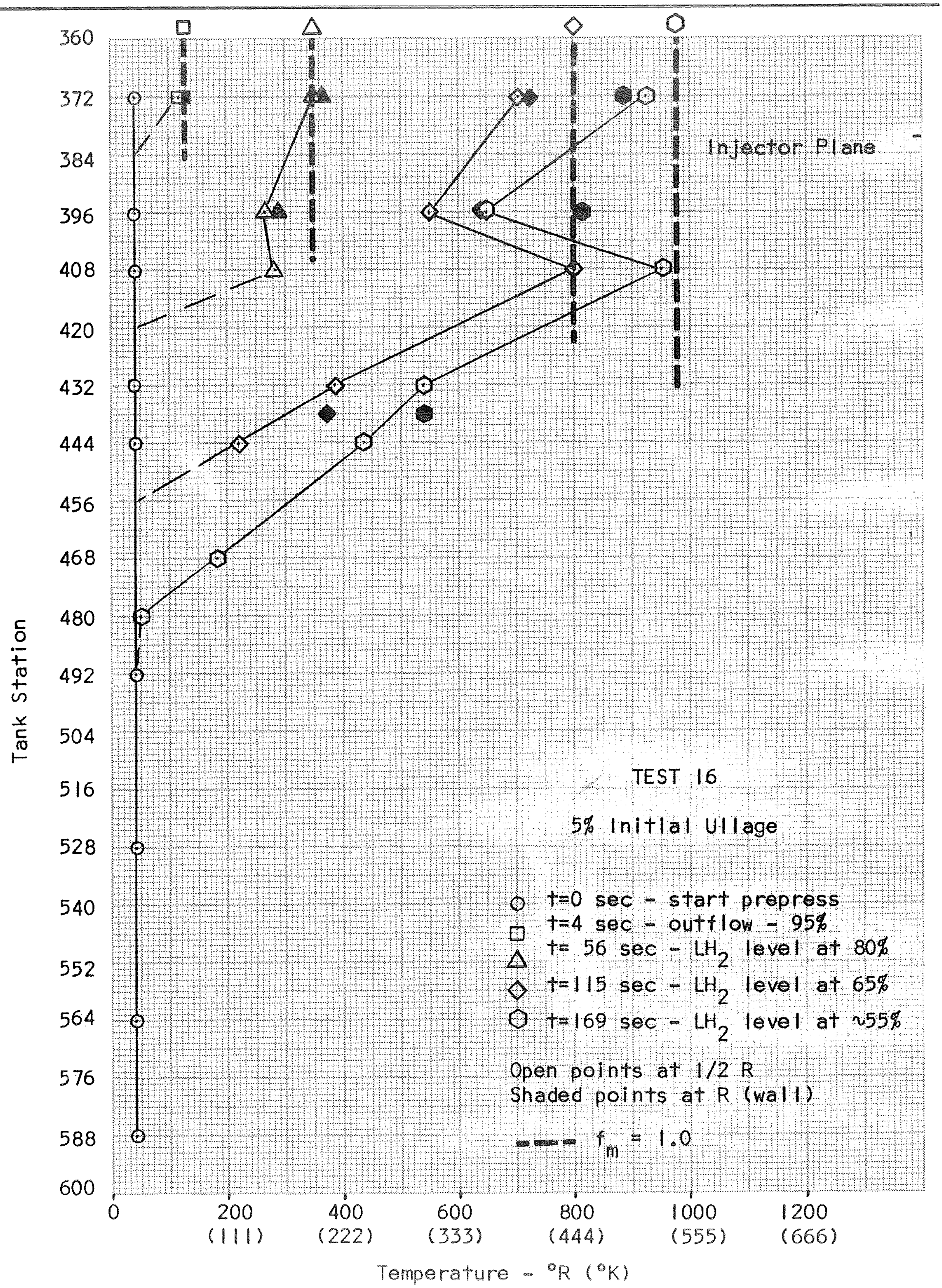

Figure 22. Temperature Correlation for Test 16

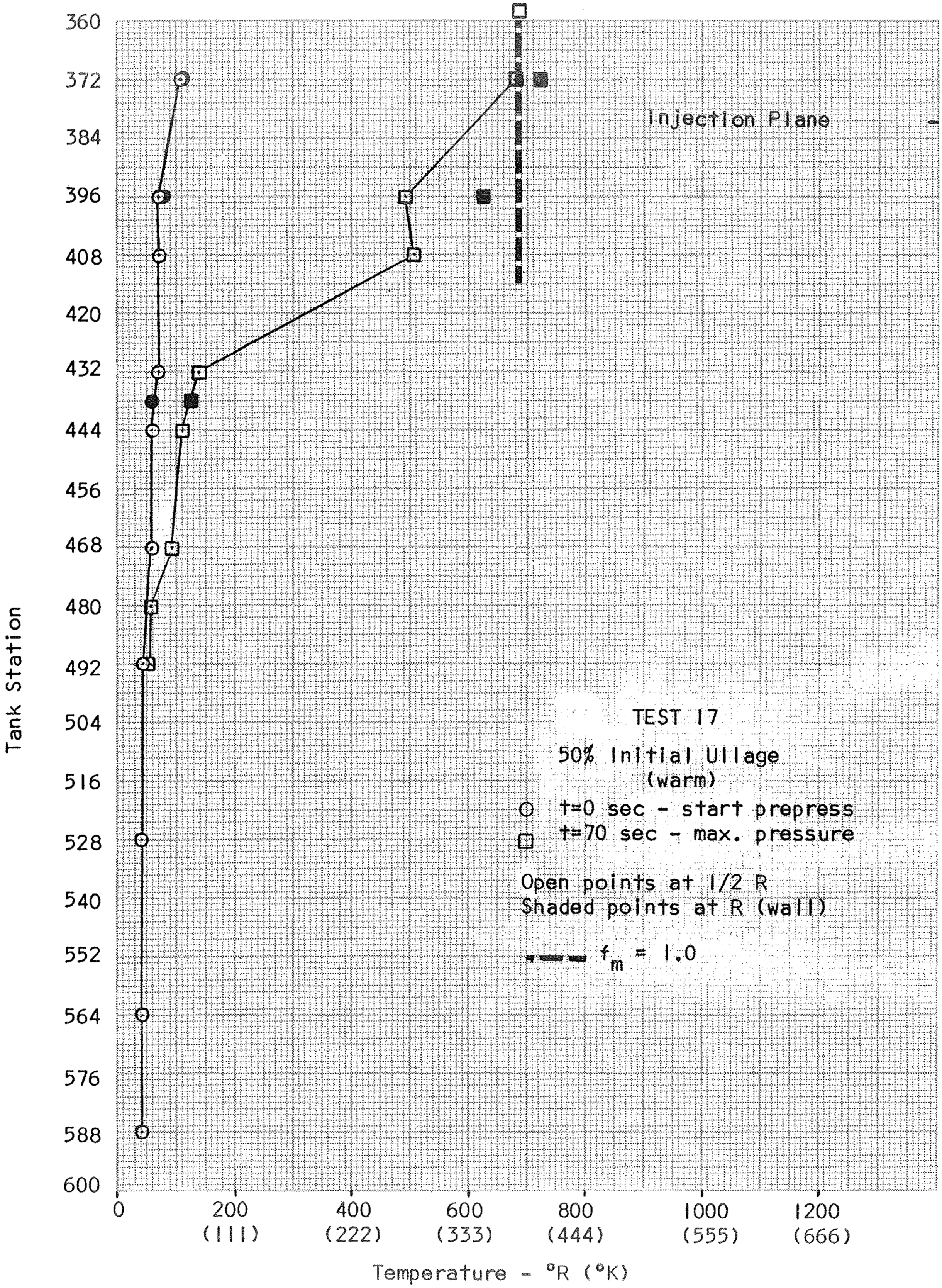

Figure 23. Temperature Correlation for Test 17

To summarize the correlation results:

1. Straight-pipe with large ullage:

   $f_m = 0.8$ gave accurate or conservative results although some runs were better correlated by $f_m = 1.0$

2. Straight-pipe with small ullage with interface heat transfer:

   $f_m = 0.8$; $\dot{q}_g = .6\ \dot{q}_c\ X_L^2$ and $\dot{q}_L = .2\ \dot{q}_g$ gives good correlation except that runs 7 and 12 were better correlated with $f_m = 0.9$; $\dot{q}_g = .25\ \dot{q}_c$; $\dot{q}_L = 0$

3. Diffuser tests were well correlated by

$$f_m = 1.0;\ \dot{q}_g = .6\ \dot{q}_c\ X_L^{\ 2};\ \dot{q}_L = .2\ \dot{q}_g \qquad (82)$$

The ability of the analysis to accurately predict MTI pressurization performance for different injectors over a wide range of operating conditions is an indication of the soundness of the fundamental assumptions of one-dimensionality, jet penetration and ullage mixing. The application of the analytical method to predict MTI pressurization performance and behavior for LH_2 - fueled space vehicles is discussed in the section on Space Vehicle Performance Predictions.

Ullage Gas Mass and Tank Enthalpy Balance

An ullage mass balance and ullage gas and tank wall enthalpy balance was computed for each test. The ullage mass was calculated from the measured pressure and local temperature conditions measured at the sensor locations; the temperature was assumed to vary linearly between the measured points. When conditions in the ullage changed slowly, the temperature sensors were able to respond adequately, and the mass balance gave reasonable results. However, when the ullage temperatures changed rapidly, as during large ullage prepressurization, the response lag of the platinum temperature sensors gave erroneous results for the mass balance. Under these conditions, the ullage was actually warmer than the sensors were recording, so that the computed mass increased by a couple of pounds. However, once conditions settled down to less rapid change, the computed mass generally returned to within 10 percent of original values. The results confirmed that LH_2 evaporation and ullage mass addition did not occur with large ullages, which agrees with the previous assumption.

The mass balances for the small ullage cases gave better results because of slower changes in temperature. These are shown in Table 3 and compared with the predicted evaporation.

Test 7 has slowly changing, well-mixed ullage conditions and gives excellent mass computations: evaporation occurs up to a time of 235 seconds, (which is when the computed liquid penetration stops) and is constant after that time. At a time of 902 seconds the computed mass jumped over 2 pounds (.91 Kg) because of the temperature reversal anomaly at Station 480. The computed evaporation data for tests 4, 5, 7, and 12 agree reasonably well with the mass balance (see Table 3).

The enthalpy balances were also rather imprecise because of temperature sensor lag and ullage nonuniformity. Typical results are shown in Figures 24 to 26 for initial ullage volumes of 5, 50 and 90 percent. The distribution of injected energy to ullage, tank, and liquid is shown. The errors could easily be due to inaccuracy in the wall temperature distributions, which were assumed to be linear between a relatively few sensor locations, or a sensor response lag error at the higher wall temperatures (and enthalpies). Other causes of heat loss from the system could be conduction from the wall into the foam insulation or down the wall into LH_2 bulk heating. The tank wall temperature predictions were consistently high, as shown in Figures 27 to 29 for typical tests 2, 7, and 8 which tends to support the thesis that wall enthalpy error due to temperature sensor lag is the major contribution to the errors in the energy balances.

TABLE 3

MASS BALANCES - 5 PERCENT ULLAGE

Test	Time (sec)	Ullage Mass Computed From Temperature Data (lb)	(Kg)	Predicted Ullage Mass (lb)	(Kg)
4	0	5.919	2.687	5.919	2.687
	23	6.483	2.945	7.935	3.602
	65	10.649	4.835	9.830	4.460
	109	10.309	4.680	9.929	4.508
5	0	5.652	2.566	5.652	2.566
	75	7.415	3.366	10.340	4.700
	130	11.995	5.450	12.649	5.746
	164	14.688	6.662	12.840	5.830
	215	11.098	5.000	12.962	5.882
7	0	6.073	2.757	6.073	2.757
	8	6.216	2.822	6.159	2.797
	134	10.435	4.740	8.926	4.052
	235	12.097	5.494	12.355	5.608
	418	12.202	5.540	12.817	5.820
	582	12.455	5.650	12.934	5.875
	780	12.209	5.547	13.055	5.925
	902	15.044	6.830	13.090	5.947
12	0	6.500	2.950	6.500	2.950
	4	6.806	3.090	6.561	2.980
	112	9.529	4.325	8.958	4.067
	200	11.906	5.408	12.683	5.756
	287	14.002	6.354	12.749	5.790

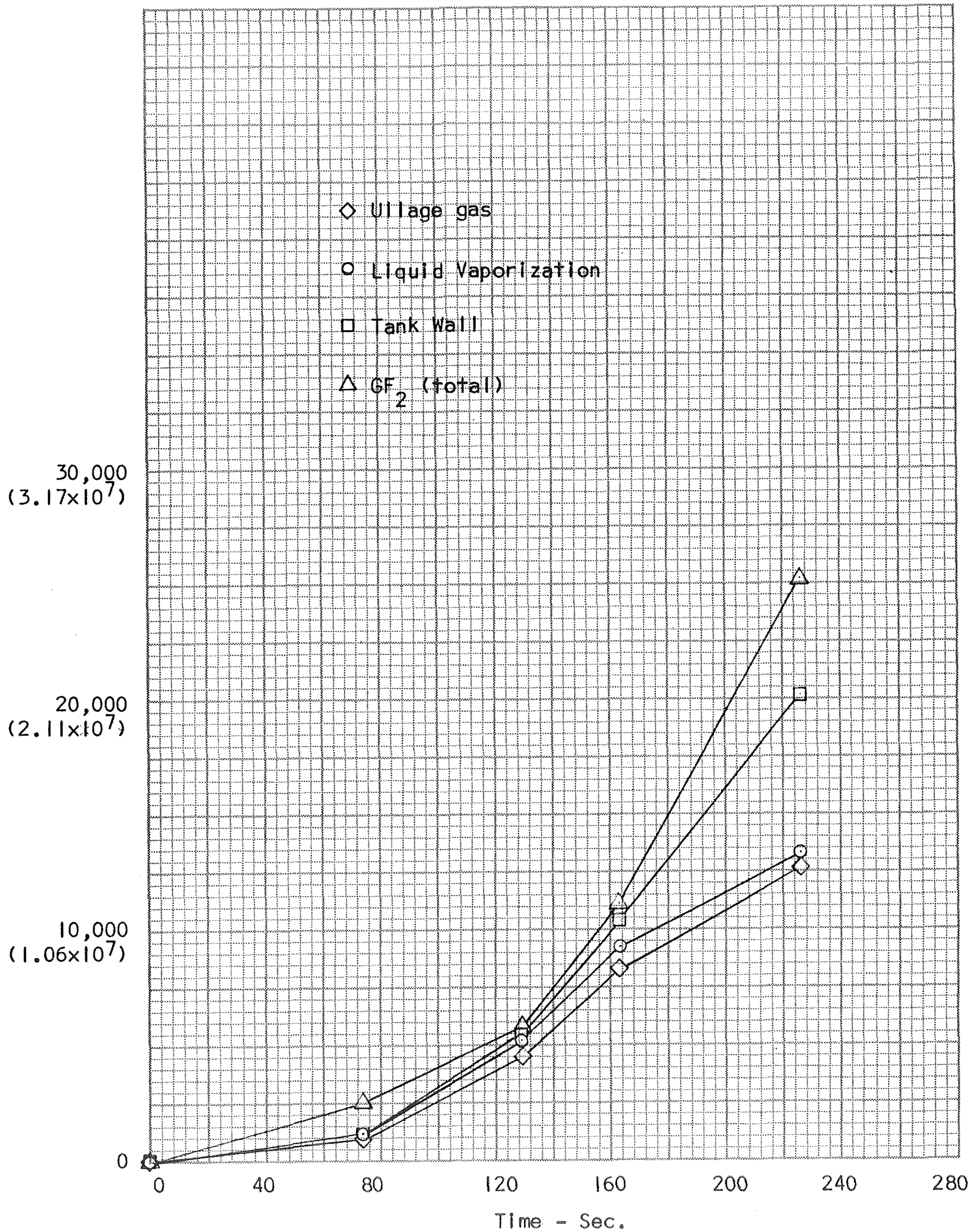

Figure 24. Energy Distribution - Test 5 - 5% Ullage

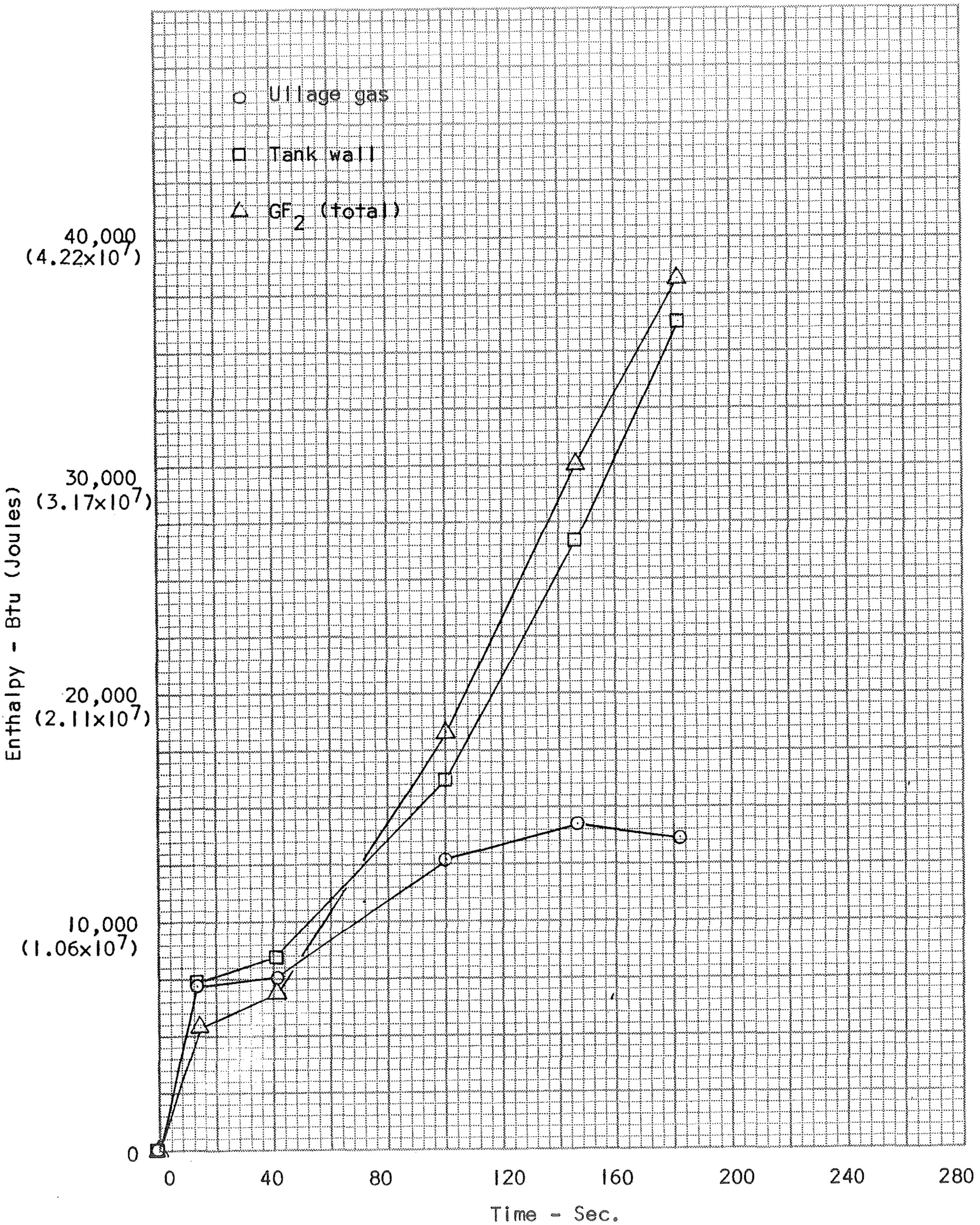

Figure 25. Energy Distribution - Test 8 - 50% Ullage

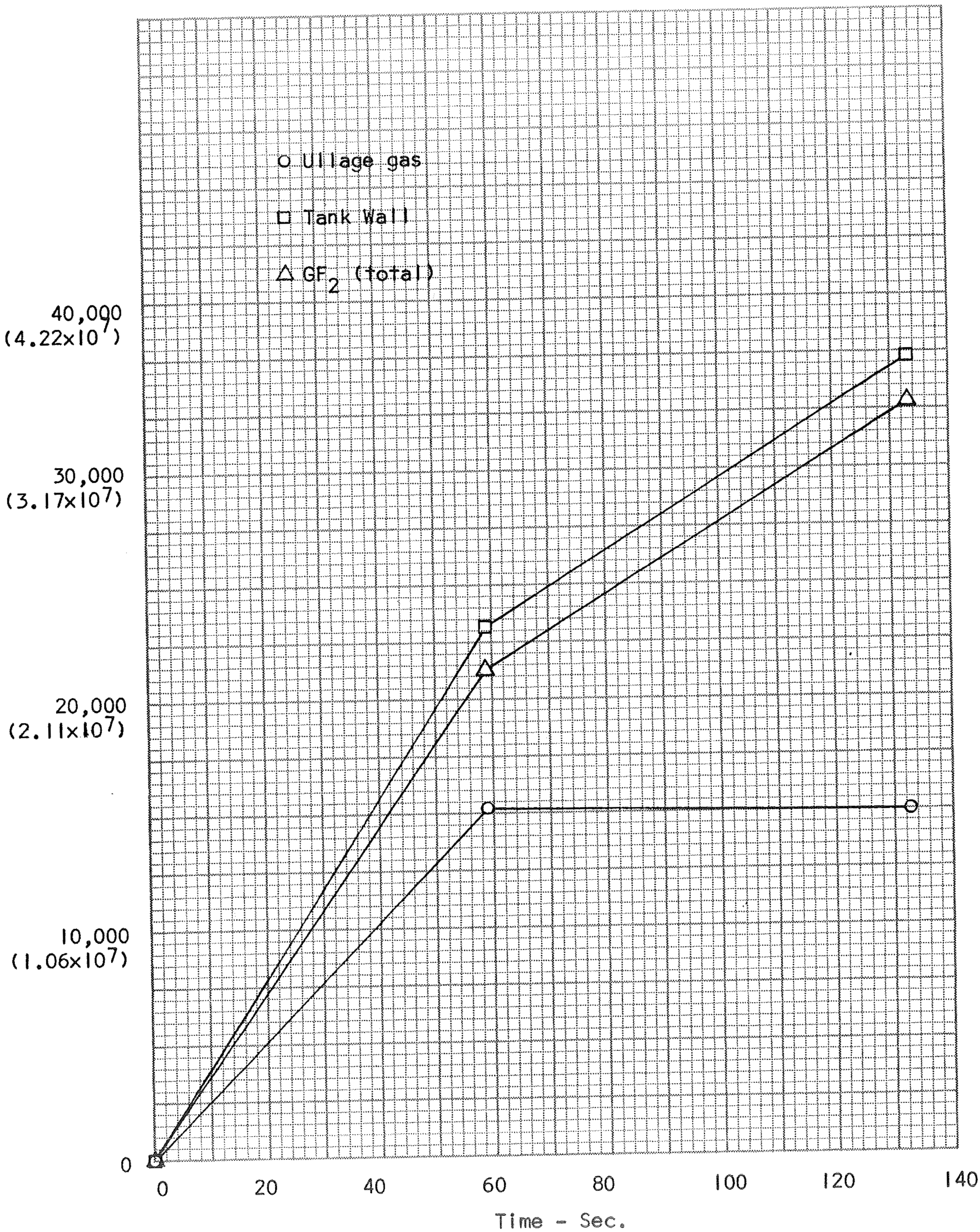

Figure 26. Energy Distribution - Test 3 - 90% Ullage

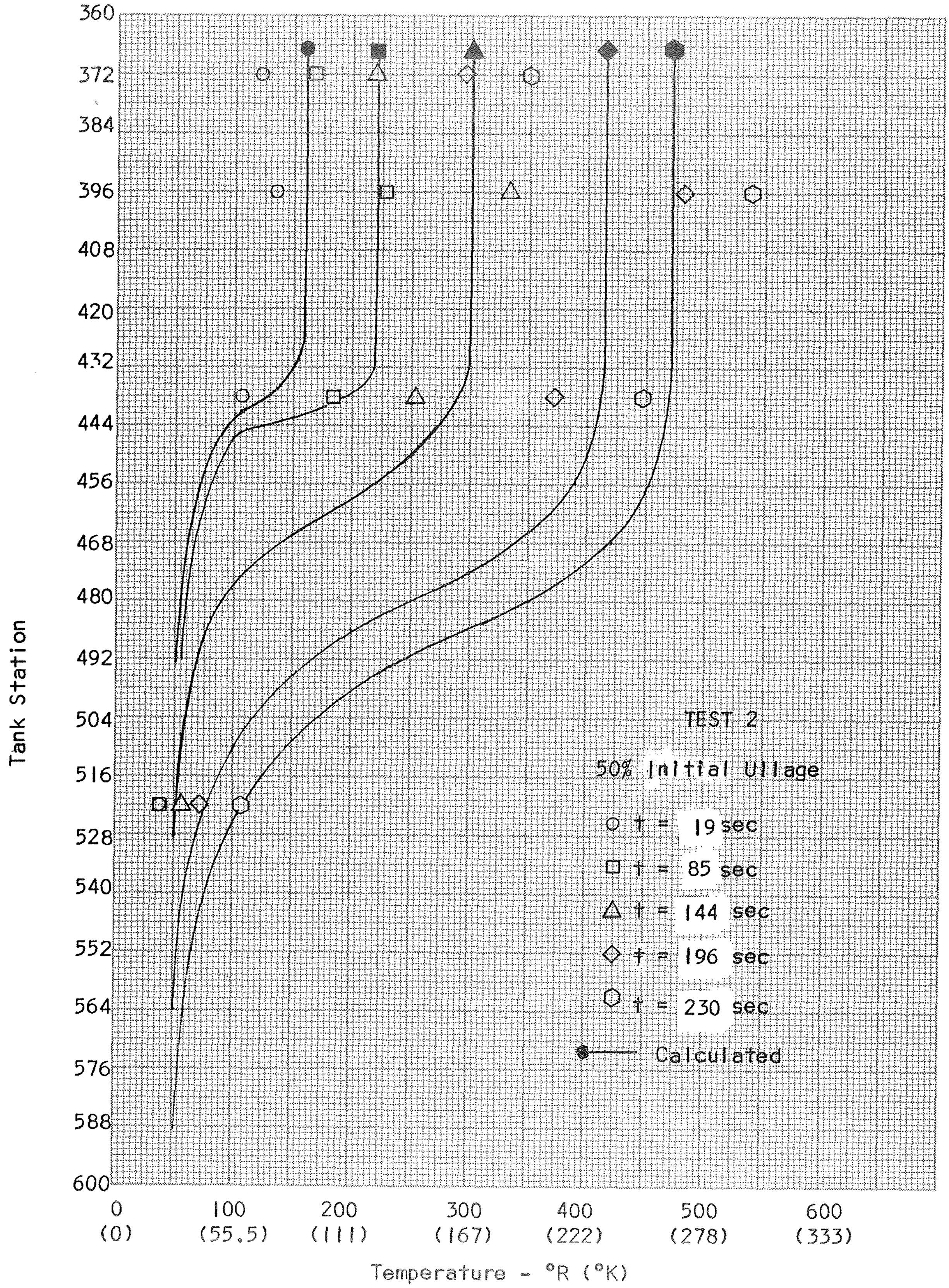

Figure 27. Tank Wall Temperature Correlation - Test 2

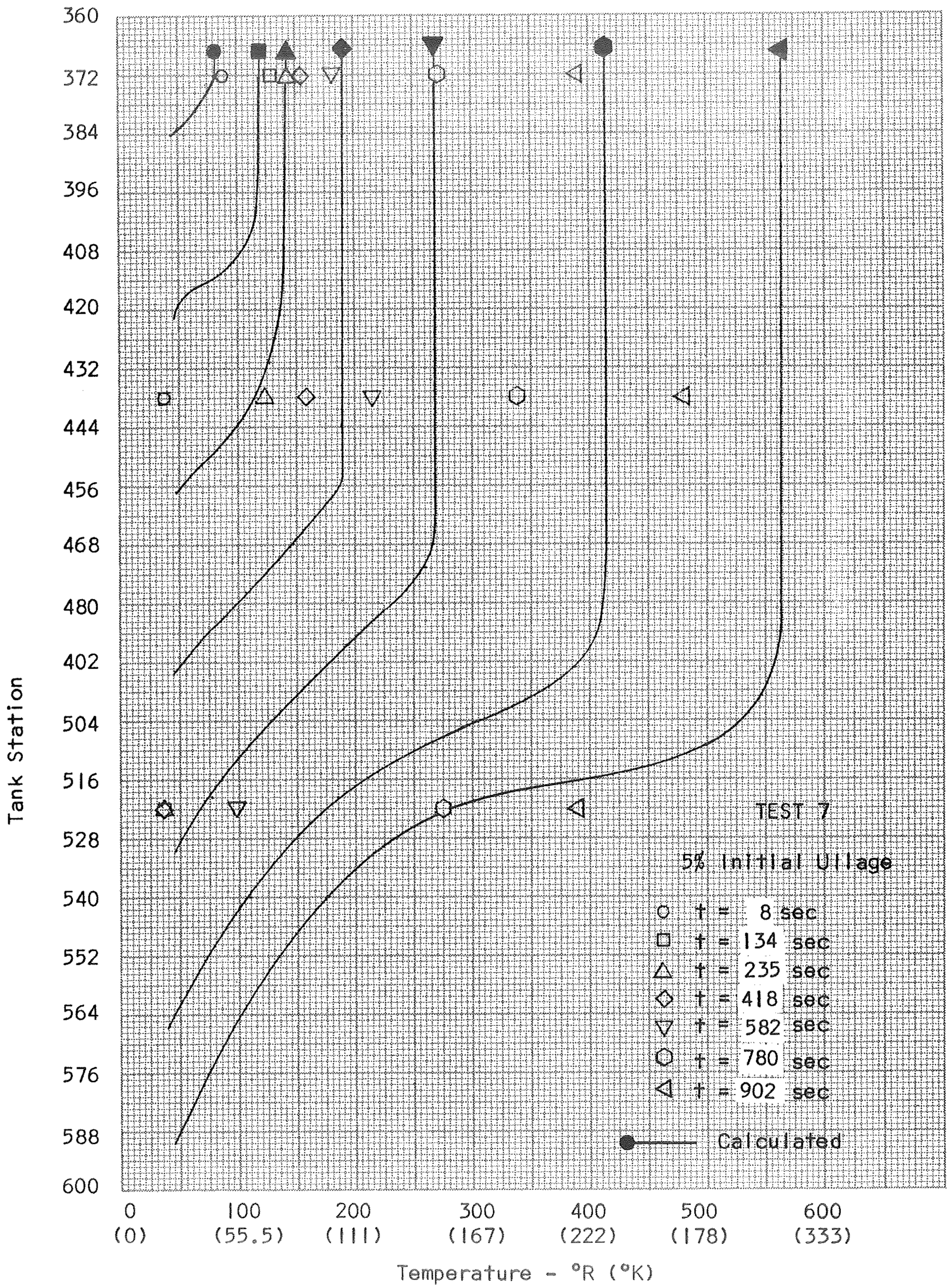

Figure 28. Tank Wall Temperature Correlation - Test 7

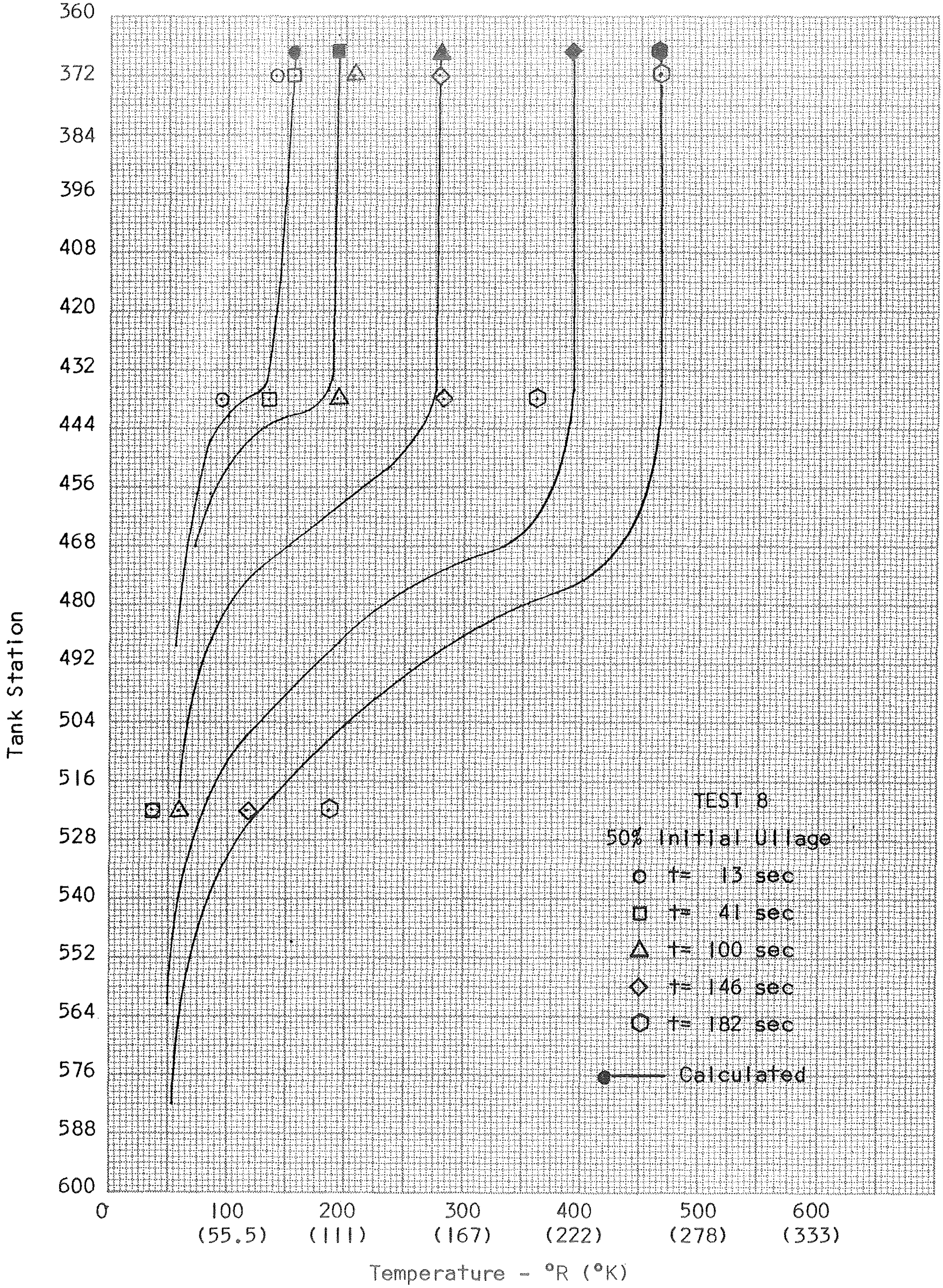

Figure 29. Tank Wall Temperature Correlation - Test 8

EXPERIMENTAL INVESTIGATION

The experimental investigation for this program had two principal objectives:

1. Provide appropriate experimental data for use in defining H819 computer program model variables to allow the prediction of realistic MTI system performance.
2. Design, fabricate, and successfully demonstrate a MTI control system and injectors in a large-scale, flight-weight LH_2 test tank.

The experiment design to satisfy these objectives is described below, followed by the results of the experiments.

EXPERIMENTAL DESIGN

MTI Control System Design

The design requirements for the MTI control system were specified in the contract and are as follows:

1. Self-regulating
2. Capable of controlled pressurization, pressure hold, and expulsion at varied outflow rates up to a maximum of 15 lbs/sec (6.8 Kg/sec) of liquid hydrogen (dependent upon tank volume).
3. Operable at any ullage volume.
4. Capable of a wide range of flowrates and operating pressures (not to exceed the working pressure of the hydrogen tank).
5. Able to pressurize the tank to within one psi (6895 N/M^2) of the desired pressure.
6. Capable of safe operation without damage to the injector or tank, freezing of fluorine in the injector, or causing minimum heat leakage into the tank when not in operation.

In addition the system was designed so that the tank and test facility would be protected against system malfunction. (This necessitated some safety requirements and redundancy which might not be appropriate for a flight system, as discussed in the section on space vehicle performance predictions).

Previous work under Contract NAS 3-7963 indicated that ullage injection of GF_2 yields a tank pressure rise followed by a pressure drop upon cessation of GF_2 injection. This pressure decay is a result of heat transfer to the cold tank walls and LH_2 from the warmer ullage. Because of these characteristics, a control system which senses tank pressure and opens and closes the GF_2 injector valve to keep the tank pressure within a narrow band (so-called "bang-bang" system) was recommended. Such a system is dynamically simple and easily analyzed, and further, allowed use of an existing injector valve proven reliable during the previous MTI tests under Contract NAS 3-7963.

In this previous MTI work it was found that non-ignition of the F_2 in the H_2 could occur, if the F_2 injectant was cold, its O_2 contaminant level was high, or there was injector damage. Although non-ignition never occurred during the previous large scale tests with ullage injection of ambient gaseous F_2, such non-ignition is potentially hazardous because the F_2 freezes in the LH_2 and then is likely to destructively detonate. It was imperative, therefore, that measures be taken to guard against F_2 non-ignition and subsequent potential detonation. The basic approach taken was to sense ignition, and, if it did not occur within a very short time period, to limit the quantity of F_2 injected by immediately closing the injector valve. In addition, since the flow rates for the large-scale, flight-weight Thor tank testing were quite high (an order of magnitude higher than the rates used in the NAS 3-7963 testing), and the tank was flight-weight and rated at reasonably low pressure, it was imperative that the capability exist for positive and reliable F_2 flow shutdown. The Thor test tank was equipped with vent/relief valves and burst discs to guard against accidental overpressure, however, burst-disc replacement would be time consuming which would be best avoided. Further, the possibility existed that the injector could fail open by burning out, so a backup GF_2 prevalve was installed in the GF_2 injection system. This prevalve was used only for additional shutdown capability in the GF_2 system and not for GF_2 flow control.

Another requirement for the control system was that it be capable of artificially cycling the injector valve during the injector demonstration tests, where the pressure switch could not be used. An adjustable on-off timer option was placed in parallel with the pressure switch option for this purpose.

The above considerations gave rise to the following ground rules for design of the control system:

1. "Bang-bang" pressurization system with pressure switch controlling on-off action of GF_2 injector valve and tank pressure to within ± 1.0 psi. (6895 N/M^2)
2. Automatic rapid shutdown of GF_2 in the event of non-ignition.
3. Total redundancy plus manual backup on all components involved in closing of the GF_2 valve.
4. Talk-back lights and alarms for malfunction and non-ignition detection.
5. Timer Cycle in parallel with pressure switch for use in injector demonstration tests and as an option for item 1.

The most important elements in the design of the MTI control system are the pressure switch, the injector valve, and the relays (required for transferring power). The pressure switches selected were completely redundant, individually plumbed mercury-type pressure switches, Mercoid type APH-41-153. The switches have a range of 15 to 45 psia (10.3 to 31 x 10^3 N/M^2) and could be individually set to any pressure within this range with a maximum actuation band (relay energize-to-denergize) of ± 0.375 psi ($\pm 2.58 \times 10^3$ N/M^2). This switch was supposed to have a maximum time delay of 15 msec and was safe for operation in an H_2 atmosphere because the contacts were sealed. This switch would not be suitable for flight vehicle use because the mercury element must be level and is thus g-vector sensitive. Bellows-type switches suitable for flight use with the same fast response and narrow actuation band are available, but must be custom made (especially for H_2 service) and are very expensive. Their use was deemed to be not cost-effective for this program. The chosen switch was available off-the-shelf, inexpensive, and suitable for ground service within an H_2 atmosphere without sacrifice of accuracy, response, or safety.

The injector valve selected was the Fox Valve Development Co. type 610851 injector valve used with great success on the previous MTI program. This valve is liquid and gaseous fluorine-compatible and has a copper-on-stainless steel seat. The valve was actuated by 500 psia (3447×10^3 N/M^2) helium through two integral solenoids, one to actuate open, and the other to actuate closed. The high pressure helium actuation enabled extremely fast valve response (closed to full-open or vice versa in less than 10 milliseconds). Use of helium to actuate closed (rather than spring-loading) was required to provide the high seat loadings necessary to effect a leak-tight metal-to-metal seal. In the event of power failure the valve would remain in its last position, which could be open. The valve, therefore, incorporated a pressurized override which was utilized by attaching a normally-open valve (energized closed by the main power) to the override. In the event of power failure, the normally-open valve would open, thus pressurizing the injector valve closed. This valve was modified to enlarge the flow orifice and adapt to the larger plumbing needed for the much larger Thor tank test system.

The relay coils and contact points involved in closing the valve were made completely redundant. The relays used were Guardian three-pole, double-throw, type 1R-1225-3C-24D (28 VDC). Similar relays performed reliably during the NAS 3-7963 tests.

The prevalve selected was a Control Components, Inc., type CM3116T valve (1-inch (.0254M) pneumatically operated-solenoid actuated open-spring-loaded closed). This valve had a relatively slow response time of the order of 200 milliseconds, and was situated at some distance from the injector valve. Therefore, a timer was incorporated in the control system to delay the initial opening of the injector valve until the prevalve had time to open and the GF_2 flow had time to fill the line between the prevalve and the injector valve.

In order to provide automatic closing of the injector valve in the event of non-ignition of the GF_2, ignition sensing was required. In the previous MTI tests under NAS 3-7963, ignition was sensed with a low-level pressure switch, which signalled the initial pressure rise accompanying ignition. For the large scale control system, a low level pressure switch would not be appropriate, because it would be saturated at the higher tank pressure level, where ignition and re-ignition is constantly occurring, and reliable ignition sensing is required with each cycle. It has been found that ignition is always accompanied by a flame (Reference 1) which radiates strongly in the infrared (IR) region (Reference 16). Thus a reliable method of detecting ignition would be to detect the accompanying flame. The IR sensors selected for the test program were Infratron type B3-SA22 lead sulfide photoconductive detectors, which have response characteristics as shown in Figure 30. The relative radiance of the F_2-H_2 flame, as reported in Reference 16, is superimposed on the figure. It can be seen that the region of maximum radiance coincides with the region of maximum detector response. These detector elements were therefore appropriate to use in the ignition sensing system.

Operation of the ignition sensor was divided into three functions:

1. Detecting and converting IR radiation into an electrical signal.
2. Amplifying this signal and establishing a threshold condition in a comparator circuit.
3. Actuating a relay with the amplified output of a comparator circuit.

The sensor is shown schematically in Figure 31, with the three functions outlined as blocks. With the detector masked from IR radiation, the threshold level is adjusted with R6 such that point "a" is more negative than point "b". As a result, the output of the comparator, an integrated circuit operational amplifier, is negative. This in turn insures that Q2-3 is cut off and relay K4 is not turned on. Radiation, from the F_2-H_2 flame, incident on the detector, causes the resistance of the detector to decrease. This decrease in resistance causes point "a" to eventually become more positive than point "b", causing the comparator output to go positive. Q2-3 is turned on, causing the relay to pull in. When the radiation level falls below the threshold level, Q2-3 turns off and the relay pulls out.

The detector configuration, shown in Figure 32, uses two detectors in series to eliminate threshold sensitivity shift with temperature. One of the detectors is permanently masked and provides a load resistance which varies with temperature exactly as does the detector. This configuration provided optimum sensitivity and threshold stability irrespective of temperature, and was used in the final sensor design.

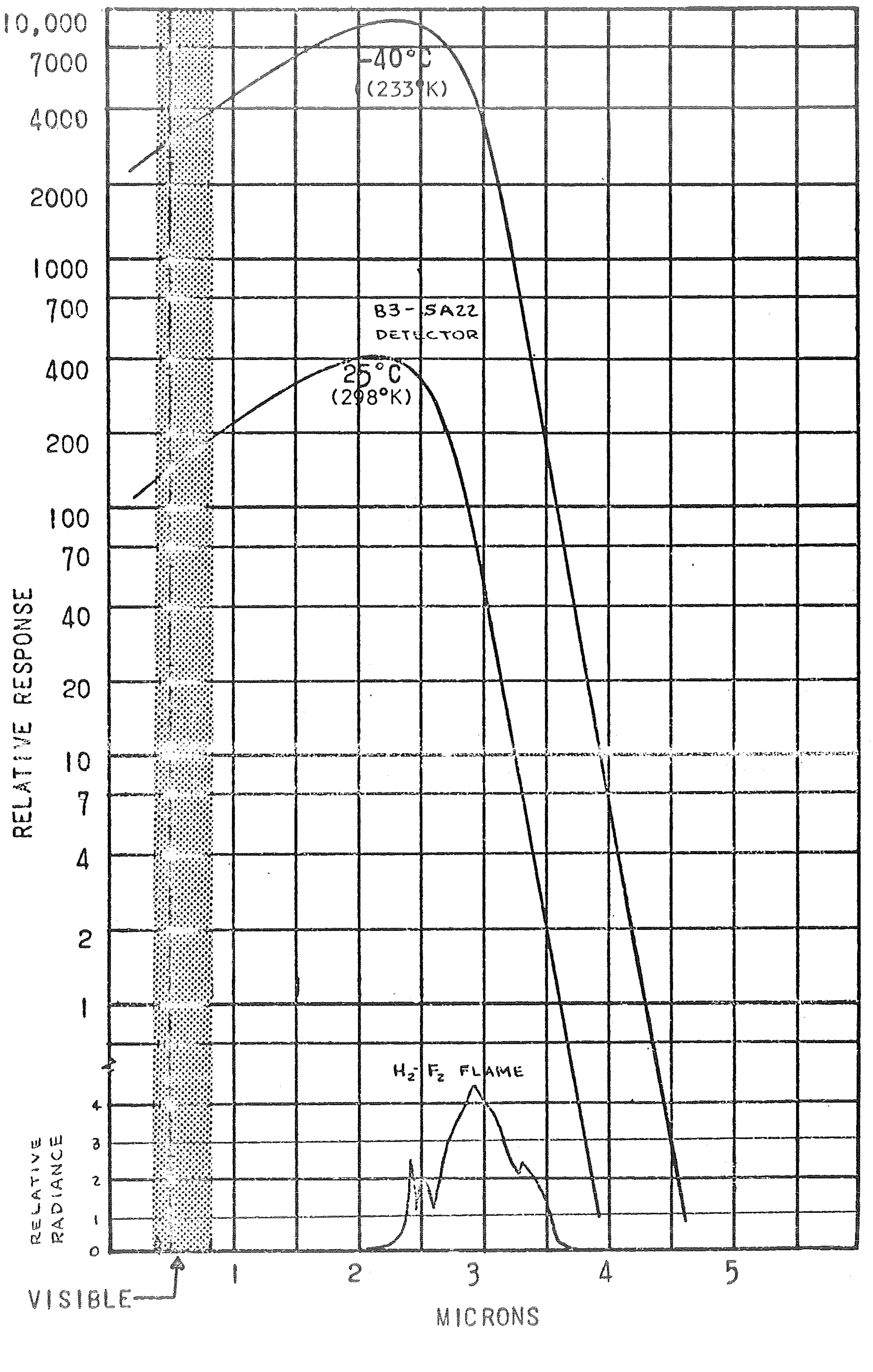

Figure 30. Spectral Response of Ignition Detector

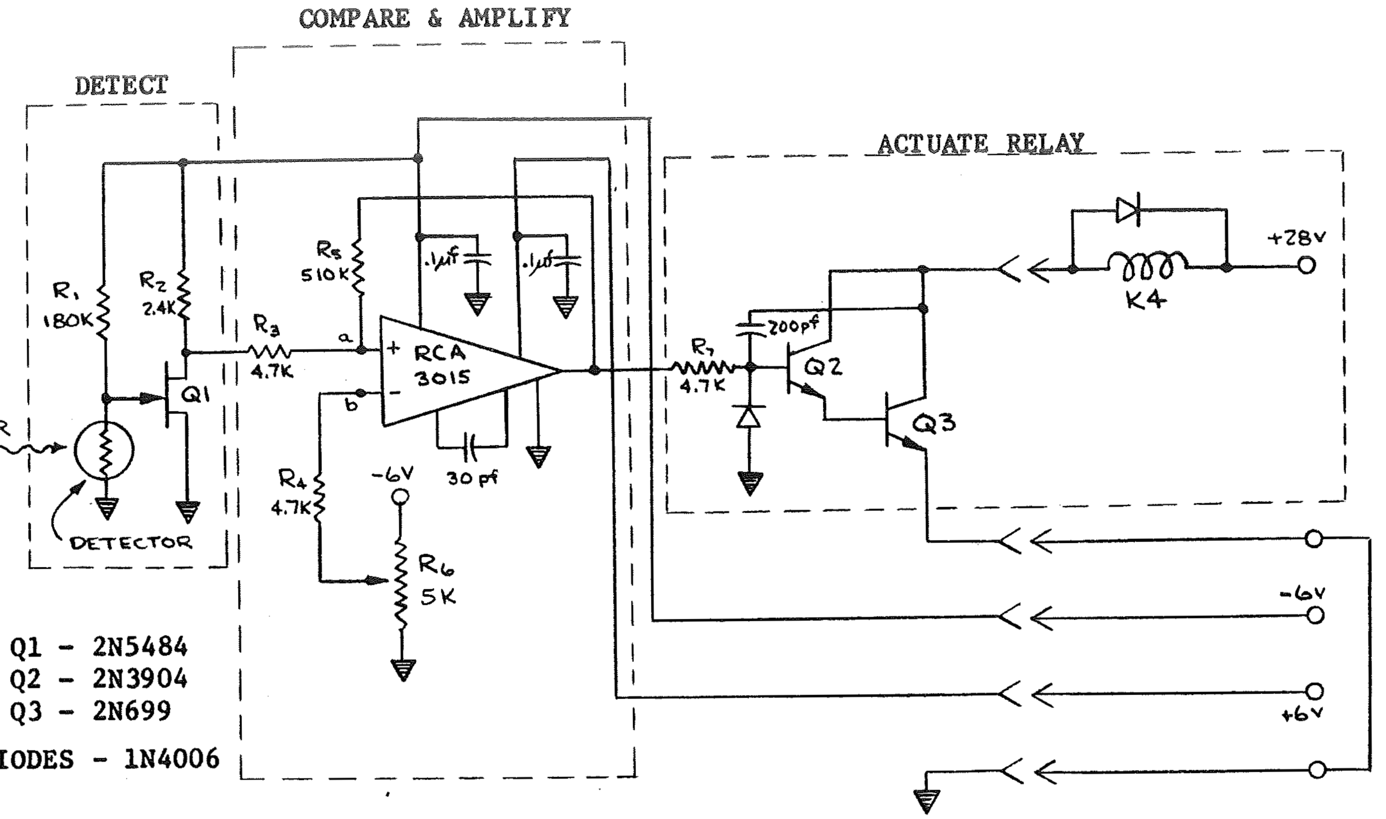

FIGURE 31 IGNITION SENSOR SCHEMATIC

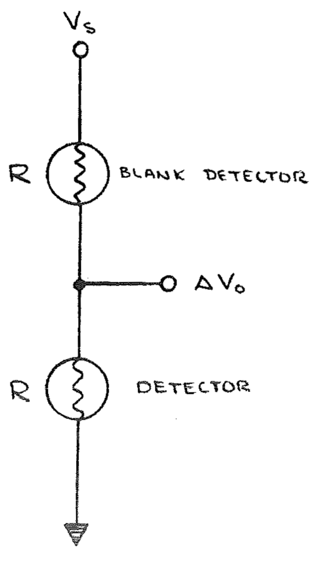

FIGURE 32 DETECTOR CONFIGURATION

The final control system design which satisfied the requirements and ground rules described previously is shown schematically in Figure 33. The apparent complexity results from the redundancy requirements. The sequence of operations is quite straightforward and is as follows:

1. Set "F_2 Prevalve" and "F_2 Inj." on "AUTO"; "F_2 Inj. Check" on "Close"; "IRD", and "ALARM" on "ON": "PS" on "ON" and "Timer Cycle" on "OFF".
2. "FIRE" to "ON", actuates K1 relay, which starts timer T-1 (K1-1), opens "F_2 Prevalve" (K1-2), and energizes the IR Detector "IRD" (K1-3) and Pressure Switch "PS" (K1-5, K1-6), enable circuits.
3. After time delay T-1, T1-1 actuates K2 relay, which opens "F_2 Inj. Valve" (K2-1, K2-2, K2-3), and starts timer T-2. (K2-4, K2-5)
4. Opening "F_2 Inj. Valve" should give reaction which actuates IRD, which in turn actuates K4 relay, which keeps open "F_2 Inj. Valve" through parallel circuit (K4-1, K4-2, K4-3), and interrupts "ALARM".
5. After time delay T-2, T2-1, 2 actuates K3 and K3A relays which close "F_2 Inj. Valve" (K3-1, K3-2, K3-3, K3A-1, K3A-2, K3A-3), and actuates "ALARM" (unless step 4 has occurred).
6. When operating pressure is reached, the pressure actuates PS1 and PS2, which actuates K5 and K5A relays, which close "F_2 Inj. Valve", (K5-2, K5A-2, K2-2, K2-3), which deactuates K3 and K3A relays.
7. Closing "F_2 Inj" should terminate reaction which should deactuate "IRD", and thus deactuate K4 relay.
8. When pressure drops to where PS1 and PS2 are deactuated, then K5 and K5A relays are deactuated, which actuates K2 relay, thus repeating steps 3 through 8.
9. An alternate sequence uses "TIMER CYCLE" on "ON" and "PS" on "OFF", to achieve steps 6, 7, and 8, by use of an alternating on-off timer.

The timers T-1, T-2, and T-3 were solid-state electronic timers made by the H. B. Abrams Co. Timer T-1 is a model TN with a maximum time of 2 sec. Timer T-2 is a model TN with a maximum time of 1 sec. Timer T-3 is a model TDS with individually adjustable on and off times, up to a maximum of 10 sec.

Other safety features incorporated in the control system design include a Mallory type SC628 alarm to signal valve shutdown caused by lack of IR signal due to non-ignition or ignition sensor failure. A light would indicate erroneous ignition sensor signals (e.g., if the ignition detector light came on before the "valve open" light). Other lights indicated that the pressure switch had energized and showed the valve positions (open or closed). In addition each relay pickup/dropout was recorded on event recorders during testing.

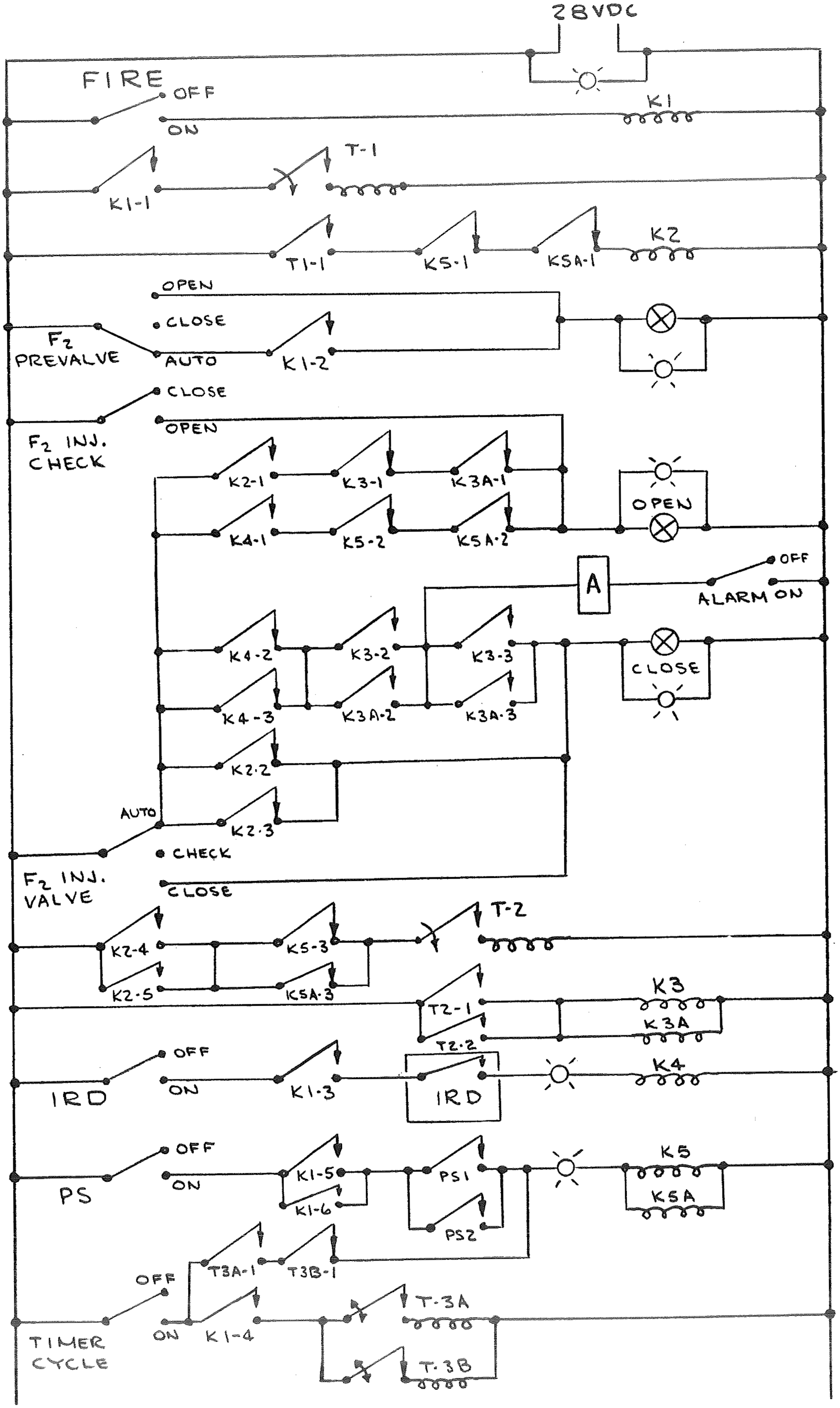

Figure 33. MTI Control System Schematic

The MTI control system shown schematically in Figure 33 was detail designed in a configuration to conform with existing cabling at the Sacramento Test Center. The system was functionally split between two panels: 1) a blockhouse panel which contained all of the enabling switches, talk-back lights, alarms, and power busses, and 2) a test pad tunnel room panel which contained all of the relays and timers. The panels were connected by existing cabling in a 500 ft (152.4 M) tunnel from the blockhouse to the test pad tunnel room. The functional split was necessary to satisfy the requirement that all control functions use only 28 VDC to avoid interference with instrumentation cabling in the tunnel. However, with 28 VDC, significant voltage drops would occur down the long tunnel length, therefore, the actuating components (relays and timers) were situated in a panel at the test pad tunnel room (under the test stand). From the tunnel room panel, relatively short cables (~50 ft) (~15.2 M) led to the valves, infrared radiation detector, and pressure switches at the Thor test tank.

The MTI control system was analyzed to determine the system dynamic response characteristics. The purpose of this analysis was to determine, by evaluation of the predicted Thor tank pressure rise and decay rates, together with the time lags inherent to the control system components, whether the system could be expected to keep the Thor tank pressure within ± 1.0 psi (± 6895 N/M^2) of the nominal tank pressure of 29.0 psia (200 x 10^3 N/M^2). Details of the analysis and a comparison of the predicted and actual performance are shown in the section on experimental results. The results of this initial analysis indicated that the control system would perform properly within the required limits.

Injector Design

Some fundamental aspects of MTI pressurization will be reviewed to facilitate understanding of the injector analysis and design. With all other pressurization techniques, mass (perhaps heated externally to the tank) is added to the tank ullage; with MTI, the injected mass is relatively minute and negligible, and essentially, only heat is added to the tank ullage.

Unacceptably high ullage temperatures will often result as a consequence of prepressurization and expulsion using only heat addition. This is shown in Figure 34 which presents the maximum ullage gas temperature as related to the basic duty-cycle requirements, the liquid mass evaporated, and the degree of ullage gas mixing. The significance of these curves can be shown by the following example: for a completely (100%) mixed ullage (the optimum case-lower curve), prepressurization from 15 to 45 psia (103.4×10^3 to 310.2×10^3 N/M^2) ($P/P_o = 3$) followed by complete expulsion from 5% ullage to empty ($V/V_o = 20$) with no mass addition ($M/M_o = 1$), yields the combined parameter $PVM_o/P_oV_oM = 60$, for which the ullage temperature is 2,400°R. (1333°K) With 50% mixed ullage the ullage temperature would need to be nearly 8000°R. (4450°K) These temperatures are clearly excessive and would endanger the tank structure.

It is clear that maximum ullage mixing is very important, because it prevents excessive local ullage temperatures and it theoretically gives higher efficiency than the stratified ullage which normally accompanies a well-diffused pressurant inflow (Reference 17). This trend toward higher efficiency with ullage mixing was shown in previous NASA experimental work on warm gas pressurization (Reference 9) which indicated not only that the straight-tube injector performance was superior, but that the performance was improved by increased jet penetration into the ullage. This was discussed previously in the Analytical Study section.

Further, mass must be added to the ullage to reduce the ullage temperature to a more acceptable maximum, say 1,000°R (556°K), for example. In this case the parameter PVM_o/P_oV_oM must be reduced to 25, which means that M/M_o must equal 2.4. Thus, 1.4 times the original ullage mass must be added to the ullage during the pressurization process to keep the temperature low. (If there is less than 100% ullage mixing, even more mass must be added.) During the previous MTI testing with the straight tube injector, the necessary mass was added to the ullage (and this lowered the ullage temperature) when the injector jet impinged on the LH_2 surface and caused LH_2 vaporization (accompanied, of course, by energy losses to the liquid). With a large initial ullage fraction or with a small partial expulsion, impingement and mass addition are not necessarily required, because the ratio V/V_o would be small.

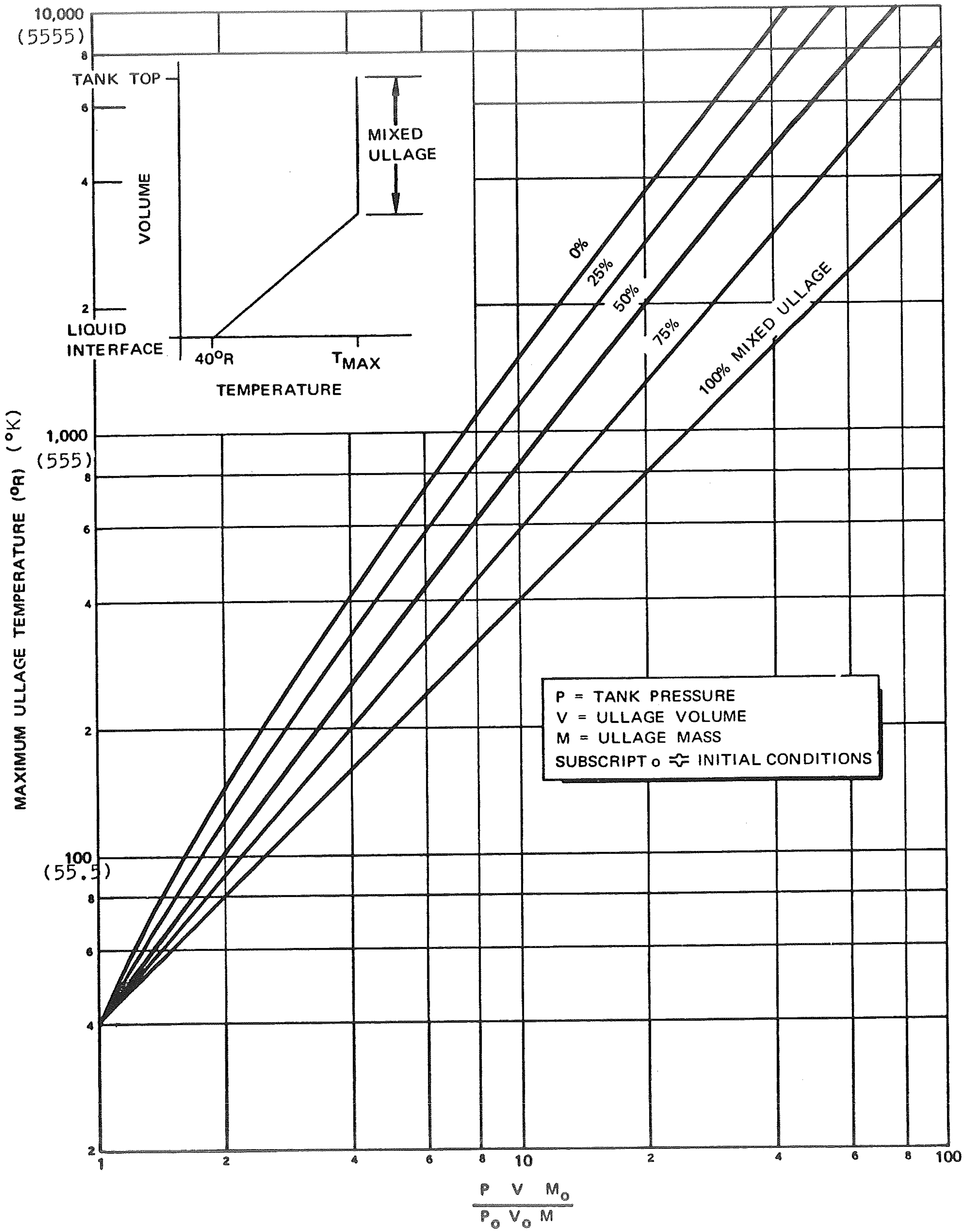

Figure 34. Tank Ullage Temperatures Due to Pressurization

The straight-pipe injector is considered to be the optimum injector for MTI pressurization for the following reasons:

1. Previous NASA experimental data (Reference 9) and the theoretical considerations mentioned in the Analytical Study indicate that the straight-pipe injector gives the greatest ullage penetration and mixing, and subsequently, the highest pressurization performance.
2. The straight-pipe injector has been successfully tested in the previous MTI testing under Contract NAS 3-7963 where it performed efficiently and demonstrated satisfactory reliability in the MTI pressurization environment.
3. The straight-pipe injector is extremely simple and easy to fabricate.

The H819 computer program described previously was used to perform a comprehensive analysis of the performance of the straight-pipe injector. The results of the analysis indicated that a 1-in. (.0254 M) diameter straight-pipe injector would give:

1. Reasonable injector inlet velocities (of the order of 100 to 20 ft/sec (30.5 to 6.1 M/sec)).
2. Excellent GH_2 ullage penetration (of the order of 10 ft (3 M)) with excellent mixing over most of the test cycles for the Thor test tank.
3. Adequate LH_2 penetration with a full tank (of the order of .6 ft (.18 M)) with sufficient LH_2 vaporization to assure reasonable ullage temperatures.

The straight-pipe injector should be located on the tank centerline to provide a uniform flow field in the tank ullage. The only available port for injection into the Thor test tank was offset from the tank centerline. The straight-pipe injector thus had to be fairly long (~35 in. (~.89 M)) to reach to the tank centerline. The offset injector port led to the idea of having an offset injector to investigate the influence of injector-to-wall distance on the convective heat transfer coefficients in the Thor test tank. The design details of the centerline and offset straight-pipe injectors are described later.

The downward penetration of the injectant from the straight-pipe injector varies inversely with the local acceleration (or g-level) as described previously in the Analytical Study. Therefore, the penetration of a straight-pipe injector may be acceptable in one-g, but may be excessive under low-g prepressurization conditions (e.g., at typical propellant settling g-levels of 10^{-2} to 10^{-3} g_e) and cause significant liquid disturbances, such as sloshing and bubble entrapment which could be deleterious to vehicle operation. Thus, reduced penetration is desirable for low-g prepressurization; this can be achieved by a diffuser-type injector.

Diffuser-type pressurant injectors have been widely used in propellant tank pressurization because they minimize ullage-gas motion and liquid interface disturbances. An ideal diffuser causes a highly stratified ullage temperature distribution with a temperature at the injector plane equal to the maximum pressurant inlet temperature. This characteristic is acceptable in most hot-gas pressurization systems, but the maximum MTI flame temperature of 7,500°R (4170°K) cannot be tolerated in close proximity to the tank wall. Thus, the conventional diffuser design with radial distribution of the pressurant (References 6 and 9) cannot be used; the high temperature reaction products must be diluted to some extent by mixing with cooler ullage gases. A conical injector would accomplish the required mixing and the affected mixing region would be smaller than with the straight-tube design. The cone injector divides the inflow into a number of small gas streams which penetrate and mix with the ullage in the same general manner as the straight tube inflow. However, due to the much smaller size of the individual gas streams, the depth of penetration and the extent of mixing is greatly reduced. The mixing region will be in contact with the interface for a shorter time, thereby reducing mass transfer and heat loss to the liquid.

The baseline diffuser design was to keep the total flow area equal to the area of the 1-in. (.0254 M) diameter straight-pipe injector, so that with equal GF_2 flowrates, equal initial flow velocities at the injector would be realized. This would reduce the number of unknown parametric differences between the two injector types.

The cone spread-angle (half angle) was arbitrarily set at 15° (.262 radian); this assures adequate spreading without danger of the flame impinging on the tank wall. Also, since the turbulent diffusion spread-angle is about 12° (.209 radian), a 15° (.262 radian) cone angle allows the diffusing flame to nearly fill the cone.

The proper number and size of diffuser holes to obtain the correct diffusing effect was analyzed using the H819 computer program, with appropriate assumptions for the interface behavior. Comparisons of the straight pipe and diffuser injectors in reduced gravity were made with interesting results. The depth of LH_2 penetration, X_L, is an important parameter in MTI pressurization since it determines evaporation rate, and indirectly reflects the degree of ullage mixing. The LH_2 penetration distance vs gravity level for both injector types is shown in Figure 35. At relatively low-gravity settling accelerations typical of a space vehicle (e.g., 10^{-3} to 10^{-2} g_e) the 25 hole 15° (.262 radian) diffuser has a penetration distance nearly identical to the straight pipe at normal (one) gravity. Thus, the pressurization performance should be similar. Conversely, at 10^{-2} g_e, the straight pipe has a LH_2 penetration distance of about 6 ft (1.83 M)! Such deep penetration would probably cause large sloshing disturbances in the LH_2 with potentially deleterious vehicle effects. As the gravity level gets smaller, even the 25-hole diffuser has excessive penetration - a finer diffuser would be required at 10^{-4} g_e for example. The analysis also compared the quantity of fluorine used and LH_2 evaporated. The fluorine usage only varies mildly with g-level, but evaporation varies strongly because of LH_2 penetration distance. For example, at 10^{-2} g_e, the straight pipe would evaporate almost 60 lb (27.2 Kg) of LH_2 during a complete expulsion - which represents a substantial weight penalty.

Naturally, the low g-level during propellant settling, would not stay low once the main engines started. The differences between injectors would not be great during prepressurization at 5% initial ullage. However, at higher ullage volumes prepressurization makes up a significant percentage of the pressurization load. For prepressurization only, the diffuser shows an insignificant performance advantage over the straight pipe - its sole operational advantage is that the diffuser has much less LH_2 penetration in reduced gravity and therefore will not cause gross liquid disturbances during prepressurization. Even this advantage is not particularly significant at large ullage volumes. For prepressurization at 10^{-2} g_e, at 50% ullage, the straight pipe flow penetrates the LH_2 by less than 5 inches (.127 meters), while at 90% ullage, no LH_2 penetration occurs with the straight pipe.

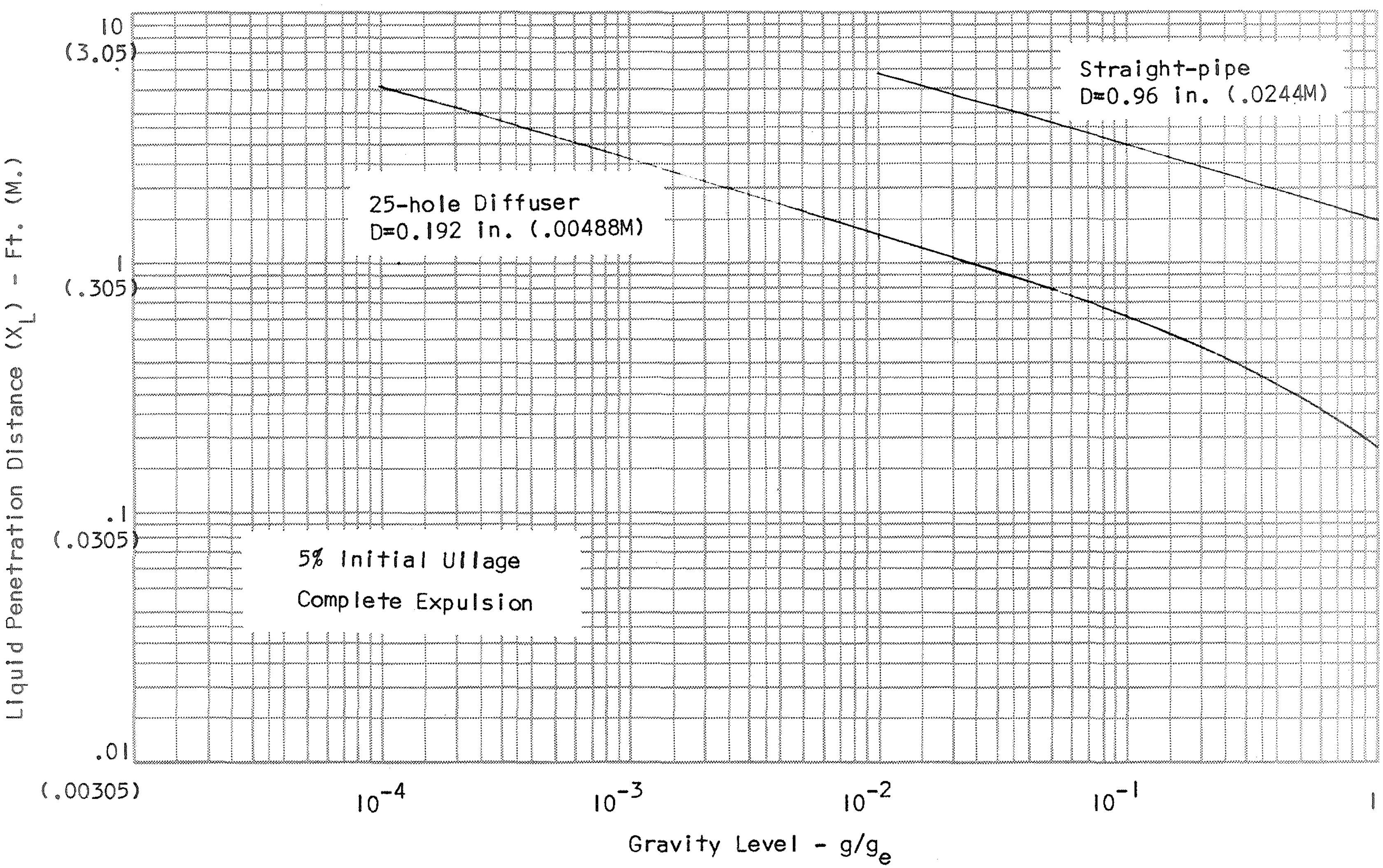

Figure 35. LH_2 Penetration Distance vs. Gravity Level

Despite the fact that the 25 hole 15° (.262 radian) diffuser showed significant advantage over the straight pipe only for reduced gravity pre-pressurization at small ullage volumes, it was recommended for limited testing during the Thor tank tests. This testing was to evaluate the adequacy of the H819 computer program to predict performance for a significantly different flow field than the straight pipe (mixed ullage), and was to uncover operational problems (if any) peculiar to diffuser-type injectors.

However, the diffuser, when tested in one-g, would give significantly higher ullage temperatures (because of reduced mixing and LH_2 evaporation) as shown in Figure 36, for complete expulsions. In order to keep the ullage gas temperature to the same level for both the diffuser and straight pipe tests, the expulsion for the diffuser must be limited to partial expulsions from about 50 ft^3 (1.42 M^3) to about 335 ft^3 (9.49 M^3) (or about 1/3 of the LH_2 expelled). This was judged to be adequate to evaluate the diffuser injector performance.

Based on the results of the above analysis, the straight-pipe and diffuser injectors were designed and fabricated. During the test program under Contract NAS 3-7963, it was found that injectors fabricated from copper provided maximum resistance to burning because of their high thermal conductivity, which tends to eliminate hot spots and injector ignition with the fluorine; therefore, both injector configurations were fabricated from oxygen-free copper. For the diffuser injector, two basic design approaches were used: the first, shown in Figure 37 was comprised of a bundle of 1/4 inch (.00635 M) diameter tubes spread out to form a 15° (.262 radian) cone in a symmetric pattern. The flow and environmental conditions for these 1/4 inch (.00635 M) tubes was expected to be essentially identical to those of the previous MTI tests under Contract NAS 3-7963, where the 1/4 inch (.00635 M) copper tubes successfully withstood the MTI test conditions. The tubes in the bundle were upset and mechanically squeezed between two plates, with the entire assembly then swagged into the expansion cone. This technique allowed each of the injector components to be scrupulously cleaned prior to assembly, and permitted mechanical assembly without the requirement of brazing or welding. This diffuser, while expected to be safe, was fairly cumbersome. A simpler design is shown in Figure 38, and was simply a showerhead of 26 holes arranged in a 15° (.262 radian) cone. In

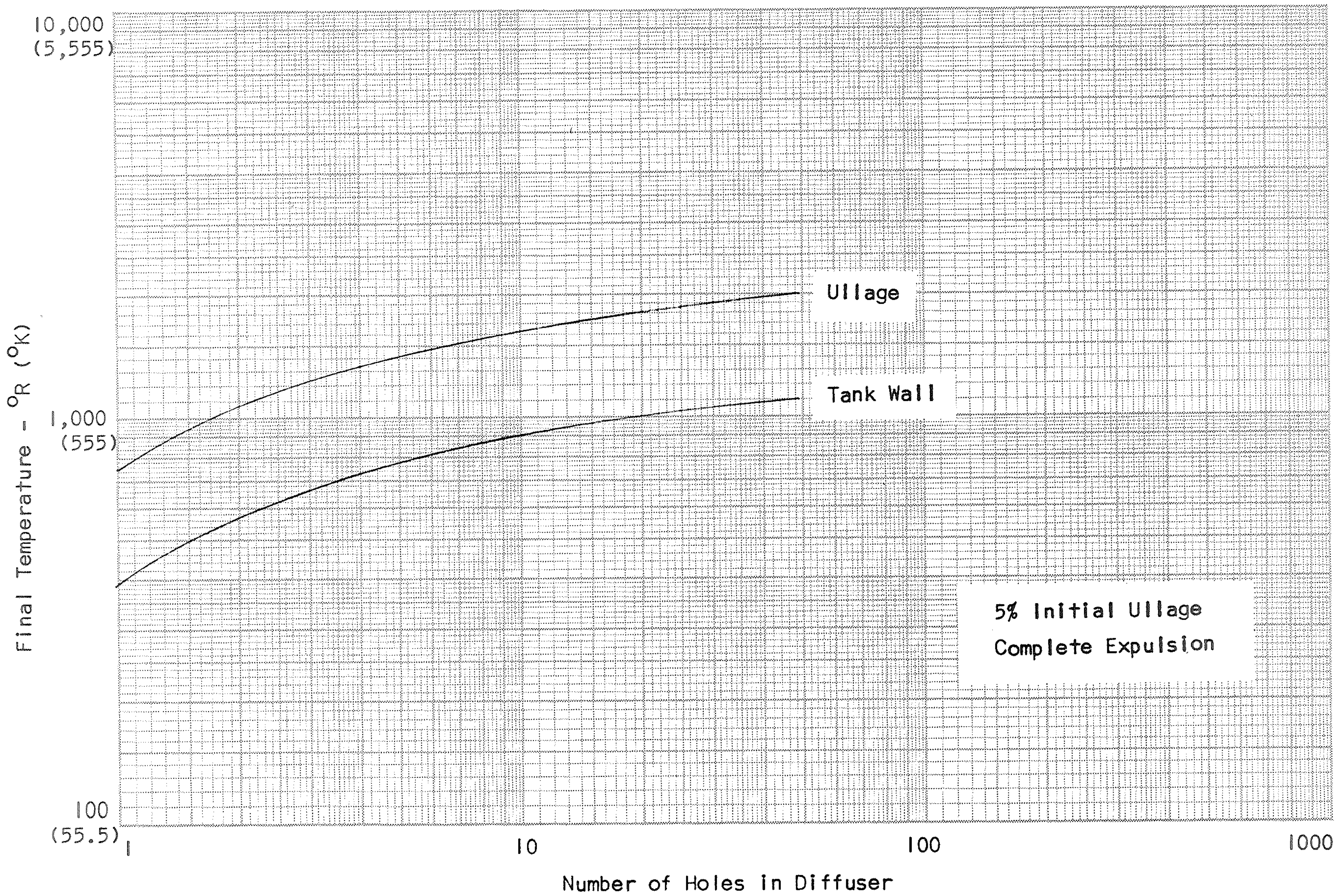

Figure 36. Ullage and Tank Wall Temperature for Various Diffusers

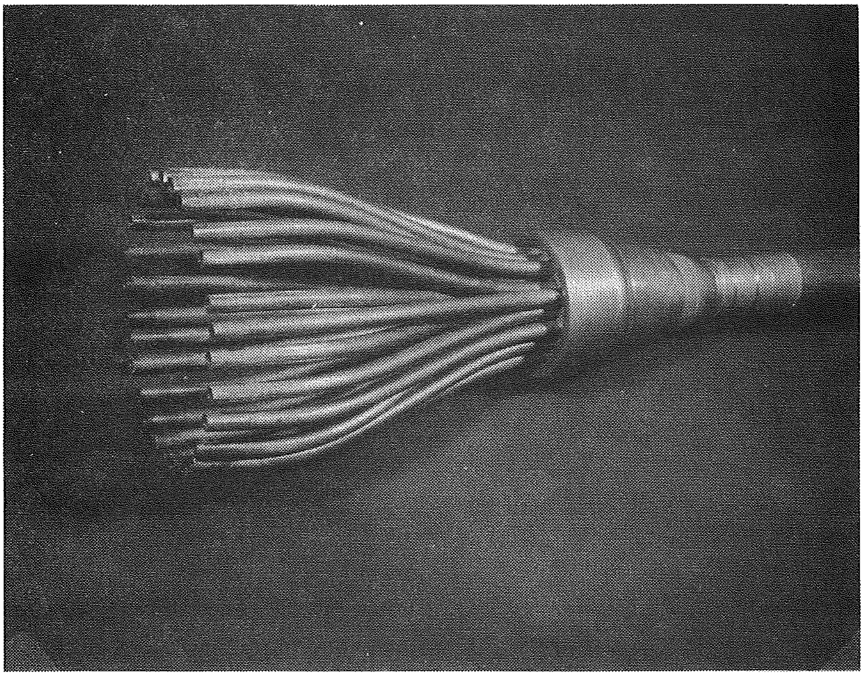

Figure 37. Tube-Bundle Diffuser Injector

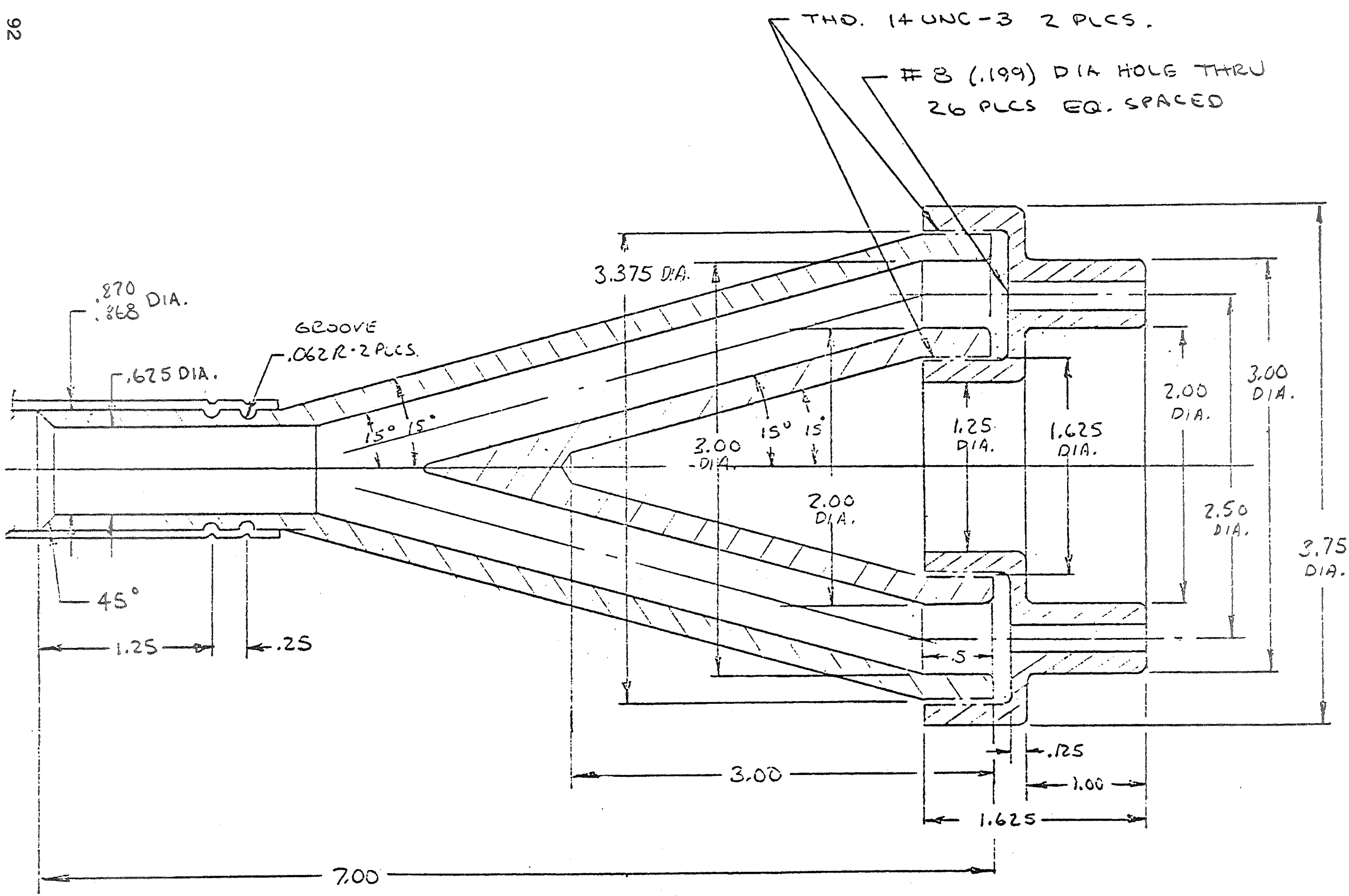

Figure 38. SHOWERHEAD DIFFUSER INJECTOR

both of these diffusers, the final flow path was straightened to be parallel to the axis of the tube: this was for testing in the injector demonstration test apparatus (as described in detail below) where a conical flow path would burn holes in the apparatus. The injector used in the Thor tank tests would be modified to provide a 15° (.262 radian) conical flow field. The components of the showerhead diffuser were screwed together, and swaged onto the injector tube. All components were scrupulously cleaned prior to assembly. There was no previous MTI test experience with the showerhead injector. It was anticipated that if it came through the injector demonstration tests in good order, it would be selected, rather than the tube-bundle injector, because of ease of fabrication.

Injector Demonstration Tests

An important part of the injector design task was to hot-fire the injectors in a cold GH_2 atmosphere with GF_2 flow on-off cycle rates simulating the injector cycling anticipated in the Thor tank tests.

The purpose of these tests was fourfold:

1. To verify the structural adequacy of the injector, and reveal any injector burning problems which could occur.
2. To determine if injectant (GF_2) freezing would occur in the rather long injector tube.
3. To verify the proper operation of the MTI Control System, including the infrared radiation (IR) ignition detector under low temperature operational conditions, and determine the proper system lag times to be set on the control system timers.
4. To verify the proper operation of the GF_2 supply system, and evaluate the accuracy of the GF_2 flowrate measurement technique.

In order to perform these tests, an injector demonstration test apparatus was designed, fabricated, and installed at the MDAC Gypsum Canyon Test Site. The injector to be tested was mounted axially along the centerline of a 12-inch (.3 M) diameter by 10 ft (3.0 M) long stainless steel pipe mounted horizontally as shown in Figure 39. The injector was mounted through a blind flange at one end of the pipe; the other end of the pipe was open. The IR detector was also mounted on the flange and looked along the injector, toward the injector tip. LH_2 flow was introduced along the bottom of the pipe, where it boiled, providing a cold GH_2 atmosphere in the pipe. The pipe and all flow lines were thoroughly purged with GN_2 prior to initiating LH_2 flow.

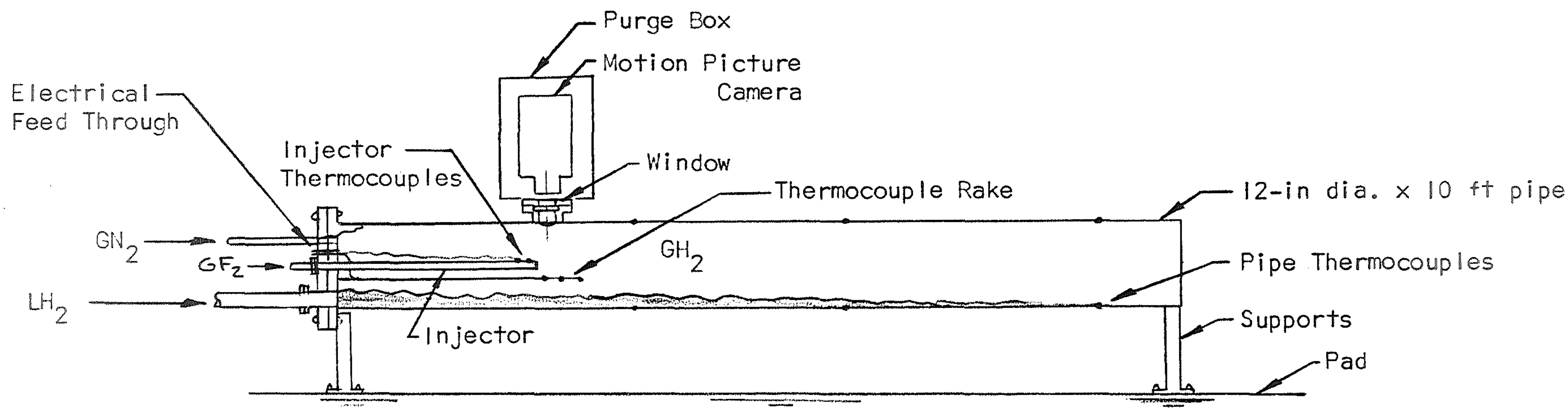

Figure 39. Injector Demonstration Test Setup

Also incorporated in the pipe (but not shown in Figure 39) was an injector support to insure that if excessive injector heating occurred, the injector would not droop and possibly ruin the test apparatus.

Two thermocouples were embedded in the injector tip and three more were situated in a rake parallel to the injector axis in the vicinity of the injector tip. Also situated in the vicinity of the injector tip was a 3-inch (.0762 M) diameter Pyrex viewing window through which high speed motion pictures at 250 pictures/second were taken with a Milliken Model 5 camera. This framing rate allowed 60 seconds of film time with the 400 foot (122 M) magazine. The high speed motion pictures and the thermocouple rake were used to determine the flame location during the cycling of the GF_2 flow.

The GF_2 supply system was designed for use in the Thor tank tests, and the same GF_2 supply complex was used for both the injector demonstration tests and for the Thor tank tests. The GF_2 supply system is described below in the section on Test Facility Design.

An overall view of the injector test facility is shown in Figure 40. The injector valve complex was mounted on the heavy flange at the right end of the large steel pipe. The GF_2 supply system, barricade, and prevalve was to the left of the test apparatus. The LH_2 trailer was situated in the right background, and the LH_2 entered the test apparatus through the insulated pipe from the right.

The injector valve complex is illustrated in Figure 41. The injector valve is oriented horizontally in the center of the picture. GF_2 flow entered the valve through the vertical stainless-steel line, and then entered the injector to the left of the valve. The IR detector was situated above the injector. The LH_2 flow entered the bottom of the test pipe through the lower insulated line. The other valves seen in Figure 41 are the injector valve emergency shutdown valve, and the GF_2 line purge valve.

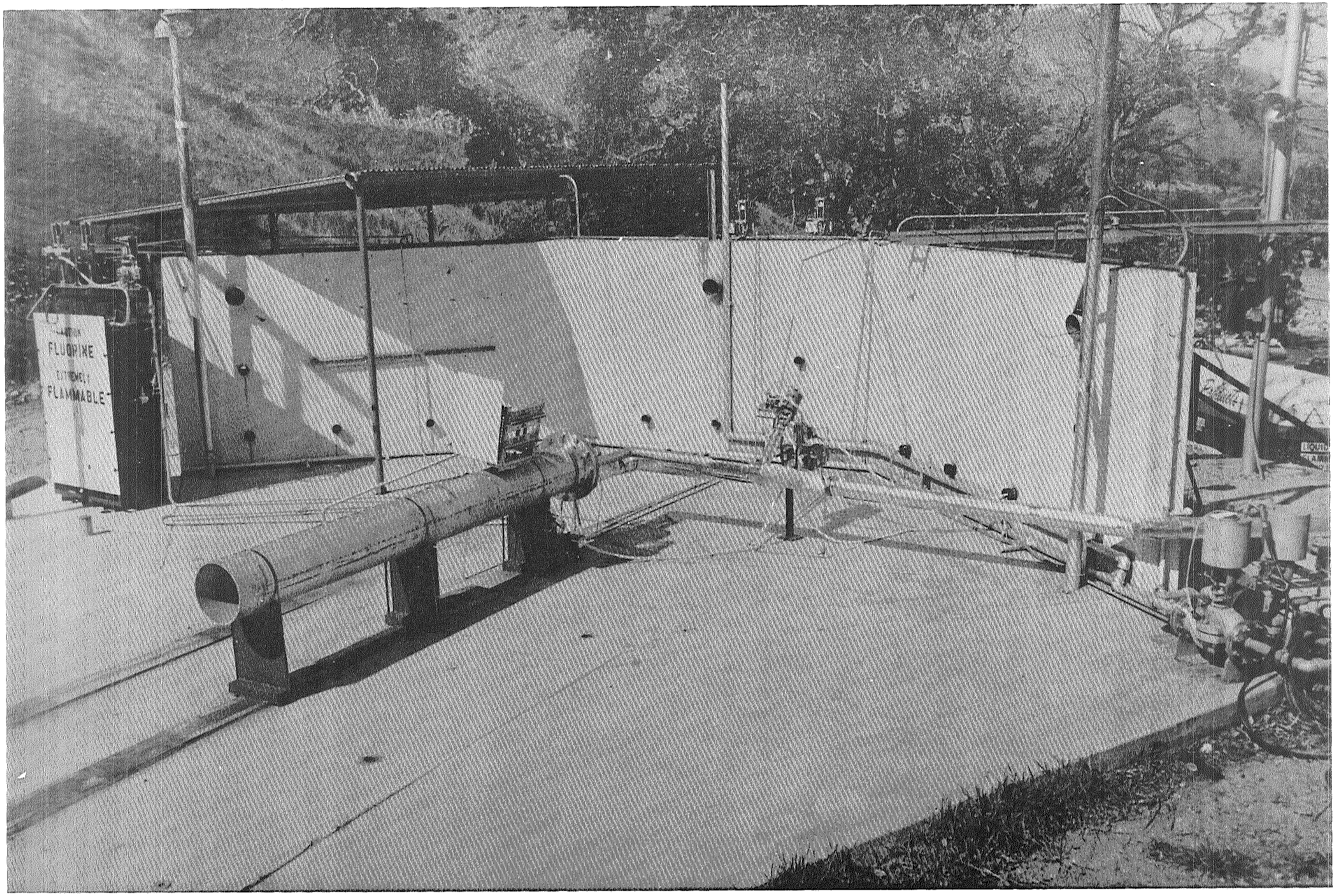

Figure 40. Overall View of Injector Test Facility

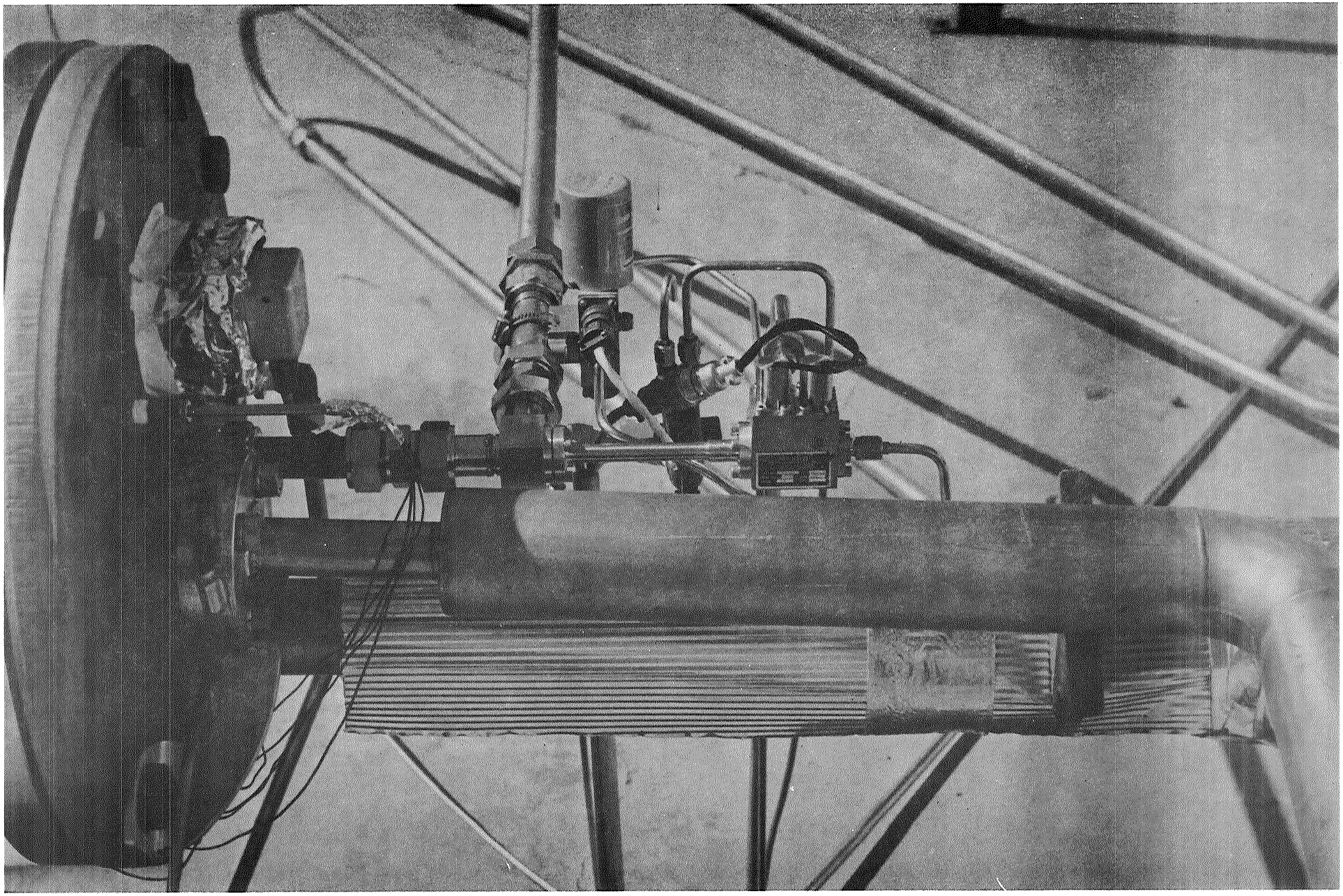

Figure 41. Injector Valve Complex

The test conditions used for the timer cycles in the injector tests were determined based on the control system response analysis mentioned previously. The conditions are:

- Test 1 - Straight pipe; ON: 0.1 sec, OFF: 0.9 sec for a duration of 60 sec.
- Test 2 - Straight pipe; ON: 1.6 sec, OFF: 1.0 sec for a duration of 60 sec.
- Test 3 - Tube-bundle diffuser; the most severe of the above 2 conditions for 40 sec, the least severe for the remaining 20 sec.
- Test 4 - Showerhead diffuser; the same as Test 3, but modified by the results of Test 3.

The ON-OFF times shown represented the limiting cases predicted for the Thor tank (nearly full and nearly empty) and were expected to fully test the capabilities of the injector, injector valve, injector control system, and IR ignition detector.

The general procedure for the injector tests was to supply GF_2 up to the prevalve and injector valve, purge the test apparatus, and initiate LH_2 flow to the test apparatus. The thermocouples near the injector were observed on the oscillograph to verify that they dropped to LH_2 temperature. The large hydrogen vapor cloud coming out the open end of the test apparatus was observed from the blockhouse window and the existence of LH_2 at the test apparatus outlet could be determined visually. At this point, a countdown from 5 was performed: On 3, the movie camera was started; on 2, the oscillograph paper speed was increased to 4 in/sec (.102 M/sec); on FIRE, the SEQUENCE START switch was actuated. From then on through the approximately 60 second test, the control system automatically actuated the injector valve, while the thermocouple traces were observed on the oscillograph. A typical oscillograph record is shown in Figure 42.

The detailed results of the test series are shown in Table 4.

The high speed movies of the first test (at 250 pictures/second) were taken with a 72° (1.26 radian) shutter at an opening of f5.6 which gave slightly under-exposed pictures: All subsequent movies were with a 160° (2.79 radian) shutter at f4.0 which gave excellent results. The movies gave excellent pictures of the flame front, which was blue-white, long (extending out of view), attached to the injector, and resembled a Bunsen-burner flame. The flame pulsed at

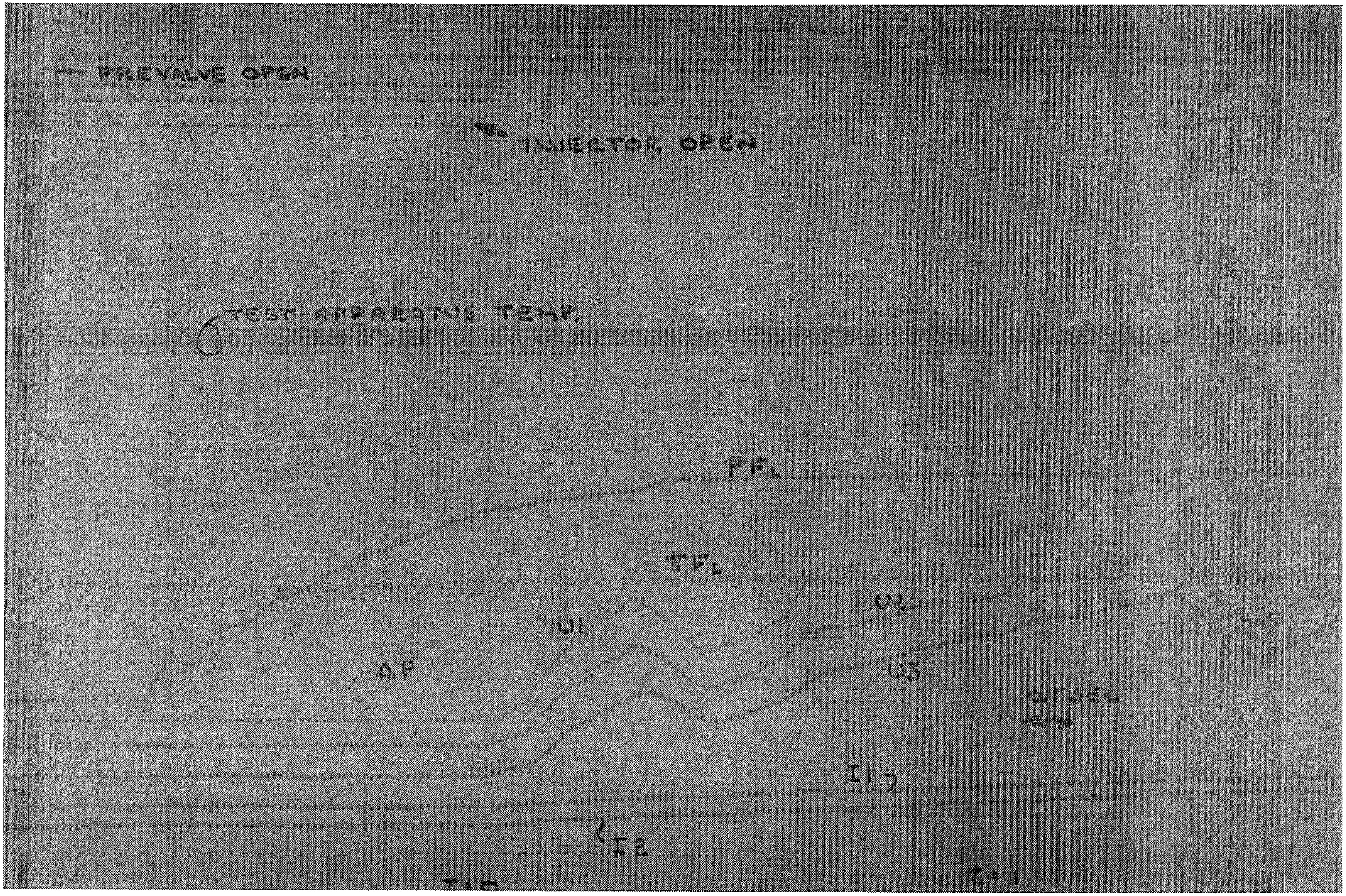

FIGURE 42. OSCILLOGRAPH RECORD - TEST 1

Table 4

INJECTOR DEMONSTRATION TEST SUMMARY

Injector Type	Cycle Conditions	Maximum Injector Temperature	Remarks
Straight Pipe	0.9 sec ON; 0.1 sec OFF* for 64 seconds	617°F (600°K)	*This was a much more severe test than the nominal cycle of 0.1 sec ON; 0.9 OFF. (Caused by operator error) yet there was no injector damage.
Straight Pipe	8.0 sec ON continuously then 1.6 sec ON; 0.9 sec OFF	109°F (316°K)	Minimum temp. of -420°F (22°K) during OFF cycle. Again no injector damage as shown in Figure 43.
Tube-Bundle Diffuser	15.0 sec ON continuously then 0.1 sec ON; 0.9 sec OFF for 20 sec.	1384°F (1024°K) in 12.4 sec, then to 2600°F (1700°K) in .4 sec	F_2 leakage around the base of the tubes bathed the injector in flame which raised the temperature of the tubes until they ignited in the F_2.
	1.6 sec ON; 0.9 sec OFF for 25 sec.		The injector damage is shown in Figure 44.
Showerhead Diffuser	IR Detector Shutdown of Control System	--	The quartz window of the IR detector was etched by HF, so that ignition could not be "seen." The sensitivity of the detector was increased, which solved the problem.
Showerhead Diffuser	15.0 sec ON continuously then 0.1 sec ON; 0.9 sec OFF for 20 sec.	(532°F)** (551°K)	**Only for 2 cycles: local heating perhaps caused by low injection velocity and flame blowback from organ-pipe pulsing in test apparatus.
	2.0 sec ON; 0.9 sec OFF for 25 sec.	263°F (402°K)	No injector damage.

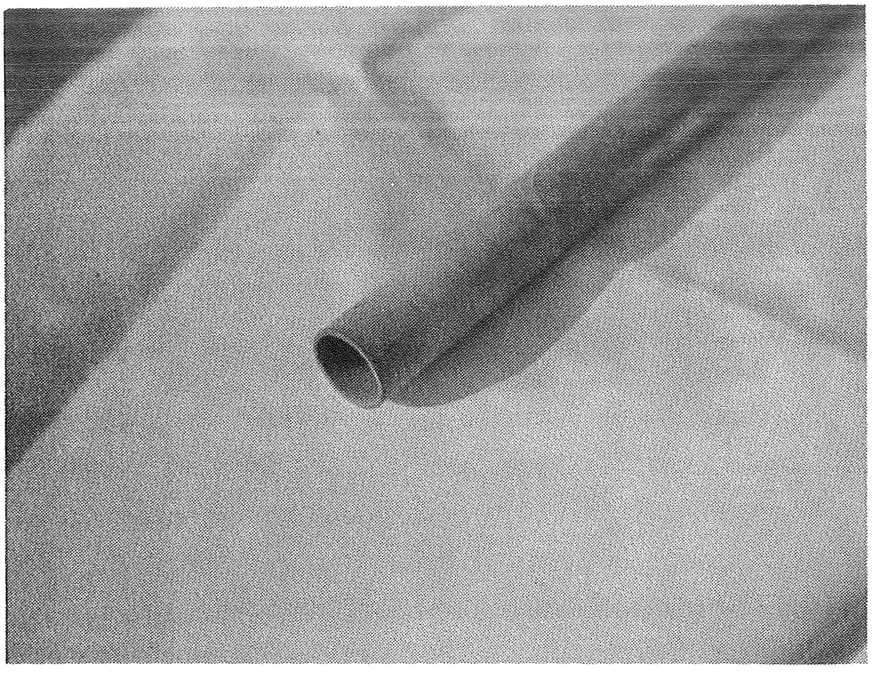

Figure 43. Straight Pipe Injector After Test 2

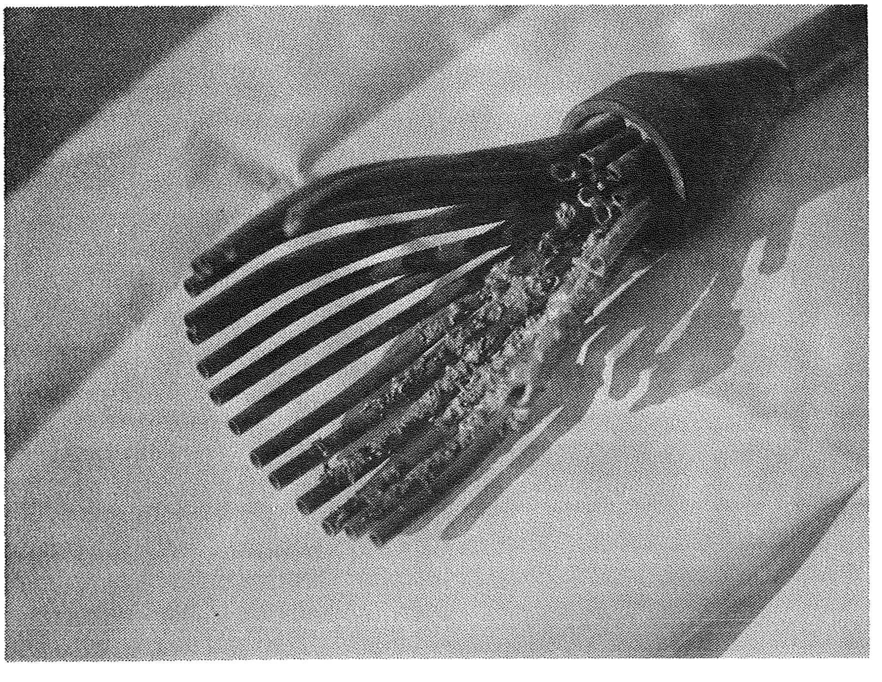

Figure 44. Tube-Bundle Diffuser Injector After Test 3

about 50 cycles/sec: this phenomenon was noted in each of the tests, regardless of the injector configuration or injectant velocity, and was attributed to an organ-pipe effect in the 10-foot (3.0 M) long test apparatus. It was observed that there apparently was considerable particulate matter being burned in the flame, which manifested itself as bright orange streaks. It is believed that the alternate cooling and heating cycles in the injector may have flaked off bits of the copper-fluoride passivation coating, which then burned in the 7100°F (4200°K) flame. As the tests progressed, the amount of particulate matter diminished noticeably.

The damage to the tube-bundle diffuser was quite severe, as shown in Figure 44. The injector damage could possibly have been averted by welding each tube in place to prevent leakage, but this would have meant a very complicated fabrication procedure combined with an already complex injector. Therefore, the showerhead diffuser was recommended for the Thor tank testing.

The showerhead diffuser injector indicated a temperature rise of 260 + 420 = 680°F (145 + 233 = 378°K) above the local ambient temperature. If the ullage temperature during the showerhead injector testing in the Thor tank were to be limited to 430°F (495°K) (the same temperature as for the straight pipe) the injector temperature could reach 1110°F (873°K), which is well below the theoretical ignition temperature of copper and fluorine (~1500°F) (~1090°K) and also below the recorded temperature at which the tube-bundle diffuser apparently ignited (1380°F) (1023°K). However, because of ullage condition uncertainties, it was recommended that both injectors (straight-tube and showerhead) be instrumented with a thermocouple, and that an injector temperature of about 1000°F (812°K) be a criterion for Thor tank test shutdown, similar to the criterion of an ullage temperature of 430°F (495°K) for the higher temperature diffuser injector Thor tank tests. The destructive leakage in the tube-bundle diffuser suggested that the showerhead diffuser be checked for leakage at the joints by flowing helium through the injector.

The shutdown of Test 4 by the IR detector because of HF etching of the quartz window presented the problem of preventing a similar occurrence in the Thor tank tests. An aluminum-oxide (sapphire) window was obtained since aluminum-oxide is unaffected by HF. The details of the IR detector installation are discussed in the section on experiment results.

There was no evidence of GF_2 injectant freezing during the injector tests, nor was freezing expected.

During the injector demonstration tests, the MTI control system functioned perfectly: the delay between prevalve and injector valve opening was set at 0.8 seconds which allowed sufficient time for injector line pressure to reach GF_2 bottle pressure. The delay between injector valve opening and allowable time for IR sensing before automatic shutdown was set at 0.050 seconds.

The data from the injector demonstration tests indicated that the pressure drop across the fluorine flow-measuring orifice was too low to provide a sufficiently large signal for accurate flow measurement. The orifice was reduced in size and GN_2 flow-calibrated to insure that the GF_2 flowrate would be accurately measured.

Following the injector tests, the injectors to be used in the Thor tank tests were designed. The configuration of the top dome of the Thor test tank is shown in Figure 45. The centerline straight-pipe injector is shown in Figure 46. The offset straight-pipe injector is shown in Figure 47. The configuration of the showerhead diffuser is shown in Figure 48. The only difference between the Thor tank injector configuration and that tested was that the 15° (.262 radian) spread angle was retained, rather than the flow being straightened (see Figure 38). The entire showerhead injector is shown in Figure 49.

Test Apparatus Design

The large scale flight-weight test tank was a Thor missile oxidizer tank. This tank was made of 2014-T6 aluminum, internal waffle-patterned milled to a minimum wall thickness of .050 in. (.00127 M). The tank had a 95.5 in. (2.43 M) inside diameter, a 228 in. (5.8 M) long cylindrical section and 16.8 in. (.427 M) high spherical segment end domes. A foam insulation system was designed and installed. The selected foam was a closed-cell polyurethane foam (Permafoam type CPR385D) with a density of 2 lb/ft^3 (3.2 Kg/M^3) and a thermal conductivity of 0.16 Btu/hr-°R-ft^2/in. (2075 Joule/M-sec-°K). Assuming an external foam temperature of 30°F (272°K), 2-1/2 inches (.0635 M) of this foam should provide a heat flux of about 30 Btu/hr-ft^2 (94.6 watt/M^2). This heat flux into the Thor tank would

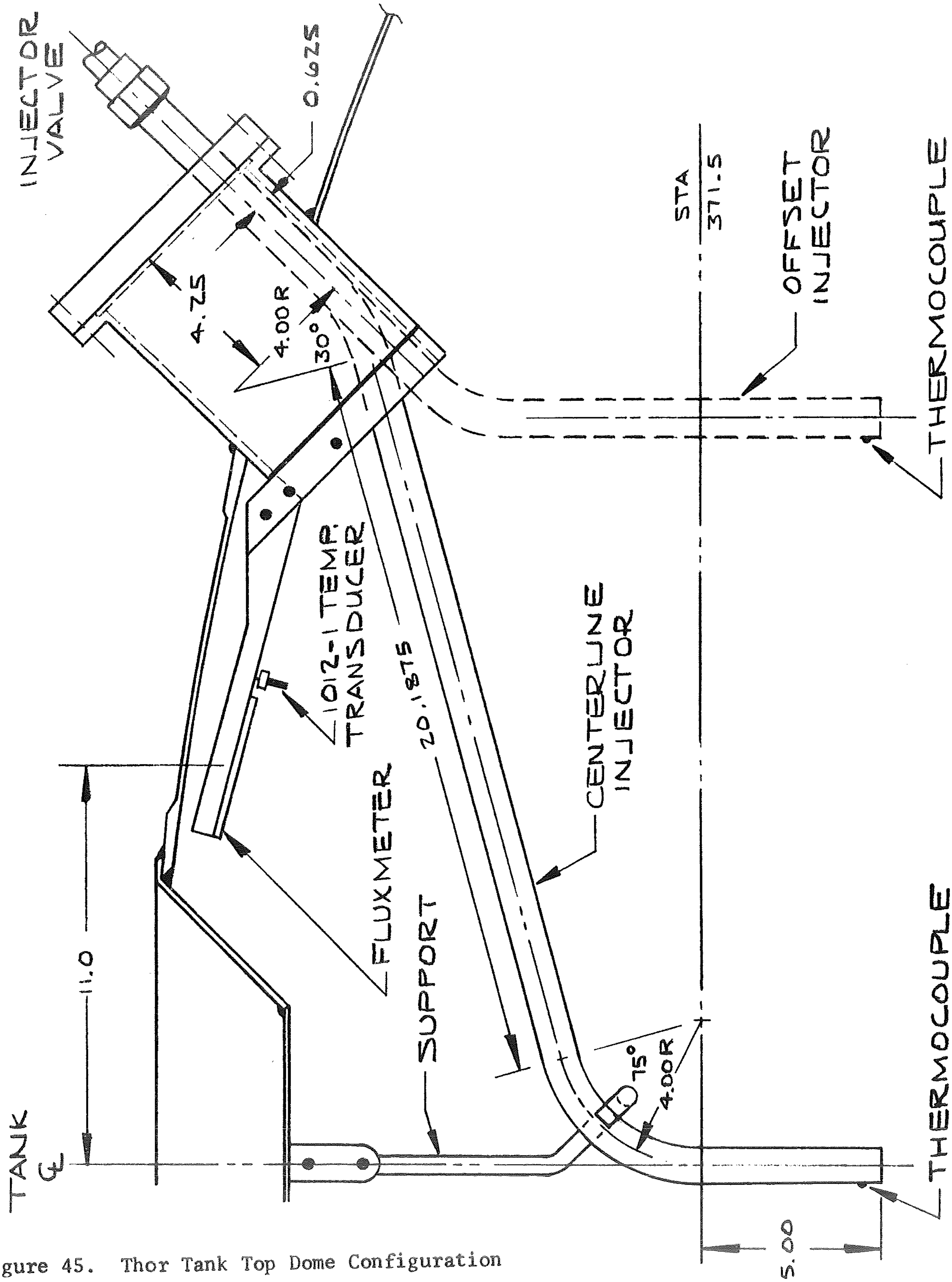

Figure 45. Thor Tank Top Dome Configuration

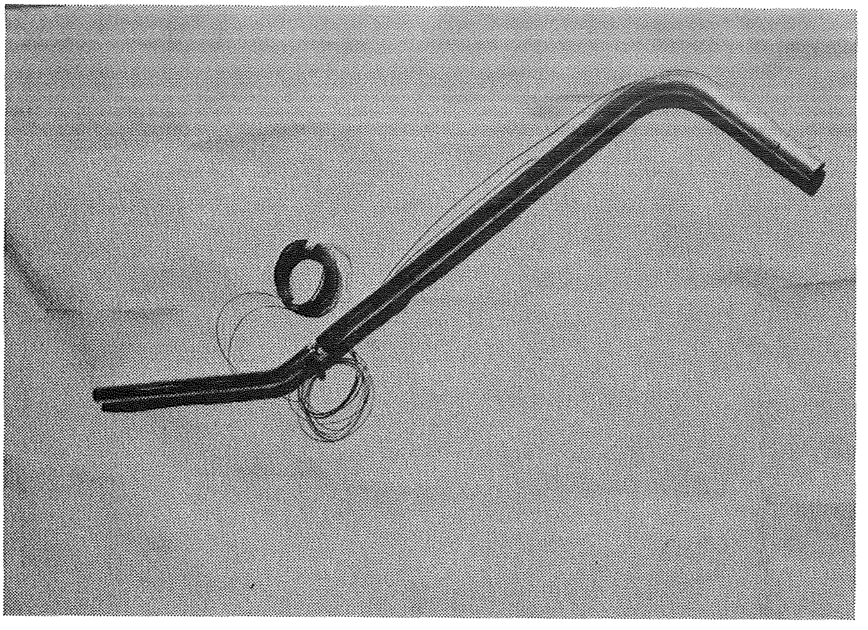

Figure 46. Centerline Straight-Pipe Injector

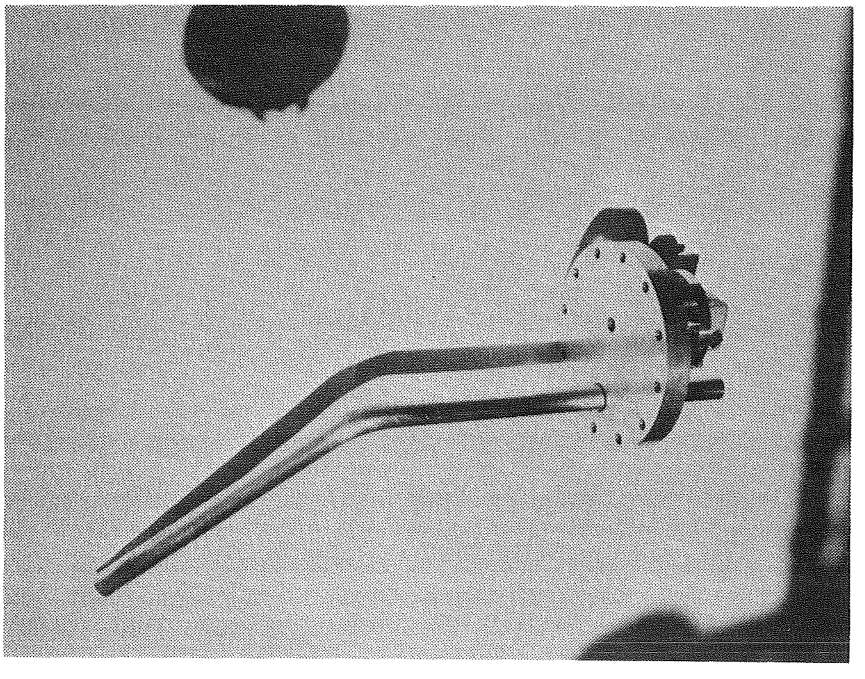

Figure 47. Offset Straight-Pipe Injector

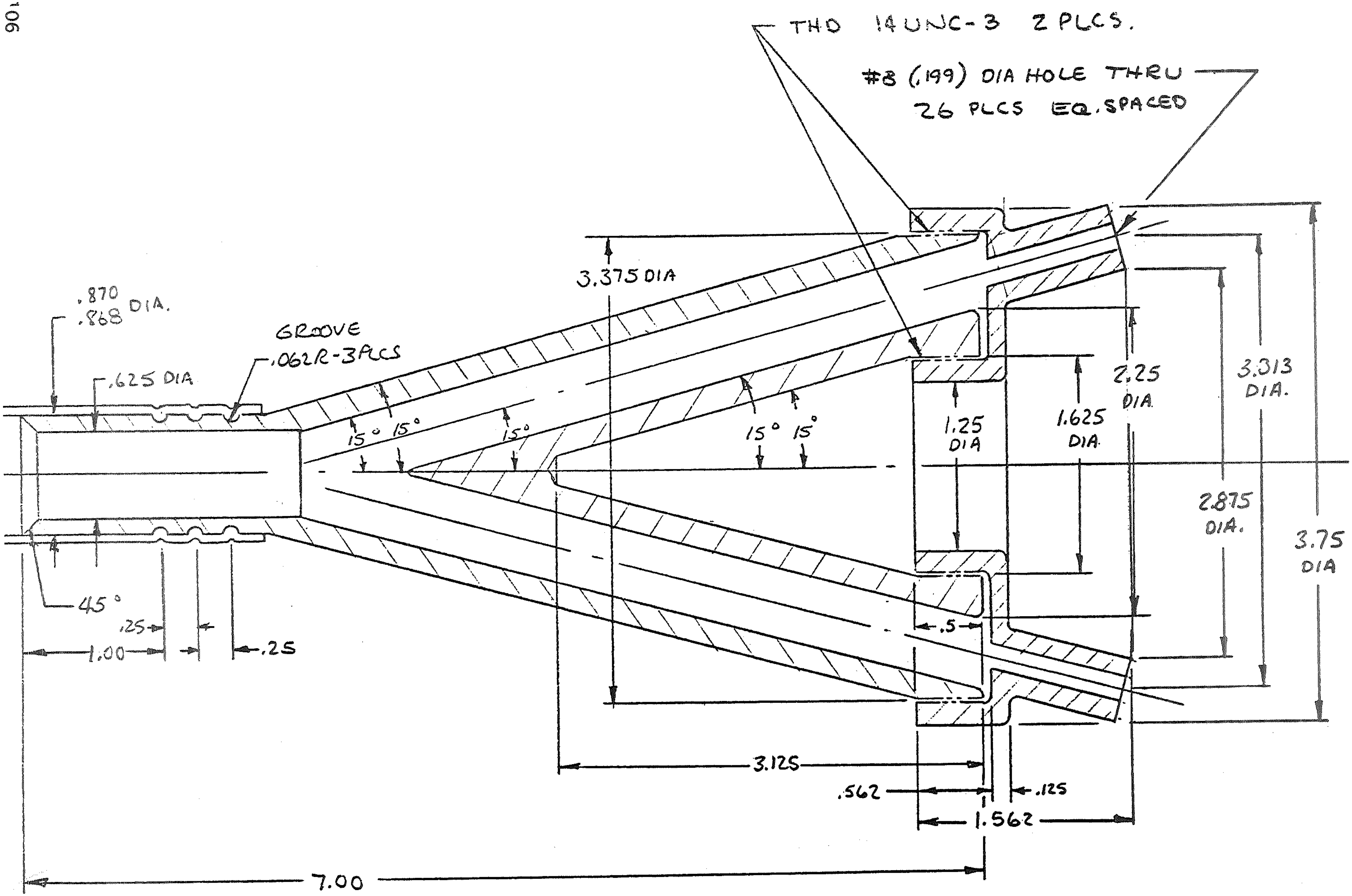

FIGURE 48.
SHOWERHEAD DIFFUSER INJECTOR FOR THOR TANK TESTS

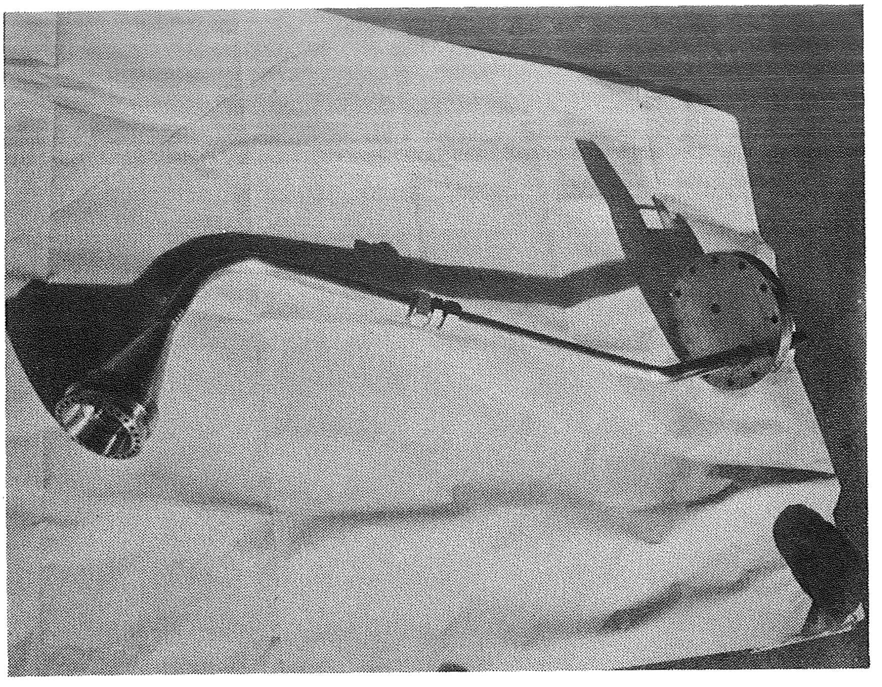

Figure 49. Shower Head Diffuser Injector

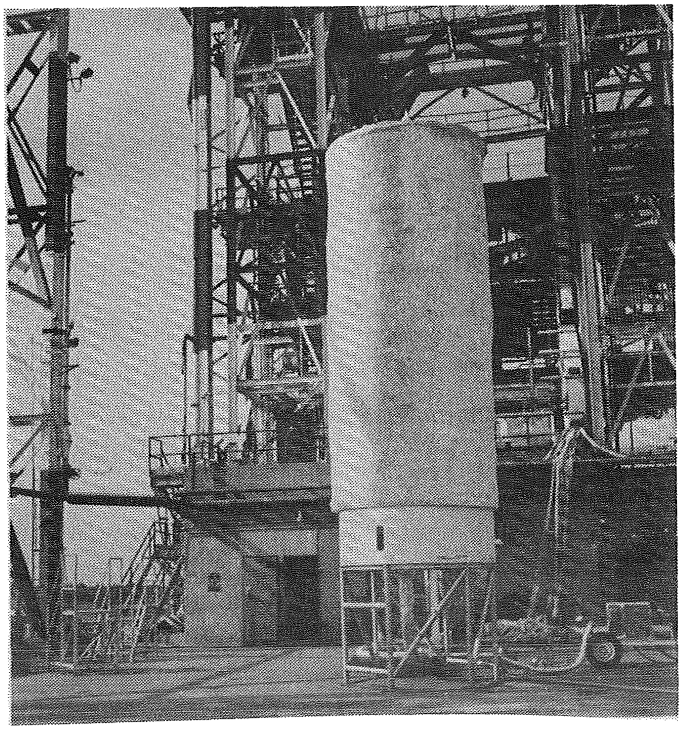

Figure 50. Thor Tank Installed at Alpha-Test Stand I

not result in excessive LH_2 boiloff. The boiloff rate was determined experimentally during testing and the insulation performance is discussed in the section on experimental results.

The tank was solvent-cleaned externally, primed with zinc-chromate primer, foamed to a minimum depth of 2-1/2 inches (.0635 M), and painted with a white vinyl-latex top coat for ultra-violet ray protection. Some small areas of the tank (e.g., access ports, handling fixture rings at the top and bottom domes, pneumatic fittings, etc.) could not be conveniently foamed at the Permafoam facility, and were foamed in place when the tank installation was complete.

Test Facility Design

The foamed Thor tank installed at the Alpha Complex-Test Stand 1 at the Sacramento Test Center (STC) is shown in Figure 50. The Alpha Complex is shown schematically in Figure 51, which also indicates the facility capacities for purge and pressurization gases.

The test apparatus installation was quite complex, as indicated by the facility schematic (Figure 52). The important subsystems making up the test facility are described below.

The GF_2 supply system is found in zones 7-8 of Figure 52. The baseline GF_2 plumbing was selected to be 1-in. (.0254 M) diameter tubing (.93 in. (.0236 M) I.D. - .035 (.00089M) wall) routed from the GF_2 gas cylinders, through the prevalve (PV431-10) to the injector valve (PV431-13). GHe and GN_2 purge valves are also shown (PV431-11, and -9). The GF_2 cylinder hand valves (HV431-1, -2, -3) can be remotely opened. The injector valve complex was essentially as used in the injector demonstration tests and is shown in Figure 53.

A compressible flow analysis indicated that the Fox Injector valve orifice must be increased to .125 in. (.00318 M) to provide sufficient choked flow with essentially cylinder pressure upstream of the valve. Preliminary analysis using the H819 program indicated that 3 cylinders (18 lb (8.16 K_g)) of GF_2 manifolded together would be sufficient to perform the individual Thor tank

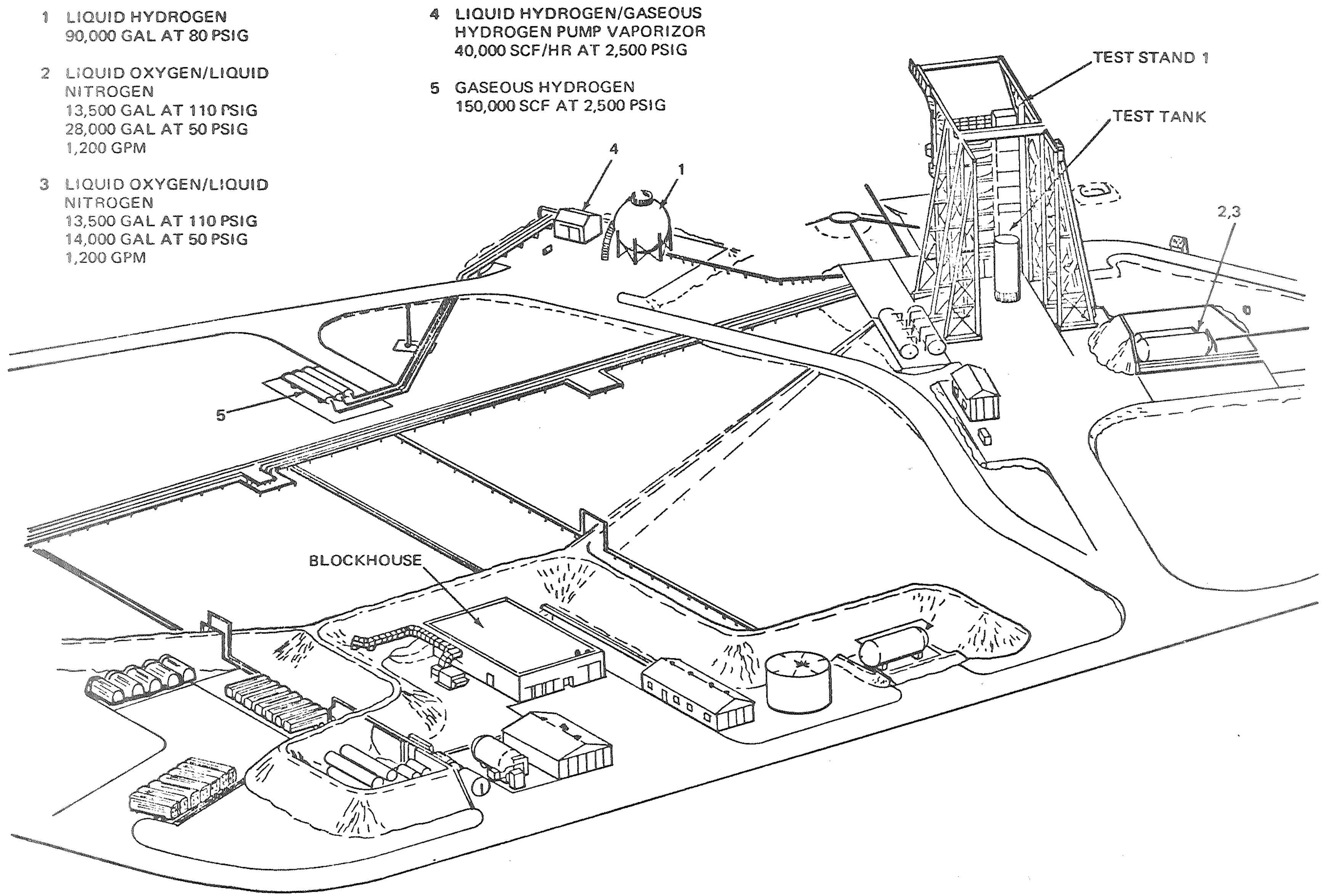

Figure 51 Alpha Complex

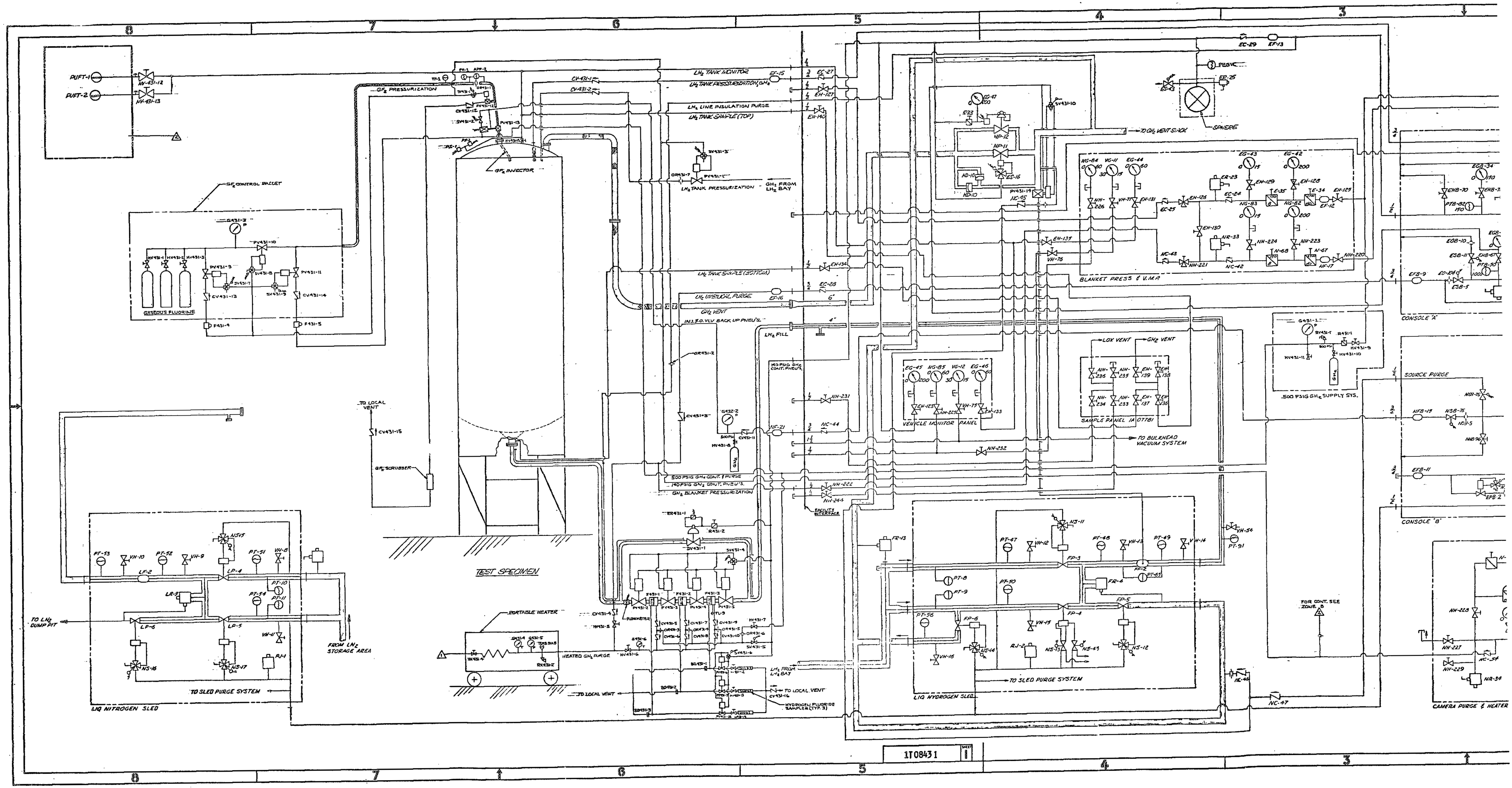

Figure 52. Schematic - MTI Test Facility

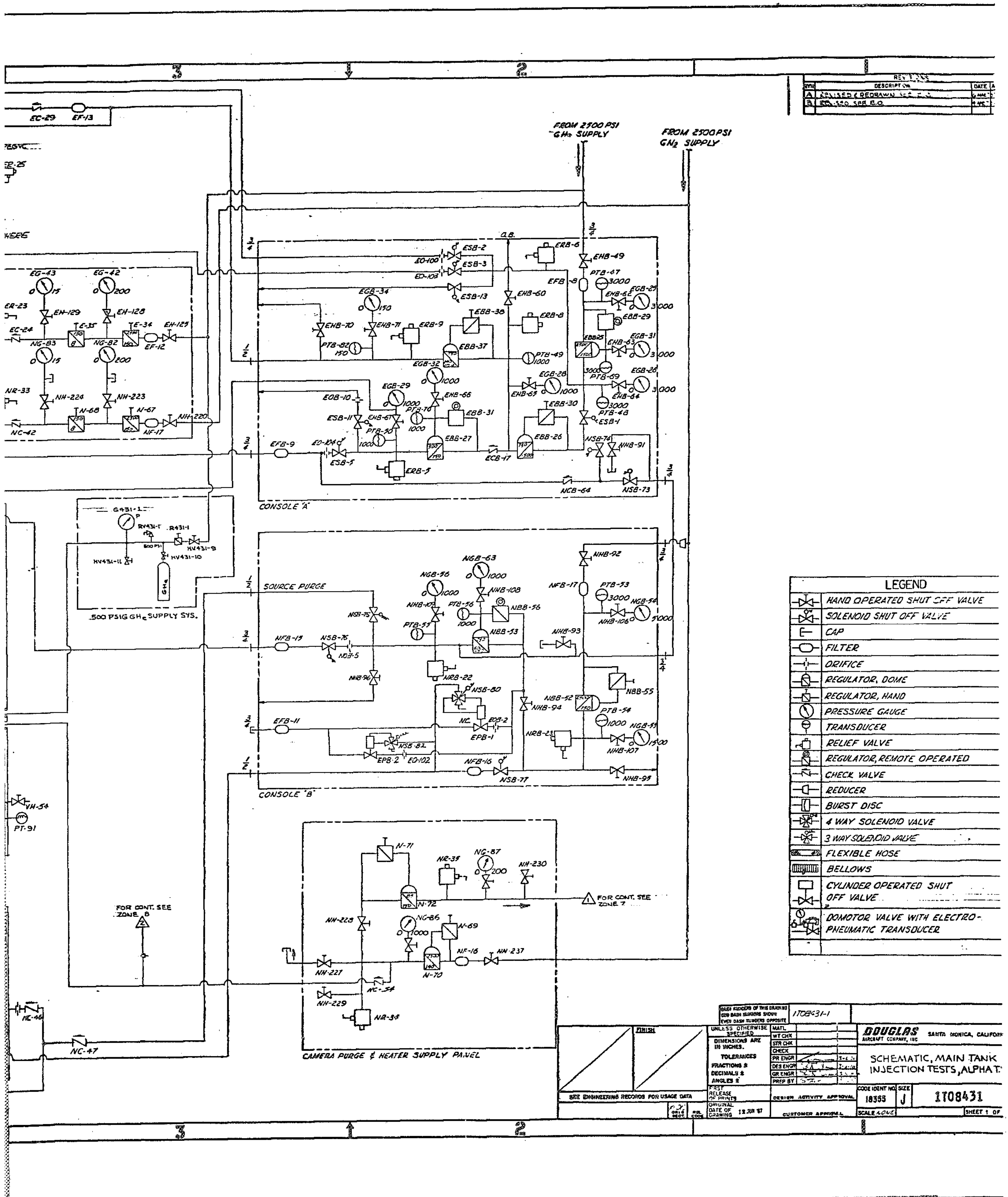
FROM 2500 PSI GHe SUPPLY
FROM 2500 PSI GN2 SUPPLY
CONSOLE 'A'
CONSOLE 'B'
SOURCE PURGE
500 PSIG GHe SUPPLY SYS.
CAMERA PURGE & HEATER SUPPLY PANEL
FOR CONT. SEE ZONE 7
FOR CONT. SEE ZONE 8
LEGEND
HAND OPERATED SHUT OFF VALVE
SOLENOID SHUT OFF VALVE
CAP
FILTER
ORIFICE
REGULATOR, DOME
REGULATOR, HAND
PRESSURE GAUGE
TRANSDUCER
RELIEF VALVE
REGULATOR, REMOTE OPERATED
CHECK VALVE
REDUCER
BURST DISC
4 WAY SOLENOID VALVE
3 WAY SOLENOID VALVE
FLEXIBLE HOSE
BELLOWS
CYLINDER OPERATED SHUT OFF VALVE
DOMOTOR VALVE WITH ELECTRO-PNEUMATIC TRANSDUCER
DOUGLAS
AIRCRAFT COMPANY, INC
SANTA MONICA, CALIFORNIA
SCHEMATIC, MAIN TANK INJECTION TESTS, ALPHA T.
18355
J
1T08431
1T08431-1
SEE ENGINEERING RECORDS FOR USAGE DATA
UNLESS OTHERWISE SPECIFIED DIMENSIONS ARE IN INCHES.
TOLERANCES
FRACTIONS ±
DECIMALS ±
ANGLES ±
DESIGN ACTIVITY APPROVAL
CUSTOMER APPROVAL
SHEET 1 OF

tests. Compressible flow analysis of the complete GF_2 supply system and the results of the injector demonstration tests indicated that the flow capacity of the system would be:

$$\dot{w} = .000211\ P_B \tag{83}$$

where $\dot{w}$ is GF_2 flowrate in lb/sec, and P_B is the GF_2 cylinder pressure in psia. This flow limit was used in the H819 program to evaluate the Thor tank pressurization performance and it appeared that the necessary flow could be achieved for the Thor tank testing. The problem with the supply system was that the F_2 flowrate would decrease during the test run as GF_2 was consumed and cylinder pressure dropped. It would be advantageous to employ a regulator to provide a constant pressure supply to the injector valve, however, no F_2-compatible regulator exists which can provide the high flow capacity needed. Fortunately, the maximum flow requirements for the system often come at the start of the test, (during prepressurization) when the cylinders are full. During hold and outflow, the average F_2 flowrate requirements would be less, since the injector valve would be cycling on and off. The F_2 flow limit meant that the "on" cycle of the valve would get longer as the test progresses. The possibility existed that there could be insufficient GF_2 flow late in the test to keep up with the outflow and heat transfer, and maintain constant tank pressure. This did occur, as is described below in the section on Experimental Results.

The LH_2 fill and outflow system is shown in zones 4, 5, 6, of Figure 52. The LH_2 was filled and emptied from the tank bottom through the main LH_2 outflow valve: a 6-in. (.1524 M) diameter Annin valve with a Domotor operator (DV431-1). This valve could be set at any position from full-open to closed and was used to control the LH_2 outflow rate to preset values. The LH_2 flow was dumped through the facility LH_2 valve complex (sled) and out the 6-in. (.1524 M) diameter facility vent line, where it was burned. The tank GH_2 vent valve was also located in the vicinity of the LH_2 valve sled, with the result that the tank vent line was about 75 ft (22.87 M) long. The tank vent line can be seen in the rear view of the Thor tank in Figure 54. The vent line was supported by the vertical beam which also provided support for all plumbing lines and wiring to the top of the tank; the pressure switches were also mounted at the

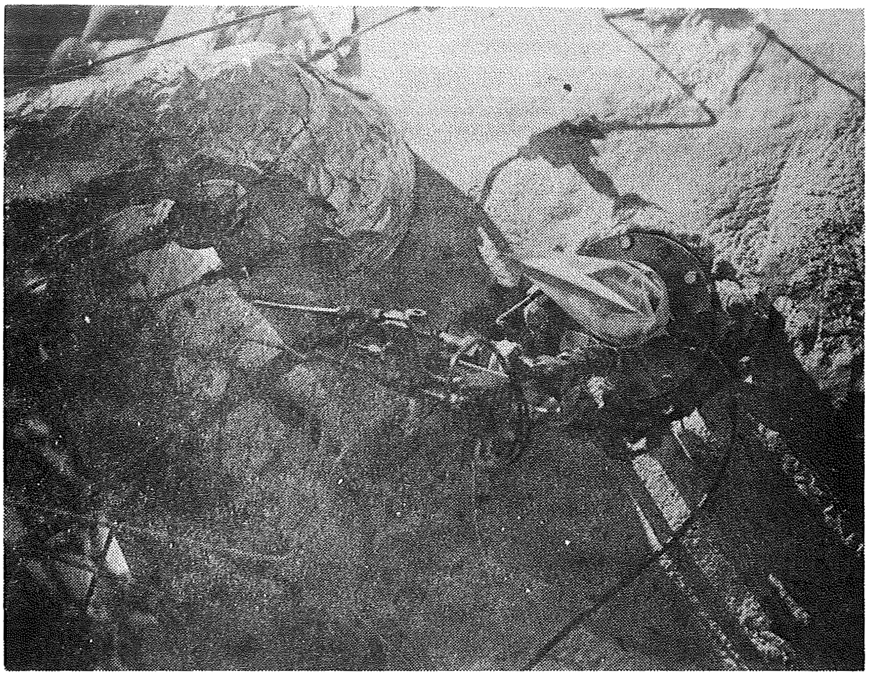

Figure 53. Injector Valve Complex on Thor Tank

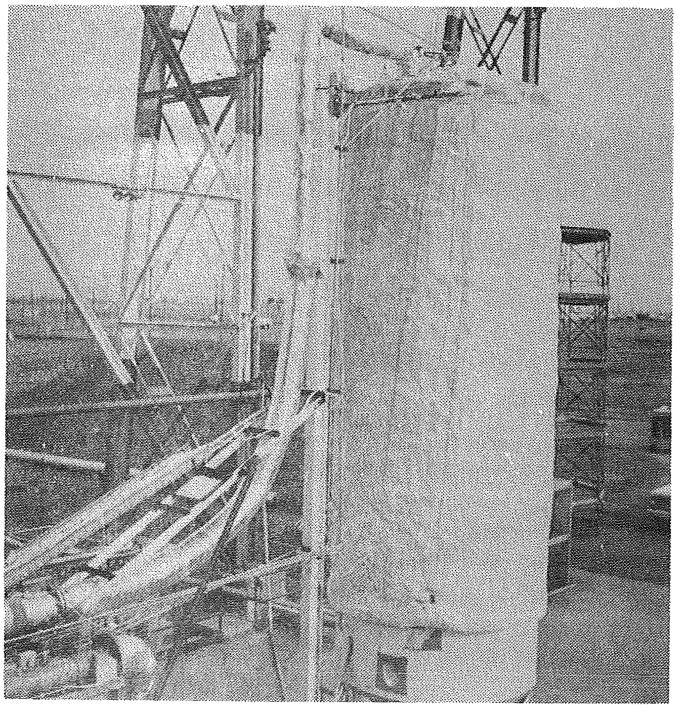

Figure 54. Rear View of Thor Tank Installation

top of the beam. This large vent line contributed 20 ft^3 (.566 M^3) to the tank ullage volume, the effects of which are described below in the Experimental Results section. All cryogenic H_2 lines were batted, wrapped, and helium-purged to resist cryopumping.

The previous MTI work under Contract NAS 3-7963 indicated that the MTI reaction product, HF, tends to condense and freeze in the LH_2 tank. Much of this HF plates out on internal tank surfaces, but a substantial quantity could be dispersed through the bulk LH_2. It was desired to sample the LH_2 outflow following an MTI test to determine the quantity and size distribution of HF contaminant. The HF sampling system is shown schematically in zone 6 of Figure 52 and actually in Figure 55. The sample system consists of three filters in series (100 μ, 30 μ, and 10 μ with an option for 30 μ, 10 μ, and 2 μ) isolated by valves. When a sample was taken, the Domotor valve was closed, and the sample filter isolation valves were opened. Any HF in the LH_2 was presumed to be trapped in the filters, with the relative quantities trapped in each filter presumed to indicate the gross size distribution of the HF particles. The isolation valves were then closed to isolate the HF trapped in each filter. The filters and valves were heated externally and the filters were individually back-purged with hot GN_2 to melt and vaporize the HF and carry it to Sodium Fluoride (NaF) Samplers. Here the HF was trapped for later analysis. Details of the HF sampling and analysis technique, and sample results are described in the section on Experimental Results.

Tank pressurization using GH_2 and helium was also provided. Ambient temperature GH_2 pressurization through another straight-pipe injector was provided to perform tests which compared single-component ullage (H_2) pressurization without reaction to MTI pressurization with reaction. Preliminary system checkout tests and various other tests throughout the test series used ambient GH_2 pressurization, as discussed in more detail in the section on Experimental Results. Also available was Helium pressurization through a diffuser for LH_2 offloading if the situation required.

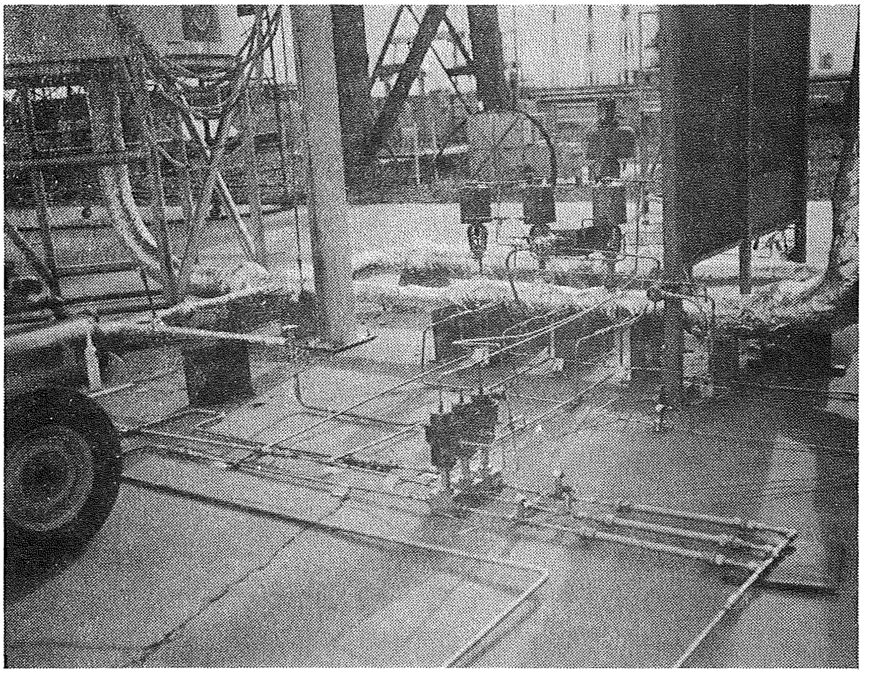

Figure 55. HF Sampling System

As mentioned previously, the NAS 3-7963 work indicated that HF would plate out on the internal tank surfaces. Although frozen HF is not particularly reactive, following MTI pressurization the tank ullage and walls could be warm enough so that the HF is liquid (or the tank could warm up between test days). Liquid anhydrous HF is quite corrosive and could attack the tank material, instrumentation, wiring, etc. A GN_2 hot purge system was designed to purge out and completely warm up the tank to remove HF between test days. The tank was warmed up to about 100°F (311°K) (HF boils at about 65°F (292°K)). The GN_2 heater cart is visible on the left side of Figure 55. The hot purge system worked reasonably well, as discussed later in the section on Experimental Results.

Instrumentation and Data Acquisition Design

The instrumentation and data acquisition equipment used in the test program was quite comprehensive and provided considerable redundancy in parameter measurement. The test tank ullage pressure was measured with two fully redundant Owens Labs type PS-254-3A10-TA (0-50 psia ($0\text{-}345 \times 10^3$ N/M^2)) strain gage pressure transducers. The GF_2 flowrate was measured with a calibrated orifice (.25 in. (.00635 M) diameter)) in the GF_2 flow line just upstream of the injector valve. The GF_2 pressure upstream of the orifice was measured with a Statham type PA347-TC-500-350 (0-500 psia ($0\text{-}3540 \times 10^3$ N/M^2)) and the pressure drop across the orifice with a Statham type PM280-TC-$\pm$5-350 ($\pm$5 psia ($\pm 34.5 \times 10^3$ N/M^2)) strain gage pressure transducers. The GF_2 temperature upstream of the orifice was measured with a Thermal Systems, Inc. type 1080-1 platinum resistance sensor. The GF_2 flowrate was found from the flow orifice equation determined from the GN_2 calibration:

$$\dot{w} = .0428 \left(\frac{P\,\Delta P}{T}\right)^{.5} \qquad (84)$$

where $\dot{w}$ is the GF_2 flowrate in lb/sec, P and T are the upstream orifice pressure in psia and temperature in °R, and ΔP is the orifice pressure drop in psi. The upstream orifice pressure is also essentially GF_2 cylinder pressure and the GF_2 flowrate was cross-checked by observing GF_2 cylinder pressure change. The pressures and GF_2 temperature were recorded (real time) on Minneapolis-Honeywell Electronic 17 Model 1070 Strip Chart recorders. The GF_2 usage during the tests is discussed in detail in the section on Experimental Results.

The location of all thermal sensors (measuring the temperature of the ullage gas, LH_2, and tank wall, and local heat flux) is shown in Figure 56, which is an exploded view from inside the tank. The instruments to measure ullage gas and liquid temperature were mounted on a vertical probe situated at the half-radius of the tank. These platinum resistance sensors were Thermal Systems, Inc., type 1070-1 (1380Ω @ 32°F (273°K)), and were situated at 1-ft. (.305 M) intervals on the probe. Initially two sensors were to be situated on the tank centerline, directly below the injector, however, due to sensor failure prior to testing, TU5 was eliminated. Essentially every third sensor was set to measure LH_2 temperature. These generally coincided with location of the level sensors, and at the basic ullage levels of 5, 50, 90% (stations 384, 492, and 588) the LH_2 temperature platinum sensors provided the reference temperature for the thermopile installations. Seven-element thermopile assemblies were situated on the vertical probe above stations 384, 492 and 588 to determine the initial conditions at the interface (as shown in Figure 57). The thermopile assemblies were configured as shown in Figure 58. Each thermopile element had 6 chromel-constantan junctions (3 at one level and 3 at a level 1-inch (.0254 M) below)) and 2 null junctions of copper-chromel. The lower junctions of each element were level with the upper junctions of the element below, with the lower junctions of the lowest element level with the LH_2 temperature sensor at that station. The thermopiles measure the temperature difference between the junction levels - 1-inch (.0254 M) apart. The thermopile output was recorded on a CEC type 5-119 Oscillograph. Level sensors were also situated on the vertical probe. These were Ohmite "Little Devil" 1KΩ resistors, overdriven to heat up (and change resistance) rapidly when the surrounding medium changed from LH_2 to gas. The level sensors were situated 1-inch (.0254 M) apart at the basic liquid fill levels (95+%, 95%, 50+%, 50%, 10+% and 10%). The initial liquid level was kept between these 1-inch-(.0254 M) apart sensors. The above level sensors, plus level sensors at 80%, 65%, 35%, and 20% liquid levels, were used for LH_2 outflow rate measurement. This technique had been successfully used previously. This outflow rate measurement technique was expected to operate satisfactorily because the tank operates at essentially

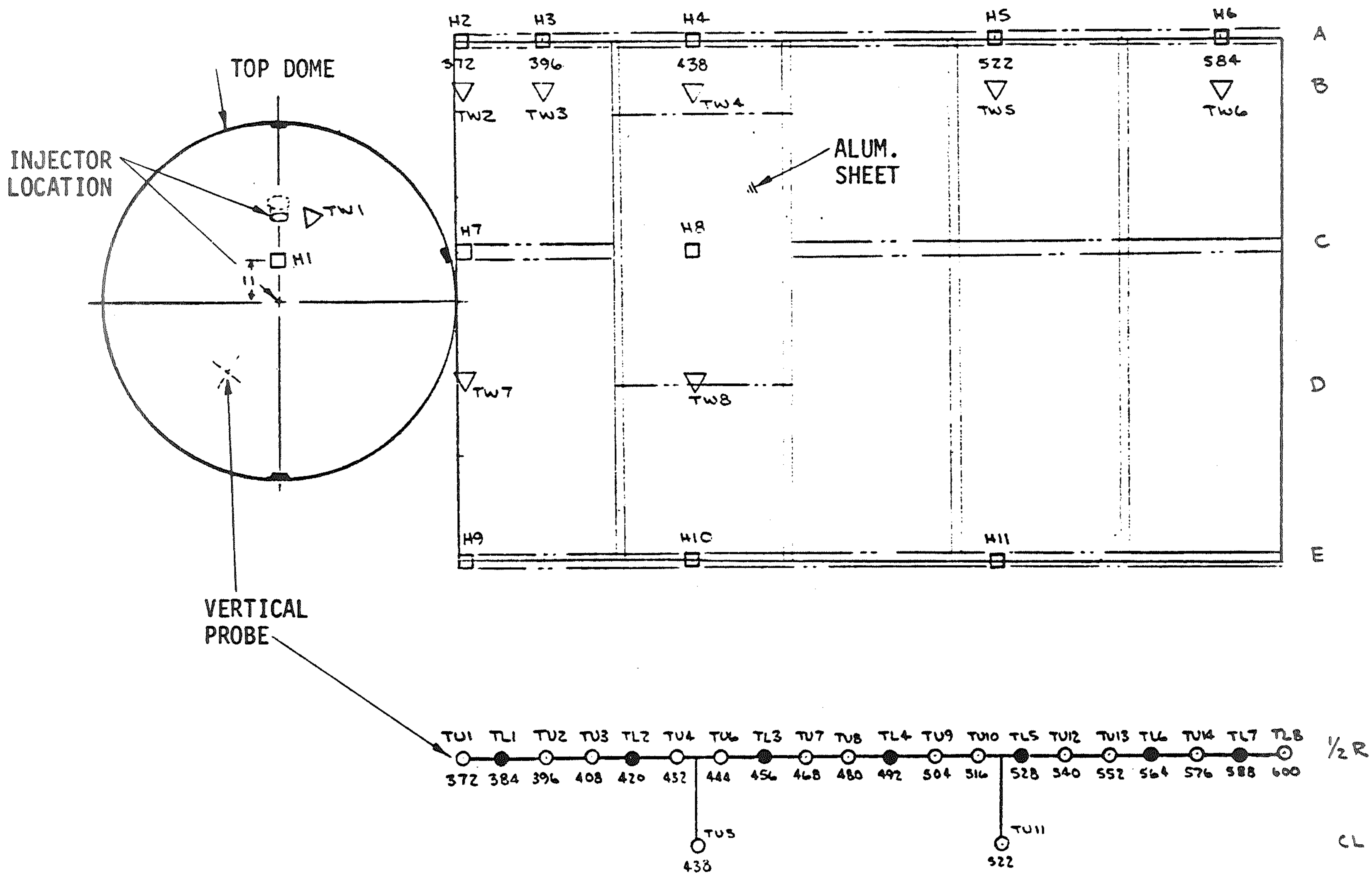

Note: Shaded points indicate level sensor locations.
Numbers indicate stations.

FIGURE 56. THOR TANK INSTRUMENTATION LOCATION AND NOMENCLATURE

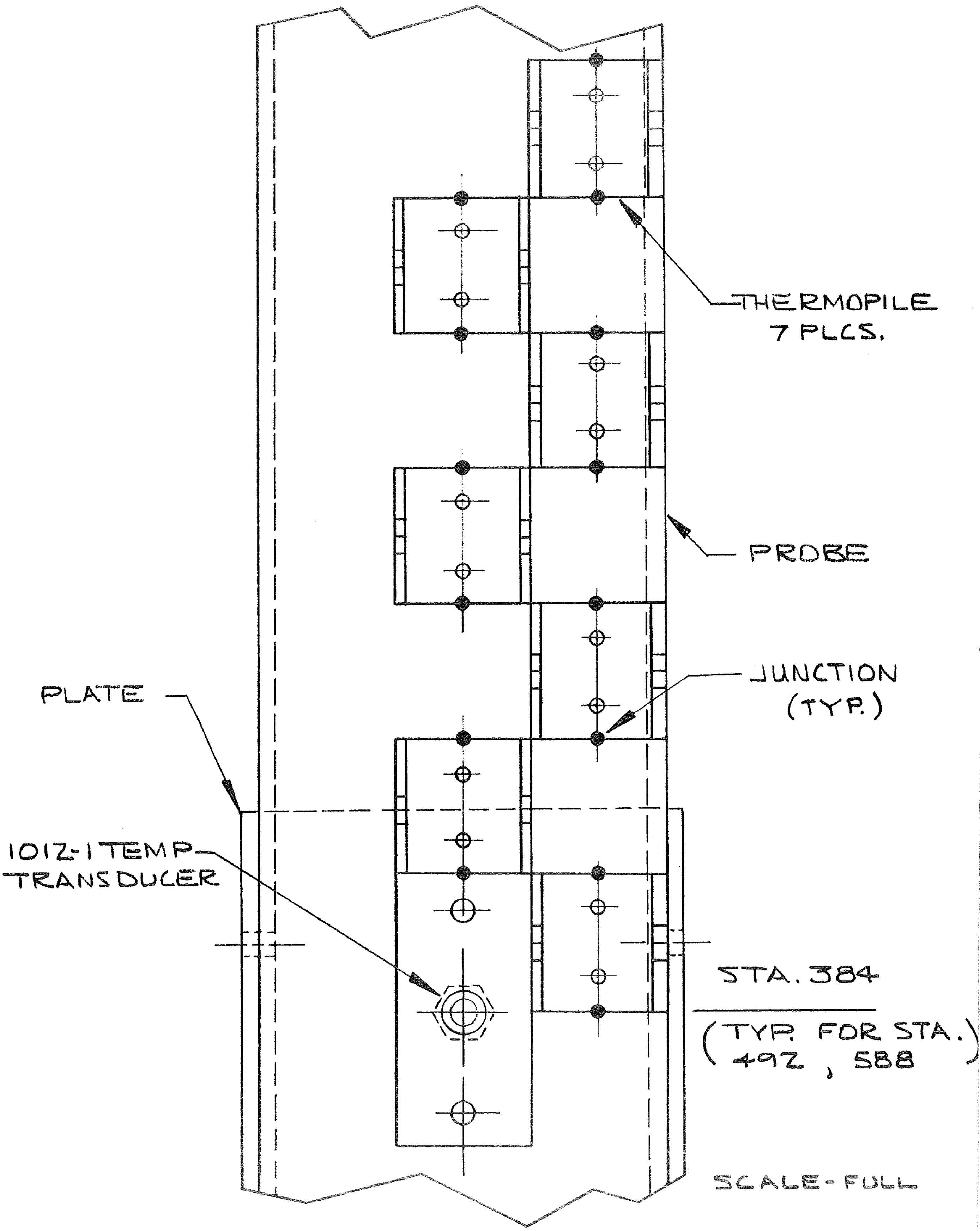

Figure 57. Thermopile Assembly

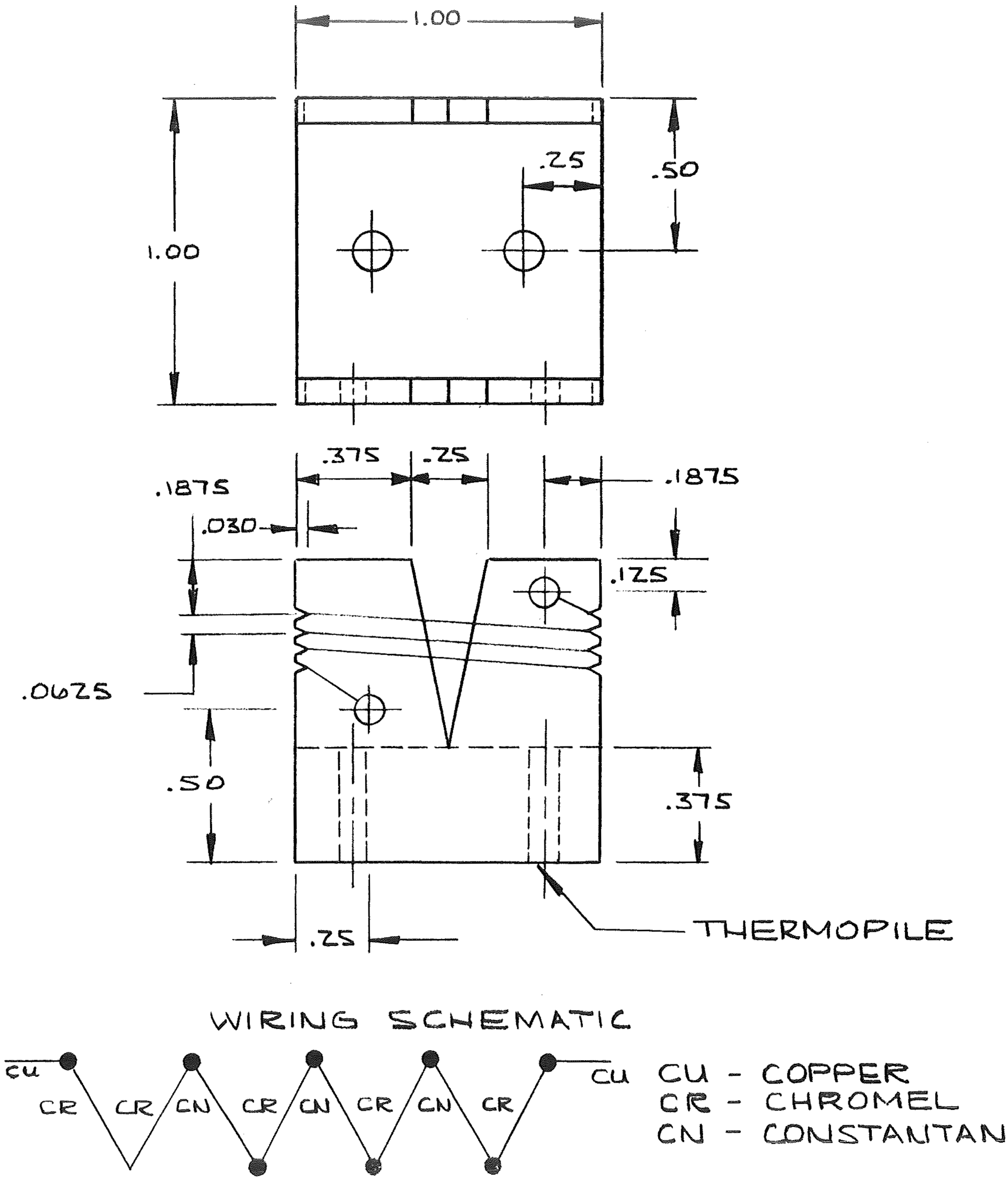

Figure 58. Thermopile Element Detail

constant pressure, exhausting to atmosphere. With a constant resistance outflow line, constant outflow should result; however, due to chilldown of the uninsulated LH_2 vent line (through which the outflow was dumped) the line resistance, and LH_2 flowrate, varied somewhat during the tests, as described below in Experimental Results.

The tank wall temperatures were measured at 8 locations as shown in Figure 56. These platinum resistance sensors were Thermal Systems, Inc., type 5001-19 (500 Ω at 32°F (273°K)) which were bonded to the outside of the tank wall, under the foam insulation.

In order to determine the heat flux and local heat transfer coefficients inside the tank it was originally proposed to use copper flat-plate calorimeters. The heat flux would be determined by measuring the temperature change of the known mass of the calorimeter. However, preliminary tests of the calorimeter installation in LH_2 indicated wide unexplained variations between the measured heat transfer coefficient, and the theoretical free-convection heat transfer coefficient. The basic problem, and probable reason for the data deviation, was that the flat plate calorimeter was apparently not well suited to measure small values of heat flux and h. In these tests with a 1/8 inch (.00318 M) thick calorimeter, the calorimeter temperature slope was about 1°R/sec (.56°K/sec). Even over a time period of 5 sec, the change in calorimeter temperature was only 5°R (2.78°K). An error of 1 or 2°R (.56 or 1.11°K) in evaluating the calorimeter temperature makes a significant error in h, which is directly proportional to this slope. If the calorimeter were made thinner, the calorimeter temperature slope would be larger, and the possible error smaller; however, then the calorimeter would more rapidly approach equilibrium with the surrounding gas, and errors in temperature sensor time constant determination would affect the results. Further the ΔT between the gas and the calorimeter would tend to become smaller, and errors in this ΔT would directly affect the accuracy of h.

Because of this questionable accuracy of the flat plate calorimeter, alternate methods of determining heat flux and h were investigated. A commercially-fabricated thermal flux meter was identified which appeared to be suitable for use in the MTI program. This meter, made by International Thermal Instrument Company, was a polyimide glass plate with plated thermopiles on each surface.

The thermopiles would directly measure the ΔT across the plate and produce a multimillivolt signal proportional to heat flux. These devices were completely compatible with the cryogenic environment and have been used on many LH_2 research programs. The instruments were individually calibrated to an accuracy of 1%. The meters were supplied clad with stainless-steel to protect the glass from HF attack.

These fluxmeters were tested in LH_2 and gave consistent and repeatable data. A typical fluxmeter installation is shown in Figure 59. The fluxmeters were bonded to the aluminum channel with a thin coating of Dow-Corning 731 RTV Silastic. The fluxmeter surface temperature was measured with a Thermal System Inc. type 5001-19 platinum resistance sensor bonded to the front of the fluxmeter with 3M Co. EC3515 epoxy. The gas temperature in the vicinity of the fluxmeter was measured with a Thermal Systems Inc. type 1012-1 platinum resistance sensor. These also provided a comparison to the gas temperature measured at the vertical probe at the tank half-radius. The local heat transfer coefficient would be determined by dividing the heat flux by the temperature difference between the gas and fluxmeter. The fluxmeters were situated in the tank as shown previously in Figure 56. The injector locations in the top dome are shown. A fluxmeter is situated in the dome midway between the injector locations. A tank wall temperature sensor is situated nearby on the outside of the dome. Row A is the tank element closest to the offset injector and in the plane containing the injector and tank centerline. Row A contains a series of 5 fluxmeter installations spread along the tank from top to bottom. Row B is offset from Row A to allow uncovered wall exposed to the ullage gas. This row contains 5 tank wall temperature sensors situated at the same stations as the fluxmeters, but on the outside of the tank wall. Row C is placed so that it is equidistant from the two injector locations and contains 2 more fluxmeters including one mounted on an aluminum sheet to introduce a smooth-walled flow field and detect any difference in heat flux compared to that near a waffle-patterned wall. Row D contains two more external tank wall temperature sensors at the same stations as the fluxmeters in Row C. Row E contains 3 more fluxmeters situated on the opposite side of the tank from Row A (farthest from the offset injector location). The results of the heat transfer measurements are described in the section on Experimental Results.

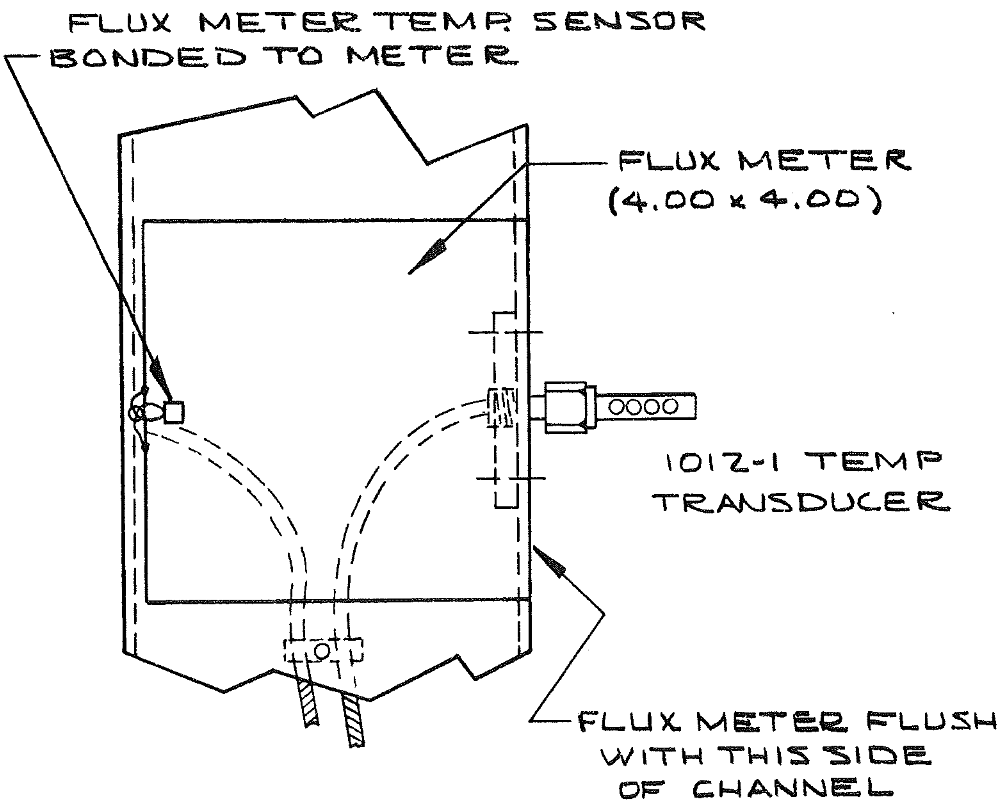

Figure 59. Fluxmeter Installation

Figure 60 shows a view looking upward inside the Thor tank prior to testing and indicates the relative position of the instrumentation in the tank. The centerline straight-pipe injector is shown installed at the top of the tank. The dome fluxmeter installation (HI) is visible behind the injector. The injector thermocouple wire is visible. The injector thermocouple was copper-constantan with the reference junction situated at the bottom of the tank where it was immersed in LH_2 during testing.

The fluxmeter output and temperatures were recorded on either Leeds and Northrup Speedomax H Model 1022 strip-charts, or on the Applied Electronics type 340-700 Pulse Duration Modulation (PDM) system. Sufficient parameters were recorded continuously on the strip-charts to evaluate test results without performing the complete automated data reduction built into the PDM system. The temperature data on strip charts included 3 fluxmeter installations (also recorded on PDM), 3 tank wall temperatures, and essentially every other ullage temperature sensor on the vertical probe.

The complete temperature-related instrumentation list, showing location, function, working range, and data acquisition method is shown in Table 5. Timing pulses were supplied by an Astrodata Model DA112-38 Time Code Generator. The relay energize signals from the MTI Control System were recorded on a Sanborn Model 125 Event Recorder. In the HF sampling system the LH_2 flow during sampling was measured with a Foxborough model 2-81-104 flowmeter and a Waugh Engineering Model 1025, 6, 7 frequency converter.

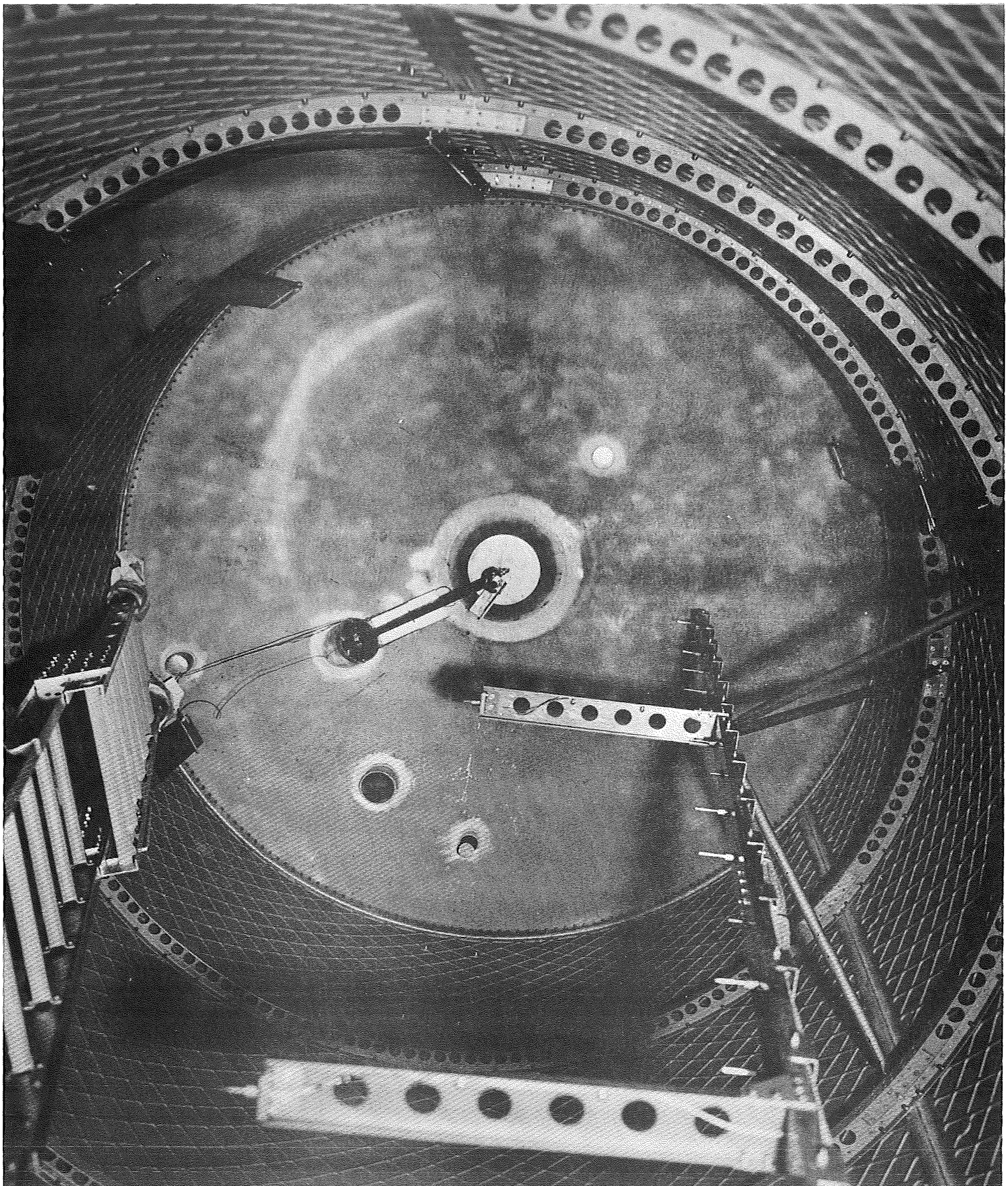

Figure 60. Internal View of Test Tank Instrumentation

Table 5

INSTRUMENTATION DATA

No.	P/N	Location Sta -Row	Function	Range °R (°K)	Wires	Data
H1		Top Dome	Heat Trans Coef			S/C &
TG1	TS1 1012-1		Ullage Gas T.	36-1000 (20-556)	(3)	PDM
TQ1	TS1 5001-19		Flux Meter T.	36-1000 (20-556)	2	
Q1	1T1 "A"		Flux		2	
H2		372-A				
TG2	TS1 1012-1		"	36-1000 (20-556)	(3)	PDM
TQ2	TS1 5001-19		"	36-1000 (20-556)	2	
Q2	1T1 "A"		"		2	
H3		396-A				
TG3	TS1 1012-1		"	36-1000 (20-556)	(3)	S/C &
TQ3	TS1 5001-19		"	36-1000 (20-556)	2	PDM
Q3	1T1 "A"		"		2	
H4		438-A				PDM
TG4	TS1 1012-1		"	36-1000 (20-556)	(3)	
TQ4	TS1 5001-19		"	36-1000 (20-556)	2	
Q4	1T1 "A"		"		2	
H5		522-A				S/C &
TG5	TS1 1012-1		"	36-1000 (20-556)	(3)	PDM
TQ5	TS1 5001-19		"	36-1000 (20-556)	2	
Q5	1T1 "A"		"		2	
H6		584-A				PDM
TG6	TS1 1012-1		"	36-500 (20-278)	(3)	
TQ6	TS1 5001-19		"	36-500 (20-278)	2	
Q6	1T1 "A"		"		2	
H7		372-C				PDM
TG7	TS1 1012-1		"	36-1000 (20-556)	(3)	
TQ7	TS1 5001-19		"	36-1000 (20-556)	2	
Q7	1T1 "A"		"		2	
H8		438-C				PDM
TG8	TS1 1012-1		"	36-1000 (20-556)	(3)	
TQ8	TS1 5001-19		"	36-1000 (20-556)	2	
Q8	1T1 "A"		"		2	
H9		372-E				PDM
TG9	TS1 1012-1		"	36-1000 (20-556)	(3)	
TQ9	TS1 5001-19		"	36-1000 (20-556)	2	
Q9	1T1 "A"		"		2	

Table 5

I.D. No.	P/N	Location Sta -Row	Function	Range °R (°K)	Wires	Data
H10		438-E	Heat Trans Coef			PDM
TG10	TS1 1012-1		Ullage Gas T.	36-1000 (20-556)	(3)	
TQ10	TS1 5001-19		Flux Meter T.	36-1000 (20-556)	2	
Q10	1T1 "A"		Flux		2	
H11		522-E				PDM
TG11	TS1 1012-1		"	36-1000 (20-556)	(3)	
TQ11	TS1 5001-19		"	36-1000 (20-556)	2	
Q11	1T1 "A"		"		2	
TW1	TS1 5001-19	Top Dome	Tank Wall T.	36-700 (20-389)	2	S/C
TW2	TS1 5001-19	372-B		36-700 (20-389)	2	PDM
TW3	TS1 5001-19	396-B		36-700 (20-389)	2	S/C
TW4	TS1 5001-19	438-B		36-700 (20-389)	2	PDM
TW5	TS1 5001-19	522-B		36-700 (20-389)	2	S/C
TW6	TS1 5001-19	584-B		36-700 (20-389)	2	PDM
TW7	TS1 5001-19	372-D		36-700 (20-389)	2	PDM
TW8	TS1 5001-19	438-D	Tank Wall T.	36-700 (20-389)	2	PDM
TU1	TS1 1080-1	372-1/2 R	Ullage Gas T.	36-1000 (20-556)	(3)	S/C
TU2	TS1 1080-1	396-1/2 R		36-1000 (20-556)	(3)	S/C
TU3	TS1 1080-1	408-1/2 R		36-1000 (20-556)	(3)	PDM
TU4	TS1 1080-1	432-1/2 R		36-1000 (20-556)	(3)	S/C
TU5	TS1 1080-1	438-CL		36-1000 (20-556)	(3)	S/C
TU6	TS1 1080-1	444-1/2 R		36-1000 (20-556)	(3)	PDM
TU7	TS1 1080-1	468-1/2 R		36-1000 (20-556)	(3)	S/C
TU8	TS1 1080-1	480-1/2 R		36-1000 (20-556)	(3)	PDM
TU9	TS1 1080-1	504-1/2 R		36-1000 (20-556)	(3)	S/C
TU10	TS1 1080-1	516-1/2 R		36-1000 (20-556)	(3)	PDM
TU11	TS1 1080-1	522-CL		36-1000 (20-556)	(3)	S/C
TU12	TS1 1080-1	540-1/2 R	Ullage Gas T.	36-1000 (20-556)	(3)	S/C

Table 5

I.D. No.	P/N	Location Sta -Row	Function	Range °R (°K)	Wires	Data
TU13	TS1 1080-1	552-1/2 R	Ullage Gas T.	36-1000 (20-556)	(3)	PDM
TU14	TS1 1080-1	476-1/2 R	"	36-500 (20-278)	(3)	PDM
TL1	TS1 1012-1	384-1/2 R	Liquid T.	36-60 (20-33)	(3)	PDM
TL2	TS1 1080-1	420-1/2 R		36-60 (20-33)	(3)	
TL3	TS1 1080-1	456-1/2 R		36-60 (20-33)	(3)	
TL4	TS1 1012-1	492-1/2 R		36-60 (20-33)	(3)	
TL5	TS1 1080-1	528-1/2 R		36-60 (20-33)	(3)	
TL6	TS1 1080-1	564-1/2 R		36-60 (20-33)	(3)	
TL7	TS1 1012-1	588-1/2 R		36-60 (20-33)	(3)	PDM
TL8	TS1 1012-1	600-1/2 R	Liquid T.	36-60 (20-33)	(3)	S/C
TL9	TS1 1012-1	LH2 Outflow Line	LH2 Sample T.	36-60 (20-33)	(3)	S/C
TP11	MDAC Thermopile	384-1/2 R	Interface T.		2	PDM
TP12		383-1/2 R			2	
TP13		382-1/2 R			2	
TP14		381-1/2 R			2	
TP15		380-1/2 R			2	
TP16		379-1/2 R			2	
TP17		378-1/2 R			2	
TP21	"	492-1/2 R			2	
TP22		491-1/2 R			2	
TP23		490-1/2 R			2	
TP24		489-1/2 R			2	
TP25		488-1/2 R	Interface T.		2	PDM

Table 5

I.D. No.	P/N	Location Sta -Row	Function	Range °R (°K)	Wires	Data	
TP26	MDAC Thermopile	487-1/2 R	Interface T.		2	PDM	
TP27		486-1/2 R			2		
TP31		588-1/2 R			2		
TP32		587-1/2 R			2		
TP33		586-1/2 R			2		
TP34		585-1/2 R			2		
TP35		584-1/2 R			2		
TP36		583-1/2 R			2		
TP37		582-1/2 R	Interface T.		2	PDM	
LL1	Ohmite Res	383-1/2 R	Liquid Level		2	S/C	*
LL2		384-1/2 R			2		
LL3		420-1/2 R			2		
LL4		456-1/2 R			2		
LL5		491-1/2 R			2		
LL6		492-1/2 R			2		
LL7		528-1/2 R			2		
LL8		564-1/2 R			2		
LL9		587-1/2 R			2		
LL10	Ohmite Res	588-1/2 R	Liquid Level		2	S/C	*
TF1	TS1 1080-1	F_2 Line	GF_2 Temperature	400-550 (222-305)	3	S/C	

* No Calibration Required.

EXPERIMENTAL RESULTS

Test Program Planning

The original test plan was a matrix allowing examination of the effects of a number of variables on the MTI pressurization process: injector configuration, initial ullage volume and condition, GF_2 injection flowrate and velocity, LH_2 outflow rate, tank pressure, and test cycle (prepressurization, hold, and expulsion. Three GF_2 injector configurations were tested in the large tank test program: the straight pipe centerline, the straight pipe offset, and the diffuser centerline. The straight pipe injector located on the tank centerline is the conventional configuration for an MTI pressurization system and was used with the most extensive range of test conditions. The straight pipe injector at the offset location provided a variation in the injector-wall distance which was thought to simulate a range of different tank configurations; the influence of the injector-wall distance on gas-wall heat transfer rates was of primary interest in these tests. The diffuser injector would tend to suppress the penetration of the GF_2 injectant into the GH_2 ullage; its behavior was of general interest in the verification of the MTI model and performance.

The major test parameters were the ullage volume (90, 50, and 5%), and the GF_2 injector inlet velocity (controlled by the GF_2 bottle pressure). Two basic tank pressures of 43 psia ($296 \times 10^3 N/M^2$) and 24 psia ($165 \times 10^3 N/M^2$) were utilized, and controlled, to some degree, the LH_2 outflow rate (5 (2.27) and 15 lb/sec (6.81 Kg/sec)), since 15 lb/sec (6.81 Kg/sec) could not be achieved with 24 psia ($165 \times 10^3 N/M^2$) tank pressure.

The MTI pressurization test plan is shown in Table 6. Prior to the GF_2 hot firing tests, a short series of checkout tests was performed using ambient (500°R (278°K)) gaseous hydrogen as pressurant; other GH_2 tests were run during the MTI test series when IR detector problems shut down a MTI test. These tests verified the operation of all instrumentation and valves as well as the general operating procedures for fill and drain, purging, etc. In addition, the test data (temperatures, pressures, GH_2 and LH_2 flowrates) obtained during these runs

Table 6

MTI PRESSURIZATION TEST PLAN

Baseline Tests Using GH_2 For Pressurization

Test No.	Injector	Initial Ullage	LH_2 Flow Rate (lb/sec)	(kg/sec)	Operating Mode
1	Straight-pipe	5%	5	2.3	C
2	Straight-pipe	50%	5	2.3	D
3	Straight-pipe	5%	15	6.8	B
4	Straight-pipe	50%	15	6.8	B

MTI Pressurization Tests

Test No.	Injector/ Location	Initial Ullage	LH_2 Flow Rate (lb/sec)	(kg/sec)	Tank Pressure (psia)	(10^3 N/M^2)	Initial GF_2 Pressure (psia)	(10^3 N/M^2)	Initial GF_2 Wt (lb)	(kg)	Operating Mode
1	Straight Pipe-- Centerline	50%	15	6.8	43	296	362	2497	17.4	7.9	A
2	Straight Pipe-- Centerline	50%	15	6.8	43	296	305	2103	17.4	7.9	A
3	Straight Pipe-- Centerline	90%	15	6.8	43	296	350	2414	17.0	7.7	A
4	Straight Pipe-- Centerline	5%	15	6.8	43	296	208	1434	17.0	7.7	B
5	Straight Pipe-- Centerline	5%	15	6.8	43	296	358	2468	17.2	7.8	C'
6	Straight Pipe-- Centerline	50%	15	6.8	43	296	262	1807	17.2	7.8	D
7	Straight Pipe-- Centerline	5%	5	2.3	24	165	368	2538	15.8	7.2	B
8	Straight Pipe-- Offset	50%	15	6.8	43	296	379	2614	13.4	6.1	B
9	Straight Pipe-- Offset	5%	15	6.8	43	296	313	2158	13.3	6.0	B
10	Straight Pipe-- Offset	50%	15	6.8	43	296	292	2014	13.3	6.0	B
11	Straight Pipe-- Offset	90%	5	2.3	24	165	200	1379	13.3	6.0	B
12	Straight Pipe-- Offset	5%	5	2.3	24	165	365	2517	17.3	7.9	C
13	Straight Pipe-- Offset	50%	5	2.3	24	165	345	2379	17.3	7.9	D
14	Straight Pipe-- Offset	50%	5	2.3	24	165	298	2054	17.3	7.9	B
15	Diffuser-- Centerline	50%	15	6.8	43	296	318	2193	7.6	3.5	B
16	Diffuser-- Centerline	5%	15	6.8	43	296	303	2089	10.7	4.9	C
17	Diffuser-- Centerline	50%	5	2.3	43	296	164	1131	10.7	4.9	D

Legend

Operating Modes

A — Prepressurize to nominal tank pressure (NTP), hold at NTP with no outflow for 60 seconds, then outflow LH_2 at the prescribed constant rate until liquid is completely expelled.

B — Prepressurize to NTP and immediately begin LH_2 outflow, continuing to complete expulsion.

C — Prepressurize to NTP, immediately begin outflow but continue only to the 50% ullage level; shut down GF_2 supply and allow tank pressure to collapse and stabilize.

C' — The same as C, but with a 60 second hold following prepressurization.

D — Begin test run with the warm ullage from the previous partial expulsion (Mode C); prepressurize to NTP, immediately begin outflow and continue to complete expulsion.

for a large scale tank using a straight pipe GH_2 injector were expected to be used to correlate with the jet penetration, interface heat transfer and gas-wall heat transfer models for the simpler one-component ullage (pure hydrogen) case. These model correlations for the one-component ullage case without the complications of the MTI flame were expected to aid in the development of the MTI analysis, however, the results of these tests were not usable. The ambient temperature ($520^oR(289^oK)$) GH_2 pressurization gas was injected through a 1-inch (.254 M) diameter straight-pipe injector to simulate the MTI injector dimensions (since an injector to simulate the MTI injector velocity could not be accommodated through available ports in the tank dome). Reasonably rapid prepressurization times (~80 sec) required a GH_2 flow rate of about .125 lb/sec (0.57 Kg/sec) which gave near-sonic injection velocity. This high velocity essentially homogenized the tank contents and resulted in a maximum measured tank internal temperature of 54^oR (30^oK).

For the MTI test series shown in Table 6, one, two, or three expulsions were run with each set of GF_2 bottles. The subsequent tests run with the partially emptied bottles provided the variation in the GF_2 injector inlet velocity. Table 6 gives the actual weight of GF_2 in the supply bottles at the start of each test group and the GF_2 pressure at the start of each test which is an indication of the resulting variation of the GF_2 inlet velocity. The operating modes provide for a hold period (at operating pressure) after the pre-pressurization, expulsion starting directly after prepressurization with no hold period, both complete and partial expulsions, and prepressurization of an initially warm as well as cold (LH_2 temperature) ullage.

Because of the complexity of the test facility, the test procedure (countdown) was also necessarily complex, long (125 pages), and detailed. The major tasks are shown in Table 7. One of the more important tasks was task 4, in which the various elements of the MTI control system were functionally checked out. It was verified that lack of IR signal would terminate injection, that with an IR signal, the injection would continue until the pressure switch (pressurized externally to the tank) actuated to terminate the injection. The pressure to the pressure switch was decreased until the injection was again initiated. The pressure switch pick-up and drop-out pressures were determined and the

TABLE 7

MTI COUNTDOWN TASKS

1 - CIRCUIT BREAKER AND POWER SETUP

2 - FACILITY WALK-AROUND

3 - TEST STAND PREPS

4 - SEQUENCE OF OPERATION CHECKS

5 - TEST STAND CLEARING

6 - FLUORINE SYSTEM SETUP

7 - COUNTDOWN INITIATION

8 - LH_2 LOADING

9 - TANK PRESSURIZATION AND OFFLOADING

10 - POST TEST TANK PURGING

11 - FLUORINE SYSTEM SECURING

12 - PANEL SECURING

13 - TANK AND TRANSFER LINE HOT PURGE

14 - TEST STAND SECURING

15 - FACILITY SECURING

16 - INSTRUMENTATION AND POWER SECURING

proper actuation of all MTI control system elements (including the injector valve) was verified.

The general technique for the tests was to load the tank to the prescribed ullage volume (indicated by level sensors 1-inch (.0254 M) apart), then chill down the LH_2 outflow system and large vent line by flowing LH_2 through it from the main storage tank (not from the test tank). The test tank vent was then closed and the tank self-pressurization rate due to external heat leak was determined. The tank was then topped (if necessary) to assure that the LH_2 level was correct, and then the MTI test was initiated.

The overall MTI test results are shown in Table 8. The times shown are the times following initial tank pressure rise until the pressure switch actuated, then the time at which outflow began, and then the time at which a particular level sensor indicated the exact ullage volume. The tank pressures shown in parentheses are not necessarily the exact pressure at that time, but indicate the low point of the initial pressure band (the most extreme). The LH_2 outflow-rate and GF_2 flowrate are averages between the time given and the previous time (e.g., for test 2, between t=85 sec and 144 sec, the average LH_2 outflow-rate was 10.8 lb/sec (4.9 Kg/sec) and the average GF_2 flowrate was 0.0556 lb/sec (.0252 Kg/sec)). The GF_2 flowrate shown is the actual flowrate while the injector valve was open. The actual total GF_2 weight consumed is shown for each time; the amount used between each time shown is the difference between the value shown and the previous value. The equivalent steady-state GF_2 flowrate (as if the injector valve were open all the time) can be computed from the GF_2 weight consumed between times divided by the time. The temperatures shown are those recorded at that time. Note also that there are a number of remarks about "IR shutdown" and "pressure decay from low GF_2 pressure." These occurrences are described in detail in the sections on Control System Performance and GF_2 Usage, below.

Control System Performance

Prior to the injector demonstration tests, the dynamic response of the MTI Control System was analyzed in some detail to determine:

1. If the control system could control the tank pressure to within ± 1.0 psi (± 6900 N/M^2) assuming reasonable models for interface heat and mass transfer.
2. The approximate rates at which the injector valve would cycle in the tank, so that these cycle rates could be simulated in the injector tests.

A block diagram of the tank pressure control system is shown in Figure 61. Each of the three primary control elements--the pressure switch, electrical relay, and electromechanical valve--was mathematically modeled as was the plant, or system to be controlled, which comprises the chemical reaction and the reactant flow. The load or disturbance, acting on the output, can be thought of as the pressure collapse due to heat transfer and the tank outflow which both contribute negatively to the rate of change of tank pressure.

Table 8

MTI PRESSURIZATION TEST DATA SUMMARY

Test No.	Injector-- Location	Time (sec)	Tank Pressure (psia)	Tank Pressure ($10^3 N/M^2$)	Ullage Vol (ft^3)	Ullage Vol (M^3)	Avg LH_2 Outflow Rate (lb/sec)	Avg LH_2 Outflow Rate (kg/sec)	Avg GF_2 Flow Rate (lb/sec)	Avg GF_2 Flow Rate (kg/sec)	Total GF_2 wt (lb)	Total GF_2 wt (kg)	Ullage Temp. TUI (max) (°R)	Ullage Temp. TUI (max) (°K)	Wall Temp. (max) (°R)	Wall Temp. (max) (°K)	Remarks
1	Straight Pipe--	0	15.5	106.9	553	15.1	Start		--	--	--	--	39	22	39	22	Prepressurization only -
	Centerline	12.7	43.3	298.5	553	15.1	Prepress		0.0719	0.0326	0.912	0.414	189	105	116	64	IR shutdown after
		16.5	42.2	290.8	553	15.1	Hold										1st cycle
2	Straight Pipe--	0	15.6	107.6	553	15.1	Start		--	--	--	--	43	24	52	29	Pressure decay from
	Centerline	19.2	42.9	295.6	553	15.1	Prepress		0.0673	0.0306	1.290	0.585	282	160	135	75	low GF_2 pressure
		85	(41.6)*	(286.8)	553	15.1	Hold		0.0612	0.0278	1.730	0.785	364	202	227	126	
		144	43.0	296.4	702	19.9	10.8	4.9	0.0556	0.0252	3.630	1.648	538	299	332	184	
		196	36.1	248.7	851	24.1	12.3	5.6	0.0463	0.0210	5.630	2.556	826	459	481	267	
		230	32.0	220.6	950	26.9	12.5	5.7	0.0388	0.0176	6.680	3.033	902	501	539	299	
3	Straight Pipe--	0	16.5	113.8	950	26.9	Start		--	--	--	--	78	43	132	73	
	Centerline	59	43.4	299.3	950	26.9	Prepress		0.0596	0.0271	3.52	1.597	672	373	332	184	
		133	(42.6)	(294.0)	950	26.9	Hold		0.0406	0.0184	5.42	2.460	777	432	504	280	
4	Straight Pipe--	0	16.8	115.9	106	3.0	Start		--	--	--	--	36	20	71	39	Pressure decay from
	Centerline	4	44.0	303.3	106	3.0	Prepress		0.0434	0.0197	0.190	0.086	64	36	71	39	low GF_2 pressure
		23	(41.8)	(288.0)	106	3.0	Hold		0.0416	0.0189	0.416	0.189	182	101	105	58	
		65	43.4	299.3	255	7.2	15.2	6.9	0.0341	0.0155	1.200	0.545	298	166	135	75	HF sample taken
		109	37.5	258.5	404	11.4	14.4	6.5	0.0326	0.0148	2.610	1.184	487	270	184	102	
5	Straight Pipe--	0	16.1	111.0	106	3.0	Start		--	--	--	--	36	20	62	34	
	Centerline	3.2	44.4	306.0	106	3.0	Prepress		0.0755	0.0343	0.236	0.107	36	20	71	39	
		75	(41.5)	(286.1)	106	3.0	Hold		0.0753	0.0342	0.417	0.189	130	72	98	54	
		130	43.5	299.9	255	7.2	11.6	5.3	0.070	0.0318	0.974	0.442	209	116	123	68	
		164	42.5	293.0	404	11.4	18.6	8.4	0.0643	0.0292	1.842	0.836	326	181	141	78	
		215	42.2	290.8	553	15.1	12.5	5.7	0.0577	0.0262	4.165	1.890	563	313	239	133	
6	Straight Pipe--	0	17.9	123.4	553	15.1	Start		--	--	--	--	335	186	254	141	Warm repressurization--
	Centerline	41	35.6	245.5	553	15.1	Prepress		0.0519	0.0235	2.125	0.965	641	356	295	164	max pressure of
		135	34.0	234.3	553	15.1	Hold		0.0317	0.0144	5.105	2.317	874	485	474	263	35.6 psia because of
		206	23.2	160.0	702	19.9	9.0	4.1	0.0229	0.0104	6.73	3.054	1,012	562	530	294	low GF_2 pressure
7	Straight Pipe--	0	17.2	118.7	106	3.0	Start		--	--	--	--	36	20	88	49	HF sample taken
	Centerline	1	26.0	179.2	106	3.0	Prepress		0.078	0.0354	0.078	0.035	36	20	88	49	
		8	(23.0)	(158.6)	106	3.0	Hold		(0.078)	(0.0354)	0.078	0.035	99	55	92	51	
		134	25.0	172.3	255	7.2	5.1	2.3	0.0768	0.0348	0.300	0.136	168	93	129	72	
		235	25.0	172.3	404	11.4	6.3	2.9	0.0752	0.0341	0.601	0.273	194	108	144	80	
		418	25.0	172.3	553	15.1	3.5	1.6	0.0715	0.0324	1.580	0.717	277	154	159	88	
		582	25.0	172.3	702	19.9	3.9	1.8	0.0650	0.0295	2.940	1.334	370	206	215	119	
		780	25.0	172.3	851	24.1	3.25	1.5	0.0471	0.0214	6.340	2.885	628	349	339	188	
		902	24.0	165.4	950	26.9	3.5	1.6	0.0413	0.0188	8.960	4.070	875	486	481	268	
8	Straight Pipe--	0	16.5	113.8	553	15.1	Start		--	--	--	--	63	35	138	77	Pressure decay from
	Offset	12.5	43.3	298.5	553	15.1	Prepress		0.072	0.0327	0.902	0.409	238	132	144	80	low GF_2 pressure
		41	(41.5)	(286.1)	553	15.1	Hold		0.068	0.0309	1.138	0.516	322	179	159	88	HF sample taken
		100	43.0	296.4	702	19.9	10.8	4.9	0.0517	0.0235	3.030	1.375	509	283	211	117	
		146	37.6	259.2	851	24.1	13.9	6.3	0.045	0.0204	5.050	2.292	706	392	286	159	
		182	32.3	222.6	950	26.9	11.8	5.4	0.0353	0.0160	6.32	2.867	836	465	359	199	
9	Straight Pipe--	0	18.0	124.1	106	3.0	Start		--	--	--	--	36	20	82	46	Prepressurization only -
	Offset	4	44.2	304.7	106	3.0	Prepress		0.0654	0.0297	0.260	0.118	90	50	91	51	IR shutdown
10	Straight Pipe--	0	16.0	110.3	553	15.1	Start		--	--	--	--	62	34	132	73	Prepressurization plus
	Offset	23	43.6	300.5	553	15.1	Prepress		0.0605	0.0274	1.27	0.576	304	169	146	81	short run without IR
		52	42.8	295.1	(553)	(15.1)	Hold		0.047	0.0213	2.42	1.098	469	260	184	102	detector in circuit -
																	HF sample taken
11	Straight Pipe--	0	17.5	120.7	950	26.9	Start		--	--	--	--	139	77	293	163	
	Offset	9	23.9	164.8	950	26.9	Prepress		0.0353	0.0160	0.317	0.144	221	123	288	160	
12	Straight Pipe--	0	18.3	126.2	106	3.0	Start		--	--	--	--	38	21	125	69	
	Offset	0.8	25.2	173.8	106	3.0	Prepress		0.077	0.0349	0.062	0.028	38	21	125	69	
		4	(23.0)	(158.6)	106	3.0	Hold		(0.077)	(0.0349)	0.062	0.028	56	31	125	69	
		112	25.0	172.3	255	7.2	5.9	2.7	0.0764	0.0347	0.284	0.129	140	78	138	77	
		200	25.0	172.3	404	11.4	7.3	3.3	0.0750	0.0340	0.544	0.247	179	99	144	80	
		287	24.0	165.4	553	15.1	7.4	3.4	0.0730	0.0331	1.030	0.468	220	122	148	82	
13	Straight Pipe--	0	18.3	126.2	553	15.1	Start		--	--	--	--	204	113	154	86	Warm repressurization -
	Offset	3	24.1	166.1	553	15.1	Prepress		0.0716	0.0325	0.287	0.130	198	110	154	86	IR shutdown when ullage
		120	(22.8)	(157.2)	702	19.9	5.5	2.5	0.069	0.0313	1.149	0.521	296	165	174	97	vol = 702 ft^2
																	HF sample taken
14	Straight Pipe--	0	17.0	117.2	553	15.1	Start		--	--	--	--	82	46	135	75	IR detector not in
	Offset	3	24.2	166.8	553	15.1	Prepress		0.0625	0.0284	0.188	0.854	104	58	135	75	circuit
		146	(23.0)	(158.6)	702	19.9	4.5	2.0	0.059	0.0268	0.549	0.249	238	132	154	86	
		266	24.0	165.4	851	24.1	5.3	2.4	0.0575	0.0261	1.595	0.724	360	200	184	102	
		334	23.0	158.6	950	26.9	6.2	2.8	0.051	0.0231	3.100	1.407	475	264	220	122	
15	Diffuser--	0	18.6	128.2	553	15.1	Start		--	--	--	--	79	44	239	133	Temperature limit test
	Centerline	25	43.0	296.4	553	15.1	Prepress		0.0486	0.0220	1.215	0.551	435	242	247	137	termination--pressure
		30	(41.4)	(285.4)	553	15.1	Hold		0.0445	0.0202	1.37	0.622	493	274	251	140	decay from low GF_2
		98	33.8	233.0	702	19.9	9.4	4.3	0.042	0.0191	3.65	1.657	888	493	343	191	pressure--HF sample taken
16	Diffuser--	0	17.7	122.0	106	3.0	Start		--	--	--	--	36	20	123	68	Temperature limit test
	Centerline	4	44.1	304.1	106	3.0	Prepress		0.063	0.0286	0.252	0.114	117	65	123	68	termination just prior to
		56	(41.2)	(284.0)	255	7.2	12.3	5.6	0.060	0.0272	0.985	0.447	352	196	144	80	reaching ullage
		115	41.2	284.0	404	11.4	10.8	4.9	0.050	0.0227	3.150	1.430	703	391	208	116	vol = 553 ft^3
		169	30.8	212.3	~553	~15.1	~11.8	~5.4	0.038	0.0173	4.730	2.147	925	514	298	166	
17	Diffuser--	0	17.5	120.7	553	15.1	Start		--	--	--	--	104	58	245	136	Warm repressurization -
	Centerline	70	34.3	236.5	553	15.1	Prepress		0.0248	0.0113	1.735	0.788	679	377	295	164	max pressure of
																	34.3 psia because of
																	low GF_2 pressure

*Pressure in parentheses is not the actual pressure at that time, but the lower limit of the initial pressure band.

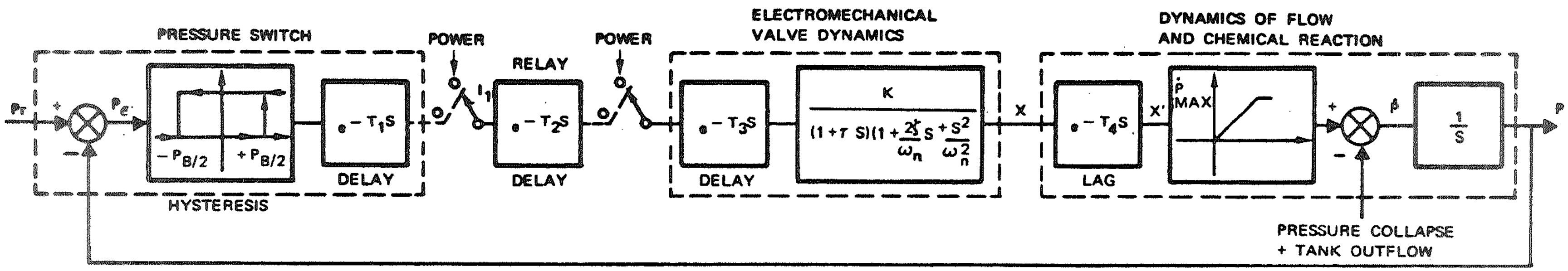

e	NATURAL LOG BASE	T_1	PURE TIME DELAY OF PRESSURE SWITCH + K5 RELAY
I_1, I_2	INTERMEDIATE SIGNALS	T_2	PURE TIME DELAY OF RELAY K2
K	VALVE GAIN	T_3	PURE TIME DELAY OF VALVE
P	OUTPUT PRESSURE	T_4	PURE TIME DELAY OF FLOW IN EXCESS OF T_3 (TRANSPORTATION LAG)
$\dot{P}$	dp/dt	X	VALVE POSITION
$\dot{P}_{MAX}$	MAXIMUM $\dot{P}$, NEGLECTING PRESSURE COLLAPSE AND TANK OUTFLOW	X'	VALVE POSITION DELAYED T_4 SEC
P_B	ACTUATION BAND OF PRESSURE SWITCH	τ	SOLENOID EDDY CURRENT TIME CONSTANT
P_ϵ	PRESSURE ERROR	ζ	DAMPING RATIO OF VALVE
P_r	REFERENCE PRESSURE	ω_n	UNDAMPED NATURAL FREQUENCY OF VALVE
S	LAPLACE OPERATOR		

Figure 61. Tank Pressure Control System Block Diagram

The 0.75 psi (5170 N/M^2) actuation band of the bistable pressure switch (p_B) was inherent in the design and due largely to the adhesion between the mercury and electrodes. The pure delay of the switch was due to the pneumatic actuation and mechanical linkage which compared the reference input pressure (p_r) with the output tank pressure (p) and produced an inclination of the mercury element that was proportional to the difference. The relay, a bistable element, was modeled as a pure time-delay equal to the interval between the application of input power and the closing of relay contacts. The electromechanical valve was described by a gain, third-order dynamics and a pure time-delay.

The latter characteristic derived from the solenoid actuation. τ was the eddy-current time constant of the solenoid and ξ and ω_n were the damping ratio and undamped natural frequency, respectively, due largely to mechanical characteristics. The dynamics of the plant included a transportation lag that was associated with the travel distance and propagation velocity of the reactant, as well as a saturation limit on the rate of tank pressure increase. Between the limits of zero and the maximum rate ($\dot{p}_{max}$), defined without regard to pressure collapse and tank outflow, linear operation was assumed although some nonlinear functional relationship may be more precise.

The primary consideration that affected the system response was the extent to which the following characteristics were known and invariant:

1. Time delays of control elements
2. Pressure switch hysteresis
3. Transportation lag of the plant and the relationship between p and the delayed valve position.

The following values for component lags were used in the analysis:

Parameter	Max. Value	Min. Value
T_1	.025 sec	.020 sec
T_2	.015 sec	.010 sec
T_3	.005 sec	.005 sec
T_4	.025 sec	.005 sec
Total Lag	.070 sec	.040 sec

The differences between the maximum and minimum delays for the relays was due to uncertainty as to the actual relay lag, which was expected to be in the range of .010 to .015 sec. The large difference in the transportation lag was caused by uncertainty as to the behavior of the F_2 flow in the injector tube. The more pessimistic assumption was that following opening of the injector valve, the F_2 flow must traverse the entire length of the injector tube, (a distance of 2.5 ft (.762 M) at an average velocity of 100 ft/sec (30.5 M/sec) for a lag of .025 sec) before ignition and pressure rise occurred. Similarly, when the injector valve closed, there was a lag of .025 seconds until the F_2 stopped flowing from the injector (and reacting). The more optimistic assumption was that following the initial injection the injector tube was full of F_2 and always stayed full of F_2. This assumed that H_2 did not propagate up the injector, burning with the F_2 inside the injector, because the HF product was a barrier to further reaction inside the injector, or the F_2 did not fall out of the injector because of negative buoyancy during the initial injector-off times. With the injector tube full of F_2, the opening of the injector valve caused essentially immediate flow from the injector tube, and the lag was thus reduced to about .005 seconds. This value was based on sonic travel time (.0025 seconds) plus pure ignition delay (.0025 seconds) as determined in Reference 1.

The equations describing the plant operation were programmed with a modification of MIMIC, a digital simulation computer program which is the digital equivalent of the analog solution of the plant equations.

The results of the analysis indicated that the control system would, in fact, control the tank pressure to within ± 1.0 psi (± 6900 N/M^2) for all conditions with pressure rise rates based on reasonable models for interface heat and mass transfer. In addition, it was determined that valve dynamics, even of slow valves, are relatively unimportant; delay times (system lags) are much more significant. Also a change in the pressure tolerance on the pressure switch (pickup-to-dropout) directly changes the magnitude of the pressure band (overshoot-undershoot).

During the injector demonstration tests, the actual system lag was .034 to .044 seconds. However, this did not include the lag of the pressure switch, which was not used. The control system timer, T-2 (See Figure 33) was set at .060 sec which was adequate to allow injection to continue with system lags of .034-.044 sec.

For the first large tank test, with the pressure switches in the system, the timer T-2 was still set at .060 sec., since it was thought that the pressure switches had a response time of the order of .010 to .015 seconds. However, the first test was shut down by the T-2 timer because ignition had not been sensed: the timer was reset to .100 sec and again the timer shut down the test. The timer was reset to .162 sec., and the initial system actuation was achieved, but the timer shut down the test on the first cycle (the first time the pressure switch was in the system). On the second test, the system operated properly (just barely) with the timer set on .162 sec., and therefore, all subsequent tests were performed with the T-2 timer set at .375 sec.

Analyses of the control system overshoots for the entire test series, indicates that with the pressure switch in the system, the average system lag is .160 sec. It can thus be concluded that the lag of the pressure switches is of the order of .120 sec. In addition, the pressure switch tolerance band (pick-up to drop-out) was supposed to be .75 psi (5170 N/M^2); in actuality, the band ranged from .8 (5510) to 1.0 psi (6900 N/M^2) at 42 psia (290 x 10^3 N/M^2) and .7 psi (4830 N/M^2) at 24 psia (165 x 10^3 N/M^2). In spite of the longer system lag time and wider pressure switch band (both of which contribute directly to increased control band), the control system functioned in a nominal manner, and generally within a 2.0 psi (13.79 x 10^3 N/M^2) band. The response of the control system is shown in Figures 62 to 67. A 5 percent initial ullage (106 ft^3 ($3M^3$)) case is shown in Figure 62. This was for test 5 which had one of the highest GF_2 bottle pressures (and flowrates) the smallest ullage, and thus represented the most difficult control problem. This particular test also had a hold period.

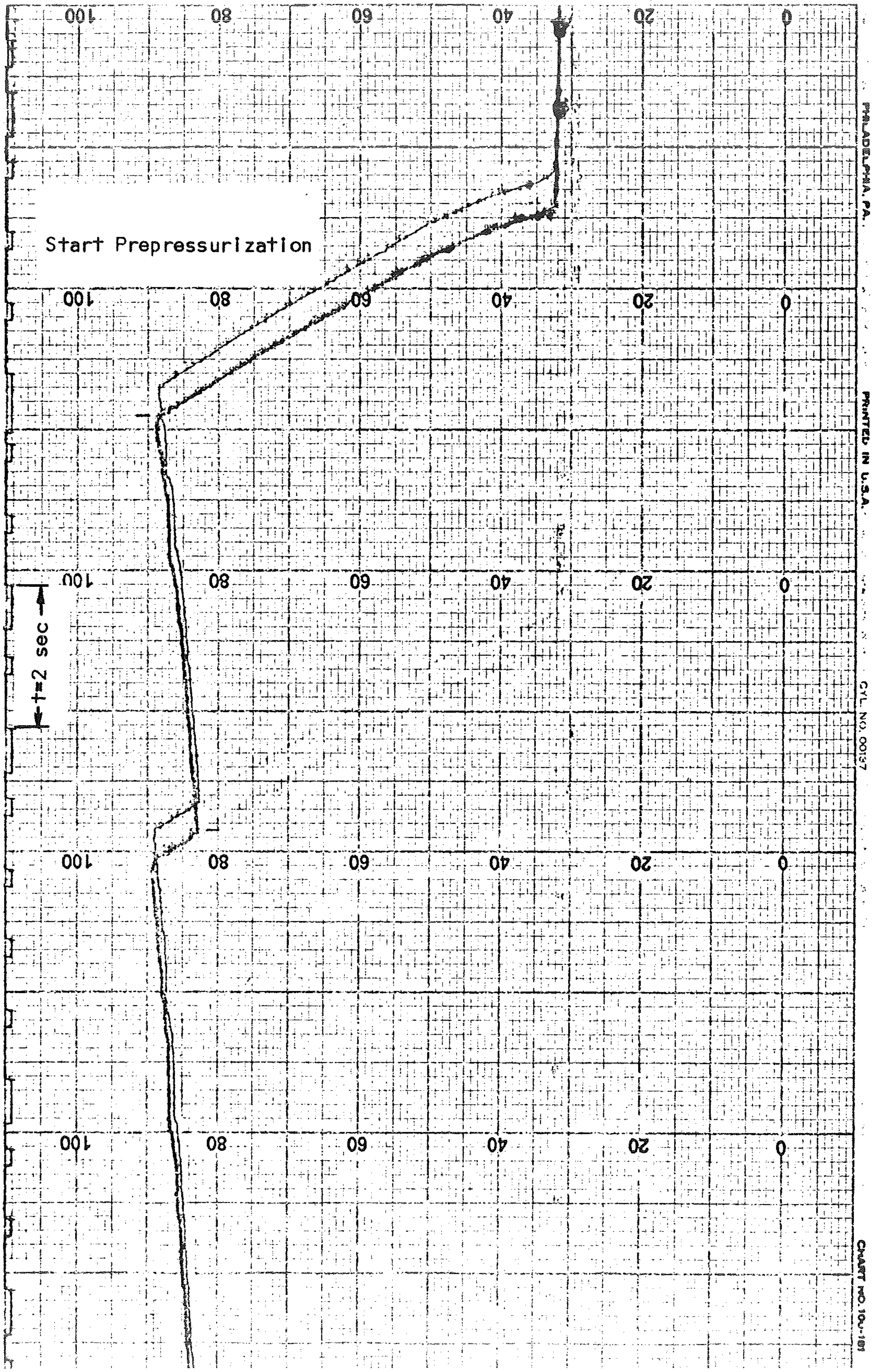

Figure 62. Control System Response - 5% Ullage - Prepressurization.

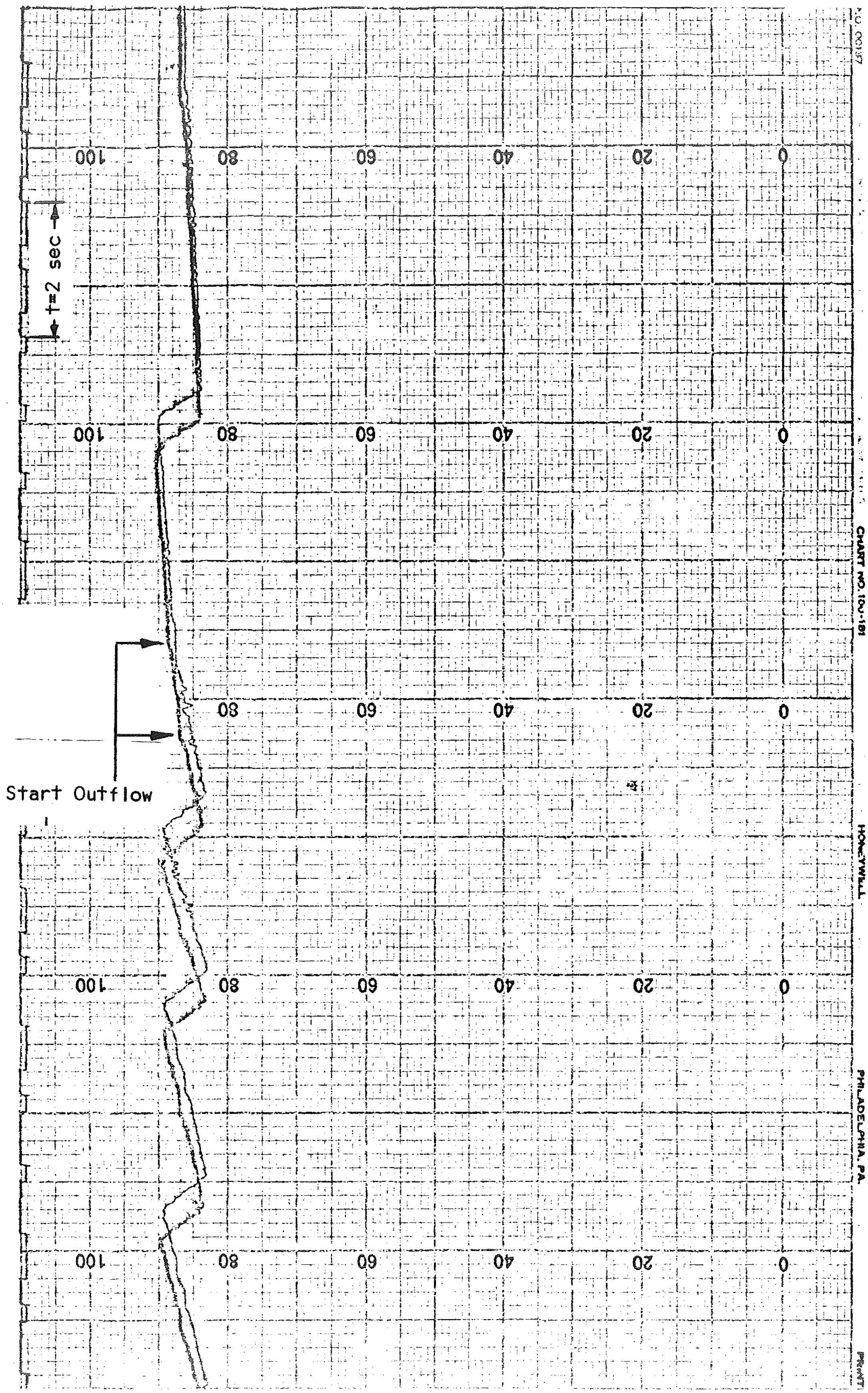

Figure 63. Control System Response - 5% Ullage - Outflow

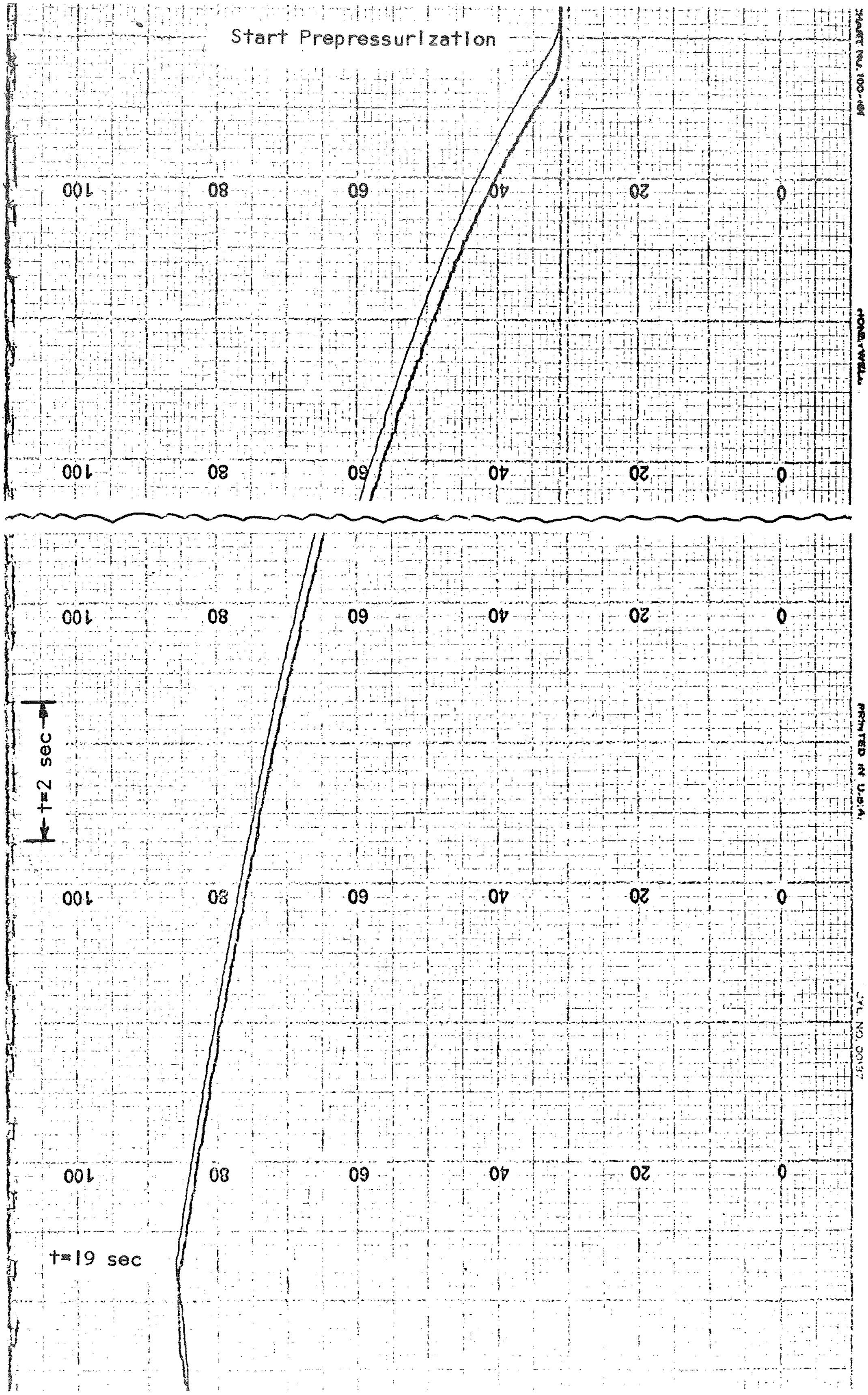

Figure 64. Control System Response - 50% Ullage - Prepressurization

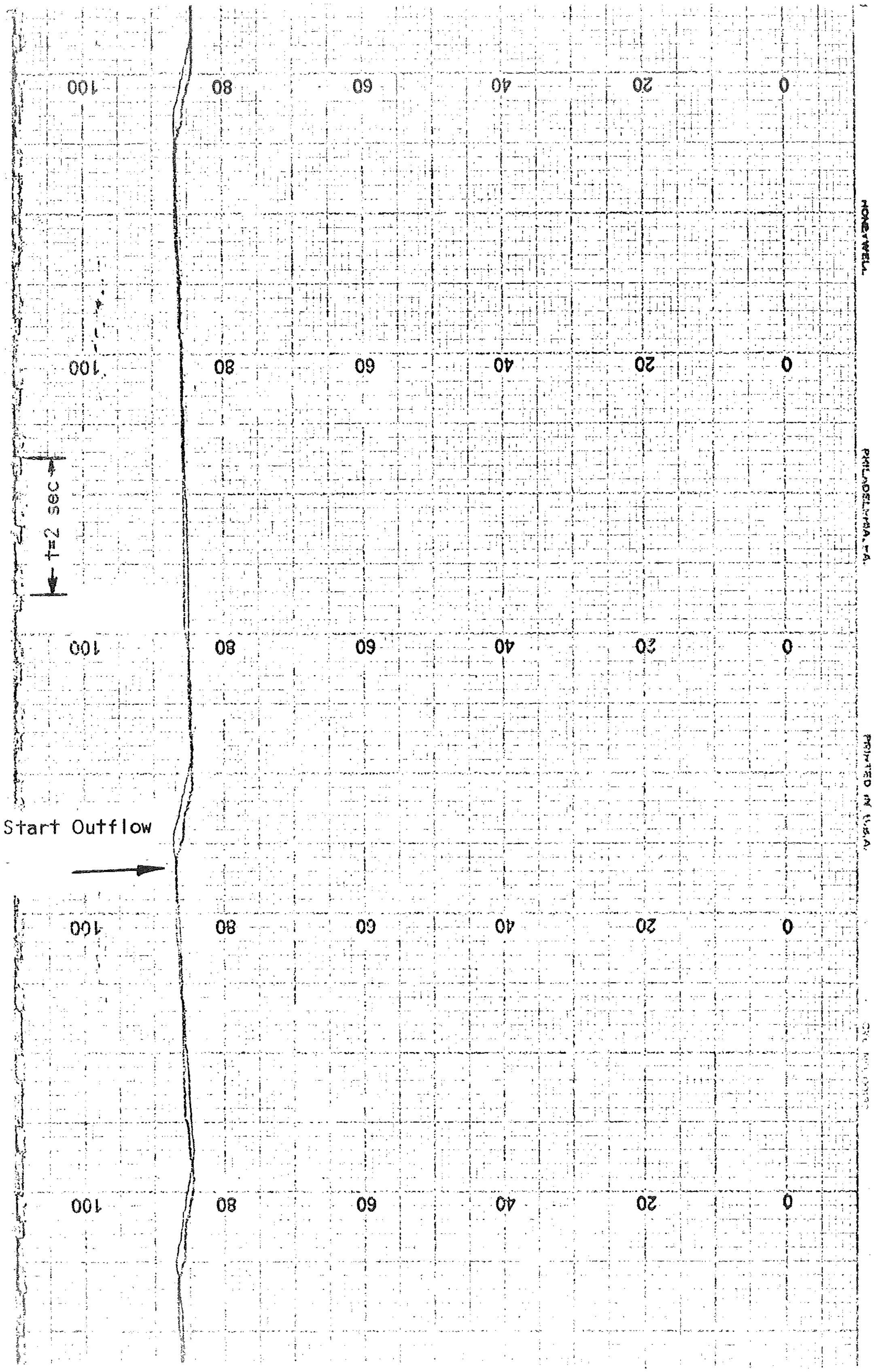

Figure 65. Control System Response - 50% Ullage - Outflow

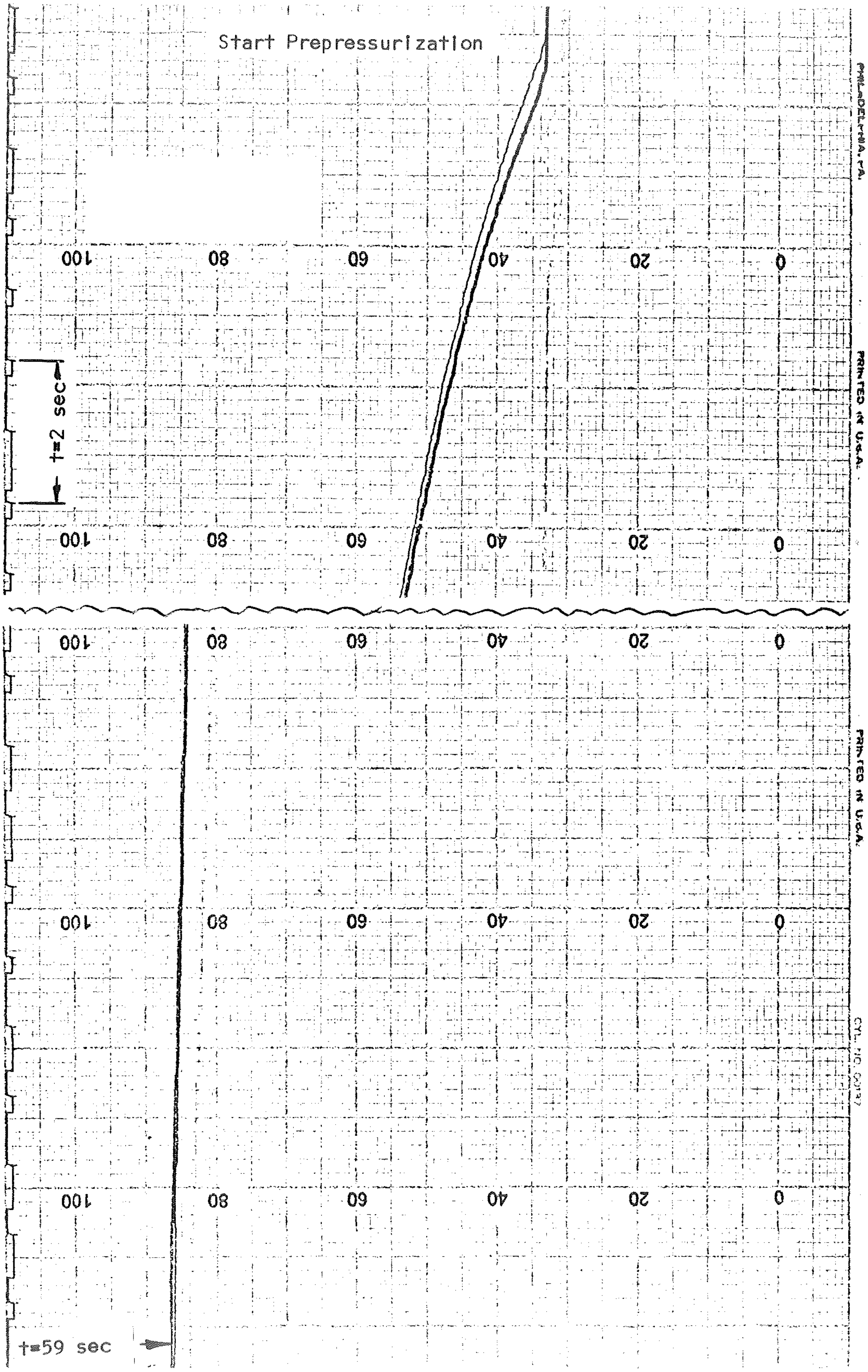

Figure 66. Control System Response - 90% Ullage - Prepressurization

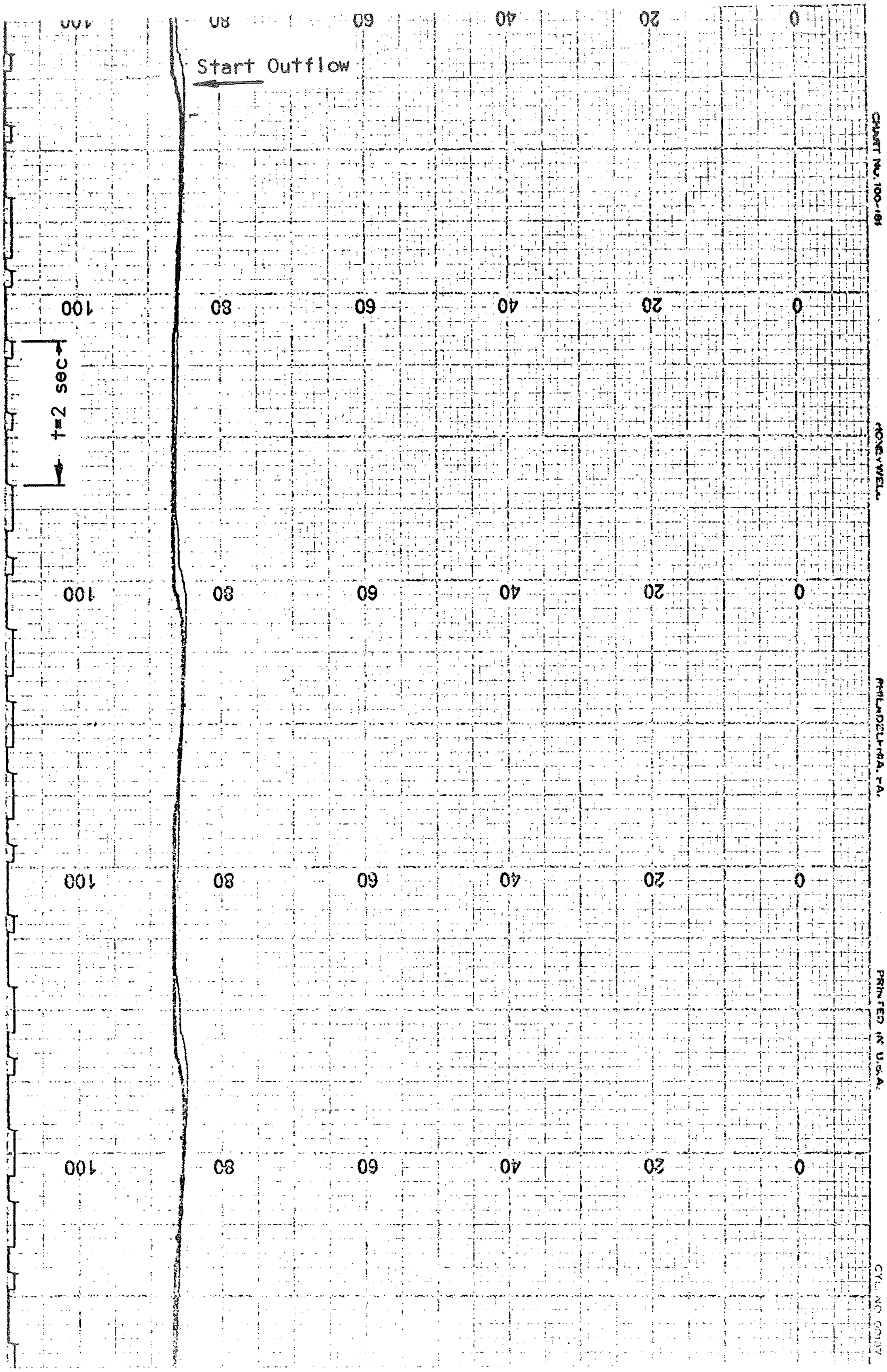

Figure 67. Control System Response - 90% Ullage - Outflow

The binary coded timing marks are visible at the top of the figures with increasing time to the left. The horizontal scale (timing) is .2 seconds per division; the vertical scale is in psia with .5 psia (3450 N/M^2) per division (100 represents 50 psia (345 x 10^3 N/M^2)). The two traces shown are for the two fully redundant pressure transducers; the right hand trace is synchronized with the timing mark pen; the left hand trace leads the timing by .4 sec. because of pen offset.

In Figure 62, the pressure rises rapidly from 15.6 psia (107.6 x 10^3 N/M^2) to 44.4 psia (306 x 10^3 N/M^2), then cycles quite slowly during the hold period, with the valve being open only 3.5 percent to 4.5 percent of the time. The maximum pressure band at this time is 3.0 psia (20.7 x 10^3 N/M^2). Figure 63 indicates the change which occurs in the pressure cycle when LH_2 outflow starts. The cycle rate changes noticeably, and now the injector valve is on about 18 percent of the time. As the test progresses, the injector-on fraction gets larger until, toward the end of the test, the valve is on all of the time. As the test progresses the control band gets narrower, as well.

The response of the control system for pressurization of a 50 percent initial ullage (553 ft^3 (15.7 M^3)) for test 2 is shown in Figures 64 and 65. Figure 64 shows the prepressurization, which is much slower, due to the increased ullage. Figure 65 shows the cycle rate transition from 11.3 percent on, before outflow, to 26.7 percent on after outflow starts. The maximum pressure band for this ullage volume is 1.3 psi (8960 N/M^2).

The control system performance for pressurization of 90 percent ullage (950 ft^3 (26.9 M^3)) for test 3 is shown in Figures 66 and 67. Figure 66 shows the rather slow prepressurization, followed by valve cycling at 76.5 percent injector on, during hold, as shown in Figure 67. The maximum pressure band for this ullage volume was 1.2 psi (8280 N/M^2) (which was essentially the pressure switch pick-up-drop-out range.)

These data indicate that the control system was capable of controlling tank pressure at any ullage volume with prepressurization, hold and expulsion cycles, and at varied LH_2 outflow rates.

Nonignition of the GF_2 in the LH_2 never occurred during the test program, however, a number of tests were terminated by the IR ignition detector. Early in the test program this occurred because of icing of the quartz window of the unit. This was solved by helium purging the unit with a configuration as shown in Figure 68. The complete purged and bagged unit is also shown in Figure 63. During the offset injector tests IR detection problems again terminated some tests (See Table 8). This was caused by the fact that the detector was no longer looking at the flame, since the injector tip was out of view, as shown previously in Figure 45. For some of these tests, the IR detector was eliminated from the control system circuitry, and ignition was monitored visually, by observing pressure rise rate and injector valve on-off condition. When the tank pressure started to decay because of reduced GF_2 pressure, it was no longer deemed a certainty that ignition was occurring, so the test was terminated.

Based on the experience of the previous MTI tests (large-scale) under contract NAS 3-7963 , where there was never a case of nonignition of ullage injection, and this test series, where, in several hundred cycles, nonignition never occurred, an ignition detector is not a requirement for a flight vehicle, or for further test programs with ullage injections; indeed, it would be a source of unreliability in the pressurization system.

Fluorine Quantities

The quantities of GF_2 required for MTI pressurization is one of the most important design considerations since this data would be used to determine weight of pressurant, GF_2 storage container weight, plumbing and injector sizes and weights, etc. The weight of GF_2 used in the test program was not known directly but was determined from a flow orifice and by monitoring GF_2 cylinder pressure. For many of the small ullage tests, the GF_2 requirement was so small that the injector valve was only open for a few tenths of a second. In this case the flow was completely in a transient condition and the flow could not be accurately measured by the flowrate equation. However, the prepressurization process usually lasted several seconds which allowed the flowrate to stabilize. In addition, because the GF_2 cylinder pressure was known, the quantity of GF_2 used could be determined from a polytropic expansion in the GF_2 cylinder. Both the polytropic expansion technique and the flowrate equation were used in conjunction to determine the GF_2 quantities. A number of test series were made from common cylinders without purging of the GF_2 plumbing

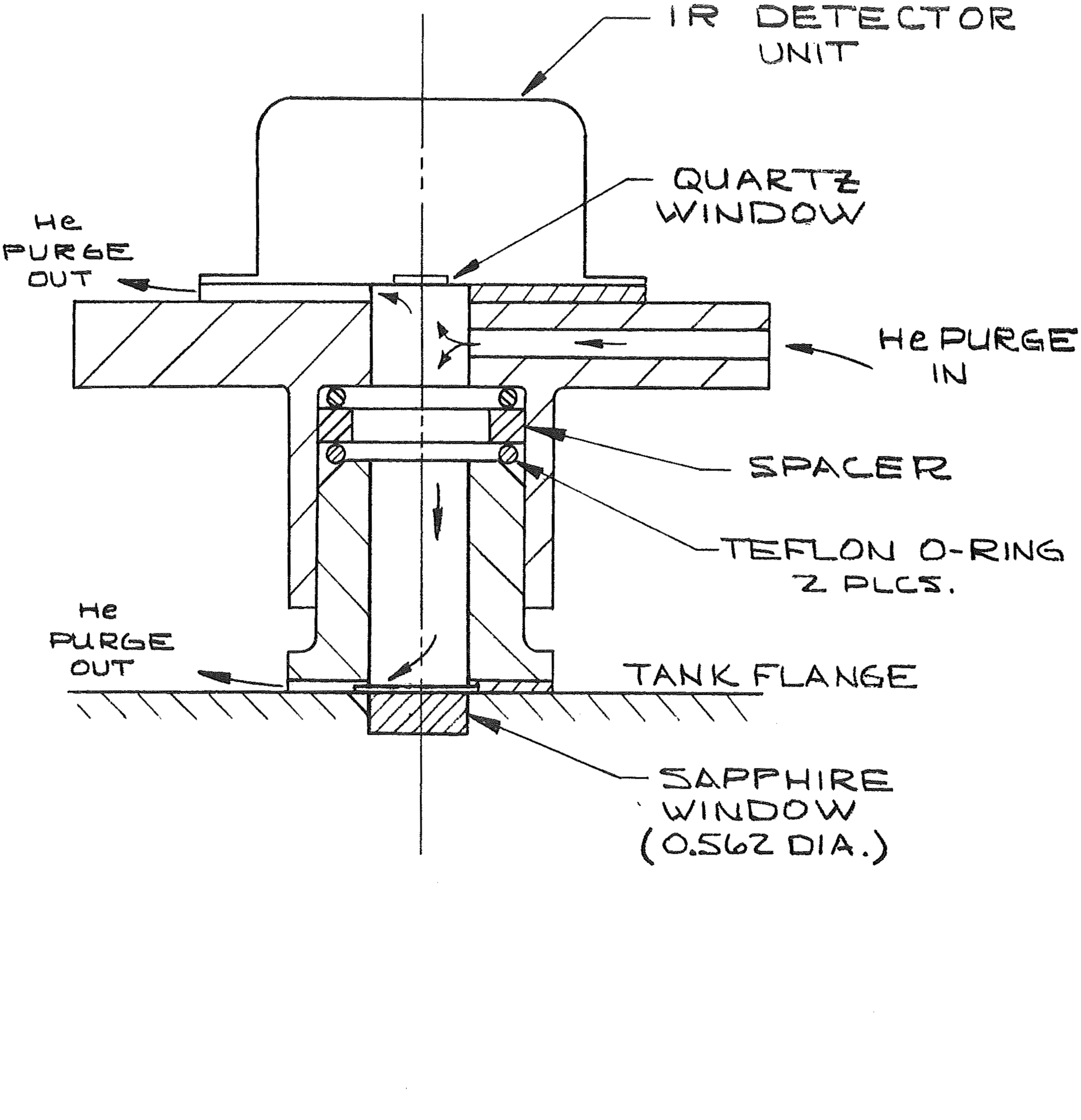

Figure 68. Purged IR Detector Installation

between tests (e.g., tests 3 and 4, 5 and 6, 12 and 13, 16 and 17). Analysis of the cylinder pressures for these complete tests, plus evaluation and comparison of the flowrate equation and polytropic blowdown of all of the pre-prepressurizations, gave an average polytropic exponent of 1.15 (compared to an isothermal exponent of 1.0 and an adiabatic exponent of 1.4). The maximum run time for any of these tests was about 300 seconds. With some GF_2 cylinder sets, only one test was made (e.g., tests 7, 8, and 15). One of these tests was quite rapid, but test 7 was a very long run ($\sim$ 900 seconds) and test 12 used small quantities in ~300 sec. It was speculated that near-isothermal expansion might be more appropriate for these tests. This is discussed further in the section on the Analytical Study, where the predicted GF_2 usage is compared to the experimental quantities. The quantities for each phase of each test, based on either the flowrate equation or polytropic expansion, as appropriate, are shown in the test summary, Table 8.

For ullage heat addition with no losses, the energy required for prepressurization of a perfect gas is

$$\Delta Q = \frac{V}{\gamma - 1} \quad \Delta P = W_{F_2} \; Q_R \tag{85}$$

where V is ullage volume, ΔP is constant volume pressure rise, W_{F_2} is quantity of GF_2 and Q_R is the specific heat of reaction (see Reference 2 for derivation). Assuming Q_R = 6050 Btu/lb (1.4 x 10^7 Joule/Kg) GF_2 and γ = 1.7 for saturated hydrogen in the ullage, the quantity of GF_2 necessary for prepressurization of an ullage volume is shown in figure 69 as line A-A.

Data from the ullage tests from Contract NAS 3-7963 together with data from this program are also shown in figure 69. Thus our MTI data spans five orders of magnitude in ullage volume with the same general trend: the losses can range from near-zero to 70 percent. Thus, the accurate prediction of these losses is essential and one of the purposes of the Analytical Study. The shaded symbols in figure 69 represent the diffuser injector tests, which tend to be generally lower in overall performance, as anticipated, but quite comparable in performance for relatively short prepressurizations.

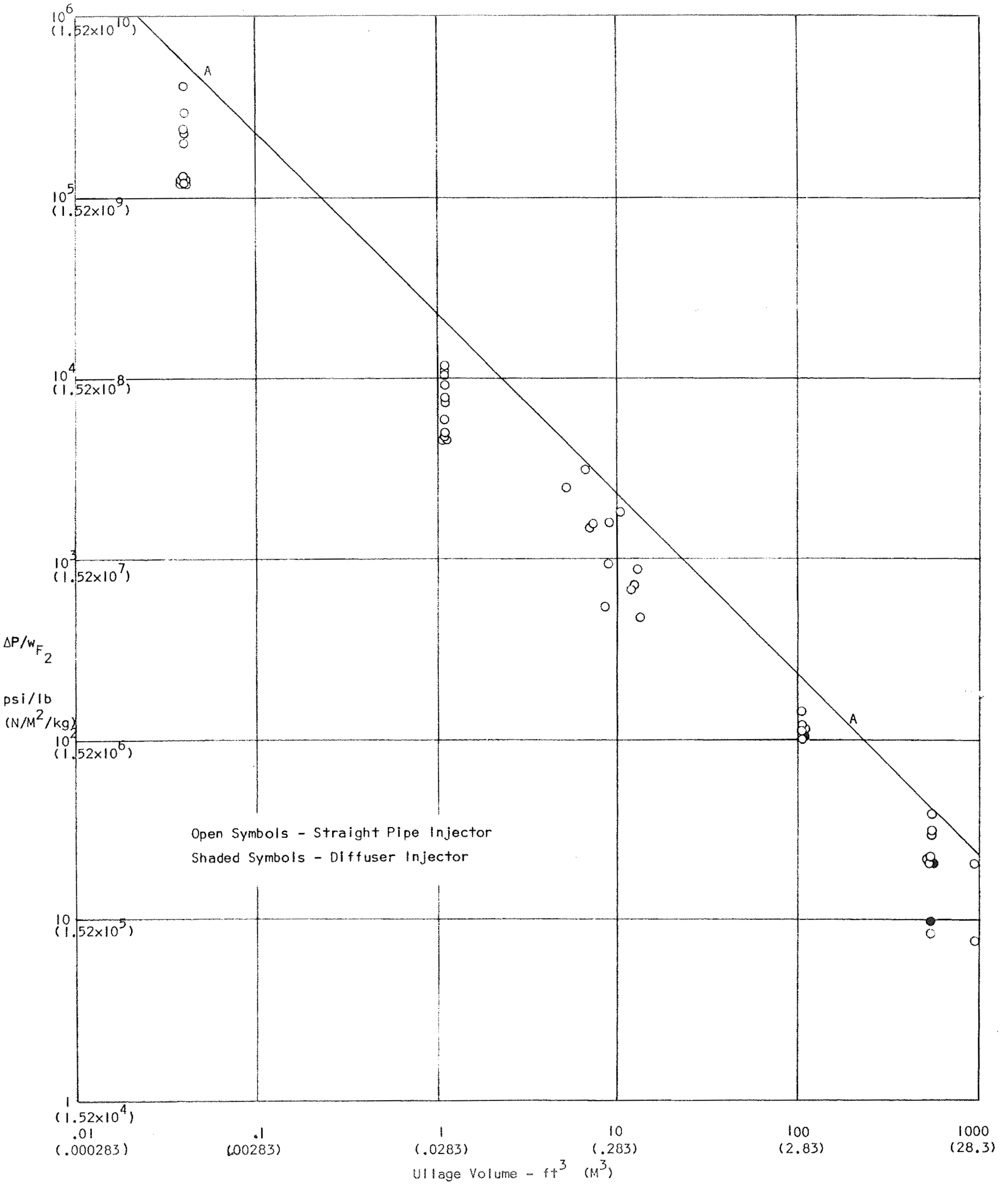

Figure 69. Fluorine Requirements for Pre-Pressurization

It was found in some of the tests, as shown in Table 8, that the energy requirements of expulsion and heat transfer was greater than the available energy of GF_2 inflow because of low GF_2 injection pressure flowrate. In these tests the pressure decayed even with the valve full on.

The GF_2 requirements for expulsion pressurizations strongly depend on the duty cycle and are not conveniently presented in graphical form. They are generally higher than equivalent prepressurization requirements because the ullage heat losses from a warm ullage (due to MTI prepressurization) must be made up. The overall GF_2 requirements for the test program are summarized in Table 8.

Temperature Distribution in the Tank

The temperature distribution in the tank is also of major concern to the designer because excessive temperatures caused by the MTI reaction could weaken the tank structure, damage equipment in the tank, etc. The ullage gas temperature distribution is of foremost concern. In the MTI tests the vertical instrumentation probe situated at the tank half-radius and the gas temperature probes in the fluxmeter installation at the tank wall provided a comprehensive picture of the ullage gas temperature distribution. The figures which follow show the distribution of tank internal temperatures for each test at various times corresponding to those in Table 8, except for tests 1 and 9 which are not shown since they were for prepressurization only. There was excellent agreement between the temperatures recorded on stripcharts and those recorded on the PDM system. The initial temperature distribution was accurately described by the liquid temperature probes (set to record between 35°R (19.5°K) and 60°R (33.3°K)) because the initial ullage was generally very cold (~40°R (22.2°K)). Exceptions were the 90 percent ullage cases, where the temperatures were of the order of 80°R (44.5°K). The data reveal a number of interesting trends. Figures 70 to 74 are for the centerline straight pipe injector at about 43 psia (296 x 10^3 N/M^2). The ullage does not appear to be completely mixed (all at a uniform temperature), although in some of the tests (2, 3, 5 and 6) the ullage temperature profile is reasonably uniform early in the test, but becomes less uniform as the test progresses. The ullage at the top of the dome gets quite warm, (tests 2-6) and the gas temperature probe TG1 failed from overheating after test 6. In

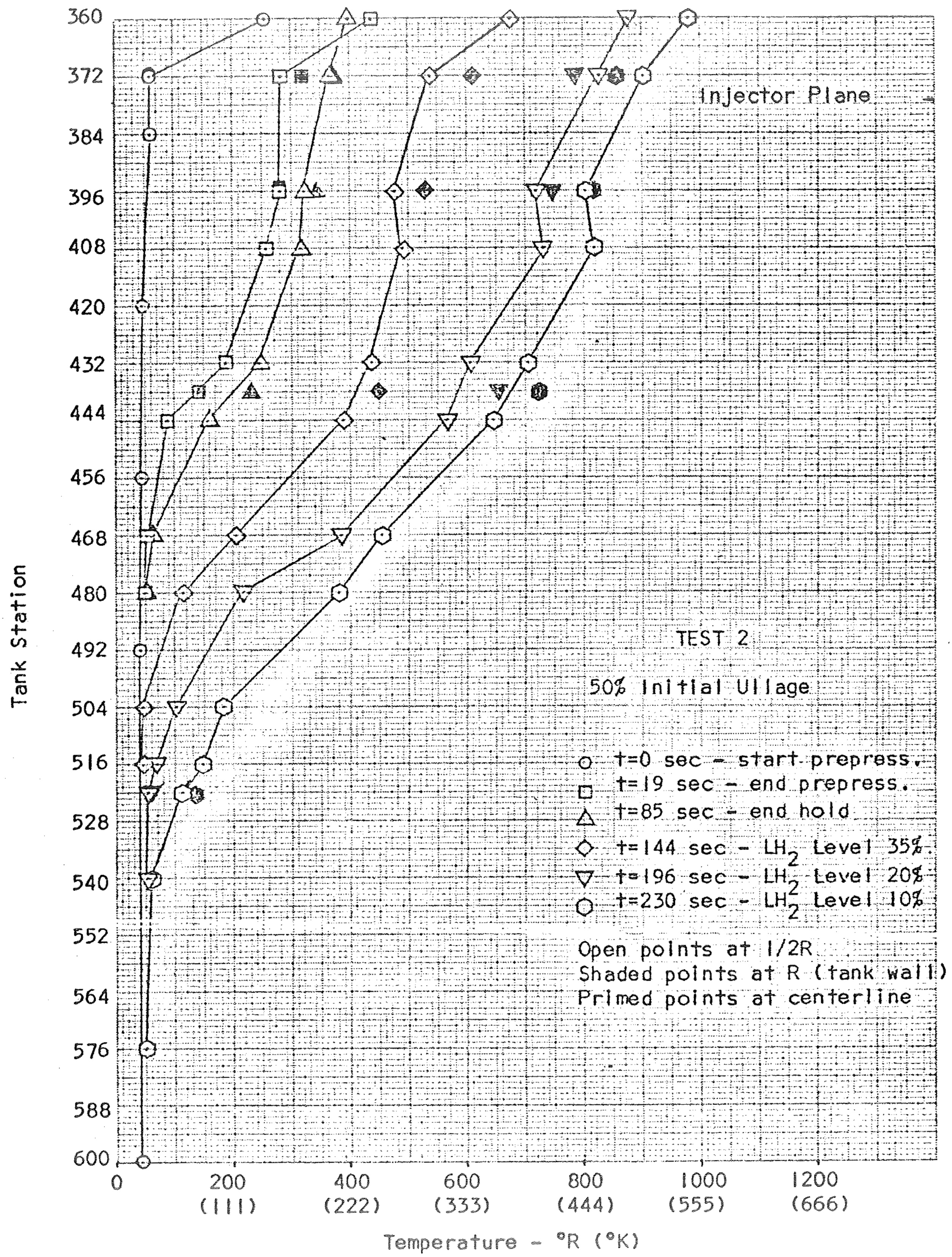

Figure 70. Axial Temperature Distribution for Test 2

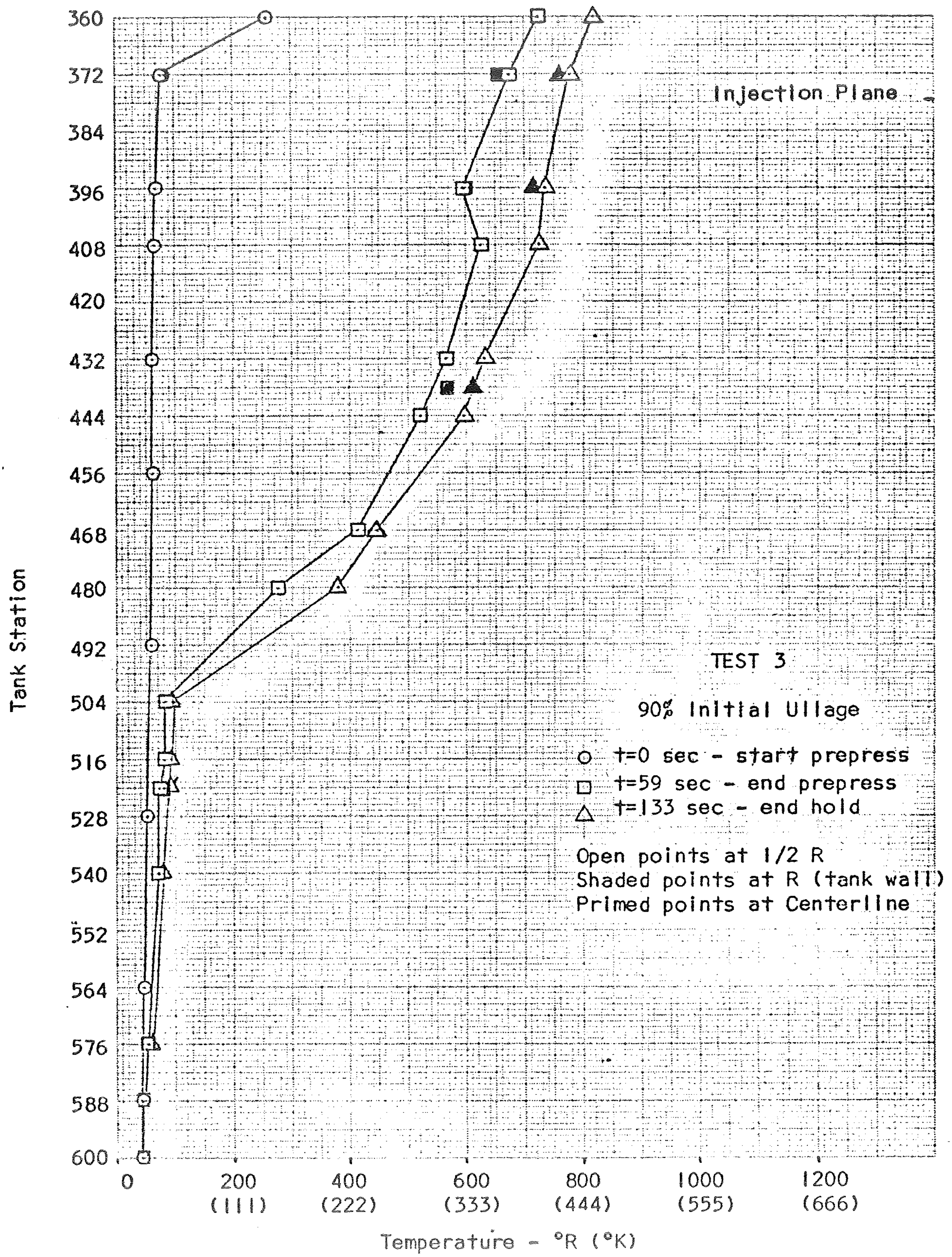

Figure 71. Axial Temperature Distribution for Test 3

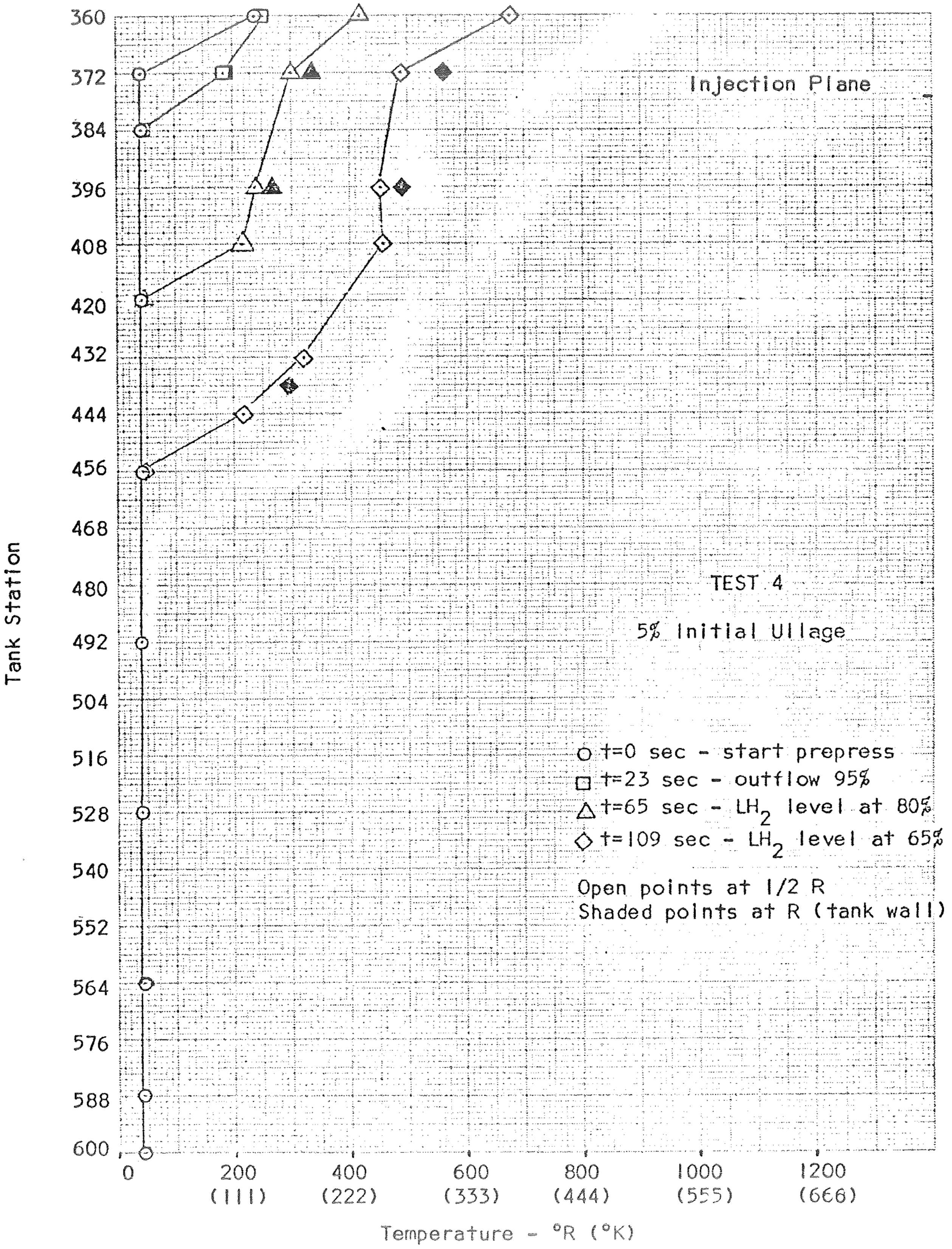

Figure 72. Axial Temperature Distribution for Test 4

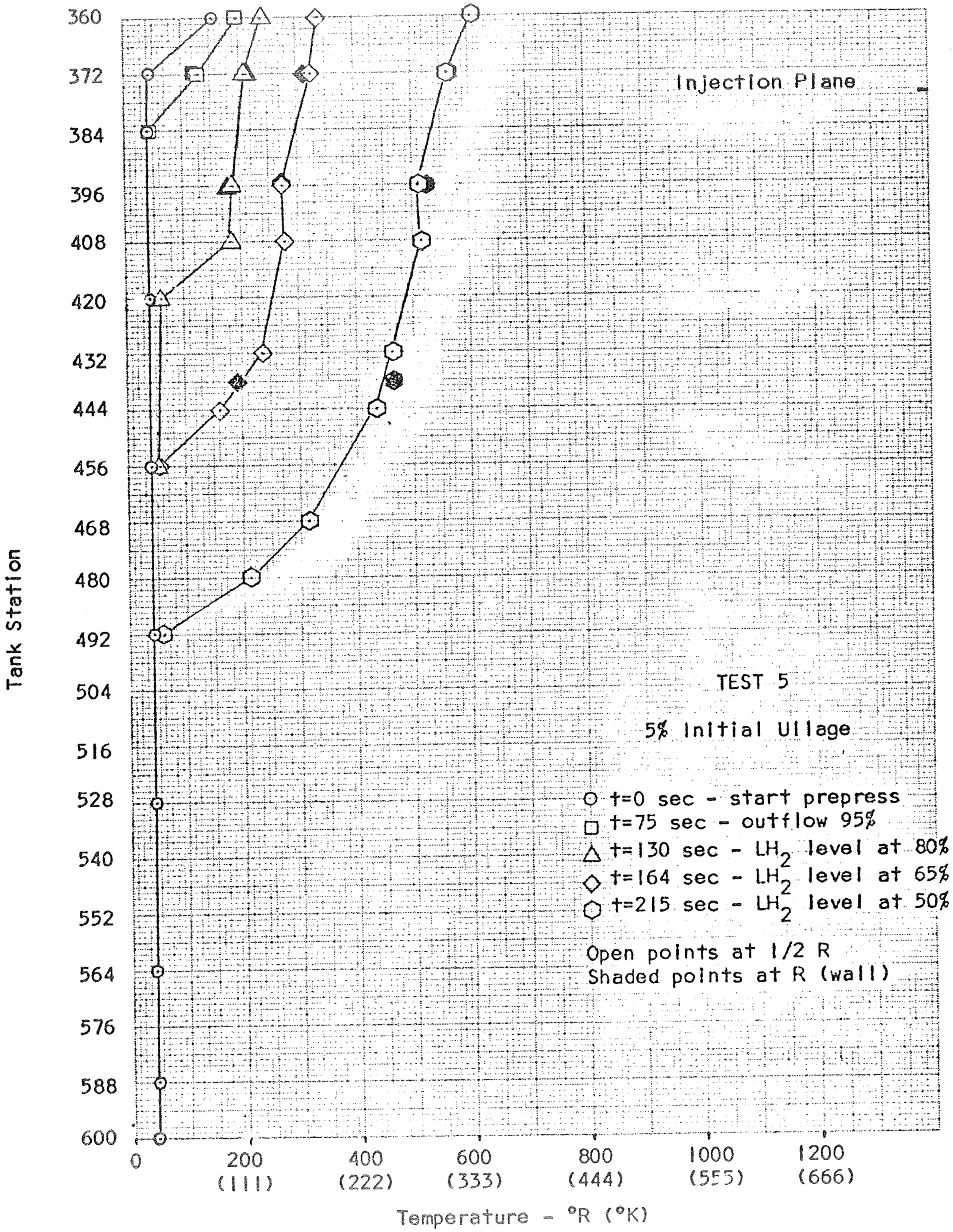

Figure 73. Axial Temperature Distribution for Test 5

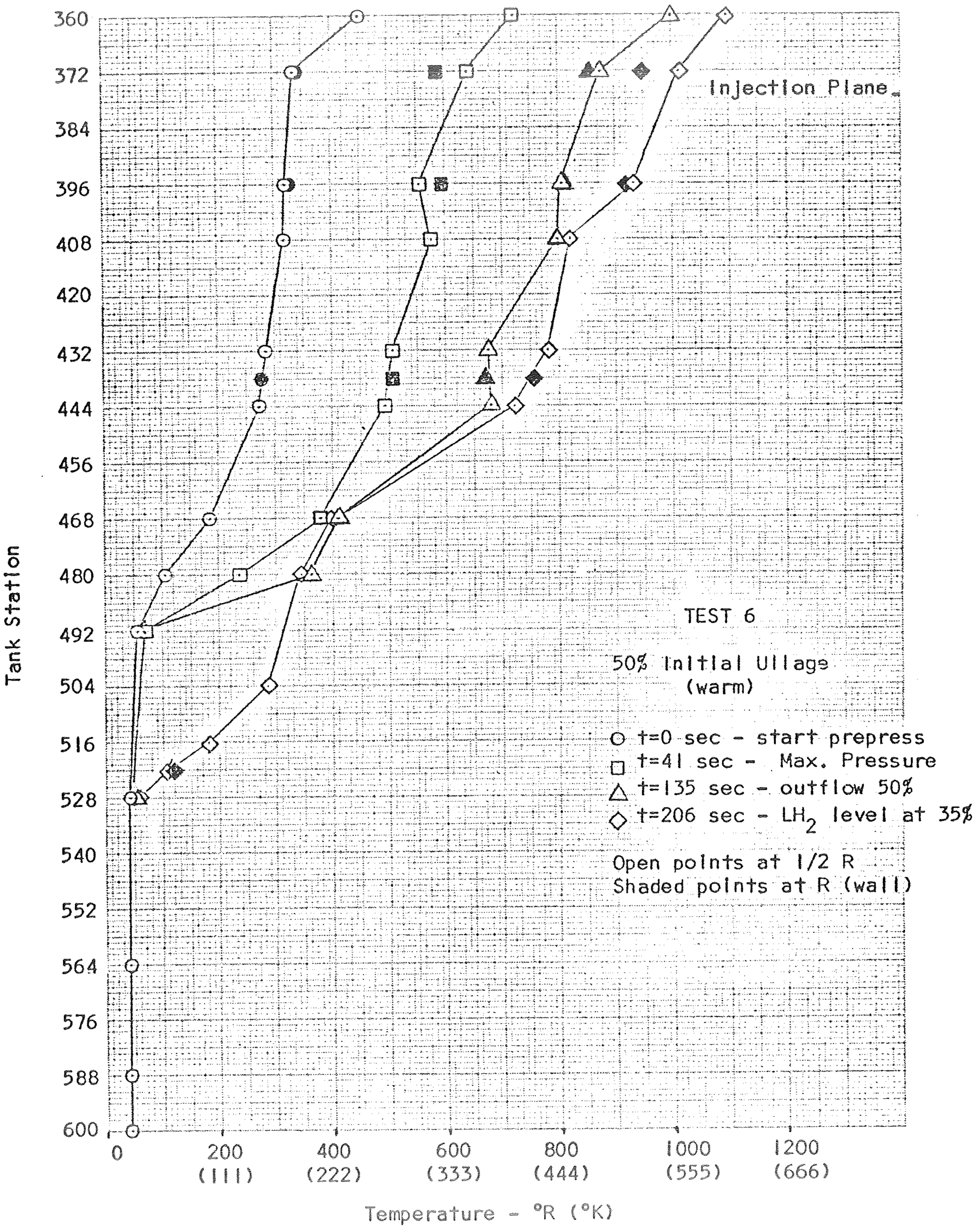

Figure 74. Axial Temperature Distribution for Test 6

many cases the gas near the wall is as warm or warmer than that at the half-radius probe, especially late in the test. Usually, however, the gas temperatures at the half-radius and wall are quite close, indicating minimal radial temperature gradient (as discussed below).

With the centerline straight pipe injector at 24 psia (165.5×10^3 N/M^2) (Figure 75), test 7, the ullage gas temperature profile is very uniform, indicating the ullage gas is very well mixed, up to a time of 584 sec, then the profile departs from uniformity, and at the end of the test appears not well-mixed, as in tests 2-6. The temperature reversal at station 480 appears to be a local anomaly on that particular sensor.

Figures 76 to 81 are for the offset straight pipe injector, which is very similar in behavior to the centerline straight-pipe. The behavior of the temperature profile at the half-radius is practically identical between the two injectors, but the gas temperature at the wall tends to be warmer than at the half radius for the offset injector (compare test 2 and test 8). However, it is the wall gas temperature farthest from the injector which gets the warmest. (The gas radial temperature profiles are discussed below.)

For the offset injector low pressure tests (24 psia (165.5×10^3 N/M^2)), the gas temperatures at the half-radius and the wall are quite close (see tests 11, 12, 13, and 14) and again the profiles are extremely uniform.

Figures 82 to 84 show the ullage gas temperature profiles for the centerline diffuser injector. As expected, the ullage gas gets warm much faster than with the straight pipe injector (compare the times to reach similar temperatures for tests 2 and 15). For this reason, the diffuser tests were terminated early. The ullage gas temperature profiles for these tests have a consistently odd shape. The half-radius sensor at station 408 is abnormally warm, and the gas temperature at the wall at station 396 is noticeably warmer than that at the half-radius. Apparently the ullage flow field caused by the diffuser is responsible for these anomalies. Figure 85 shows the relationship of the half-radius and wall temperature probes to the diffuser. The flame zone virtually impinges on the half-radius sensor at station 408 (TU3), then flows up the wall to the wall sensor at station 396 (TG3), but leaves the half-radius sensor at station 396 (TU2) in a cooler zone. The sensor below TU3 is a liquid temperature sensor (TL2) which was set at 35-60°R (19.5 - 33.3°K).

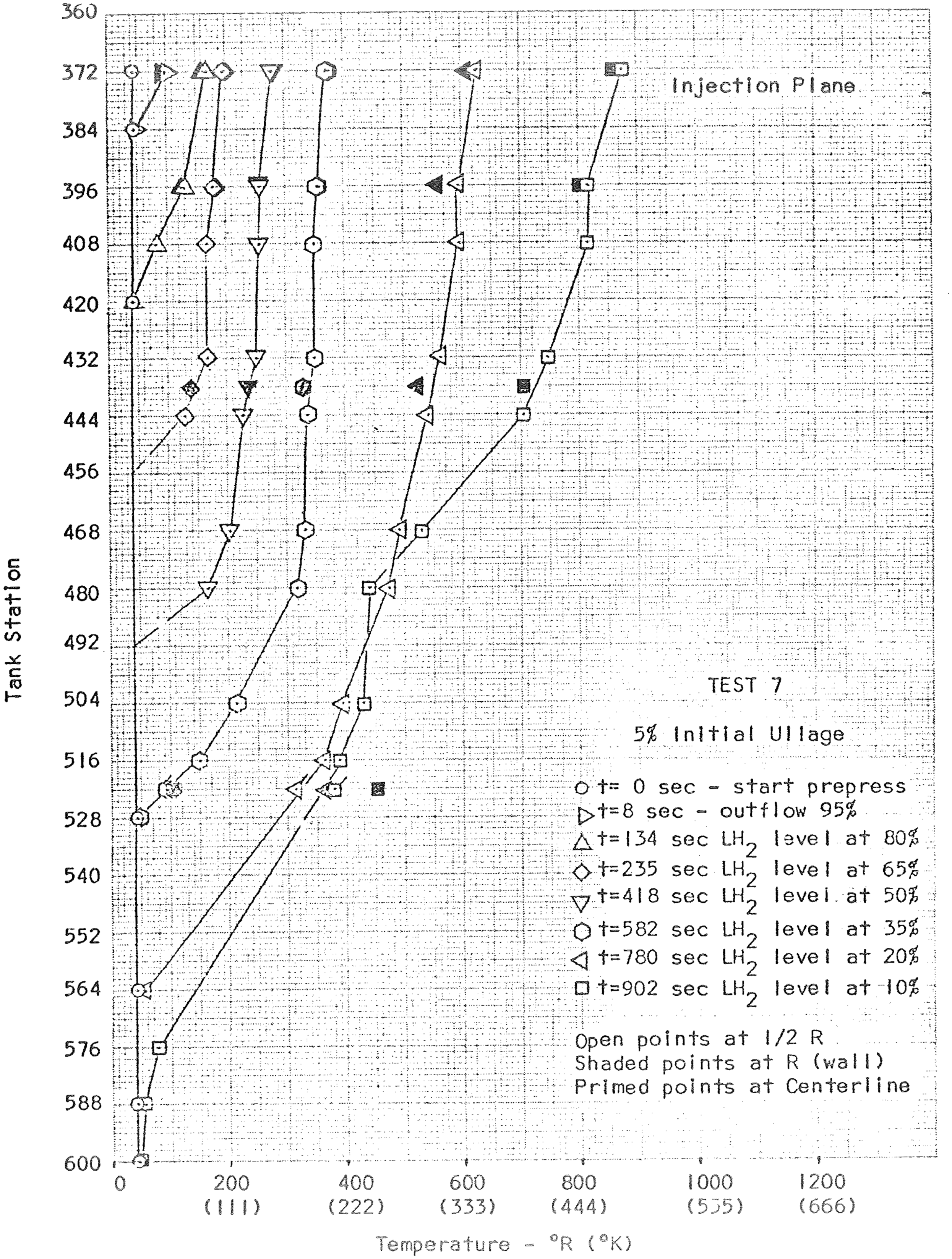

Figure 75. Axial Temperature Distribution for Test 7

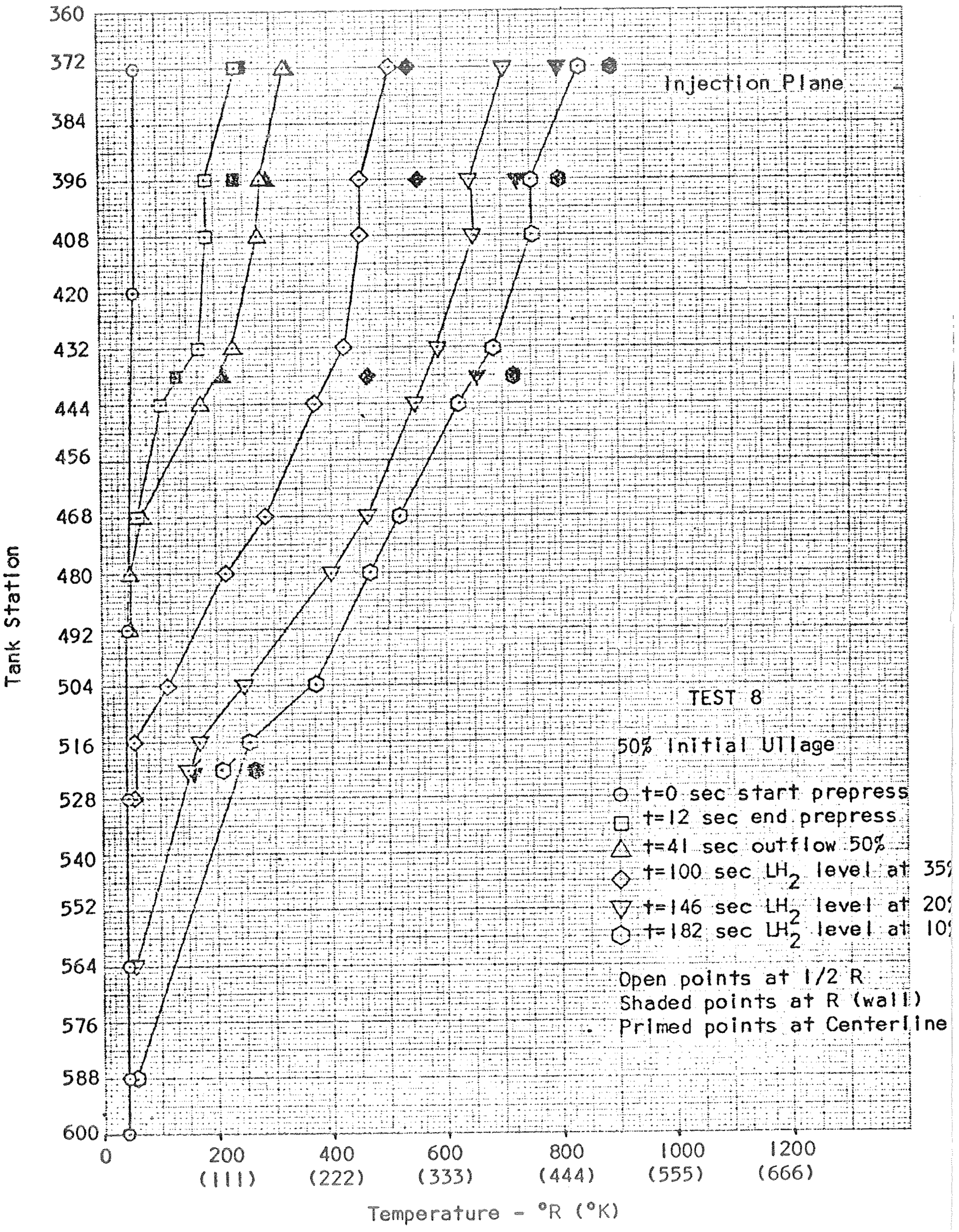

Figure 76. Axial Temperature Distribution for Test 8

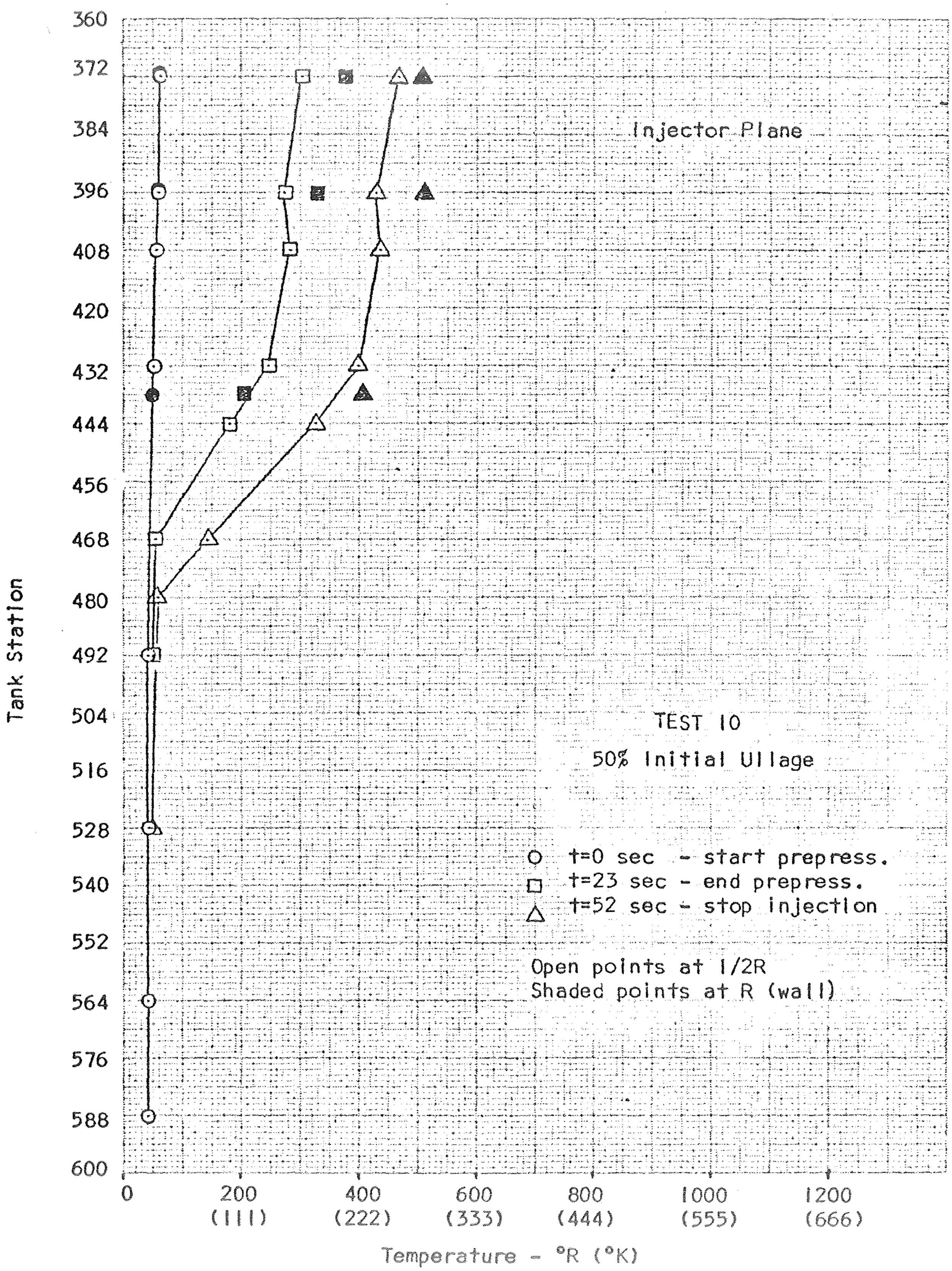

Figure 77. Axial Temperature Distribution for Test 10.

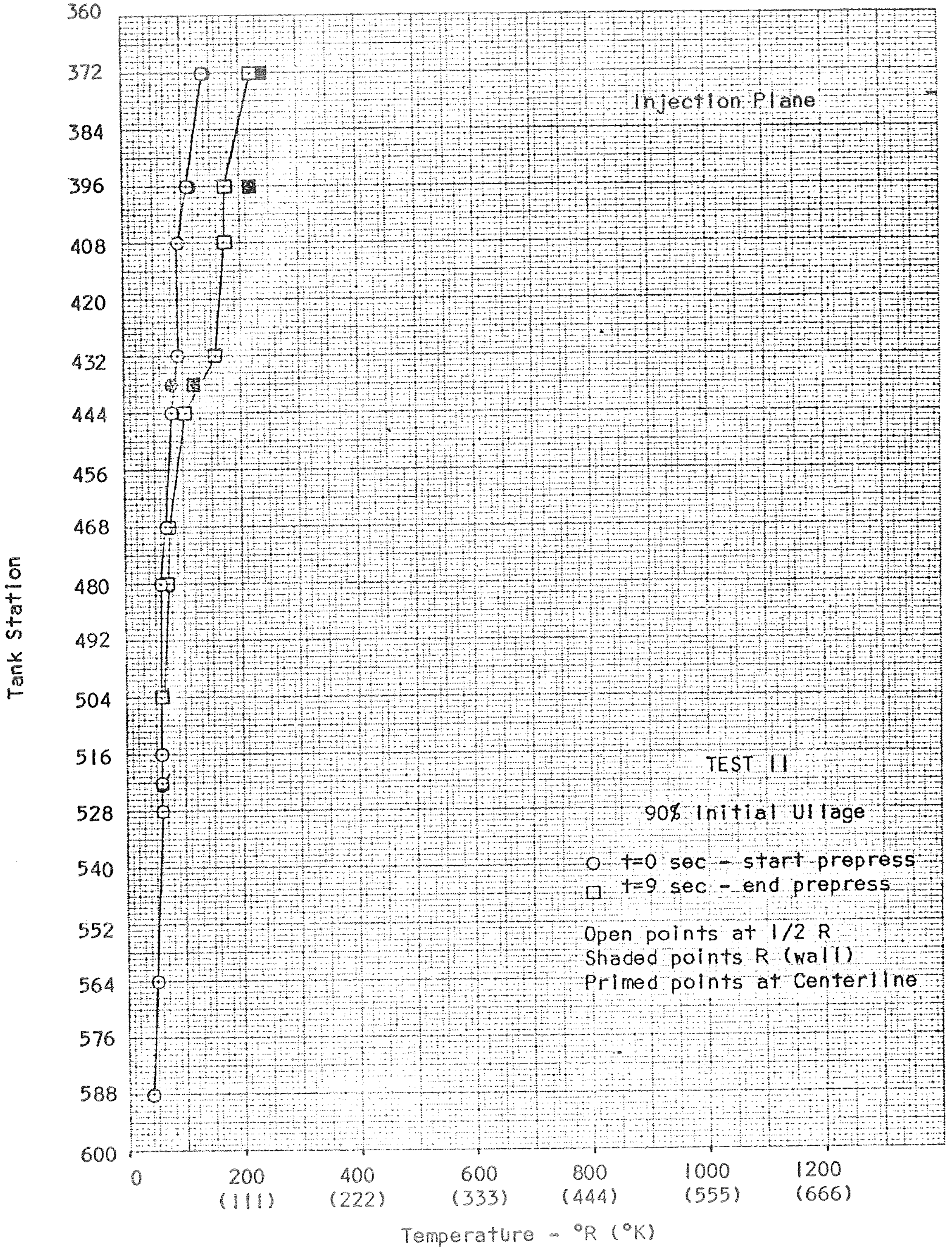

Figure 78. Axial Temperature Distribution for Test II

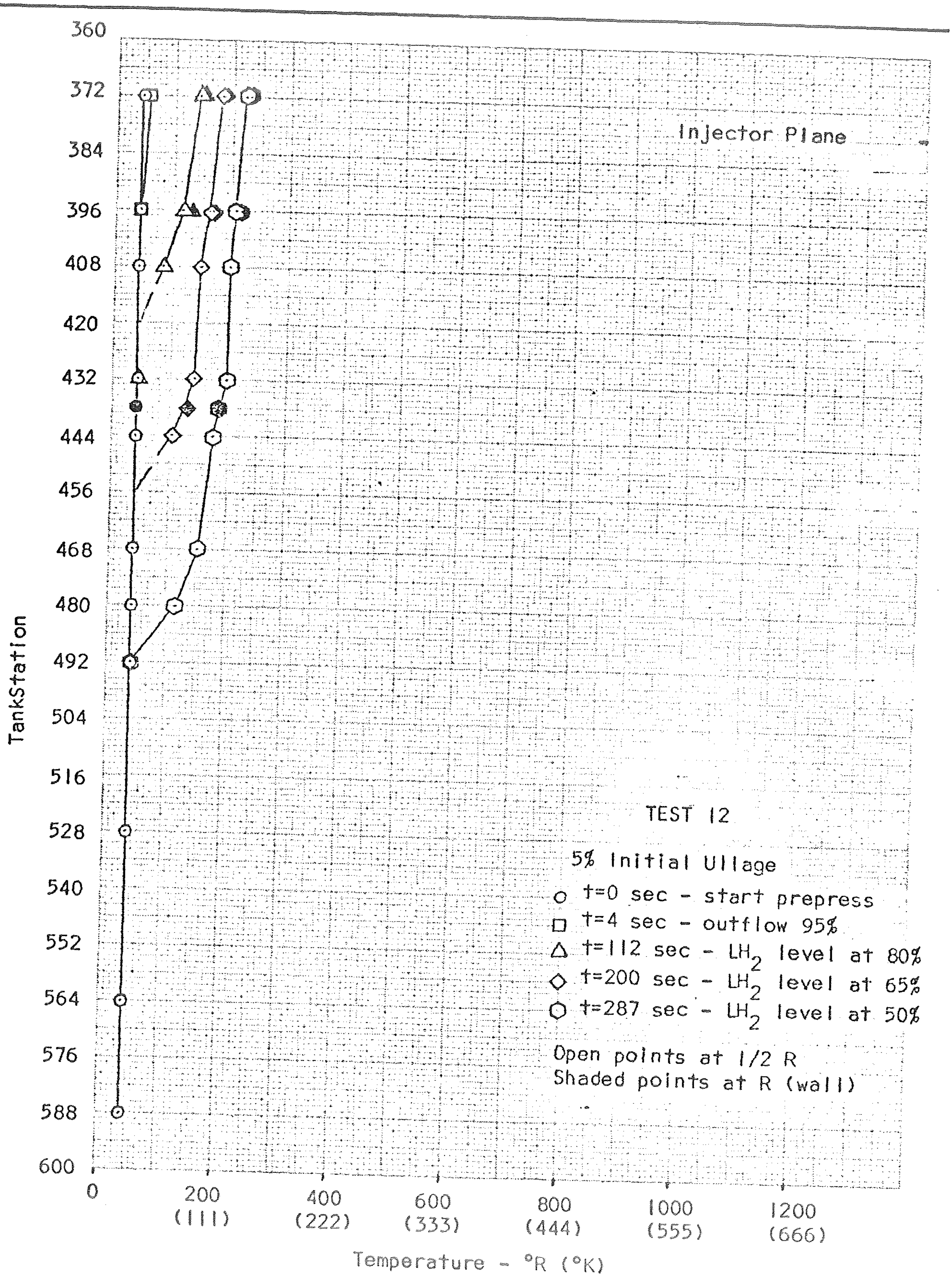

Figure 79. Axial Temperature Distribution for Test 12

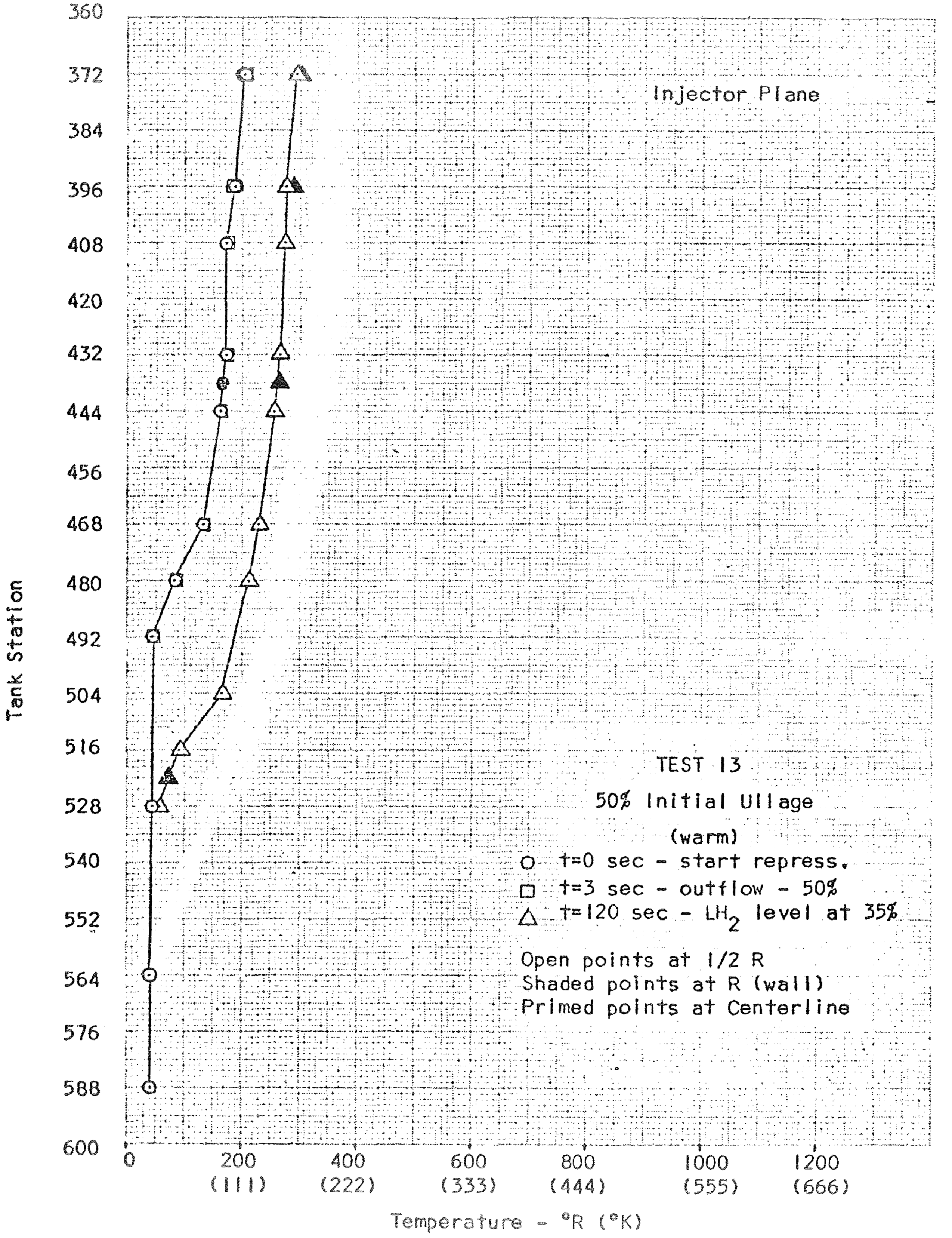

Figure 80. Axial Temperature Distribution for Test 13

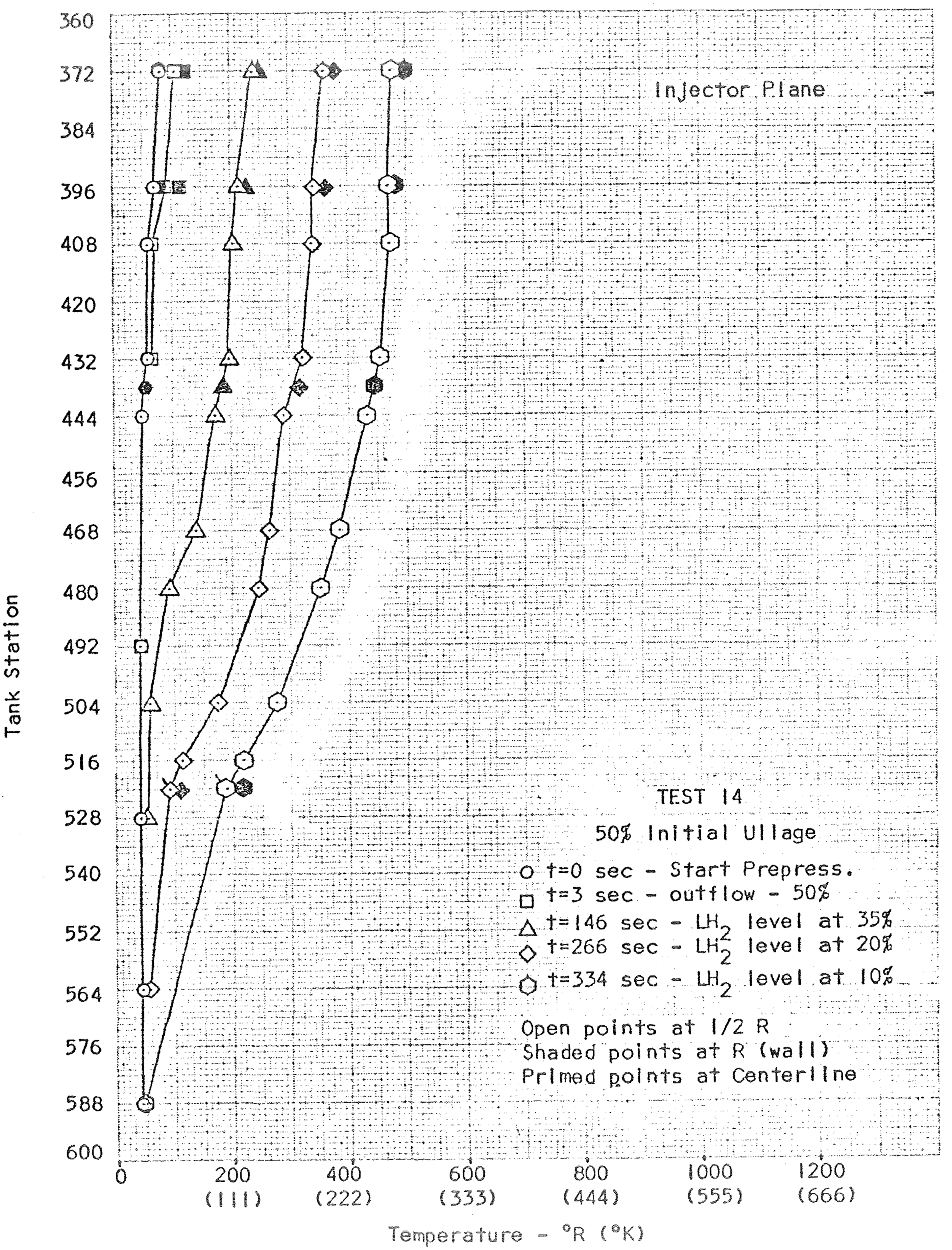

Figure 81. Axial Temperature Distribution for Test 14

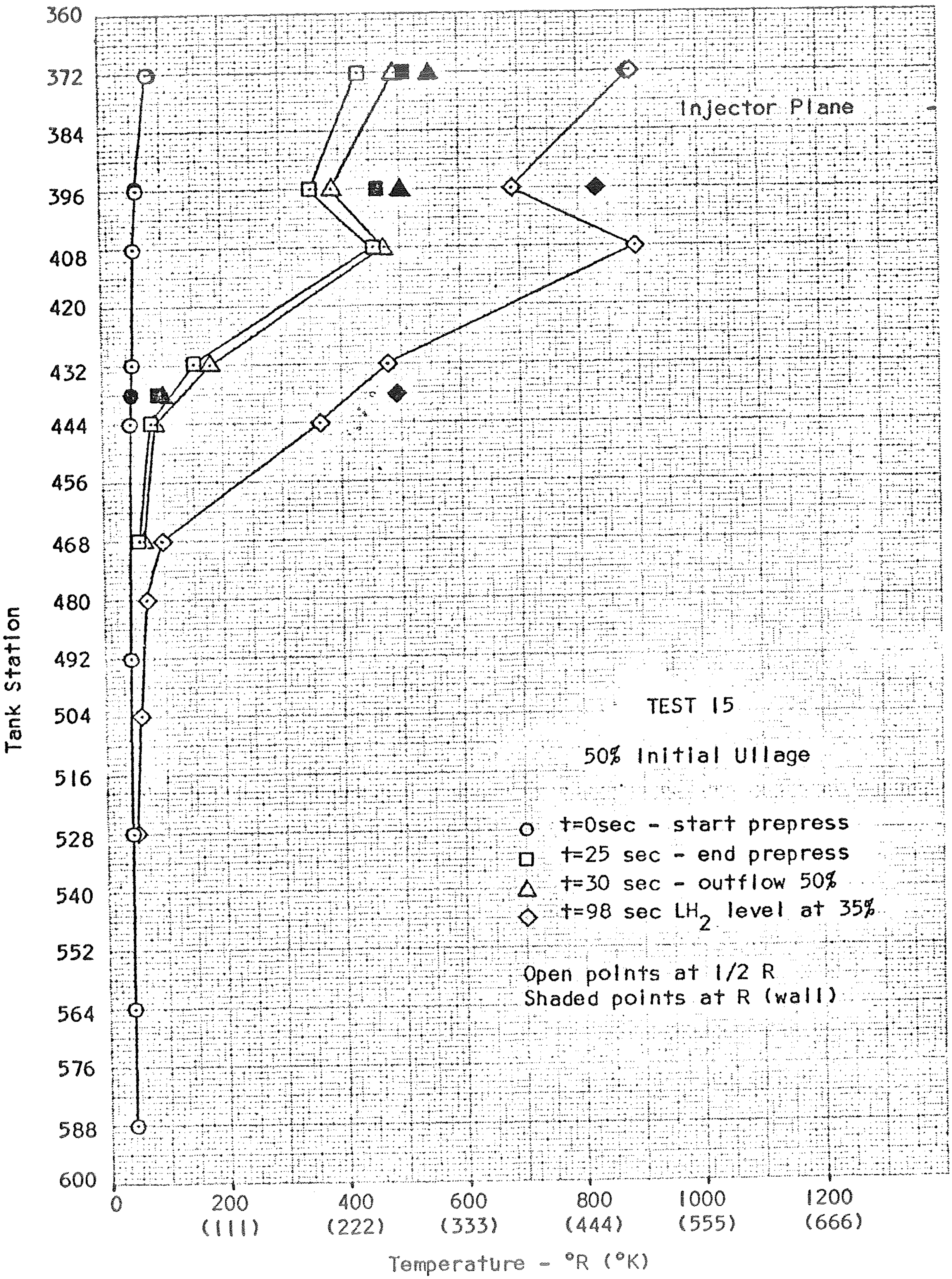

Figure 82. Axial Temperature Distribution for Test 15

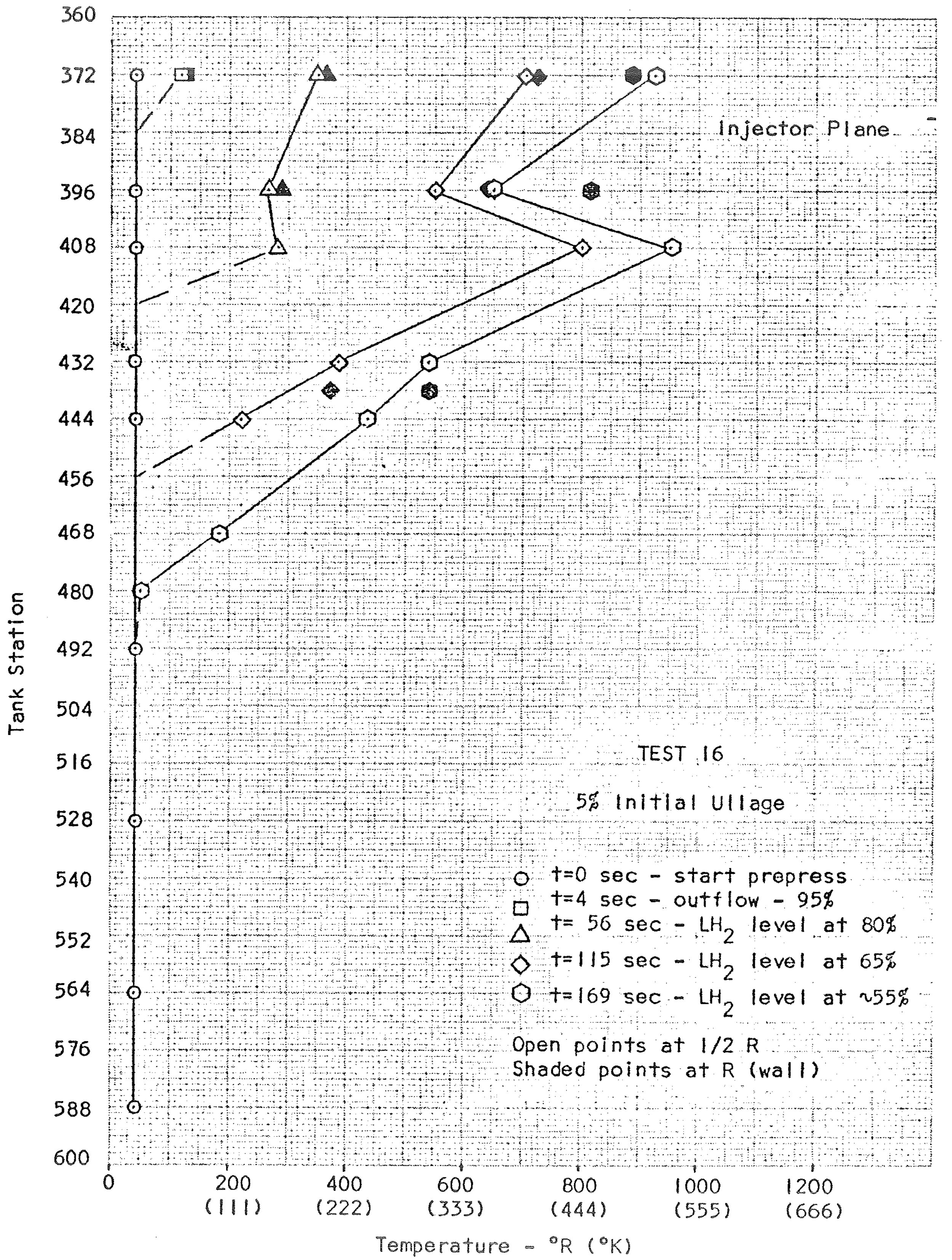

Figure 83. Axial Temperature Distribution for Test 16

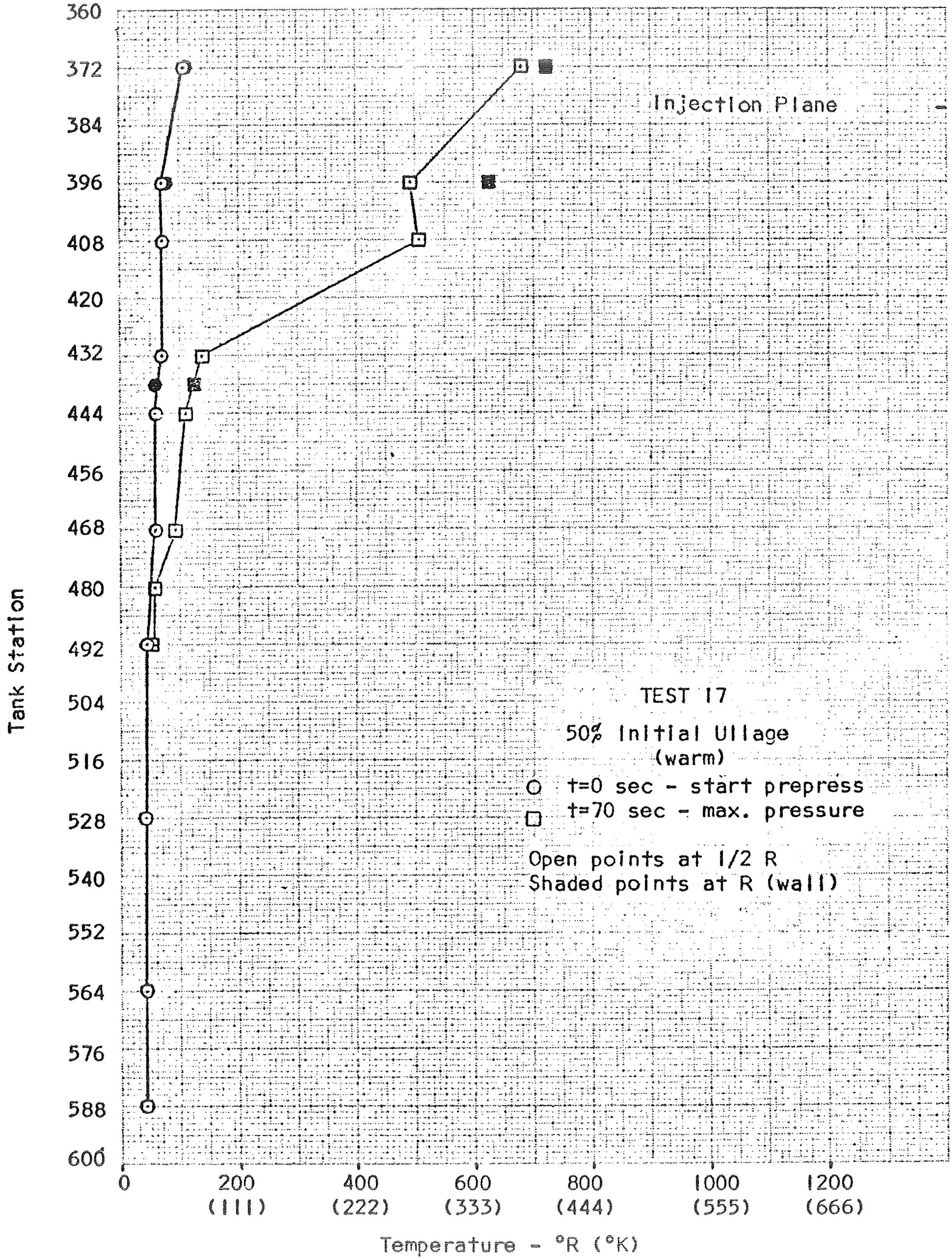

Figure 84. Axial Temperature Distribution for Test 17

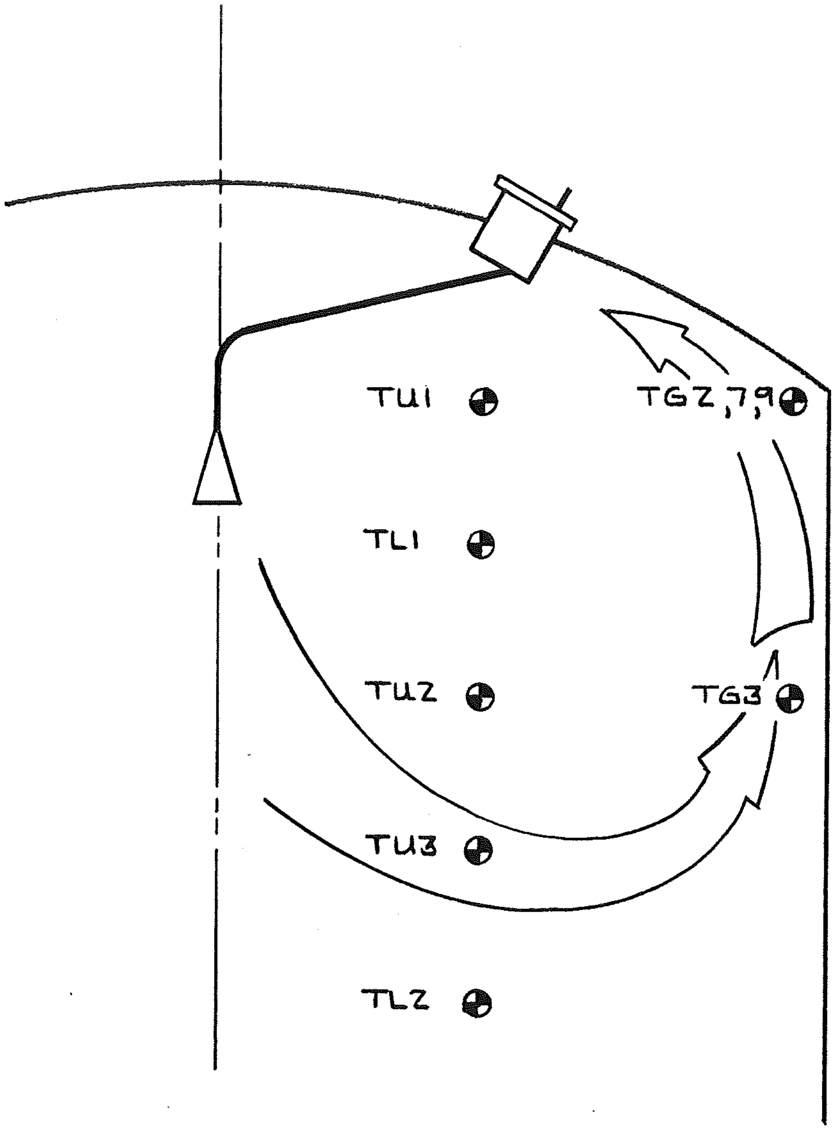

Figure 85. Diffuser Flow Field-Temperature Sensor Configuration

The same kind of flow field (but less severe) may be occurring with the straight pipe injectors, with the half-radius sensors in a cooler region of the circulating gas, while the wall sensors are in a warmer region. The implications of this flow field on ullage gas mixing and GF_2 usage were discussed previously in the Analytical Study section.

Uniform radial temperature distribution in the ullage gas is an assumption central to the one-dimensional nodal analysis. The data indicate that the radial temperature distribution is quite uniform between the half-radius and wall sensors. At station 438 there are three gas temperature probes at the wall fluxmeter installations (TG4, TG8, TG10), and two sensors on the half-radius probe, TU4 at station 432 and TU6 at station 444. The temperatures at TG4, TG8 TG10, and the average of TU4 and TU6, are shown in Figures 86 and 87 for tests 6 and 7, at times late in the test. At times early in the tests, all of these temperatures agree within a few degrees. The later times represent the maximum deviation of the gas temperatures from uniformity. The figures show the relative angular location of the sensors, and the distances from the injector to the sensor. The gas temperatures are quite uniform despite the disparity in distance from the half-radius probe to the wall, except for the gas temperature at TG8, which is lower than the other wall gas temperatures. The difference is perhaps due to the fact that the TG8 probe is aimed radially, from the center of a smooth sheet while the TG4, and TG10 probes are aimed tangentially from the side of a channel, and thus sense a different local flow field.

With the offset injector, the gas temperatures are also very uniform as shown in Figures 88 and 89 for tests 8 and 14. In test 8, the gas temperature 24 inches (.609 M) from the injector is essentially identical to that at 65 inches (1.65 M) from the injector. TG8 and TU 4-6 are at the same distance from the injector (~40 inches (1.02 M)) and record essentially the same gas temperature. Figure 89 for test 14 shows all four gas temperatures within 10°R (5.6°K) at 334 seconds, and nearly equal at 372 seconds. For earlier times, all four gas temperatures were essentially equal. Because there is very little gas temperature difference at various injector-wall distances, there should be very little difference in heat transfer. This was found to be true, as is discussed further in the next section. The ullage gas appears to be well mixed radially with the straight pipe injector.

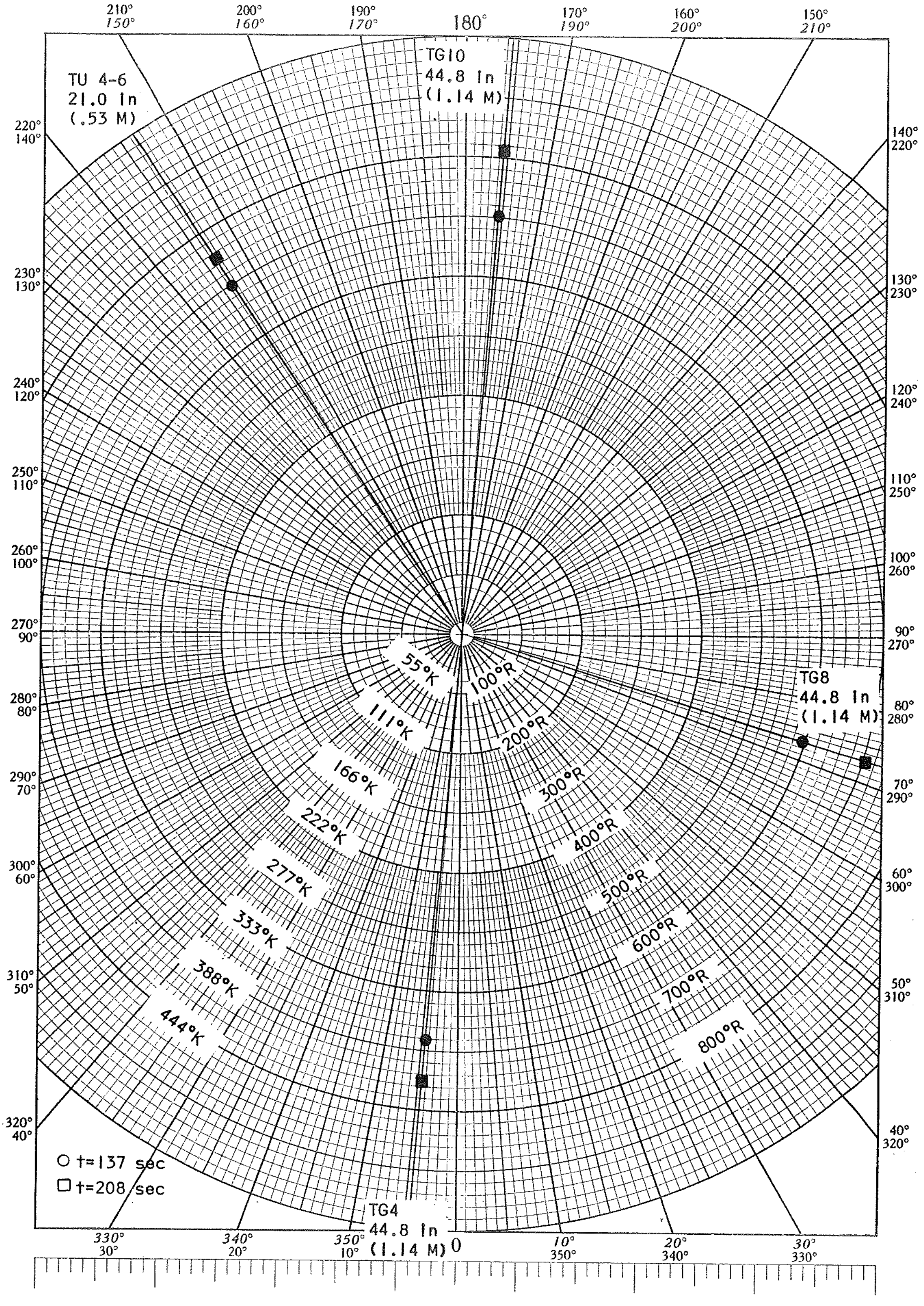

Figure 86. Radial Temperature Distribution - Test 6

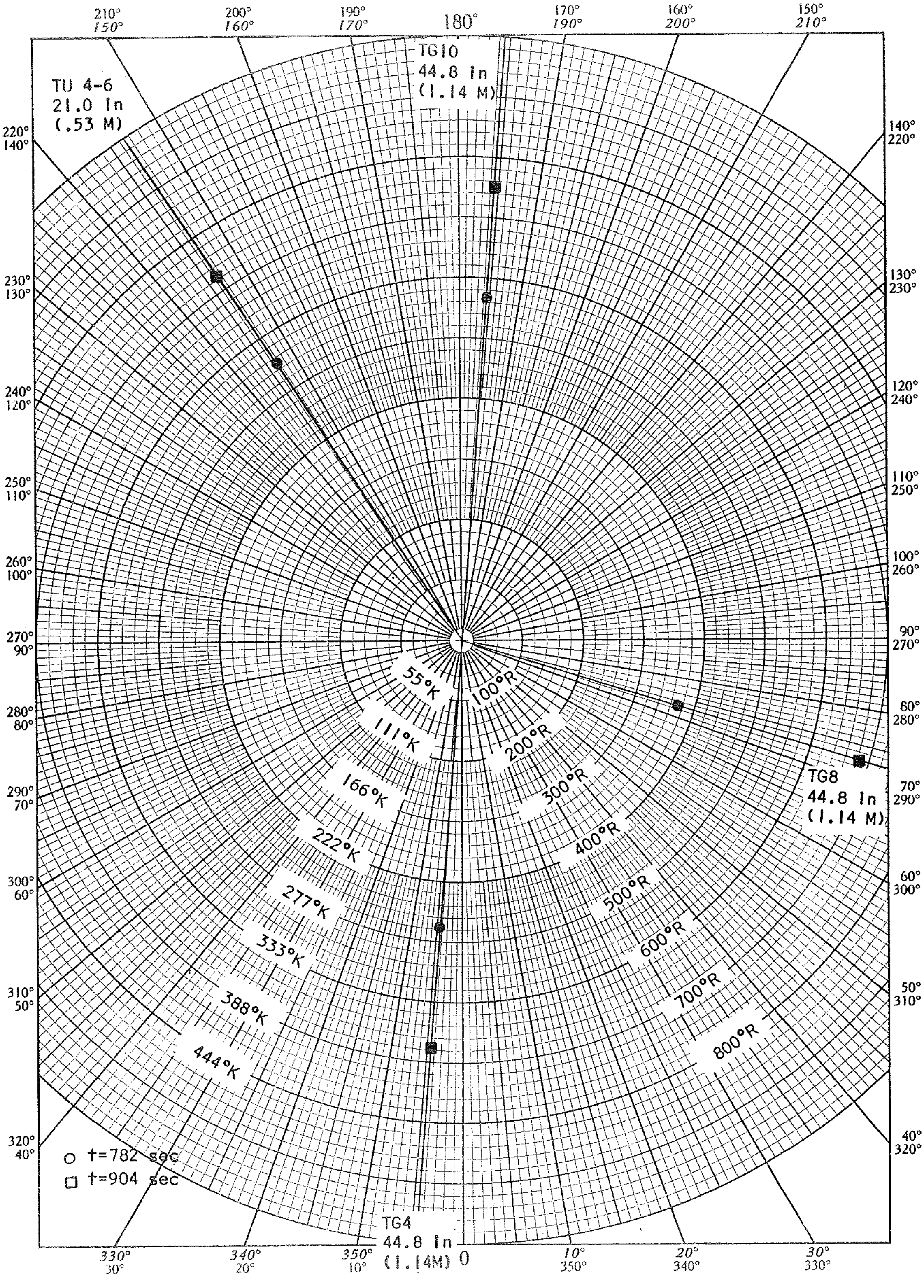

Figure 87. Radial Temperature Distribution - Test 7

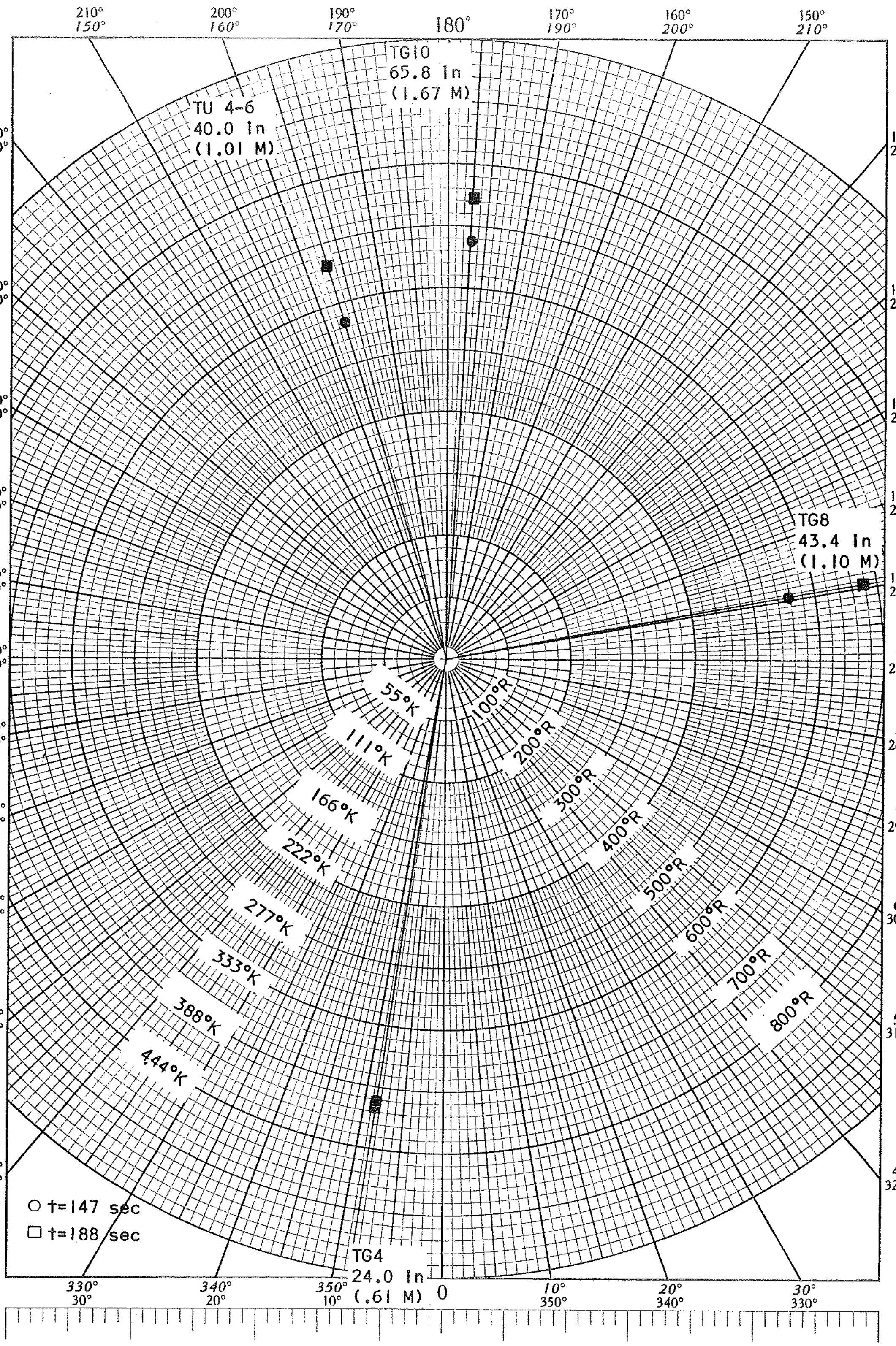

Figure 88. Radial Temperature Distribution - Test 8

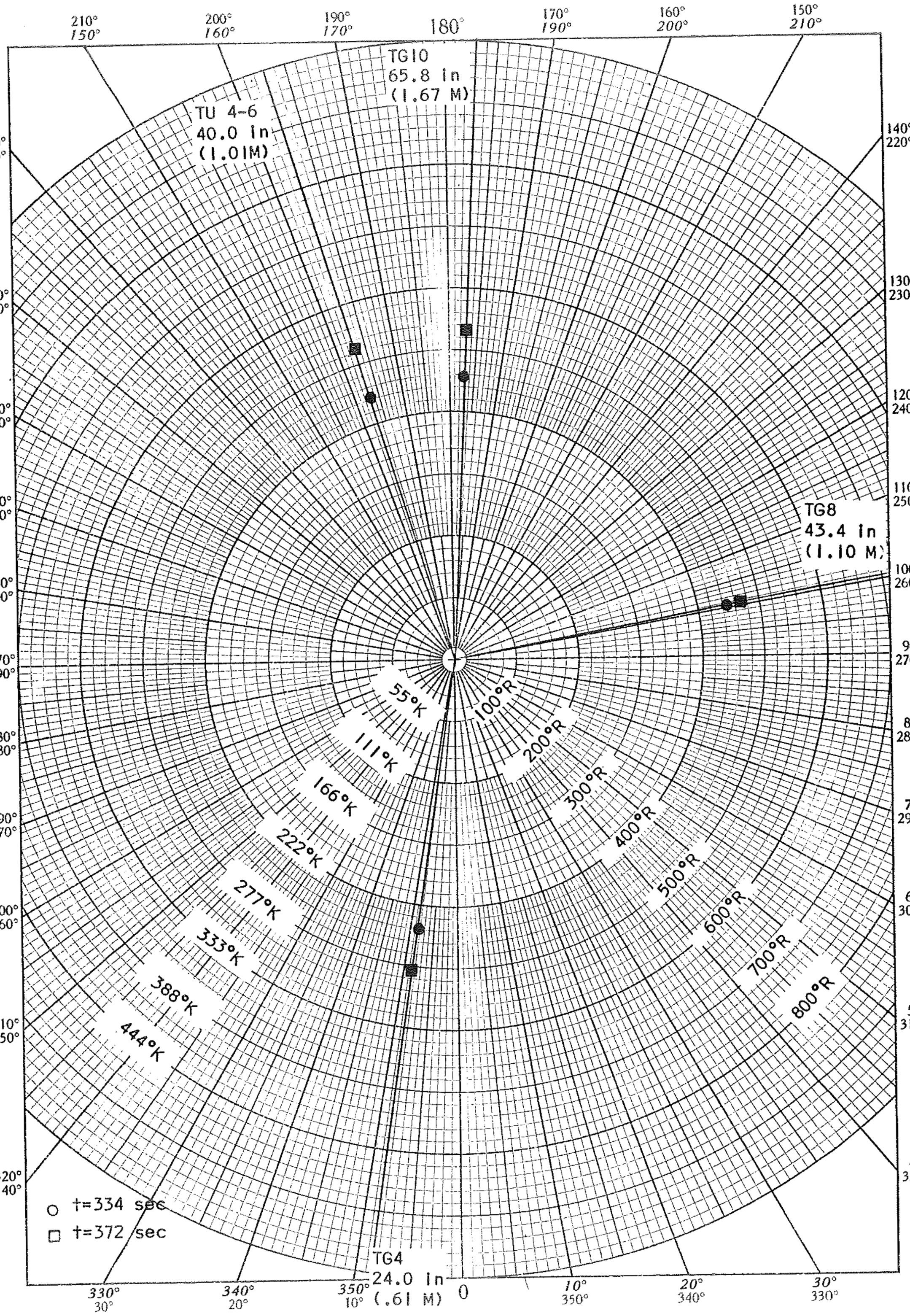

Figure 89. Radial Temperature Distribution - Test 14

The ullage gas temperatures with the diffuser injector were also quite uniform radially except for the anomaly at station 396, described above. At stations 372 and 438, the temperatures recorded by the half-radius and wall sensors were nearly as uniform as those with the straight-pipe injector. Again, the temperature at TG8 was consistently lower than at TG4 and TG10.

The ullage gas temperatures near the LH_2 interface were measured with the thermopile assemblies. It was found that the temperatures measured with the thermopiles agreed closely with the temperatures measured by the half-radius gas sensors near the interface. The thermopile assemblies provided reliable temperature measurements only if the liquid temperature reference sensor is immersed in LH_2. Thus, the thermopile gives reliable data on the initial conditions at the interface up to the time the reference sensor is uncovered, as well as data when the interface passes a thermopile location during outflow. None of the thermopiles indicated any initial stratification near the interface even with so-called "warm" ullages. However, they did indicate that very large gradients could occur at the interface within a few seconds after prepressurization. The data for test 7 are shown in Figures 90 to 92. The 5 percent ullage prepressurization is shown in Figure 90. There is initially a large gradient, which cools down until outflow occurs. The gradient then follows the interface downward. In Figure 91, as the interface approaches the thermopiles at the 50 percent level, the temperature gradient is quite steep and variable. This indicates how well the ullage is mixed and penetrated by injection. In Figure 92, as the interface approaches the thermopiles at the 90 percent ullage level, the temperature gradient is much less severe and quite cold.

Figure 93 shows the end of test 12, as the interface approaches the 50 percent level (where outflow was stopped) and the start of test 13 with prepressurization at the same level. The temperature gradient is quite steep, and varies erratically when carried along with the interface during outflow. During prepressurization, the gradient is much better behaved.

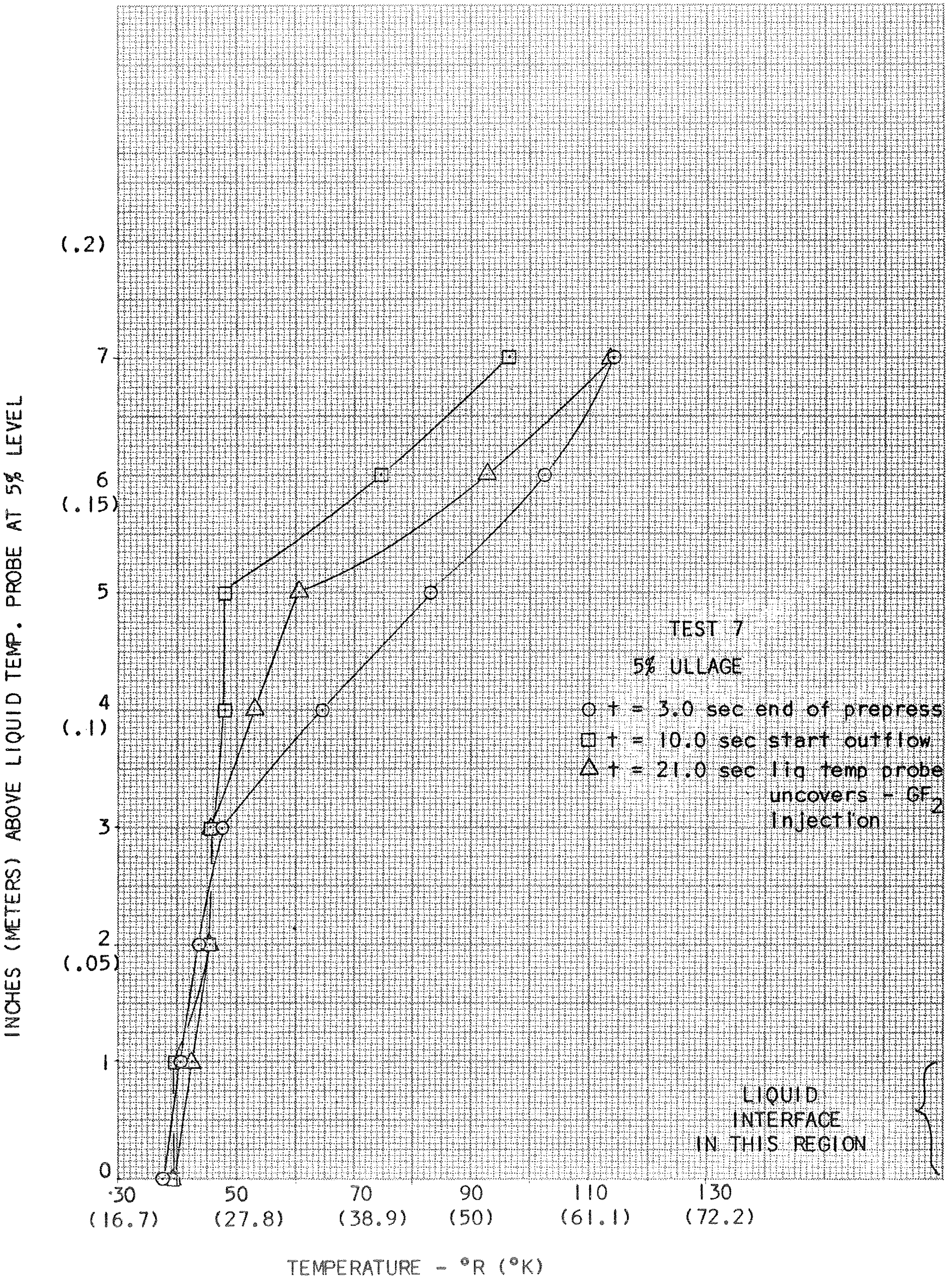

Figure 90. Temperature Gradient at 5% Level-Test 7

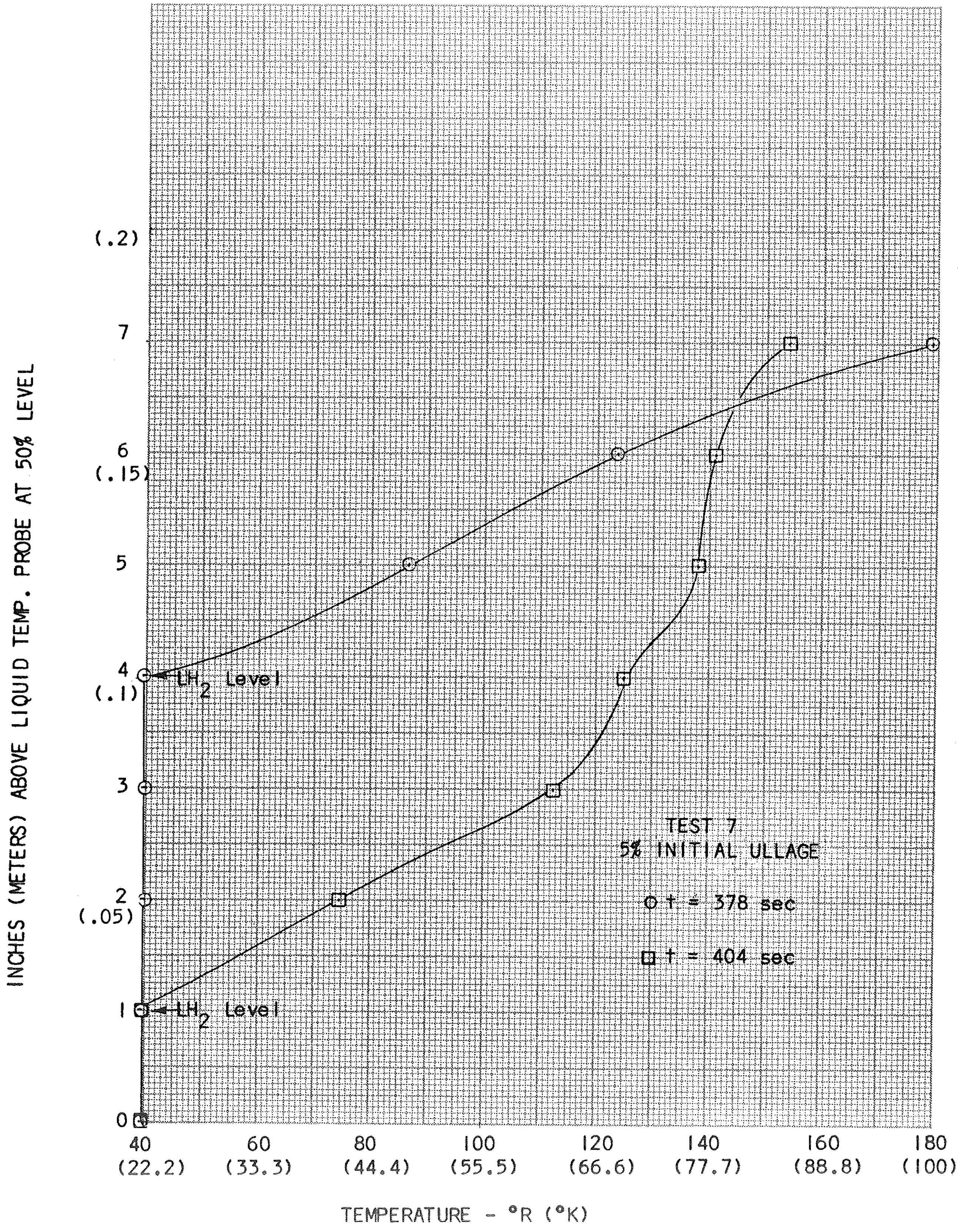

Figure 91. Temperature Gradient at 50% Level-Test 7

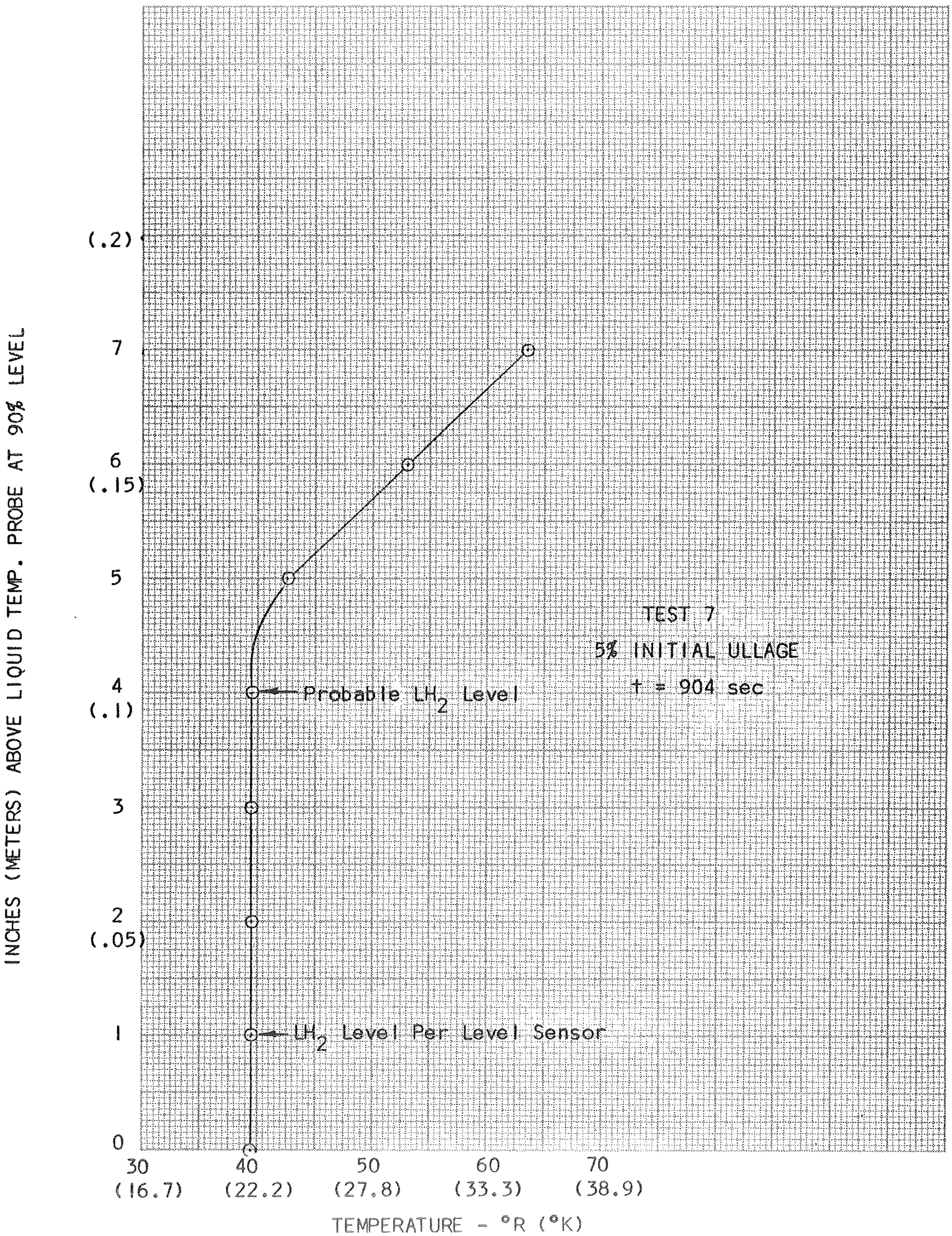

Figure 92. Temperature Gradient at 90% Level-Test 7

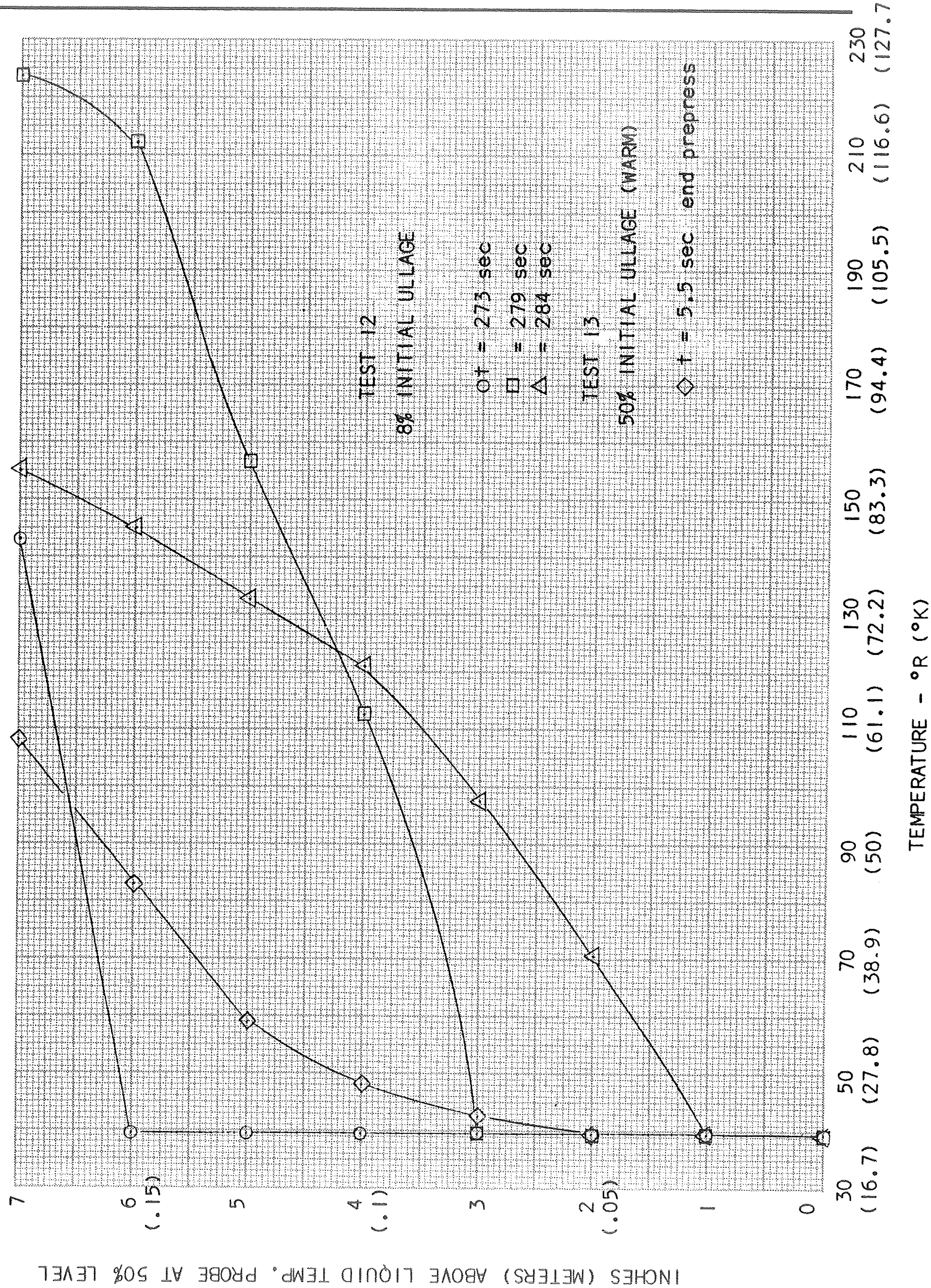

Figure 93. Temperature Gradient at 50% Level-Test 12 and 13

Figure 94 shows the gradients for the prepressurization at 5 percent ullage with the diffuser injector (test 16). The gradients are not much different from those of the straight-pipe injector (test 7) except that the ullage is warmer, because test 16 was at higher pressure (43 psia (296 x 10^3 N/M^2) compared to 24 psia (165.5 x 10^3 N/M^2)).

The existence of thermal gradients in the LH_2 was not revealed by the thermopiles; they only reacted measurably to the passage of the gas-liquid interface. This may have been because the gradient in the LH_2 was so shallow that the thermopiles could not detect it. The liquid temperature sensors, on the other hand, did reveal the existence of a layer of saturated LH_2 in many of the tests. This layer usually grew during the test and ranged up to nearly 3 feet (.915 M) thick; e.g., in test 7, the saturated LH_2 layer thickness grew from .22 ft (.067 M) at 136 seconds to 2.84 feet (.866 M) at 782 seconds. This growth would require a heat input of 4740 Btu (5.0 x 10^6 joules), or 7.2 Btu/sec (7600 watts). The external heat leak to the tank during this time averaged about 7.5 Btu/sec (7910 watts), thus it appears that the growth of the saturated LH_2 layer during this long test can be explained as caused by the external heat leak. Even in much shorter tests, such as test 4, where the saturated LH_2 layer was apparently about .24 ft (.073 M) thick after 109 seconds, and test 12, where the layer was .48 ft (.146 M) thick after 287 seconds, the external heat leak would account for most, but not all, of the layer growth. In a space vehicle, where the external heat leak is much less than in the test tank, the MTI process may contribute more significantly to LH_2 saturation. However, for prepressurization, where MTI has the most utility, the saturated layer caused by MTI was shown in our tests to be insignificant (of the order of a couple of inches (.05 M), at most).

The tank wall temperatures were distributed axially in much the same way as the ullage gas temperatures, and showed little tangential variation at a given station. The wall temperature distribution is shown in Figure 95 for a typical centerline straight-pipe test (test 2), and in figure 96 for a typical offset straight-pipe test (test 8). Even for very hot ullage gas temperatures, the tank wall never got much above room temperature on the side walls. This was probably due to the good thermal conduction path down the walls to the LH_2. With thinner, less conductive walls, the wall temperature would more closely approach the ullage gas temperature.

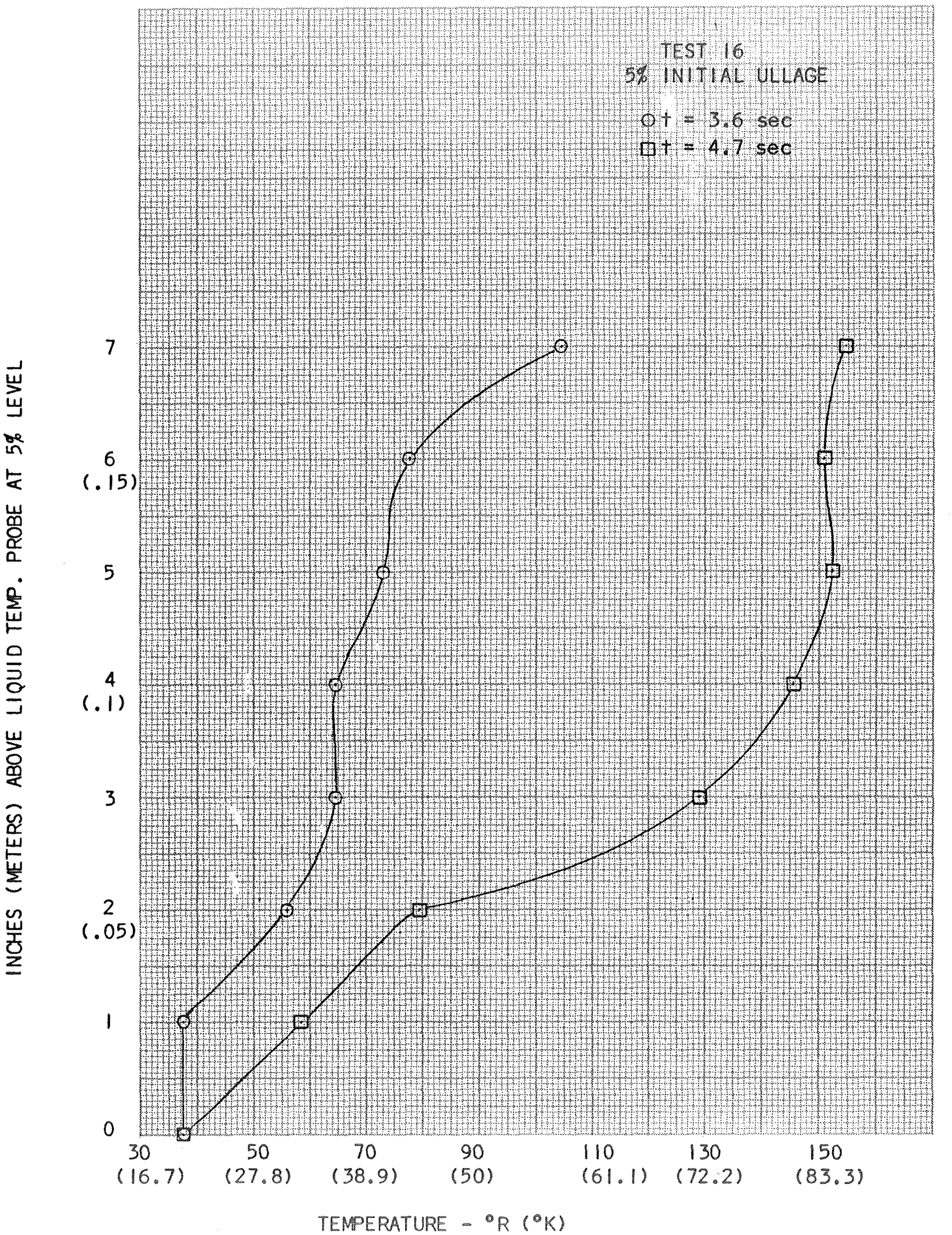

Figure 94. Temperature Gradient at 5% Level-Test 16

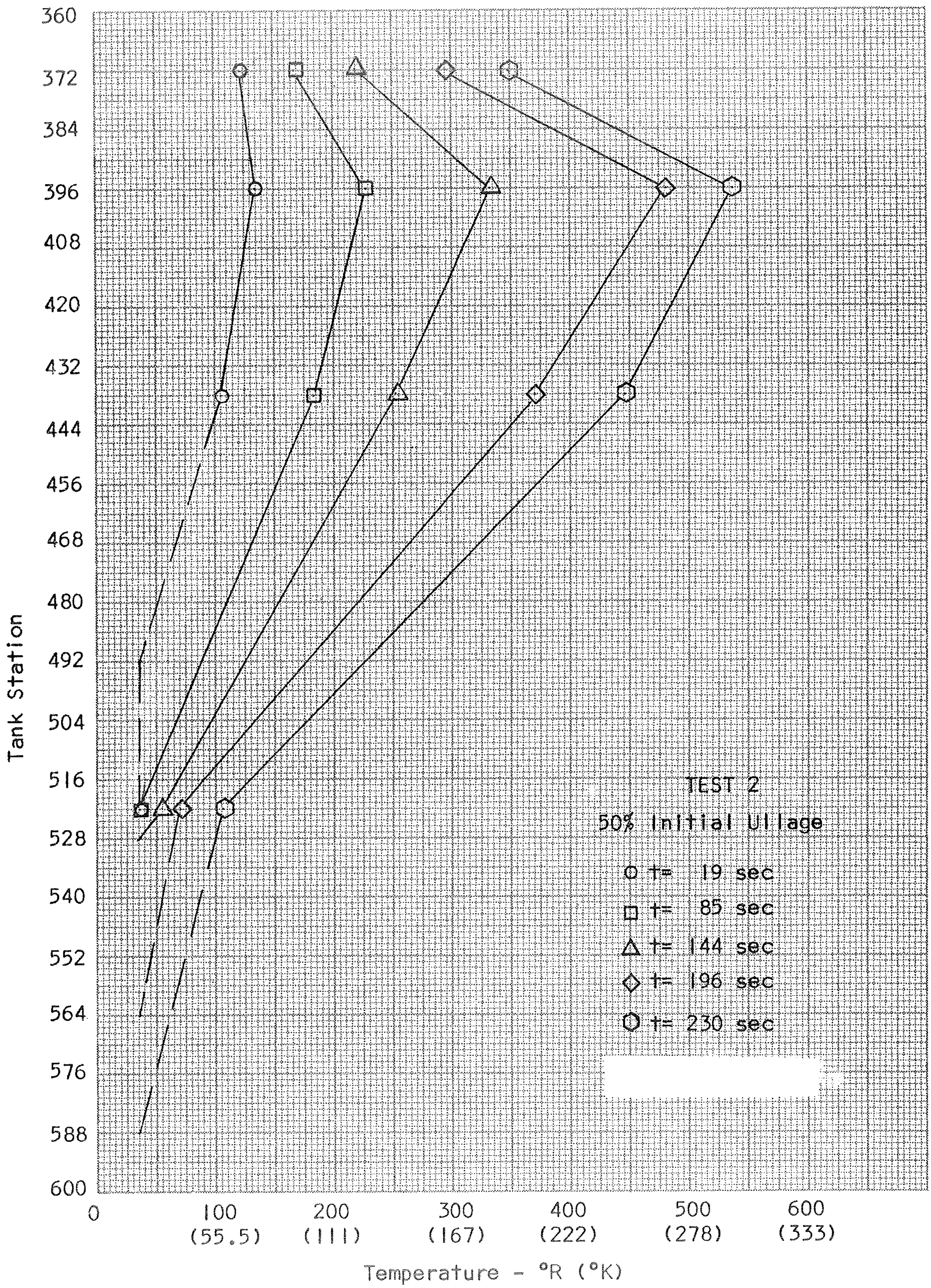

Figure 95. Tank Wall Temperature Distribution-Test 2

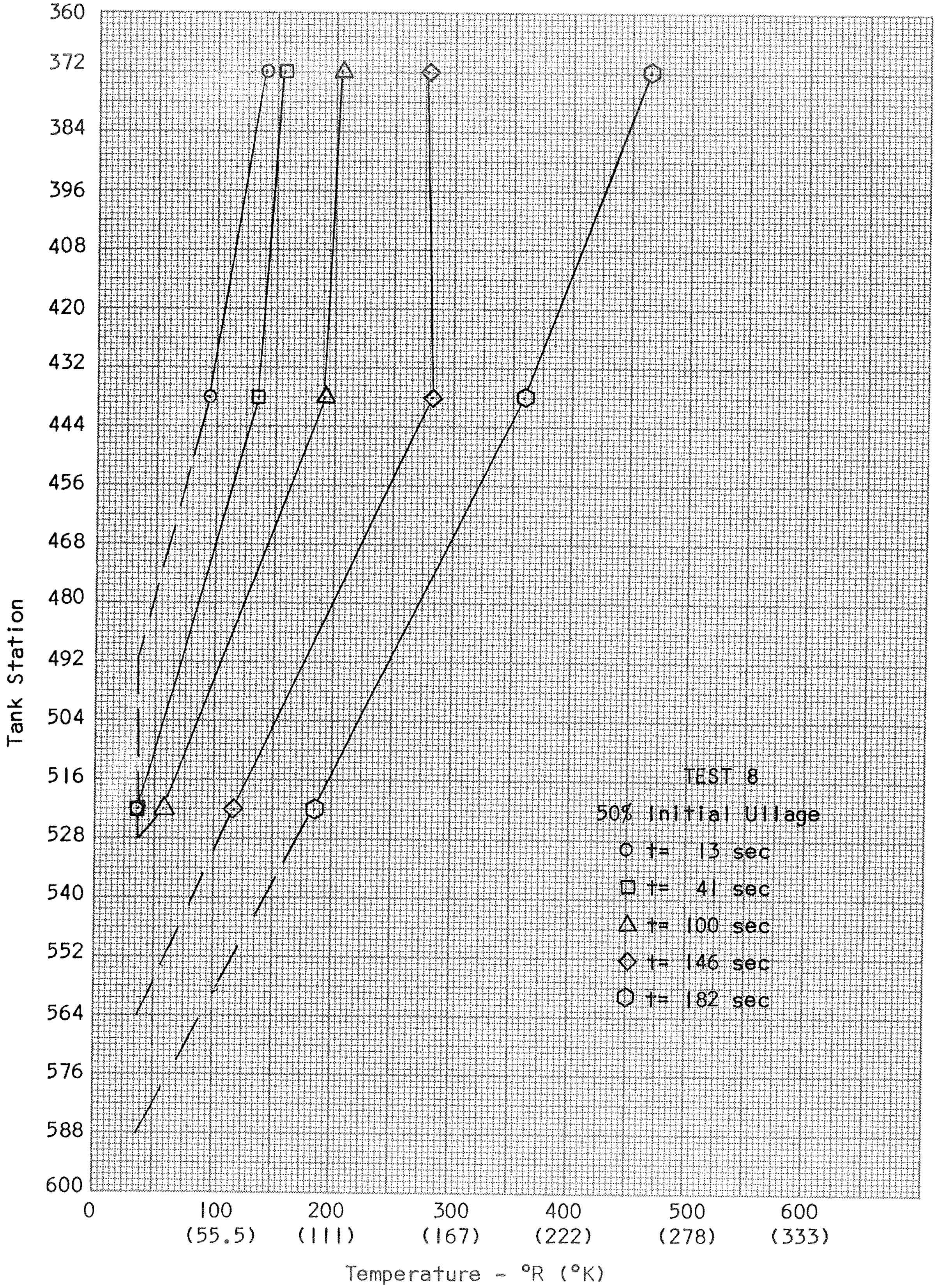

Figure 96. Tank Wall Temperature Distribution-Test 8

Tank Heat Flux and Heat Transfer

The heat flux measurements made in the large tank were somewhat limited. The fluxmeter installations near the top of the tank were exposed to rather high temperatures (~1000°R (556°K)) and a number of them failed in the course of the test program. Sometimes, the fluxmeter continued to function, but the temperature sensor on the fluxmeter failed. The fluxmeter in the dome, HI, failed after the first test, debonded, and fell to the bottom of the tank (see the section on Other Vehicle Effects). The fluxmeters which were lower in the tank, which were not exposed to high temperatures, were not damaged, but did not measure any appreciable heat flux.

The data determined from the centerline injector tests indicated heat transfer in excess of that accounted for by free convection. The difference in the measured heat transfer coefficient and the free convection heat transfer coefficient was assumed to be the forced convection heat transfer coefficient. From Reference 13, the equation for forced convection to a vertical flat plate is:

$$\frac{h_{fo} d}{K} = 0.037 \left(\frac{\rho U d}{\mu}\right)^{4/5} \left(\frac{C_p \mu}{K}\right)^{1/3} \tag{86}$$

The forced convection heat transfer coefficient is weakly dependent on a characteristic dimension ($d^{-1/5}$) which was arbitrarily set at 4 inches (.1017 M), (the width and height of the fluxmeter). The velocity needed to give the correct forced convection coefficient was determined. It was observed that this velocity was related to the GF_2 velocity in the injector and to the injector on-time fraction for the fluxmeters in the mixed zone (top of the ullage). This is shown in Figure 97. The observed correlation is

$$U = .12\, U_{Jo} f \tag{87}$$

where U_{Jo} is the injector velocity and f is the on-time fraction. The dependence of the forced convection heat transfer on the injector on-time was a real effect — the heat flux at the top of the tank often pulsed in approximate synchronization with the injector flow. In the lower portion of the ullage, the velocity was not a function of the on-time fraction, and, while initially

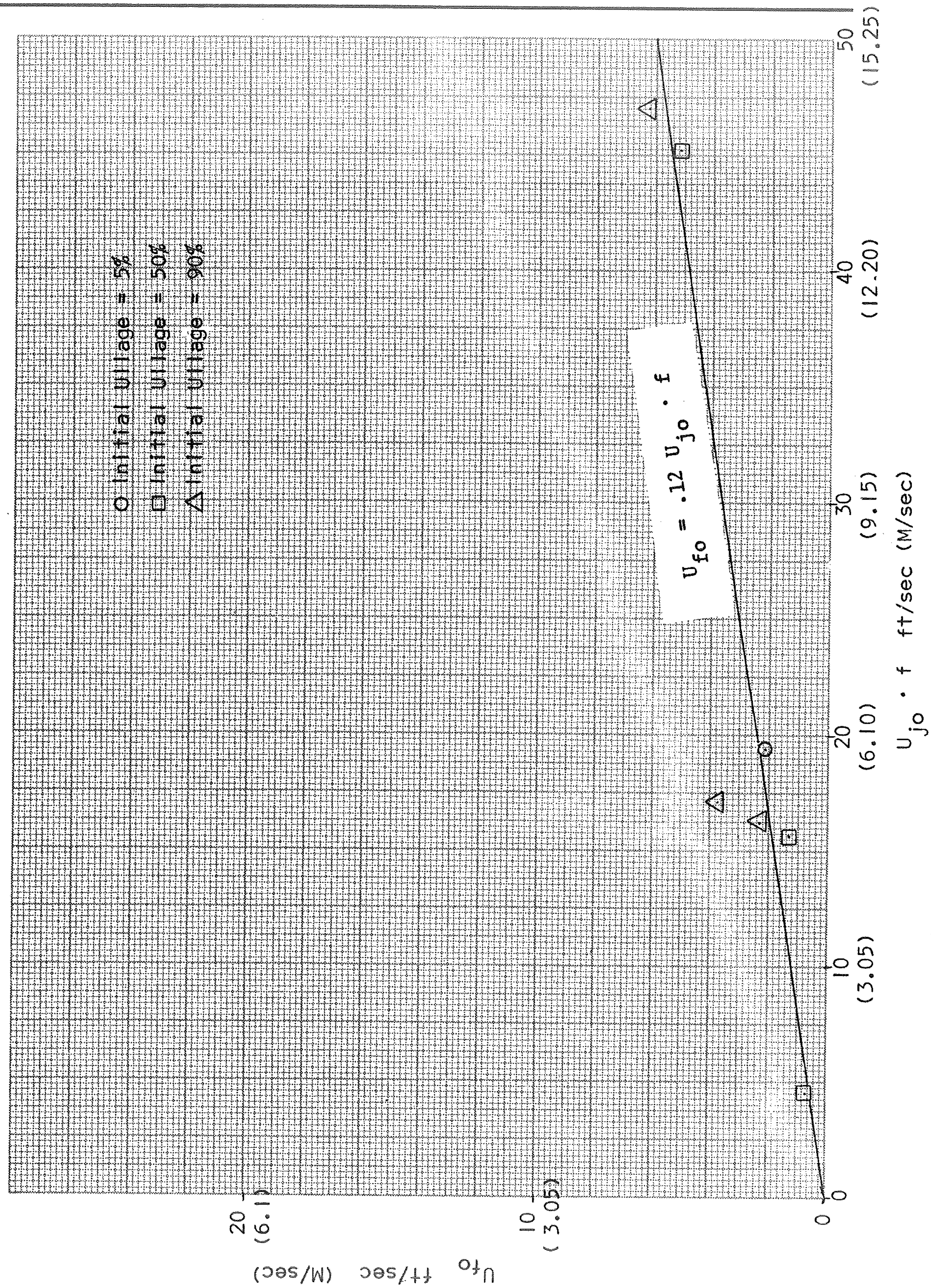

Figure 97. Forced Convection Heat Transfer Velocity Correlation

related to the injection velocity, rapidly decayed to zero. Thus, the overall heat transfer coefficient quickly approached free convection in this region.

One of the objectives of the offset injector tests was to determine the effect of various radial distances on heat transfer. There were no conclusive results of any such effect. This may have been due to the uniformity of the well-mixed flow field in the tank, as evidenced by the lack of significant temperature anomalies, (as discussed previously in the section on Temperature Distribution).

It was observed that the heat flux to the fluxmeter on the smooth aluminum sheet was consistently somewhat lower than the flux to a channel-mounted flux-meter near the waffle-patterned wall at the same station, as shown in Figure 98.

This variation could be due to increased turbulence and heat transfer from flow field variations near the waffle-patterned wall, or could simply be due to the greater capacity of the channel-mounted fluxmeter to transmit heat to the LH_2 through the rather good conductive path of the thick channel. The difference could also be attributed to the differences in gas temperature sensor location or other geometric variances. It is difficult, therefore, to draw any firm conclusions about heat transfer to smooth or waffle-patterned walls from the limited data.

HF Sampling

The HF sampling system was described previously in the section on Test Facility Design. Once the HF was trapped in the filters, and purged out to the HF absorber tubes, the absorber tubes were removed and chemically analyzed in the laboratory to determine the HF quantity trapped in each filter. The chemical analysis procedure was as follows:

1. Remove top fitting from HF absorber tube.
2. Pour contents of tube into 1 liter polyethylene beaker, making certain that no caked material remains in the tube.
3. Macerate the powder in the beaker until all lumps are broken up.
4. Add 500 ml of water to the beaker and stir the mixture for 3-4 minutes (180-240 sec).
5. Take pH of suspension. pH of blank is 6.8.

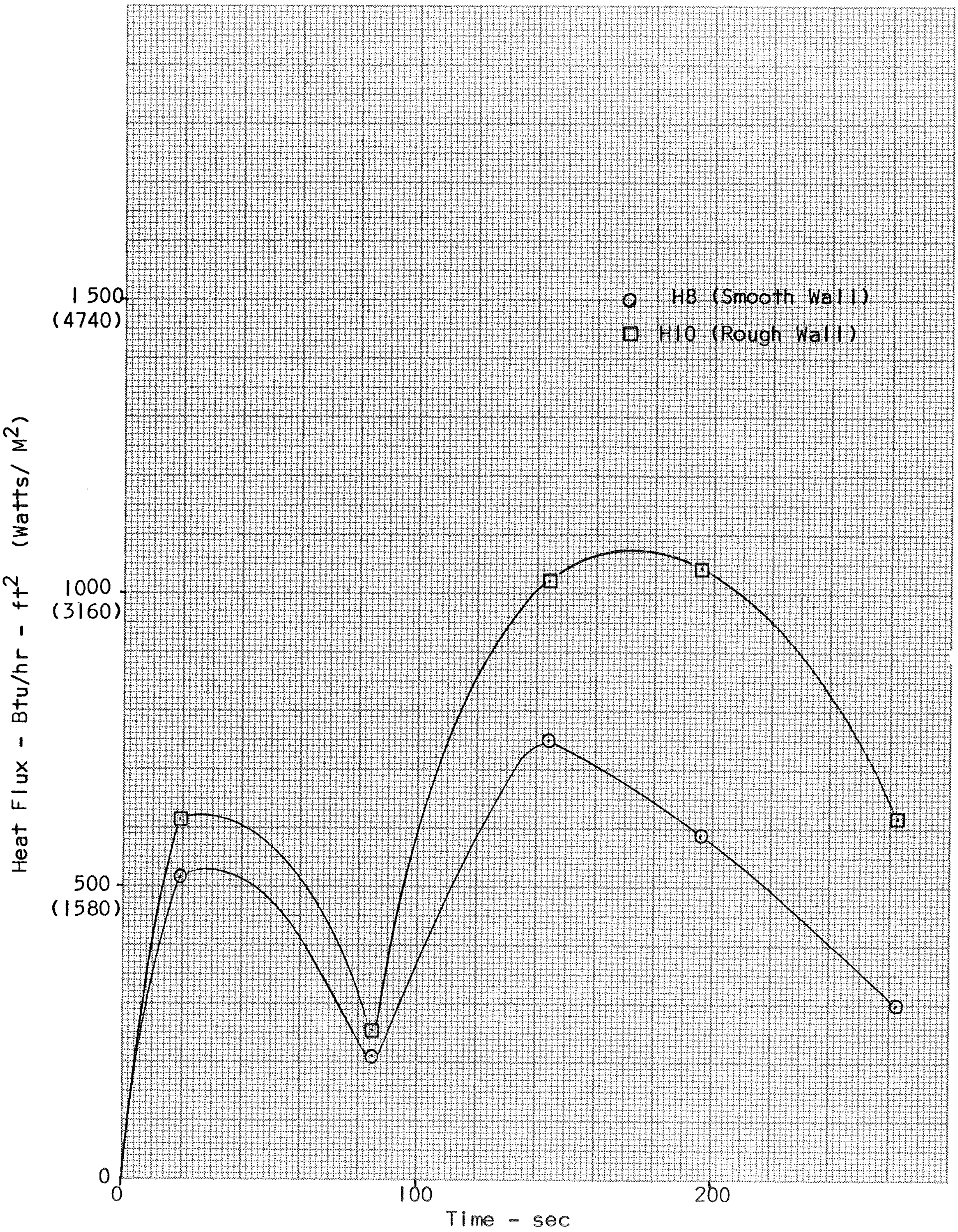

Figure 98. Smooth Wall Heat Flux Compared to Rough Wall Heat Flux

If pH of Suspension is Above 2:

6. Add 1-2 ml of phenolphthalein indicator and, stirring rapidly, titrate with 0.1024 N NaOH solution to pink end-point that remains permanent for fiteen seconds. The titration of the blank with this solution is 4.3 ml.

   Calculations: (mls sample titration - mls of blank titration) x 0.2048 = HF % by weight.

If pH of Suspension is Strongly Acid, Below 2:

7. Put suspension in one liter volumetric flask and dilute to the mark with water.
8. Stir thoroughly. Allow powder to settle.
9. Pipet suitable aliquot (probably 50 ml) into polyethylene beaker.
10. Dilute with water to 500 ml.
11. Add 1-2 phenolphthalein indicator and with rapid stirring, titrate with 1.034 N NaOH solution to pink end-point that remains permanent for fifteen seconds. The titration of the blank with this solution is 0.1 ml.

    Calculations: (mls of sample titration - mls of blank titration) x 2.068 = HF % by weight.

The results of the analysis for the tests which were sampled for HF quantity are shown in Table 9.

The uncertainty in the LH_2 quantity is due to the presence of two-phase flow through the sample filter system, while the system chills down. In the test 7 sample, however, the LH_2 outflow was sampled from the 10+ percent level sensor to the 10 percent level sensor (which were one-inch (.0254 M) apart). Thus, the equivalent of one-inch (.0254 M) of LH_2 in the tank (or 17.85 lb (8.10 Kg)) was passed through the sample system. It was unlikely that much LH_2 in the tank boiled off during sampling because the LH_2 was saturated at 25 psia (172.3×10^3 N/M^2) from test 7, and the tank was pressurized to 45 psia (310×10^3 N/M^2) during the sampling. From Table 9 it will be noted that except for test 7, only traces of HF were found in the absorbers. The possible reasons for this are:

1. HF trapped in the filters is not efficiently purged through to the absorbers.
2. The filter sampling technique does not provide a fair sample of the HF which might be present in the bulk LH_2.
3. Little HF is present in the bulk LH_2 outflow.

TABLE 9

HF SAMPLING RESULTS

Test No.	HF Quantity-Grams (10^{-3} Kg)			LH2 Quantity-Grams (10^{-3} Kg)		Remarks
	100 μFilter	30 μFilter	10 μFilter	Max	Min	
4	0.0215	0.0000	0.0016	4640	1990	Flowmeter not working
7	0.47	0.31	0.0057	8100		Sampled from 10+% to 10%-flowmeter not working
8	0.0018	0.0000	0.0000	1030	790	Burst disc blew. LH2 quantity questionable
10	0.0000	0.0000	0.0000	4070	3520	
13	0.0000	0.0016	0.0000	3840	2690	
15	0.0000	0.0000	0.0000	0		No apparent LH2 flow

The filters and the valves isolating them were a sizable mass of metal which was difficult to warm up; therefore, thermocouples were installed under the insulation to determine when the filters were warm enough to vaporize the HF (HF boils at 527°R (293°K). Generally the filters were warmed up to 535-540°R (297-300°K)). It is thought that all HF was removed from the filters, which always looked very clean and dry when inspected during the course of the test program.

In order to evaluate possibilities (2) and (3) above, the characteristics of test 7, which provided an apparently reasonable sample, will be examined in detail. During the initial phase of test 7, the ullage is very cold (see Table 8), and the HF would tend to condense out and freeze in the ullage and fall into the LH_2 or condense and freeze directly in the LH_2 (with a nearly full tank). However, during this time the GF_2 usage, and HF production is very low. Later in the test the GF_2 usage and HF production is much higher, but the ullage is large and warm, so that HF condensation would not occur. Therefore, the quantity of HF which could end up in the LH_2 is much less than the total quantity produced during the entire test. Further, the previous MTI work under contract NAS 3-7963 indicated that considerable HF froze on the tank walls because they were colder than the ullage. As an example, in test 7, the ullage temperature is below the HF freezing point of 326°R (181°K) up to a time of 582 sec, (when the ullage is 702 ft^3 (19.9 M^3)). The ullage temperature is above the HF boiling point of 527°R (293°K) from a time of 780 sec until the end of the test at 902 sec. However, between the times of 582 and 780 sec when the HF could be in liquid form in the ullage, the tank walls are still below the HF freezing point.

Therefore, up to the time of 582 sec, 3.1 lbs (1.41 Kg) of HF is produced which could freeze in the ullage or freeze on the walls, and which could credibly end up in the LH_2. Between the times of 582 and 780 sec, the 3.58 lbs (1.62 Kg) of HF produced would condense in the ullage, but tend to freeze out on the cold tank walls. Probably very little of this HF would end up in the LH_2. From a time of 780 sec on, the 2.76 lbs (1.25 Kg) of HF produced would be in vapor form in the ullage, but would tend to condense on the colder walls and run down the wall and freeze. Again, little of this HF would end up in the LH_2. The thesis that most of the HF ends up on the tank walls and internal hardware is supported by evidence of noticeable HF etching effects on the tank walls at about station 480. This is just about where the HF condensation/freezing line is located for the end of test 7. This condition is further described in the section on Other Vehicle/Hardware Effects, and Figure 103 in that section shows the etch marks on the tank wall.

It appears that the maximum credible quantity of HF which would end up in the LH_2 is about 3.1 lbs (1.41 Kg) in 3910 lbs (1772 Kg) of LH_2, or if evenly distributed, about one part in 10^3. Although frozen HF is heavier than LH_2, it tends to sink very slowly (see Reference 1) but since it tends to freeze in the LH_2 early in the test, there would be plenty of time for it to sink to the tank bottom. It is believed that a substantial portion of the HF remains behind on the tank bottom, or trapped in the outflow sump, or in crevices in the outflow line, instrumentation wiring, etc. It is thought that the test 7 sample of 1 part HF per 10^4 parts LH_2 is a valid sample representing a credible maximum that would be found when there is plenty of time for the HF to sink to the tank bottom. With the other tests shown in Table 9, the credible quantity of HF reaching the LH_2 ranged from 2.4 (1.1 Kg) to 2.75 lbs (1.25 Kg), but the rapid test times made it less likely that much HF would reach the sample system; however, with rapid outflows, more HF could be concentrated in the last LH_2 leaving the tank.

The conclusions reached about the HF sampling are that the quantity of HF in the LH_2 would range from 1 part per 10^3 to 1 part per 10^4. Further, a 10μ filter appears adequate to filter the HF that is present. On the other hand, considerable HF passes through the 100μ filter so that HF clogging of small orifices (engine injectors) appears not to be a problem.

Other Vehicle/Hardware Effects

None of the injectors used in the test program were damaged, and showed only heat discoloration. The maximum injector temperatures recorded during the test program are shown in Table 10. In general, the temperatures are quite reasonable and in line with that predicted from the injector demonstration tests. In the diffuser tests the thermocouple wire burned off, but recorded 1460°R (811°K) in the process - this was not the injector temperature. The centerline straight-pipe injector after testing is shown in Figure 99.

Table 10

MAXIMUM INJECTOR TEMPERATURE

Test	Injector	Temperature (°R)	Temperature (°K)
1	Straight-Pipe - Centerline	477	265
2		1007	559
3		968	538
4		939	522
5		1005	558
6		1036	575
7	Straight-Pipe - Centerline	823	457
8	Straight-Pipe - Offset	1063	590
9		445	347
10		745	414
11		323	179
12		291	167
13		463	257
14	Straight-Pipe - Offset	819	455
15.	Diffuser - Centerline	Thermocouple wire	
16		Burned off - Maximum	
17	Diffuser - Centerline	1460	811

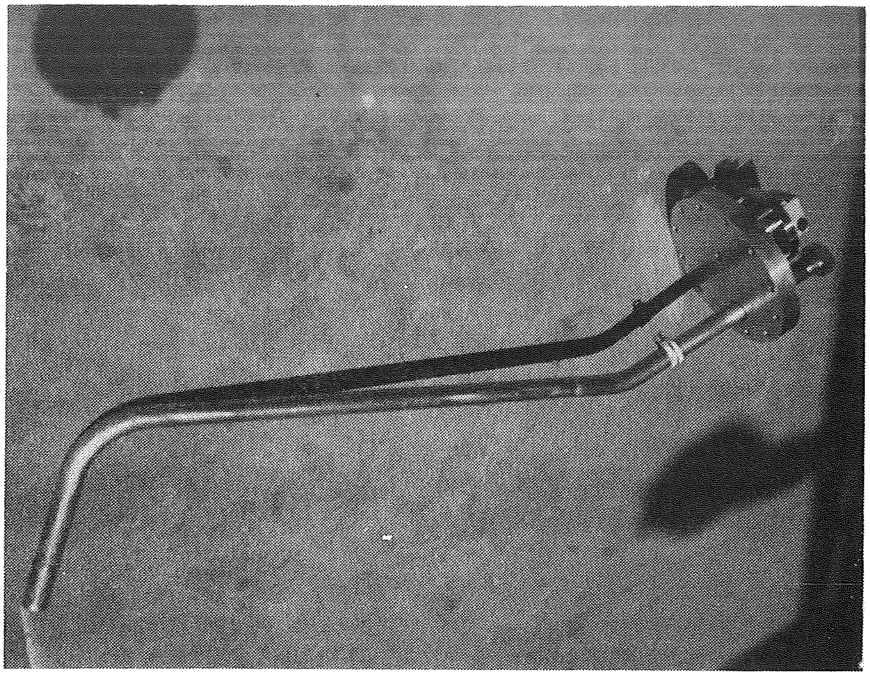

Figure 99. Centerline Straight-Pipe Injector Following Testing

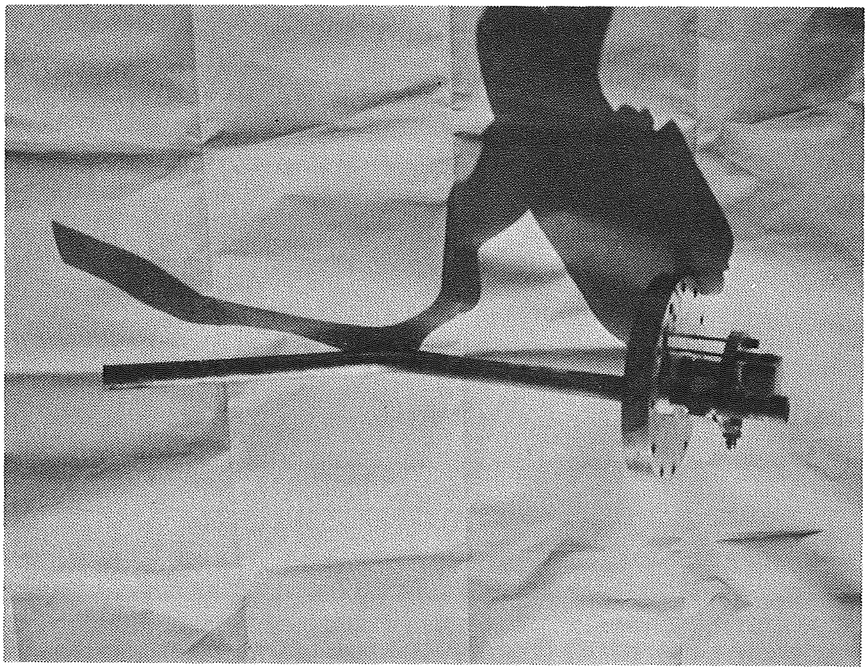

Figure 100. Offset Straight-Pipe Injector Following Testing

The offset straight-pipe injector is shown in Figure 100. The IR detector installation is clearly visible attached to the outside of the flange. The diffuser injector is shown in Figure 101. Note the heat/flow patterns near the holes in the injector.

Following the straight-pipe/centerline injector tests, some of the critical instrumentation had apparently failed; especially the level sensors and fluxmeter installations. The tank was opened and entered while changing to the straight-pipe/offset injector. During this time the tank interior was inspected and the instrumentation repaired. When the tank was opened after hot GN_2 purging for several hours the smell of HF was still quite strong. The tank sump is shown in Figure 102. It was coated with a white powdery film, and many lumps of white caked powder were found. The fluxmeter from the top dome was found in the sump. It is shown lying on the flow diverter in Figure 102 and was severely abused by overheating. The white powder was identified as the 731 RTV silastic used to bond the fluxmeters to the channels. Apparently the childown/heating cycles had removed all of the excess RTV used for potting of the fragile fluxmeter wires, plus any excess used in the bonding process. The tank interior is shown in Figure 103. The tank was very clean and apparently undamaged. Heat marks may be seen in the top dome which follow the external ribs (compare with Figure 60). HF etching marks were visible on the tank sidewall about halfway down at tank station 480. This was probably the HF melting region from the previous test (No. 7). Some of the instrumentation damage can be seen from close examination of Figure 103. The fluxmeter on the smooth sheet had debonded and was hanging by its wires. The severe heat had debonded several of the fluxmeter temperature sensors, and the ceramic coating on several of these sensors had been attacked by the HF until the platinum element was exposed and broken. These sensors were replaced. The carbon resistors which had failed had been severely attacked by HF - others nearby had not been affected. This was perhaps due to some shielding of the resistor from the ullage flow field. A few of the type 1012-1 gas temperature sensors (which were not completely shielded as were the 1080-1 sensors) had the ceramic element attacked by HF. Generally, however, these sensors survived better than the wafer type sensors. The thermopiles and teflon-covered wire were unaffected by the testing.

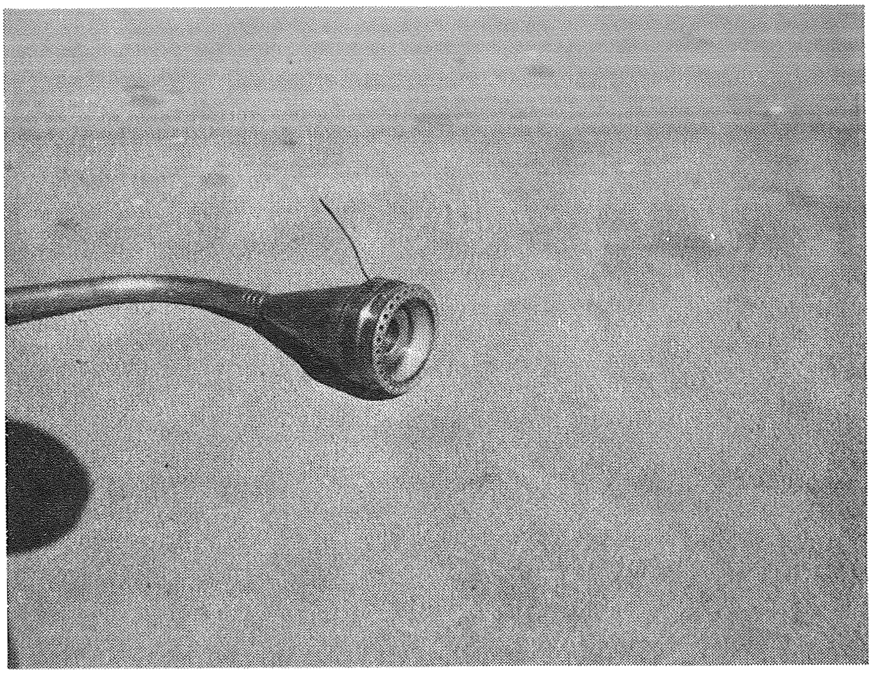

Figure 101. Centerline Diffuser Injector Following Testing

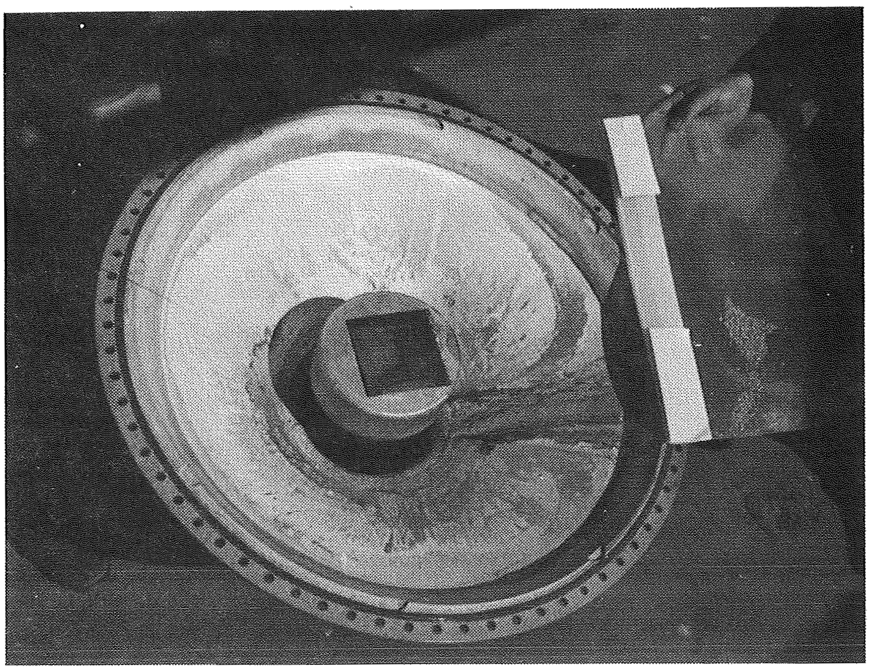

Figure 102. Test Tank Sump Following Test 7

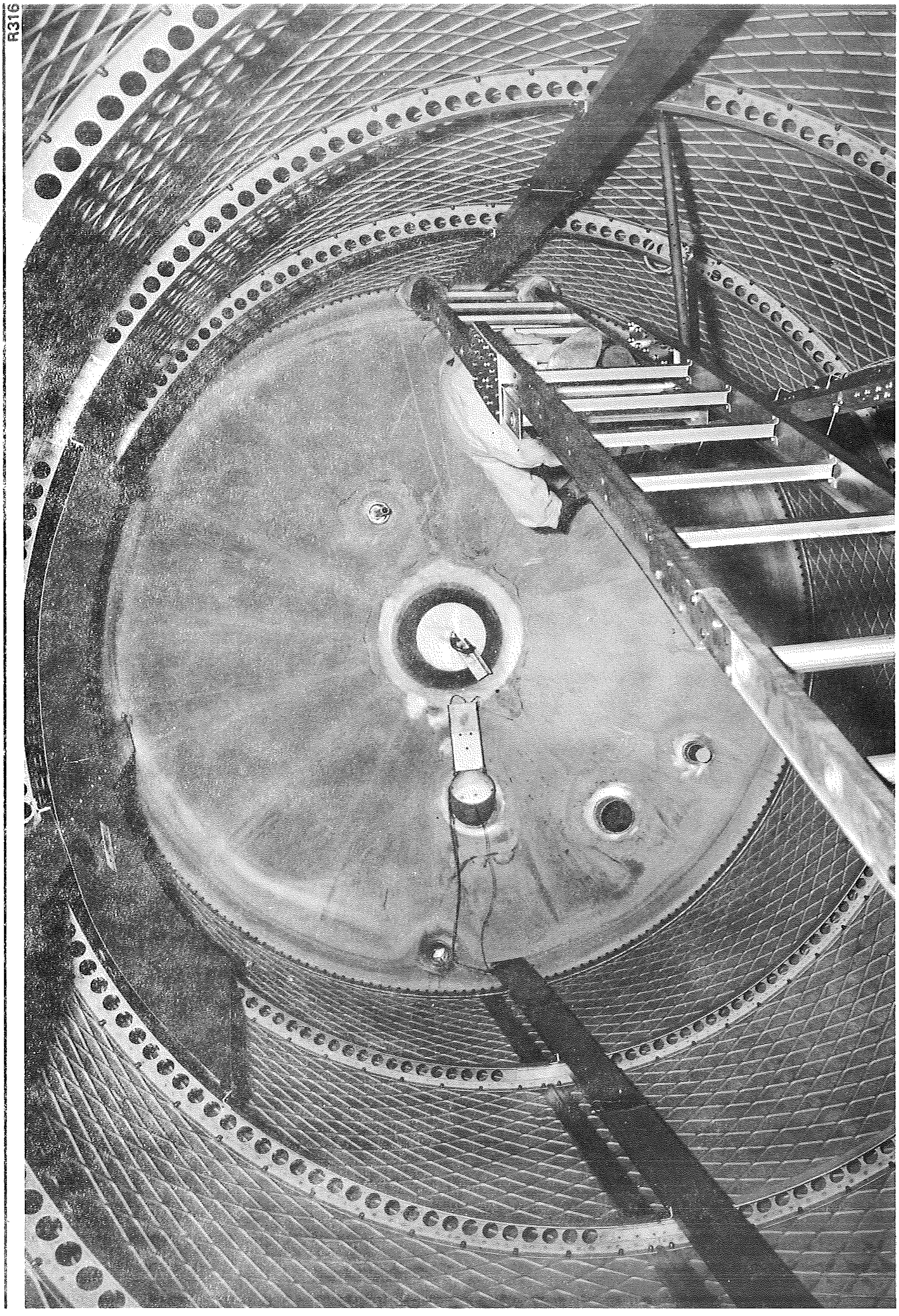

Figure 103. Interior of Test Tank Following Test 7

During the test program, the foam insulation also deteriorated to some degree. This was not unexpected because of the fairly large thickness. The foam cracked from a combination of thermal stress and tank pressurization. The cracks averaged about 1/8 inch (.00318M) wide and were repaired each day with RTV silastic potting compound. The external heat leak through the insulation increased somewhat as the test program progressed.

Analysis of the tank self-pressurization rate (with the vent closed) gave the apparent tank heat leak shown in Figure 104. The large deviation above the line by the 50 percent and 90 percent ullage cases is thought to be caused by continuing chilldown of the tank and insulation with low liquid levels. The conditions in the tank system had not yet stabilized in the short times shown in Figure 104, and thus an apparent excessive heat leak was computed. Actually, boiling in the bulk liquid as the system chilled down after loading was probably the reason. The heat leak through the tank walls was used in the analysis of the data for the analytical model, but the heat leak was not significant compared to the pressurization heat input, except for test 11, where it was calculated to reduce the GF_2 pressurant requirements by about 27 percent.

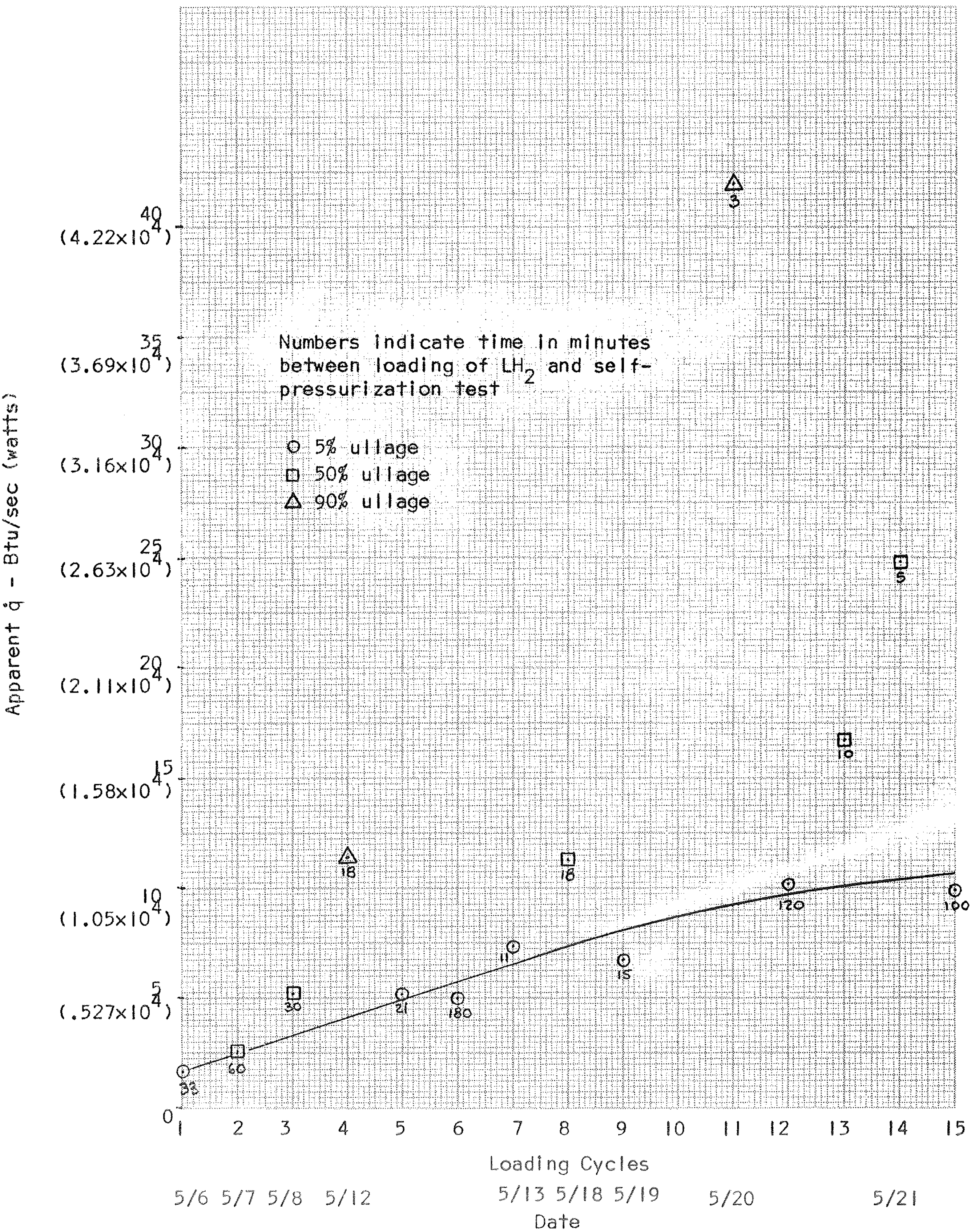

Figure 104. Apparent Test Tank External Heat Leak

SPACE VEHICLE PERFORMANCE PREDICTIONS

APPLICABILITY TO THE FULL RANGE OF HYDROGEN-FUELED SPACE VEHICLES

The MTI pressurization computer program H819 was developed for use over the full range of hydrogen fueled space vehicles. The generalized tabular inputs utilized in the program enable the user to specify virtually any reasonable tank configuration, duty cycle and operating conditions and to compute a mathematical solution for the GF_2 usage and resulting gas and wall temperatures. While the operation of the computer program is straightforward, its use in the study of a new vehicle and/or mission should include three general steps: first, assessment of the applicability of the model for the imposed conditions; second, selection and sizing of the injector system for the most effective operation; and third, calculation of the fluorine usage and other performance data. These steps are interrelated and iterative, but are discussed separately below.

The applicability of the model is related to the tank configuration, duty cycle and operating conditions. The most critical aspect of the model is the ullage mixing process and its effectiveness. The ullage mixing model correlates quite well with the experimental MTI results. The test tank configuration was a cylindrical tank of 1000 ft^3 (28.3 M^3) volume and L/D = 2.5. The original GH_2/LH_2 data correlated with the ullage mixing analysis was obtained with a 29 ft^3 (.82 M^3) cylindrical tank and L/D = 3 (Reference 9). Additional GH_2/LH_2 pressurization data showing ullage mixing with straight pipe injectors are reported for spherical tanks (L/D = 1) of 65 ft^3 (1.84 M^3) and 1150 ft^3 (32.5 M^3) in References 18 and 19, respectively. It was not possible for this investigation to correlate these data with the ullage mixing analysis; however, the presence of the mixed ullage region is quite evident from the reported test data. The ullage mixing model is expected to be valid for an L/D range of at least 1 to 3. The ullage volume should not directly influence the validity of the model although the injector must be properly scaled. For low L/D, a smaller value of the mixing factor f_m may be appropriate.

The ullage mixing effectiveness and the mixing fraction f_m are discussed in the section on Analysis of Experimental Results. The attainment of less than complete mixing to the full jet penetration depth is apparently a flow field effect in the ullage. The resulting flow field could be influenced by the tank configuration as well as duty cycle factors such as the ullage volume, injectant velocity, on-time fraction, etc. The flow field could not be precisely defined from the present test results but its effect on the data was apparent. Use of the value $f_m = 0.8$ for straight-pipe injectors gave good results and was generally conservative in predicting performance of the few cases which did not agree well with this assumption. The factor f_m appears to compensate for flow field effects; however, this aspect of the analysis is not fully understood.

A wide range of the various duty cycle parameters were used in the test program and correlated by the theoretical computations. Any physically reasonable duty cycle is expected to produce valid results from the computer program.

The most important factor in the general vehicle operating conditions is the acceleration level, particularly the low-g environment. The gravity level is included in the analysis as an input variable and influences both the free convection component of gas-wall heat transfer and the buoyancy force term in the jet penetration analysis. The equations should remain valid; however, no test data have been obtained under low-g conditions to check this part of the MTI analysis. Ullage mixing is essentially a forced convection process driven by the inlet jet energy and should not be adversely affected by low-g levels. The occurrence of excessive jet penetration depth into the liquid (X_L) may have effects not pred icted by the program. The possible disorientation of the propellant is not desirable, and the interface heat transfer empirical factors were evaluated at moderate values of X_L. Injector configuration and injectant conditions should be chosen to avoid excessively high X_L in low-g. Ullage injection is assumed; therefore, the LH_2 should be reasonably well settled, with a reasonably flat interface.

While any general system can be input to the program, it may not be clear at the outset how the injector configuration and conditions should be specified. This information must be developed iteratively by successive computer program calculations. The primary influence on the solution is the jet penetration depth and the resultant ullage mixing. Going from a straight tube injector to a multiple-tube or diffuser injector will decrease the penetration depth for a given GF_2 flowrate. Increasing the GF_2 flowrate for a given injector will increase the penetration depth. An increased flowrate will require a smaller on-time fraction for the pressure switch to give the same total GF_2 usage rate. This flexibility in determining jet penetration depth independent of the total GF_2 usage makes the pressure switch a desirable type of pressure control technique for an MTI system.

SPECIFIC SPACE VEHICLE PERFORMANCE ANALYSIS

To demonstrate the applicability of the H819 analysis to large-scale flight vehicles, a vehicle configuration and mission specified by NASA was analyzed to determine the performance of an MTI Pressurization System. The vehicle specified was the LH_2 tank of the Centaur vehicle with a total LH_2 tank volume of 1240 ft^3 (35.1 M^3) and a 316 stainless steel tank wall which was .016-in. (.0004 M) thick. The general configuration of the tank is shown in Figure 1 of Reference 20, (except for the volume and tank wall thickness). Reference 20 also gives experimental and predicted ambient stored helium requirements for pressurizing the same tank. The mission requirements were generally to provide 3 prepressurization cycles (at different ullage volumes) plus hold periods of low outflow for engine chilldown. The expulsion pressurization requirements are assumed to be provided by high-pressure GH_2 bled from the engines and thus MTI was not used for expulsion. The mission details are shown in Table 11.

The basic pressurization system design is straightforward, simple and conservative, and is shown schematically in figure 105. The system uses unregulated GF_2 storage bottle blowdown with the injector valve controlled by a pressure switch. A prevalve is not required, since proper design of the injector valve makes the prevalve superfluous. Further, if the injector valve fails, the entire system has failed. There is no system for detecting ignition, since for a vehicle application it is unnecessary and reduces overall reliability. (If the GF_2 fails to ignite, an ignition detector is not necessary to detect this fact - the tank pressure won't go up.)

TABLE 11

CENTAUR MISSION REQUIREMENTS

Prepressurization Cycle	Ullage Volume ft^3	Ullage Volume M^3	Prepressurization Time-sec	Hold Time sec*	Computed g-level g/g_e
1	40-65	1.13-1.84	< 5	< 15	6×10^{-4}
2	380	10.76	< 20	< 40	7.5×10^{-4}
3	1000	28.32	< 50	< 40	14.5×10^{-4}

*1.5 lb/sec (.68 Kg/sec) outflow during hold.

Pressure Rise Requirements

LH_2 Saturation Conditions:	18.5 - 20.5 psia (127.7×10^3 - 141.4×10^3 N/M^2)
Engine NPSP Requirements	8.3 psi (57.2×10^3 N/M^2)
Pressure Switch Range	2.0 psi (13.8×10^3 N/M^2)
Tank Pressure Range (assumed)	30.0 - 32.0 psi (207×10^3 - 221×10^3 N/M^2)

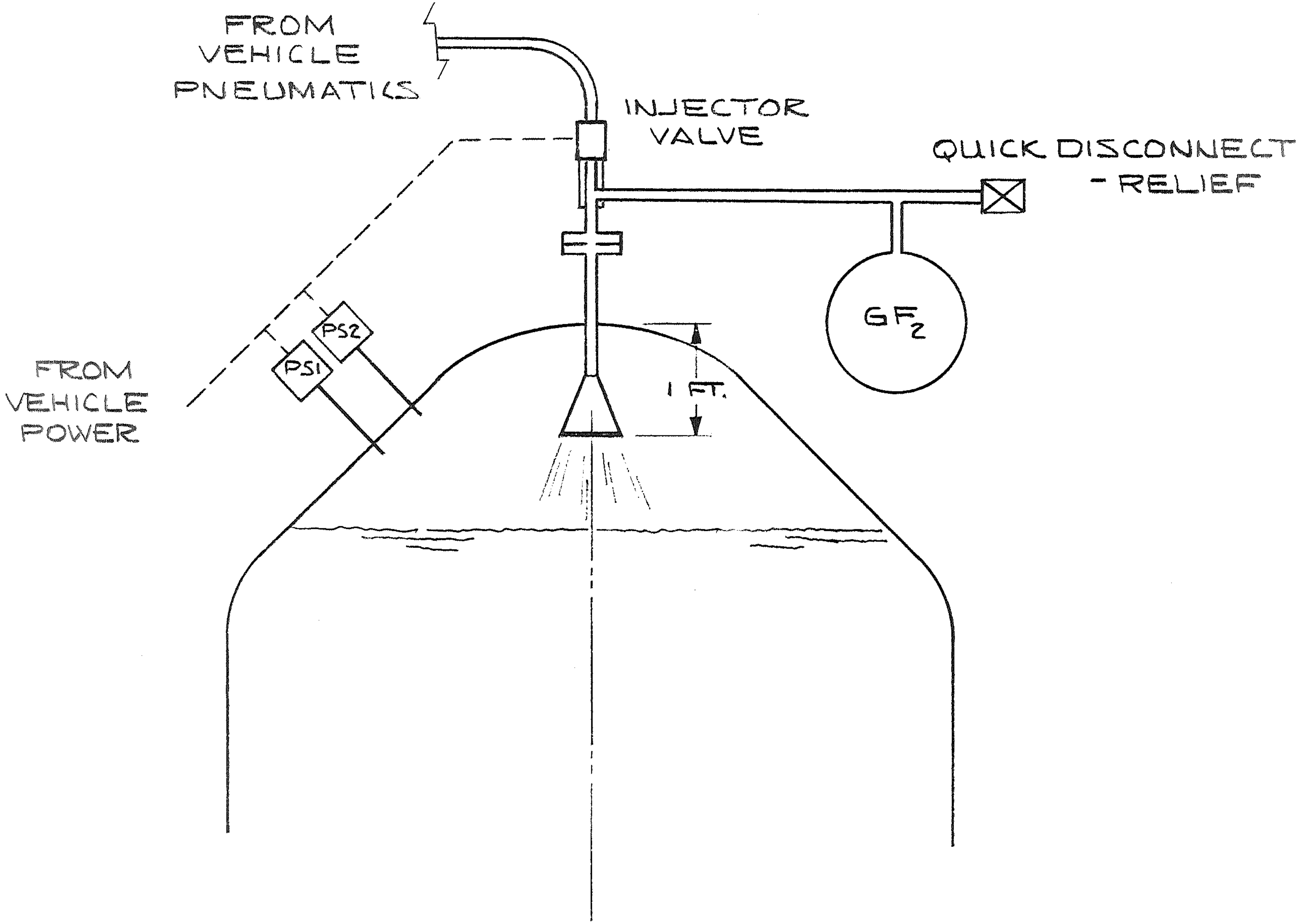

Figure 105. Centaur MTI System Schematic

The GF_2 flow control orifice is integral to the injector valve. The pressure switches may be made redundant if failure analysis indicated that such redundancy would contribute significantly to system reliability. The GF_2 storage conditions are assumed to be at 400 psia (2760×10^3 N/M^2) and 500°R (278°K). The low storage pressure was chosen because it is appropriate for adequate injection velocity, yet avoids the storage, filling, handling, and leakage problems inherent in high pressure GF_2 storage. The ambient temperature (500°R (278°K)) is assumed since this provides ease of loading, and will assure reliable ignition with controllable levels of O_2 contaminant in the GF_2. The system is at the forward (payload) end of the tank. Achieving this warm temperature through the proper use of standoffs from the LH_2 tank, orientation, thermal control coatings, etc., should not be a problem.

It was assumed that during prepressurization the propellants were settled with the g-levels shown in Table 11, and that ullage injection of GF_2 was used. Previous studies of MTI performance in low gravity (see the section on Experiment Design) indicated that a diffuser injector should be used to reduce liquid penetration to acceptable levels. Figure 35 indicated that in 10^{-3} - 10^{-2} g_e, a 26-hole -15° (.262 radian) diffuser would have about the same penetration characteristics as a straight-pipe injector of equal flow area in 1-g_e.

The maximum ullage volume and GF_2 flow requirements were about the same as the Thor test tank, and therefore it was assumed, as a first trial, that the diffuser should have 26 holes of .200-inch (.0051 M) diameter arranged in a 15° (.262 radian) cone. This is equivalent to a one-inch (.0254 M) diameter basic GF_2 flow and plumbing system. It was assumed that the diffuser was situated inside the tank one-foot (.3048 M) from the wall as shown in figure 105. A preliminary calculation indicated that less than one pound (.45 Kg) total GF_2 would be required. It was assumed that 3 pounds (1.36 Kg) of GF_2 would be stored at 400 psia (2760×10^3 N/M^2) and 500°R (278°K) to assure that at the end of the third (1000 ft^3 (28.3 M^3)) pressurization, there would be sufficient GF_2 storage pressure to provide adequate penetration of the large ullage. A summary of the study results is shown in Table 12. The total GF_2 required is .863 lb (.392 Kg). The injector valve cycled on twice during prepressurization cycles 1 and 2, but only once during prepressurization in cycle 3. The required hold times could almost be performed

TABLE 12

CENTAUR MISSION STUDY RESULTS

Prepressurization Cycle	Time (sec)	WF_2		WH_2 Evaporated		T Ullage		Penetration Depth	
		lb	(Kg)	lb	(Kg)	°R	(°K)	ft	(M)
1. Prepress	0.58	.0486	.0221	.1583	.0719	61	33.9	2.78 *(.483)	.848 *(.147)
Hold (Total)	20.0	.0577	.0262	.1886	.0855	63.4	35.2	2.78 *(.471)	.875 *(.144)
2. Prepress	2.79	.2193	.0995	0	0	64.2	35.7	5.93	1.809
Hold (Total)	60.0	.2559	.1161	0	0	66.6	37.0	6.03	1.839
3. Prepress	8.78	.5492	.2488	0	0	120.0	66.7	6.08	1.853
Hold (Total)	90.0	.5492	.2488	0	0	116.9	65.0	6.08	1.853

*LH_2 Penetration Depth

with no injector valve cycles at all. This was because the ullage stayed very cold, and the tank wall, because of its very low heat capacity, was essentially always in thermal equilibrium with the ullage; hence, very little energy loss to the wall, and very slow pressure decay in the tank.

The final GF_2 storage sphere pressure was 250 psia (1724 x 10^3 N/M^2) which gives adequate GF_2 reserve in case the interface heat transfer uncertainties with the small ullage case cause errors in GF_2 usage predictions. The 1.06 ft^3 (.03 M^3) GF_2 storage sphere is 15.2 inches (.386 M) in diameter, has an .050-inch (.0013 M) thick wall, is fabricated from 2014-T6 aluminum and weighs 3.6 lbs (1.63 Kg) (assuming a 50 percent boss weight factor, and a safety factor of 1.25 on yield strength.) The 2014-T6 aluminum alloy has a high strength/weight ratio and is fully compatible with GF_2. Because of the low ullage temperatures, the diffuser injector requires less heat-soak capacity, and can be fabricated from thin (.060-inch (.0015 M)) copper sheet at an approximate weight of 2.0 lbs (.91 Kg). The injector valve and flow plumbing weigh about 3.6 lbs (1.63 Kg) and 0.5 lbs (.227 Kg), respectively. The flightweight pressure switches and quick disconnect/relief valve could weigh 0.5 lbs (.227 Kg) and 3.5 lbs (1.59 Kg), respectively for a total system weight of 16.7 lbs (7.59 Kg).

The system is quite simple and lightweight, and compared to an ambient helium system, should save about 150 lbs (68.1 Kg), (based on the experimental helium requirements in Reference 20).

CONCLUSIONS

As a result of this comprehensive analytical and experimental program utilizing a large-scale flight-weight test tank, a number of significant conclusions can be drawn regarding the applicability of a fluorine-hydrogen MTI pressurization system to a large-scale hydrogen-fueled flight vehicle:

1. A sophisticated analytical technique has been developed which incorporates models for heat transfer, injection jet penetration, and ullage mixing, and which accurately predicts the performance of large-scale MTI pressurization systems. The model was used to successfully correlate the large-scale experimental results. The correlations indicated that there was little radial temperature variation, that the ullage gas was generally deeply penetrated by the injectant jet, and generally well-mixed, (although usually not completely mixed.) The analytical method accurately predicted the GF_2 usage, the tank temperature distributions, and the quantities of LH_2 evaporated, over a wide range of operating conditions and injector configurations.

2. The experimental program successfully demonstrated the operation of a complete MTI pressurization control system in a large-scale flight-weight LH_2 tank. The tests indicated controllable pressurization, reasonable ullage gas and tank wall temperatures, and efficient GF_2 usage. The straight-pipe injectors provided more efficient (cooler) pressurization than the diffuser injector, as predicted by the analysis.

3. The MTI reaction product, HF, had been of concern with large-scale MTI application . The tankage and major structural components were unaffected by the HF. Some of the instrumentation, when unprotected, was attacked by HF (together with severe heating/cooling temperature cycles.) This could be avoided with suitable design. Sampling for HF in the LH_2 expelled from the tank was inconclusive, but the results implied that there was very little HF in the effluent LH_2 (less than 1 part per thousand.)

4. Fluorine-hydrogen MTI pressurization has been tested and evaluated extensively enough that flight-vehicle application can be confidently undertaken. Analysis of a typical advanced upper-stage vehicle with multiple-burn mission, performed with the MTI pressurization computer program, has indicated superior performance and substantial weight savings, compared to conventional helium prepressurization.

REFERENCES

1. Cady, E.C., Hypergolicity of F_2-H_2 and Reaction Product Freezing Under Main Tank Injection Pressurization Conditions, NASA CR-72253, (DAC-60975), September 1967.

2. Cady, E.C., An Investigation of Fluorine-Hydrogen Main Tank Injection Pressurization, NASA CR-72408, (DAC-62233), April 1968.

3. Cady, E.C., "An Investigation of Fluorine-Hydrogen Main-Tank Injection Pressurization," Journal of Spacecraft and Rockets, Vol. 6, No. 11, November 1969, pp. 1248-1253.

4. Roudebush, W.H., An Analysis of the Problem of Tank Pressurization During Outflow, NASA TN D-2585, January 1965.

5. Fortran Program for the Analysis of a Single-Propellant Tank Pressurization System, Rocketdyne Report S&ID IDWA 5835, 15 June 1964.

6. Nein, M.E., and J.F. Thompson, Experimental and Analytical Studies of Cryogenic Propellant Tank Pressurant Requirements, NASA TN D-3177, February 1966.

7. Kendle, D.W., A Numerical Analysis of Cryogenic Tank Pressurization, MDAC Report DAC-60863, November 1967.

8. Kendle, D.W., A Tank Pressurization Computer Program for Research Applications, MDAC Report DAC-63076, December 1968.

9. DeWitt, R.L., R.J. Stochl, and W.R. Johnson, Experimental Evaluation of Pressurant Gas Injectors During the Pressurized Discharge of Liquid Hydrogen, NASA TN D-3458, June 1966.

10. Kleinstein, G., "Mixing in Turbulent Axially Symmetric Free Jets," Journal of Spacecraft and Rockets, Vol. 1, No. 4, July-August 1964, p. 403.

11. Laufer, J., "Turbulent Shear Flows of Variable Density," AIAA Journal, Vol. 7, No. 4, April 1969, p. 706.

12. Hawthorne, W.R., D.S. Weddell, and H.C. Hottel, "Mixing and Combustion in Turbulent Gas Jets," Third Symposium on Combustion, Flame and Explosion Phenomena, The William and Wilkins Co., 1949.

13. McAdams, W. H., Heat Transmission, McGraw-Hill Book Co., 1954.

14. Eckert, E.R.G. and R.M. Drake, Jr., Heat and Mass Transfer, McGraw-Hill Book Co., 1959.

15. Roder, H.M., and R.D. Goodwin, Provisional Thermodynamic Functions for Para-Hydrogen, National Bureau of Standards Technical Note 130, December 1961.

16. Simmons, F.S., C.B. Arnold, and E.F. Lirette, Infrared Spectroscopic Study of Hydrogen-Fluorine Flame, BAMIRAC Report 4613-122-T, March 1966.

17. Kendle, D.W., Ullage Mixing Effects on Cryogenic Tank Pressurization, MDAC Report DAC-63168, March 1968.

18. Stochl, R.J., P.A. Masters, R.L. DeWitt and J.E. Maloy, Gaseous-Hydrogen Requirements for the Discharge of Liquid Hydrogen from a 1.52-Meter-(5 ft) Diameter Spherical Tank, NASA TN D-5336, August 1969.

19. Stochl, R.J., P.A. Masters, R.L. DeWitt and J.E. Maloy, Gaseous-Hydrogen Pressurant Requirements for the Discharge of Liquid Hydrogen from a 3.96-Meter-(13 ft) Diameter Spherical Tank, NASA TN D-5387, August 1969.

20. Lacovic, R., A Comparison of Experimental and Calculated Helium Requirements for the Pressurization of a Centaur Liquid Hydrogen Tank, NASA TM X-1870, September 1969.

DISTRIBUTION LIST FOR FINAL REPORT, NASA CR-72756

RECIPIENT	DESIGNEE	COPIES
National Aeronautics & Space Administration Lewis Research Center 21000 Brookpark Road Cleveland, Ohio 44135		
Attn: Contracting Officer, MS 500-313		1
Liquid Rocket Technology Branch, MS 500-209		5
Technical Report Control Office, MS 5-5		1
Technology Utilization Office, MS 3-16		1
AFSC Liaison Office, 501-3		2
Library		2
Office of Reliability & Quality Assurance, MS 500-111		1
D. L. Nored, Chief, LRTB, MS 500-209		1
E. A. Edelman, Project Manager MS 500-209		3
E. W. Conrad, MS 500-204		1
R. J. Stochl, MS 500-204		1
R. L. Dewitt, MS 500-204		1
A. J. Stofan, MS 500-103		1
W. R. Dunbar, MS 500-106		1
Chief, Liquid Experimental Engineering, RPX Office of Advanced Research & Technology NASA Headquarters Washington, D.C. 20546		2
Chief, Liquid Propulsion Technology, RPL Office of Advanced Research & Technology NASA Headquarters Washington, D.C. 20546		2
Director, Launch Vehicles & Propulsion, SV Office of Space Science & Applications NASA Headquarters Washington, D.C. 20546		1

RECIPIENT	DESIGNEE	COPIES
Chief, Environmental Factors & Aerodynamics Code RV-1 Office of Advanced Research & Technology NASA Headquarters Washington, D.C. 20546		1
Chief, Space Vehicles Structures Office of Advanced Research & Technology NASA Headquarters Washington, D.C. 20546		1
Director, Advanced Manned Missions, MT Office of Manned Space Flight NASA Headquarters Washington, D.C. 20546		1
NASA Scientific & Technical Information Facility P.O. Box 33 College Park, Maryland 20740		6
Director, Technology Utilization Division Office of Technology Utilization NASA Headquarters Washington, D.C. 20546		1
National Aeronautics & Space Administration Ames Research Center Moffett Field, California 94035 Attn: Library	Hans M. Mark Mission Analysis Division	1
National Aeronautics & Space Administration Flight Research Center P.O. Box 273 Edwards, California 93523 Attn: Library		1
National Aeronautics & Space Administration Goddard Space Flight Center Greenbelt, Maryland 20771 Attn: Library	Merland L. Moseson, Code 620	1

RECIPIENT	DESIGNEE	COPIES
National Aeronautics & Space Administration John F. Kennedy Space Center Cocoa Beach, Florida 32931 Attn: Library	Dr. Kurt H. Debus	1
National Aeronautics & Space Administration Langley Research Center Langley Station Hampton, Virginia 23365 Attn: Library	E. Cortwright Director	1
National Aeronautics & Space Administration Manned Spacecraft Center Houston, Texas 77001 Attn: Library	J. G. Thiobodaux, Jr. Chief, Propulsion & Power Division	1
National Aeronautics & Space Administration George C. Marshall Space Flight Center Huntsville, Alabama 35812 Attn: Library	Hans G. Paul James Thomas	1
Jet Propulsion Laboratory 4800 Oak Grove Drive Pasadena, California 91103 Attn: Library	J. Blumrich Henry Burlage, Jr.	1
Defense Documentation Center Cameron Station Building 5 5010 Duke Street Alexandria, Virginia 22314 Attn: TISIA		1
Office of the Director of Defense Research & Engineering Washington, D.C. 20301 Attn: Office of Asst. Dir. (Chem. Technology)		1
RTD (RTNP) Bolling Air Force Base Washington, D.C. 20332		1

RECIPIENT	DESIGNEE	COPIES
Arnold Engineering Development Center Air Force Systems Command Tullahoma, Tennessee 37389 Attn: Library	Dr. H. K. Doetsch	1
Advanced Research Projects Agency Washington, D.C. 20525 Attn: Library		1
Aeronautical Systems Division Air Force Systems Command Wright-Patterson Air Force Base, Dayton, Ohio Attn: Library		1
Air Force Missile Test Center Patrick Air Force Base, Florida Attn: Library	L. J. Ullian	1
Air Force Systems Command Andrews Air Force Base Washington, D.C. 20332 Attn: Library	Capt. S.W. Bowen SCLT	1
Air Force Rocket Propulsion Laboratory (RPR) Edwards, California 93523 Attn: Library		1
Air Force FTC (FTAT-2) Edwards Air Force Base, California 93523 Attn: Library	Donald Ross	1
Air Force Office of Scientific Research Washington, D.C. 20333 Attn: Library	SREP Dr. J.F. Masi	1
Space & Missile Systems Organization Air Force Unit Post Office Los Angeles, California 90045 Attn: Technical Data Center		1
Office of Research Analyses (OAR) Holloman Air Force Base, New Mexico Attn: Library 88330 RRRD		1

RECIPIENT	DESIGNEE	COPIES
U.S. Air Force Washington, D.C. Attn: Library	Col. C.K. Stambaugh Code AFRST	1
Commanding Officer U.S. Army Research Office (Durham) Box CM, Duke Station Durham, North Carolina 27706 Attn: Library		1
U.S. Army Missile Command Redstone Scientific Information Center Redstone Arsenal, Alabama 35808 Attn: Document Section	Dr. W. Wharton	1
Bureau of Naval Weapons Department of the Navy Washington, D.C. Attn: Library	J. Kay Code RTMS-41	1
Commander U.S. Naval Missile Center Point Mugu, California 93041 Attn: Technical Library		1
Commander U.S. Naval Weapons Center China Lake, California 93557 Attn: Library		1
Commanding Officer Naval Research Branch Office 1030 E. Green Street Pasadena, California 91101 Attn: Library		1
Director (Code 6180) U.S. Naval Research Laboratory Washington, D.C. 20390 Attn: Library	H. W. Carhart J. M. Krafft	1
Picatinny Arsenal Dover, New Jersey 07801 Attn: Library	I. Forsten	1
Air Force Aero Propulsion Laboratory Research & Technology Division Air Force Systems Command United States Air Force Wright-Patterson AFB, Ohio 45433 Attn: APRP (Library)	R. Quigley C. M. Donaldson	1

RECIPIENT	DESIGNEE	COPIES
Electronics Division Aerojet-General Corporation P.O. Box 296 Azusa, California 91703 Attn: Library	W. L. Rogers	1
Space Division Aerojet-General Corporation 9200 East Flair Drive El Monte, California 91734 Attn: Library	S. Machlawski	1
Aerojet Ordnance and Manufacturing Aerojet-General Corporation 11711 South Woodruff Avenue Fullerton, California 90241 Attn: Library		1
Aerojet Liquid Rocket Company P.O. Box 13222 Sacramento, California 95813 Attn: Technical Library 2484-2015A	R. Stiff	1
Aeronutronic Division of Philco Ford Corp. Ford Road Newport Beach, California 92663 Attn: Technical Information Department	Dr. L. H. Linder	1
Aerospace Corporation 2400 E. El Segundo Blvd. Los Angeles, California 90045 Attn: Library-Documents	J. G. Wilder	1
Arthur D. Little, Inc. 20 Acorn Park Cambridge, Massachusetts 02140 Attn: Library	A. C. Tobey	1
ARO, Incorporated Arnold Engineering Development Center Arnold AF Station, Tennessee 37389 Attn: Library		1
Battelle Memorial Institute 505 King Avenue Columbus, Ohio 43201 Attn: Report Library, Room 6A		1

RECIPIENT	DESIGNEE	COPIES
Beech Aircraft Corporation Boulder Facility Box 631 Boulder, Colorado Attn: Library	Douglas Pope	1
Bell Aerosystems, Inc. Box 1 Buffalo, New York 14240 Attn: Library	W. M. Smith	1
Bendix Systems Division Bendix Corporation 3300 Plymouth Street Ann Arbor, Michigan Attn: Library	John M. Brueger	1
Bellcomm 955 L'Enfant Plaza, S.W. Washington, D.C. Attn: Library	H. S. London	1
Boeing Company Space Division P.O. Box 868 Seattle, Washington 98124 Attn: Library	J. D. Alexander C. F. Tiffany	1
Boeing Company 1625 K Street, N.W. Washington, D.C. 20006		1
Chemical Propulsion Information Agency Applied Physics Laboratory 8621 Georgia Avenue Silver Spring, Maryland 20910	Tom Reedy	1
Chrysler Corporation Missile Division P.O. Box 2628 Detroit, Michigan Attn: Library	John Gates	1
Chrysler Corporation Space Division P.O. Box 29200 New Orleans, Louisiana 70129 Attn: Librarian		1

RECIPIENT	DESIGNEE	COPIES
Curtiss-Wright Corporation Wright Aeronautical Division Woodridge, New Jersey Attn: Library	G. Kelley	1
University of Denver Denver Research Institute P.O. Box 10127 Denver, Colorado 80210 Attn: Security Office		1
Fairchild Stratos Corporation Aircraft Missiles Division Hagerstown, Maryland Attn: Library		1
Research Center Fairchild Hiller Corporation Germantown, Maryland Attn: Library	Ralph Hall	1
Republic Aviation Fairchild Hiller Corporation Farmington, Long Island New York		1
General Dynamics/Convair P.O. Box 1128 San Diego, California 92112 Attn: Library	Frank Dore	1
Missiles and Space Systems Center General Electric Company Valley Forge Space Technology Center P.O. Box 8555 Philadelphia, Pa. 19101 Attn: Library		1
Grumman Aircraft Engineering Corporation Bethpage, Long Island, New York Attn: Library	Joseph Gavin	1
Hercules Powder Company Allegheny Ballistics Laboratory P.O. Box 210 Cumberland, Maryland 21501 Attn: Library		1

RECIPIENT	DESIGNEE	COPIES
Honeywell, Inc. Aerospace Division 2600 Ridgeway Road Minneapolis, Minnesota Attn: Library		1
IIT Research Institute Technology Center Chicago, Illinois 60616 Attn: Library	C. K. Hersh	1
Kidde Aerospace Division Walter Kidde & Company, Inc. 567 Main Street Belleville, New Jersey 07109	R. J. Hanville	1
Ling-Temco-Vought Corporation P.O. Box 5907 Dallas, Texas 75222 Attn: Library		1
Lockheed Missiles and Space Company P.O. Box 504 Sunnyvale, California 94087 Attn: Library		1
Lockheed Propulsion Company P.O. Box 111 Redlands, California 92374 Attn: Library	H. L. Thackwell	1
Marquardt Corporation 16555 Saticoy Street Box 2013 - South Annex Van Nuys, California 91409	L. R. Bell Jr.	1
Martin-Marietta Corporation (Baltimore Division) Baltimore, Maryland 21203 Attn: Library		1
Denver Division Martin-Marietta Corporation P.O. Box 179 Denver, Colorado 80201 Attn: Library	Dr. Morganthaler F. R. Schwartzberg	1
Orlando Division Martin-Marietta Corporation Box 5827 Orlando, Florida Attn: Library	J. Fern	1

RECIPIENT	DESIGNEE	COPIES
Western Division McDonnell Douglas Astronautics 5301 Bolsa Ave. Huntington Beach, California 92647 Attn: Library	R. W. Hallet G. W. Burge P. Klevatt	1
McDonnell Douglas Aircraft Corporation P.O. Box 516 Lambert Field, Missouri 63166 Attn: Library	R. A. Herzmark	1
Rocketdyne Division North American Rockwell, Inc. 6633 Canoga Avenue Canoga Park, California 91304 Attn: Library, Department 596-306	Dr. R. J. Thompson S. F. Jacobellis	1
Space & Information Systems Division North American Rockwell 12214 Lakewood Blvd. Downey, California Attn: Library		1
Northrop Space Laboratories 3401 West Broadway Hawthorne, California Attn: Library	Dr. William Howard	1
Purdue University Lafayette, Indiana 47907 Attn: Library (Technical)	Dr. Bruce Reese	1
Rocket Research Corporation Willow Road at 116th Street Redmond, Washington 98052 Attn: Library	F. McCullough, Jr.	1
Stanford Research Institute 333 Ravenswood Avenue Menlo Park, California 94025 Attn: Library	Dr. Gerald Marksman	1
Thiokol Chemical Corporation Redstone Division Huntsville, Alabama Attn: Library	John Goodloe	1

RECIPIENT	DESIGNEE	COPIES
TRW Systems, Inc. 1 Space Park Redondo Beach, California 90278 Attn: Tech. Lib. Doc. Acquisitions	D. H. Lee	1
TRW TAPCO Division 23555 Euclid Avenue Cleveland, Ohio 44117	P. T. Angell	1
United Aircraft Corporation Corporation Library 400 Main Street East Hartford, Connecticut 06108 Attn: Library		1
United Aircraft Corporation Pratt & Whitney Division Florida Research & Development Center P.O. Box 2691 West Palm Beach, Florida 33402 Attn: Library	R. J. Coar Dr. Schmitke	1
United Aircraft Corporation United Technology Center P.O. Box 358 Sunnyvale, California 94038 Attn: Library	Dr. David Altman	1
Vickers Incorporated Box 302 Troy, Michigan		1
Vought Astronautics Box 5907 Dallas, Texas Attn: Library		1